YOKOHAMA NATIONAL UNIVERSITY
INSTITUTE OF URBAN INNOVATION

AN EXPERIMENTAL STUDY ON THE SEISMIC PERFORMANCE OF RC BEAMS WITH NON-STRUCTURAL WALLS

A dissertation presented in partial fulfilment
of the requirements for the
Doctor's Degree in Engineering

Supervisor

Prof. TASAI Akira

by

Mhmoud SAUOD

2016

The Dissertation Committee for Mhmoud SAUOD Certifies that this is the approved version of the following dissertation:

An Experimental Study on the Seismic Performance of RC Beams with Non-Structural Walls

Committee:

TASAI Akira,
Supervisor

TSUBAKI Tatsuya,
Professor

KAWABATA Masaya,
Associate Professor

MATSUMOTO Yuka,
Associate Professor

SUGIMOTO Kunyoshi,
Associate Professor

KUSUNOKI Koichi,
Associate Professor

An Experimental Study on the Seismic Performance of RC Beams with Non-Structural Walls

by

M.Eng. Mhmoud SAUOD, 2013

Dissertation

Presented to the Graduate School of Urban Innovation

Yokohama National University

in Partial Fulfillment

of the Requirements

for the Degree of

Doctor's Degree in Engineering

Yokohama National University

September 2016

Dedicated to

my beloved wife and my parents

Acknowledgements

All praise be to God.

Many special thanks to my supervisors, Prof. TASAI Akira, Prof. SUGIMOTO Kunyoshi and Prof. KUSUNOKI Koichi for the invaluable guidance they gave during the study. I am also grateful for the assistance provided by laboratory members of Institute of Urban Innovation.

I want to express my thanks and gratitude to my wife and family for their prayers, endless love, support and encouragement.

This research has been supported by Scientific Research Grant Program under Grant-in-aid No. 25420572.

MHMOUD SAUOD

September, 2016

An Experimental Study on the Seismic Performance of RC Beams with Non-Structural Walls

Ph.D., Mhmoud SAUOD

Yokohama National University, 2016

Supervisor: Prof. TASAI Akira

The impact of constructing non-structural walls with structural gaps in RC beams was not highlighted enough previously, although its importance. Experimentally, it was found that shear failure occurred in these beams even they were designed to fail in flexural manner. Six specimens were designed with specific parameters; shear margin, increasing shear reinforcement and the influence of slab. The experimental results showed that increasing of shear reinforcement and the presence of slab improved the seismic performance of the beams; large deformation capacity and flexural failure. Comparing with other beams where shear failure occurred, as well fracture of stirrups was remarked. To calculate the amount of shear reinforcement for safe design, strut-and-tie model was proposed. FEA was done as a necessary step to build the strut-and-tie model. Three main beams without slab were modeled. The numerical results corresponded with the experimental and analytical results. The proposed model is expected to be helpful to the designer, especially for checking the shear reinforcement at plastic hinge regions of studied beams. In addition, the proposed model is very flexible to be used for wide range of RC beams with non-structural walls.

Table of Contents

List of Tables

List of Figures

CHAPTER 1
INTRODUCTION

- Introduction of Shear Failure of RC Beams
- Problem Definition and Previous Researches
- Introduction to Strut-and-Tie Model Essentials
- Research Objective

1.1 Introduction of Shear Failure of RC Beams

Thousands of tests have been performed on longitudinally reinforced concrete beams in shear during the past century, and many design equations [1] have been proposed. Most of these equations account for only the most basic mechanisms which induce failure or they are empirically based and do not account for the different mechanisms of shear resistance. Shear failure is a very complex combination of conditions which are still not fully understood. Two primary sources which contribute to the lack of understanding of shear failures are that the mechanisms which lead to failure change depending on beam geometry and the brittleness of shear failures. The components which constitute shear resistance of longitudinally reinforced concrete beams can be roughly categorized as aggregate interlock, resistance of the compression zone, and dowel resistance of the reinforcement. The final failure of the beam can be contributed to the loss of anyone of these components. The amount which these mechanisms contribute to the overall resistance are dependent on one another and varies during the process of failure. These components are also functions of the beam's geometry such as the steel ratio, concrete strength, shear span ratio of the beam, and loading conditions. Shear failure is normally extremely brittle, and sudden, explosive failure results. Due to this brittleness, the progression of shear failure has not been documented. Often, several components resisting the shear force seemingly fail at once, which may lead to misdiagnosis of which mechanism actually leads to the final failure.

The behavior of RC beams under reversed loading is different than it in case of monotonic loading [2, 3, 4].

The reinforcement details, amount and arrangement, should be designed well to prevent brittle behavior of RC beams especially in case of reversed loading. Where RC beams are designed to have a ductile behavior under external loads such as, earthquakes. The ductile behavior requires forming plastic hinges at ends of the beam after yielding of the longitudinal bars. These hinges should be strong to not collapse in case of high inelastic rotation angles and to dissipate enough amount of energy.

1.2 Problem Definition and Previous Researches

By investigation of RC building in damaged area due to earthquakes (5 ,6).
Shear failure of columns was observed in some buildings which have a beams with non-structural walls. X-shaped cracks formed in the columns between the non-structural walls of beams.

The non-structural walls constructed with the beams, hanging walls or standing walls, shortened the height of connected column. And as a result, the columns became stiffer and the brittle behavior is dominant.

Figure (1.1) shows illustration about the impact of non-structural walls on the connected columns.

For same drift angle of floor, the applied shear force on the columns with shorter height is higher than the taller ones.

To keep the columns safe, structural gaps are constructed to disconnect between the walls and the columns without any initial study on the influence of these gaps on the seismic performance of beams.

There is a lack in the experimental works done on the RC beams with non-structural wall with/without structural gaps.

Previous researches (7, 8, 9) studied the RC beams with non-structural walls in different cases as the followings:

- The walls at two sides of beam without structural gaps.
- The walls at two sides of beam with structural gaps.
- The walls at one side of beam with structural gaps with different heights of wall.

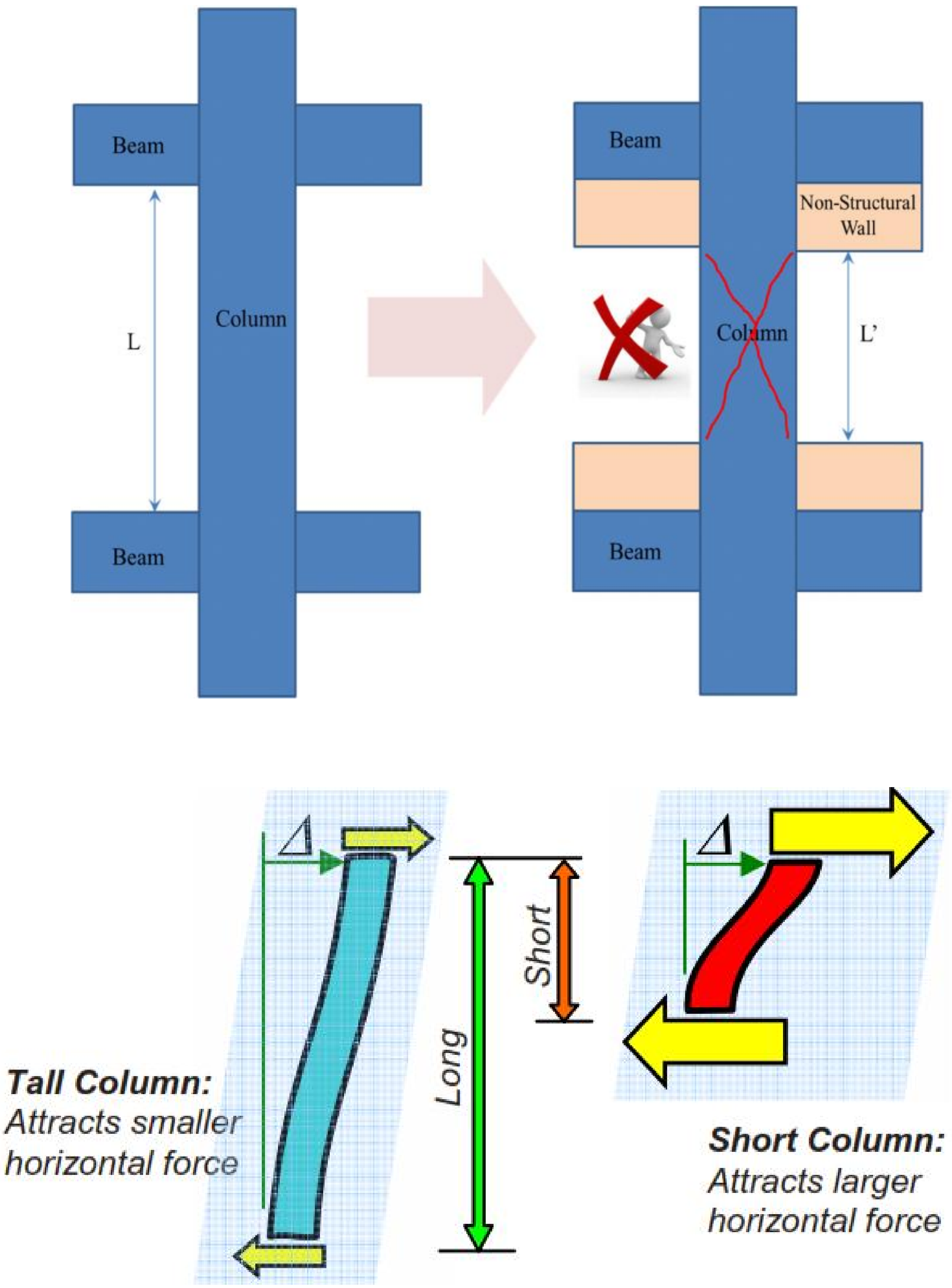

Fig(1.1) Shortening the height of columns by non-structural walls

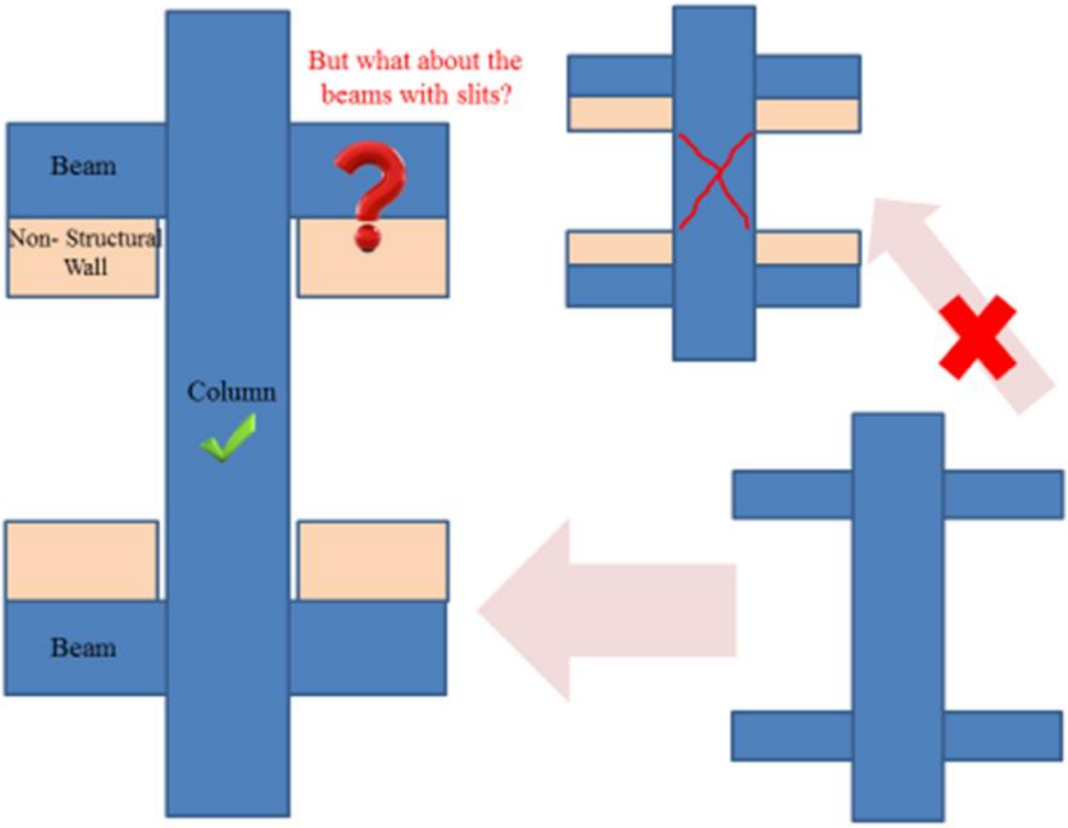

Fig(1.2) Constructing slits, structural gaps, between the walls and the connected columns

Table (1.1) shows the dimensions and details of specimens of previous experimental works. Figures (1.3) to (1.7) show dimensions and reinforcement details of these specimens.

Appendix A, shows the experimental results of mentioned specimens; shear force and lateral displacement curves and cracks patterns.

Flexural failure occurred in all the beams with deformation capacity larger than 1/25 rad. And touching between the wall and the support occurred in case of beams with structural gaps.

In case of the walls at one side of beam, yielding of stirrups occurred, even though the height of wall was increased from 350mm to 1400 mm.

This research highlights this case, the walls at one side of beam, where some stirrups at plastic hinge regions yielded.

New beam with shorter length comparing with the beams studied in the previous researches, were designed and various situations were studied. Taking into consideration the influence of shear span ratio, shear reinforcement and the slab.

Table 1.1 Dimensions and details of specimens of previous experimental works[7]

Beam	SP-B1	SP-S1	SP-S2	SP-S3	SP-S4
Width	200				
Depth	300				
Main Bars	3D13				
P_t %	0.71 %				
Stirrups	2D6@100				
P_w %	0.32 %				
Non-Structural Wall					
Thickness	-	80			
Height	-	350	700	350	1400
Position	-	Two Sides		One Side	
Transverse Reinforcement	-	2D4@50 , 0.23 %			
Longitudinal Reinforcement	-	2D4@50 , 0.23 %			
Edge's Bars	-	4D6			
Fc (MPa)	21.0				
Length of Beam	2500.0				
Shear Span Ratio	4.17				

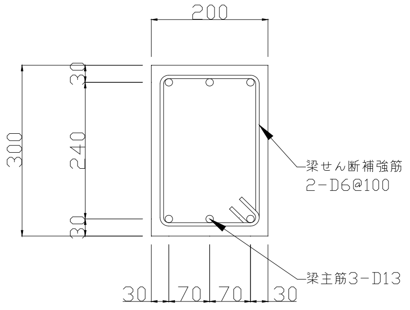

Fig (1.3) SP-B1(7)

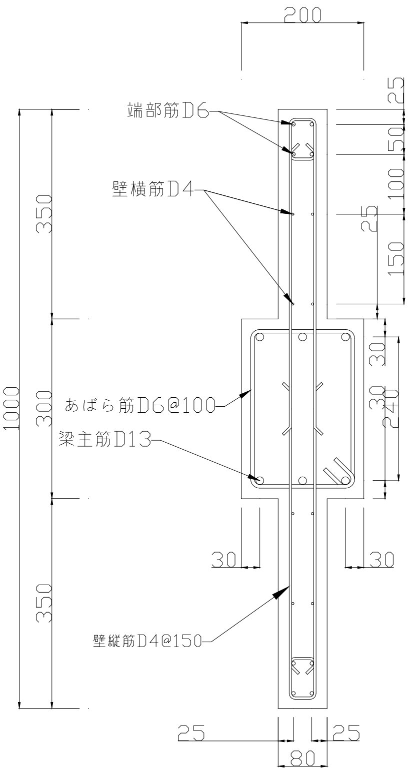

Fig (1.4) SP-S1(7)

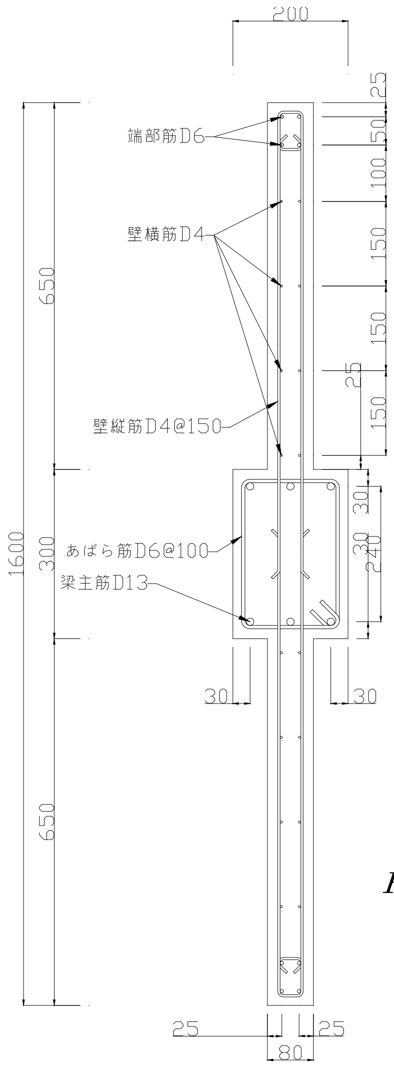

Fig (1.5) SP-S2(7)

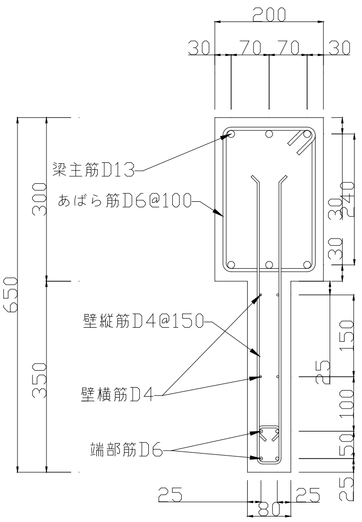

Fig (1.6) SP-S3(7)

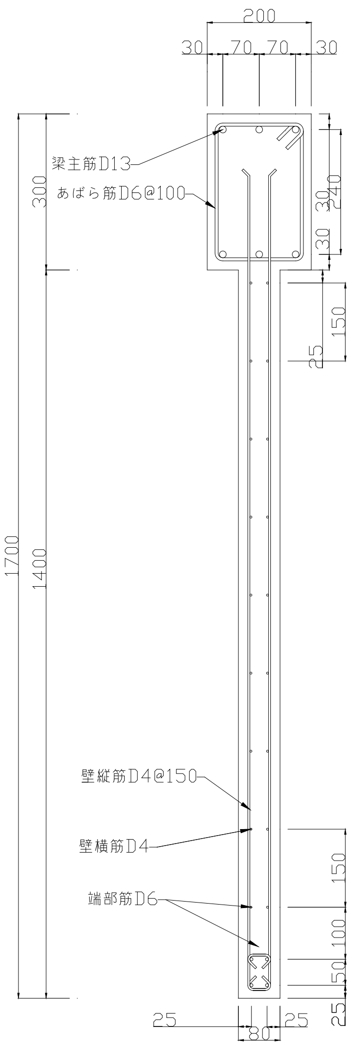

Fig (1.7) SP-S4(7)

1.3 Introduction to Strut and Tie Modeling Essentials

The concept of strut-and-tie model is simple, and depends on determining the paths of forces or stresses in the studied structural members. The compression stresses will be represented in the struts and the tensile stresses will be represented in the ties. The struts usually are concrete members with or without reinforcement and the ties are steel bars.

The struts and ties are the main members of the STM, and they intersect in the nodes, so the STM consists of struts, ties and nodes.
The dimensions of the STM; spacing between the members, depends on the dimension of the structural member and reinforcement details.
The main principles (10) of STM are:

1- The truss of STM is in equilibrium with the external loads.
2- The concrete struts should have enough strength to avoid the crushing.

The stresses in each of STM members must be less than the allowable stresses determined in the adopted codes. After considering the factored external loads and the reduction of STM strength members.
Calculating the strength of the STM is not easy due to difficulty in calculating the strength of STM members; struts, ties and nodes (11).
STM (12, 13) is very flexible to different situation of structural members and this characteristic means that there is no right or wrong STM for the same structural member. In another word, there is better and worse STM according to choosing the positions of struts and ties.

1.4 Research Objective

From the previous researches, the case of RC beams with non-structural walls at one side of beam and with structural gaps is a critical case, yielding and fracture of stirrups of beam, and should be highlighted. The influence of the wall with structural gaps on the beam is the goal of this research. And proposing a proper method to design the RC beam in this situation where the adopted codes in Japan did not refer to a specific methodology of designing and left it up to the designer.

CHAPTER 2
OUTLINES OF SPECIMENS

- Dimensions and Reinforcement Details
- Estimation of Hysteresis Characteristics
- Ultimate Flexural Strength
- Ultimate Shear Strength

2.1 Dimensions and Reinforcement Details

Six beams were designed according to the adopted specifications and regulations of designing RC beams in Japan.

Tables (2.1) and (2.2) show the dimensions and reinforcement details of studied specimens.

Table 2.1 Dimensions of studied specimens

<table>
<tr><th rowspan="2">Specimen</th><th colspan="2">Cross-Section</th><th rowspan="2">Gap Width</th><th rowspan="2">Cross-Section of the Wall</th><th rowspan="2">Cross-Section of the Slab</th></tr>
<tr><th>Width</th><th>Height</th></tr>
<tr><td>SP-S5</td><td rowspan="6">200</td><td>300</td><td rowspan="2">15</td><td rowspan="6">350 X 80
Height X Thickness</td><td rowspan="3">No Slab</td></tr>
<tr><td>SP-S6</td><td rowspan="4">400</td></tr>
<tr><td>SP-S6-AR</td><td rowspan="3">25</td></tr>
<tr><td>SP-S6-Slab T</td><td rowspan="3">1000* X 100
Flange* X Thickness</td></tr>
<tr><td>SP-S6-Slab K</td></tr>
<tr><td>SP-S5-Slab T</td><td>300</td><td>15</td></tr>
<tr><td colspan="6">*: Flange of slab is 1000 mm without the width of beam. Units: mm.</td></tr>
</table>

Table 2.2 Reinforcement details of studied beams

<table>
<tr><th rowspan="2">Specimen</th><th colspan="4">Beam Bars</th></tr>
<tr><th>Main</th><th>Pt%</th><th>Stirrups</th><th>Pw%</th></tr>
<tr><td>SP-S5</td><td>2-D19</td><td>1.10</td><td>D4@70</td><td>0.20</td></tr>
<tr><td>SP-S6</td><td rowspan="2">3-D19</td><td rowspan="2">1.19</td><td>D6@50</td><td>0.64</td></tr>
<tr><td>SP-S6-AR</td><td>D6@35</td><td>0.91</td></tr>
<tr><td>SP-S6-Slab T</td><td rowspan="2">2-D19+
1-D10</td><td rowspan="2">0.89</td><td rowspan="2">D6@40</td><td rowspan="2">0.79</td></tr>
<tr><td>SP-S6-Slab K</td></tr>
<tr><td>SP-S5-Slab T</td><td>2-D16</td><td>0.76</td><td>D6@100</td><td>0.32</td></tr>
</table>

The non-structural walls and the slabs were designed with same dimensions and reinforcement details for all specimens as the following:

For the non- structural wall, 2-D4@150mm were used for longitudinal and transverse bars and 4-D6 at the edge of wall.

For the slab, 2-D5@75mm were used for longitudinal and horizontal bars in two layers.

In case of SP-S6-AR, The spacing between the stirrups was decreased from 50 mm to 35 mm along 335mm ≒ 0.9·d at the plastic hinge regions keeping 50mm in the middle of beam.

The width of structural gap was calculated as the following:

$$\frac{W_s}{H} = \frac{\delta}{L} = R \qquad \text{Eqn.2.1}$$

Where:

Ws: Width of structural gap (*mm*),

H: Height of non-structural wall (*H= 350 mm*),

δ: Lateral displacement of whole specimen (*mm*), and

L: Length of beam (*L= 1700 mm*).

R: Drift angle, deformation angle (*rad*).

In case of width of the gap is 15 mm, the maximum lateral displacement of specimen is:

$$\frac{15}{350} = \frac{\delta}{1700} \Rightarrow \delta \approx 72.85mm \Rightarrow R \approx \frac{1}{23.33} rad$$

In the other case where width of slit is 25 mm:

$$\frac{25}{350} = \frac{\delta}{1700} \Rightarrow \delta \approx 121.42mm \Rightarrow R \approx \frac{1}{14} rad$$

Width of the gap was determined in both beams SP-S5 and SP-S6 as same to the gap width in the previous researches and kept for SP-S5-Slab T because this beam was designed to consider the impact of slab on the seismic behavior of SP-S5.

For the other specimens, the width of gap was increased to be 25 mm taking into consideration the expected increasing in the strength and deformation capacity due to slab and strengthening by adding more stirrups in plastic hinge regions.

Figures (2.1) to (2.7) show the dimensions and reinforcement details of studied specimens.

Fig(2.1) Dimensions and reinforcement details of SP-S5

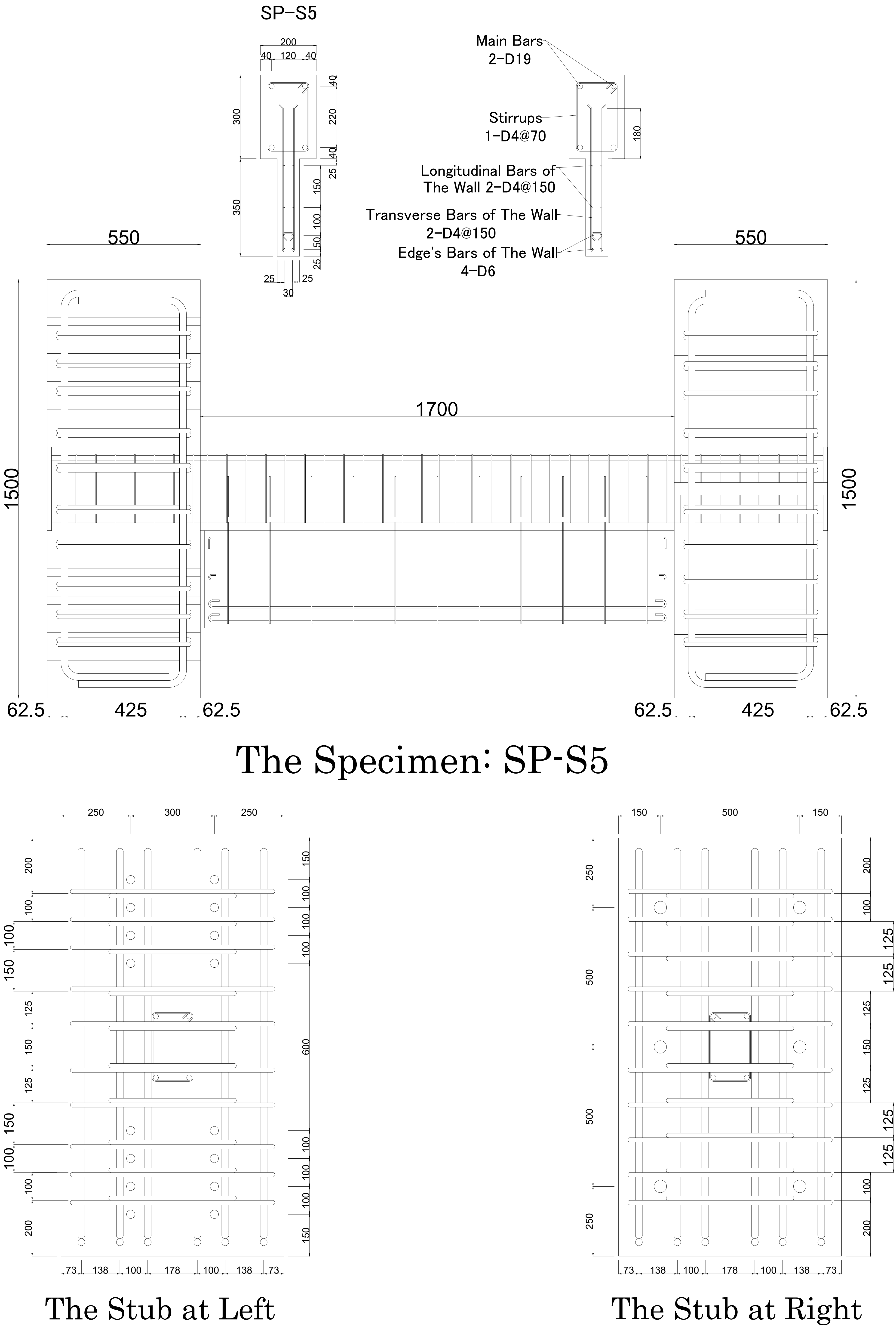

Fig(2.2) Dimensions and reinforcement details of SP-S6

SP-S6

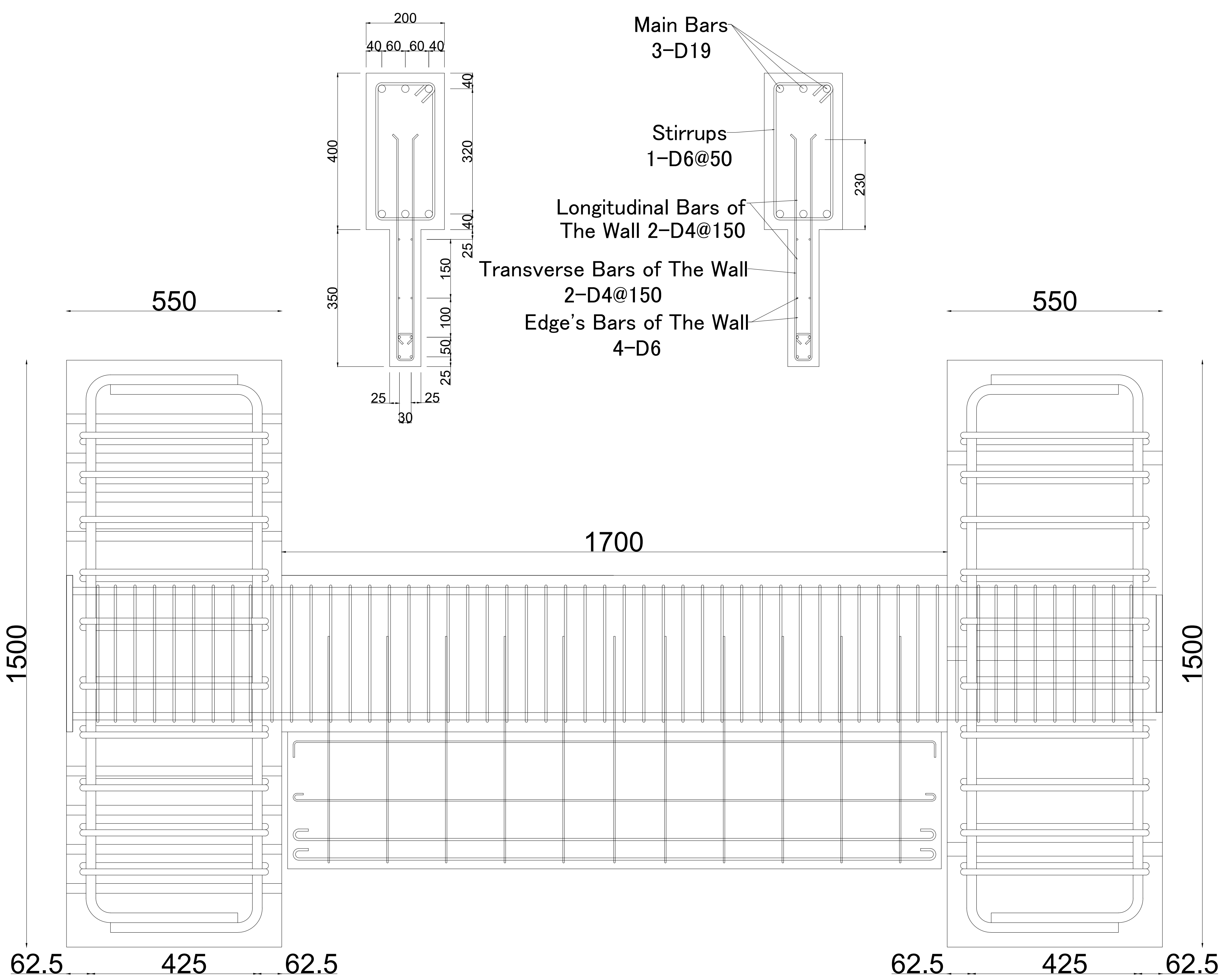

The Specimen: SP-S6

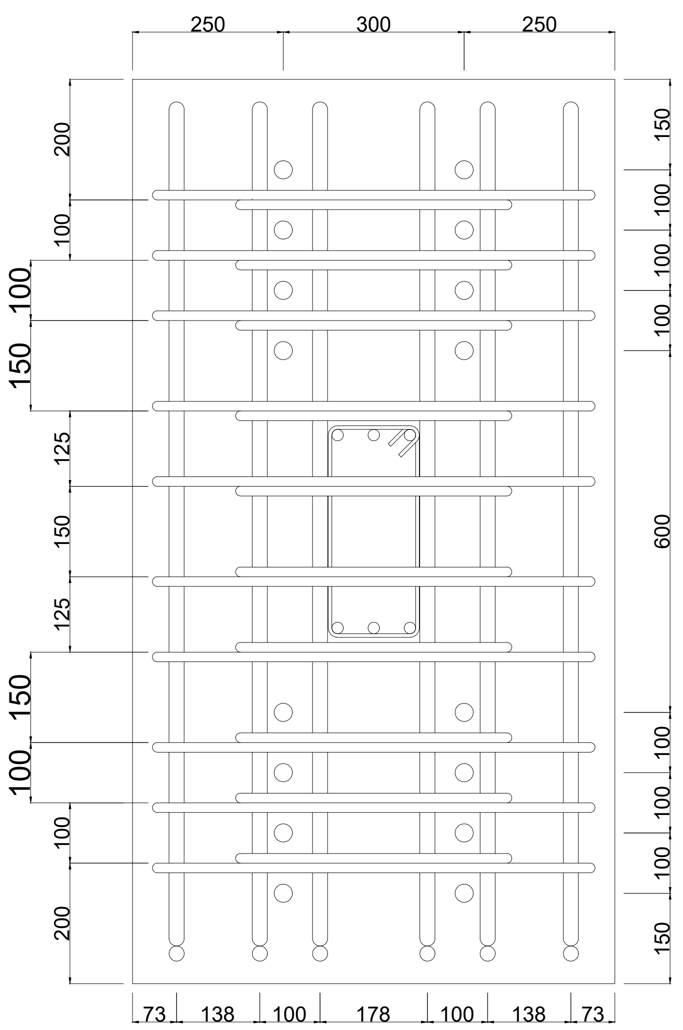

The Stub at Left

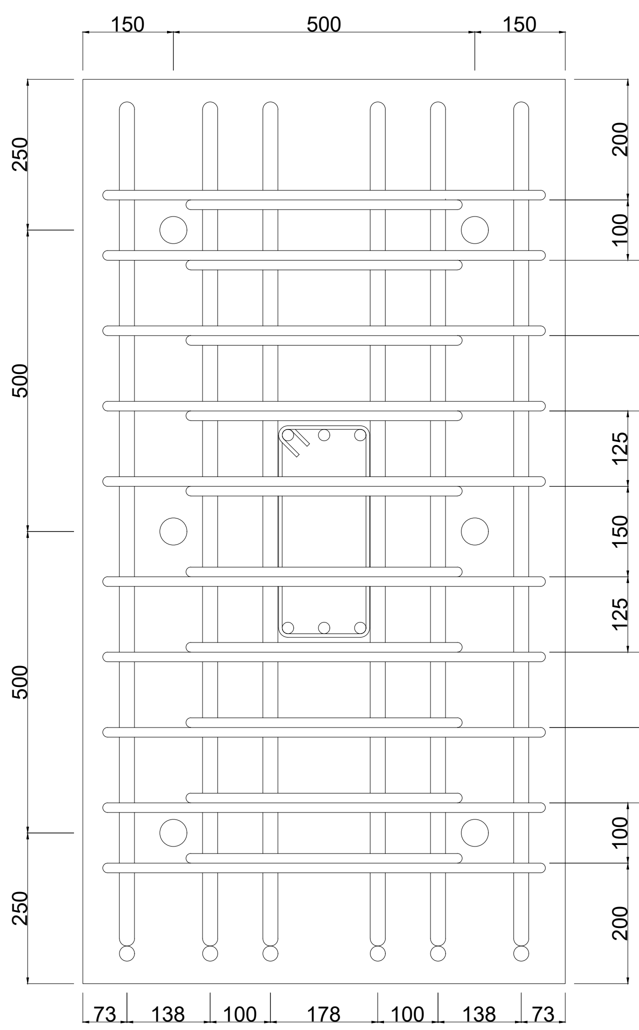

The Stub at Right

Fig(2.3) Dimensions and reinforcement details of SP-S6-AR

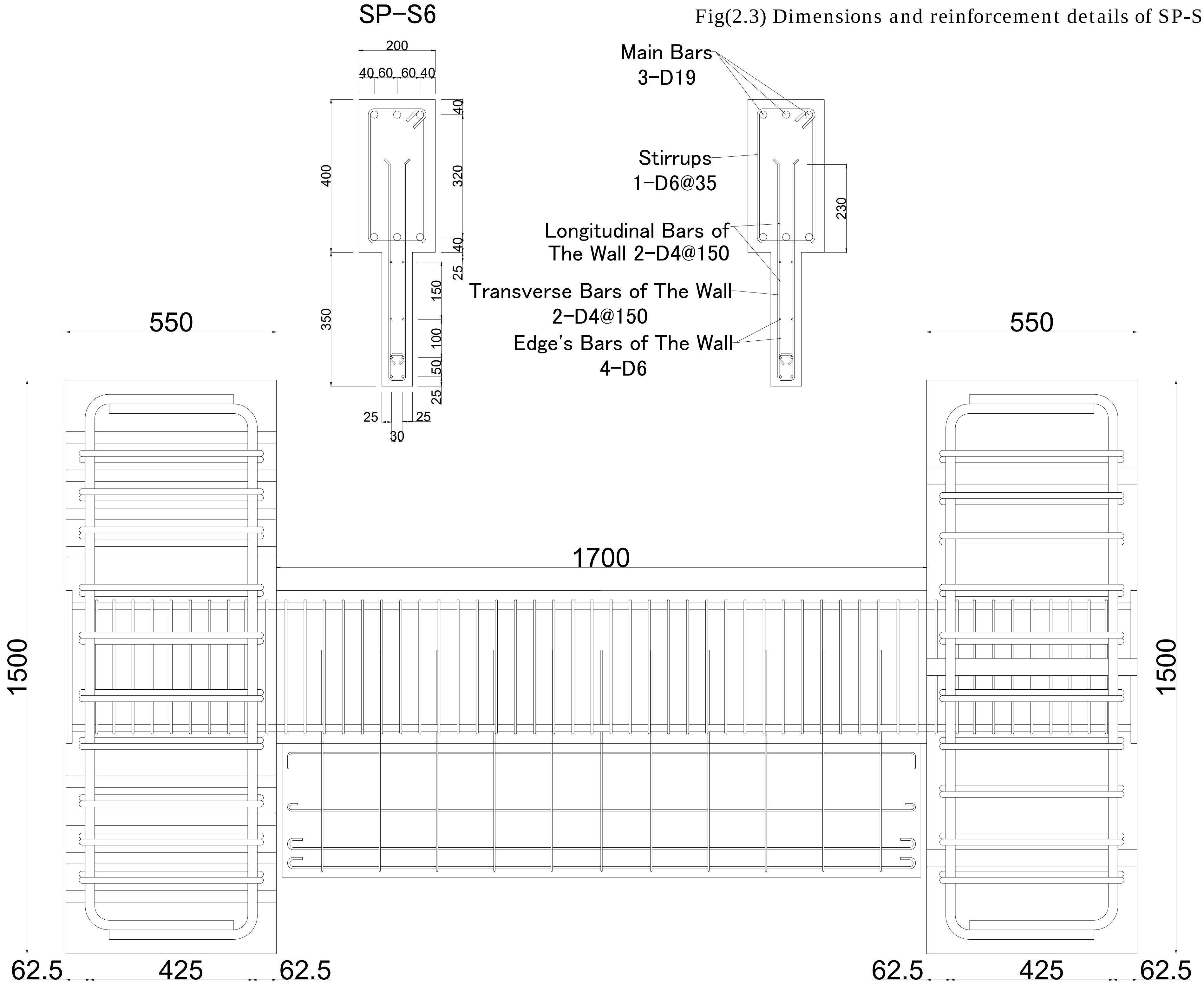

The Specimen: SP-S6-AR

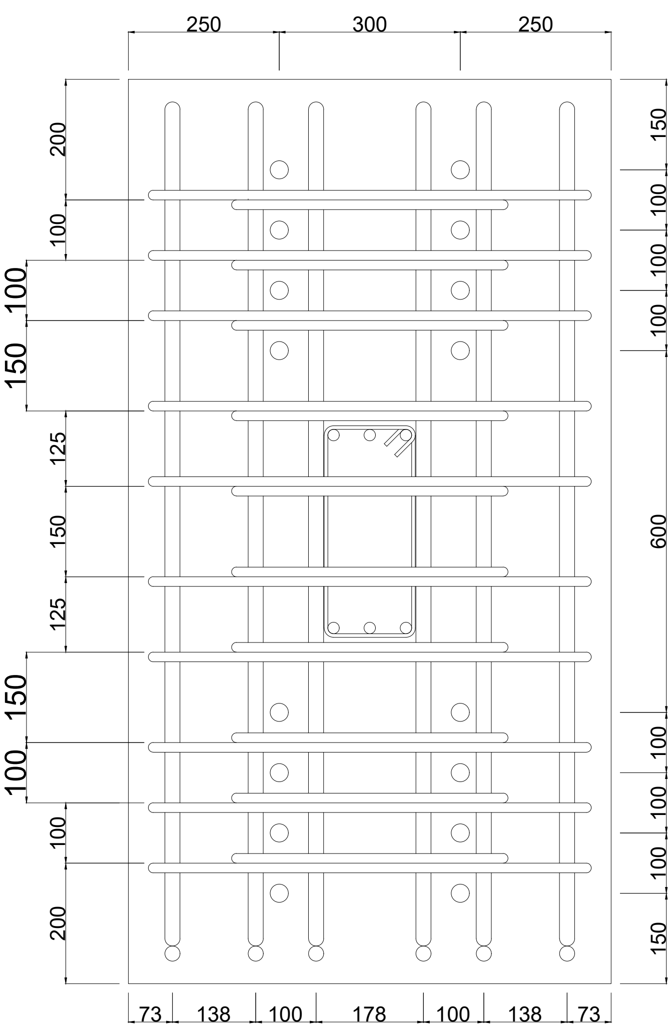

The Stub at Left

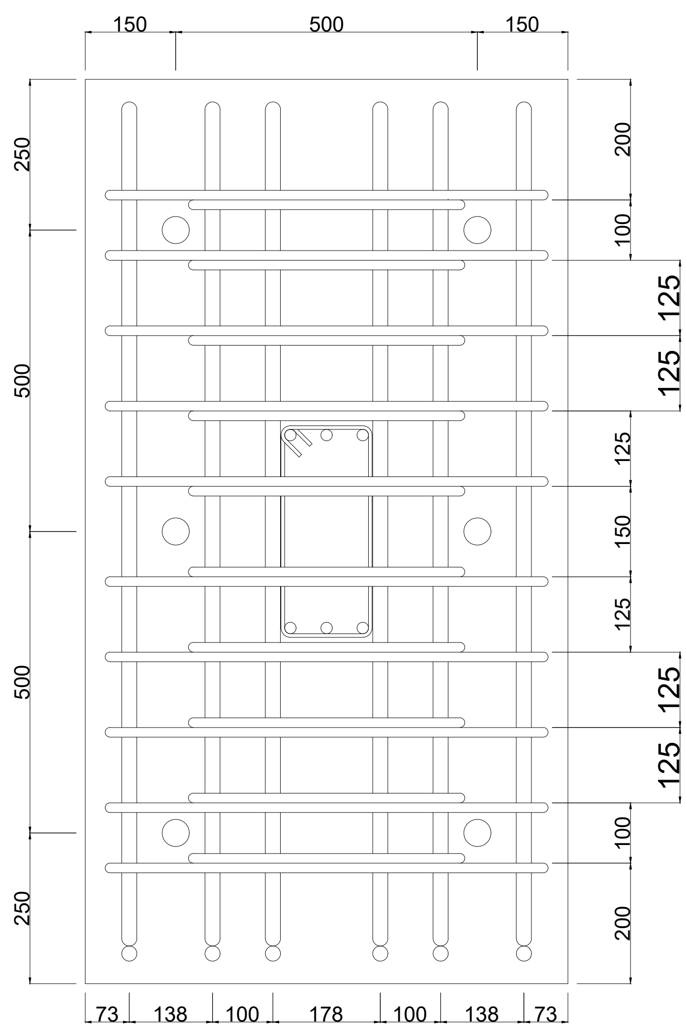

The Stub at Right

Fig(2.4) Dimensions and reinforcement details of SP-S6-Slab T

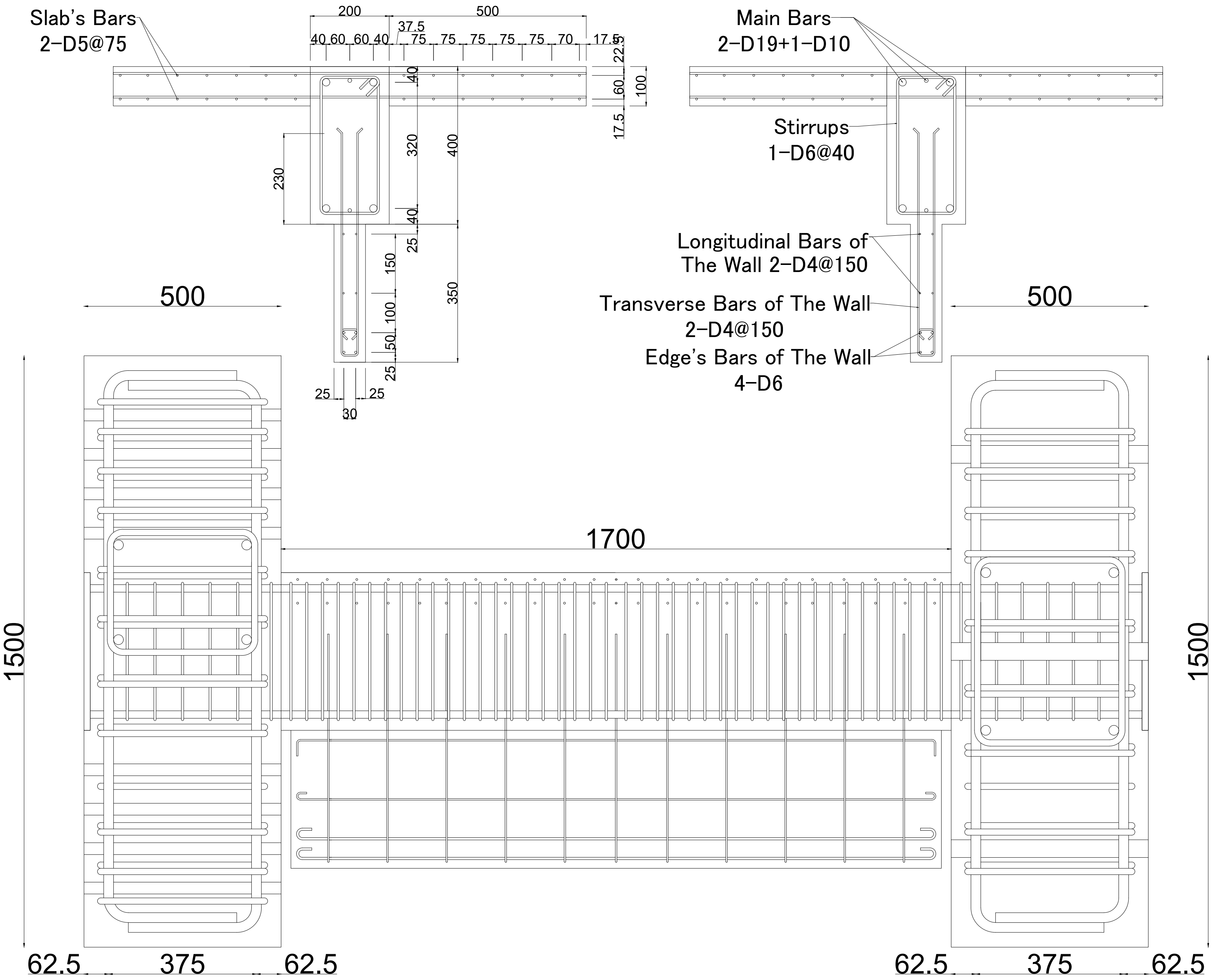

The Specimen: SP-S6-Slab T

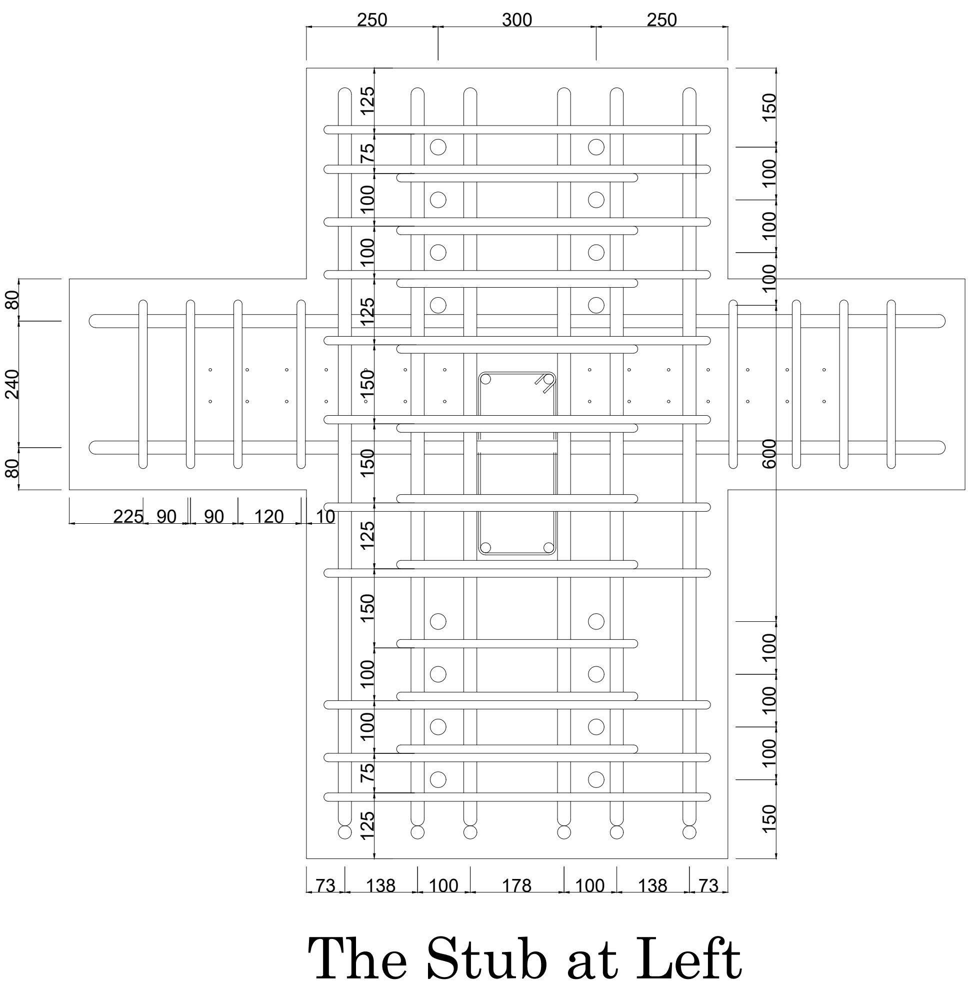

The Stub at Left

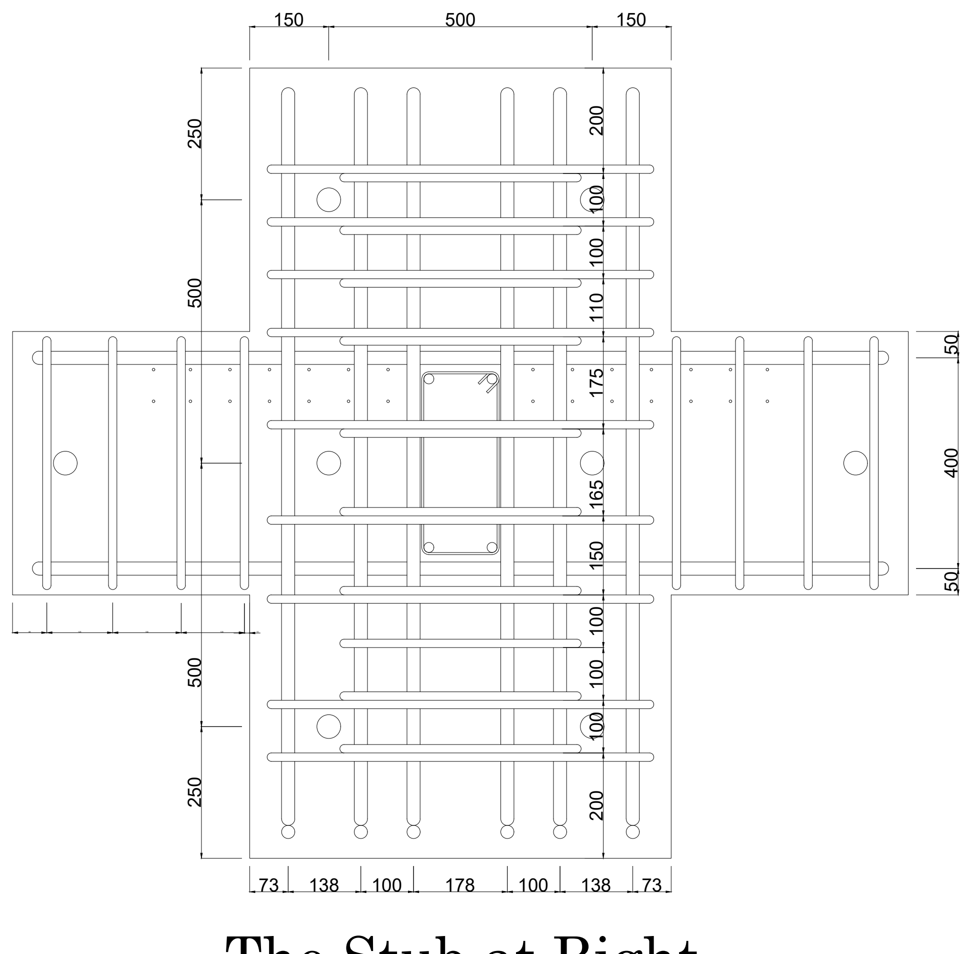

The Stub at Right

Fig(2.5) Dimensions and reinforcement details of SP-S6-Slab K

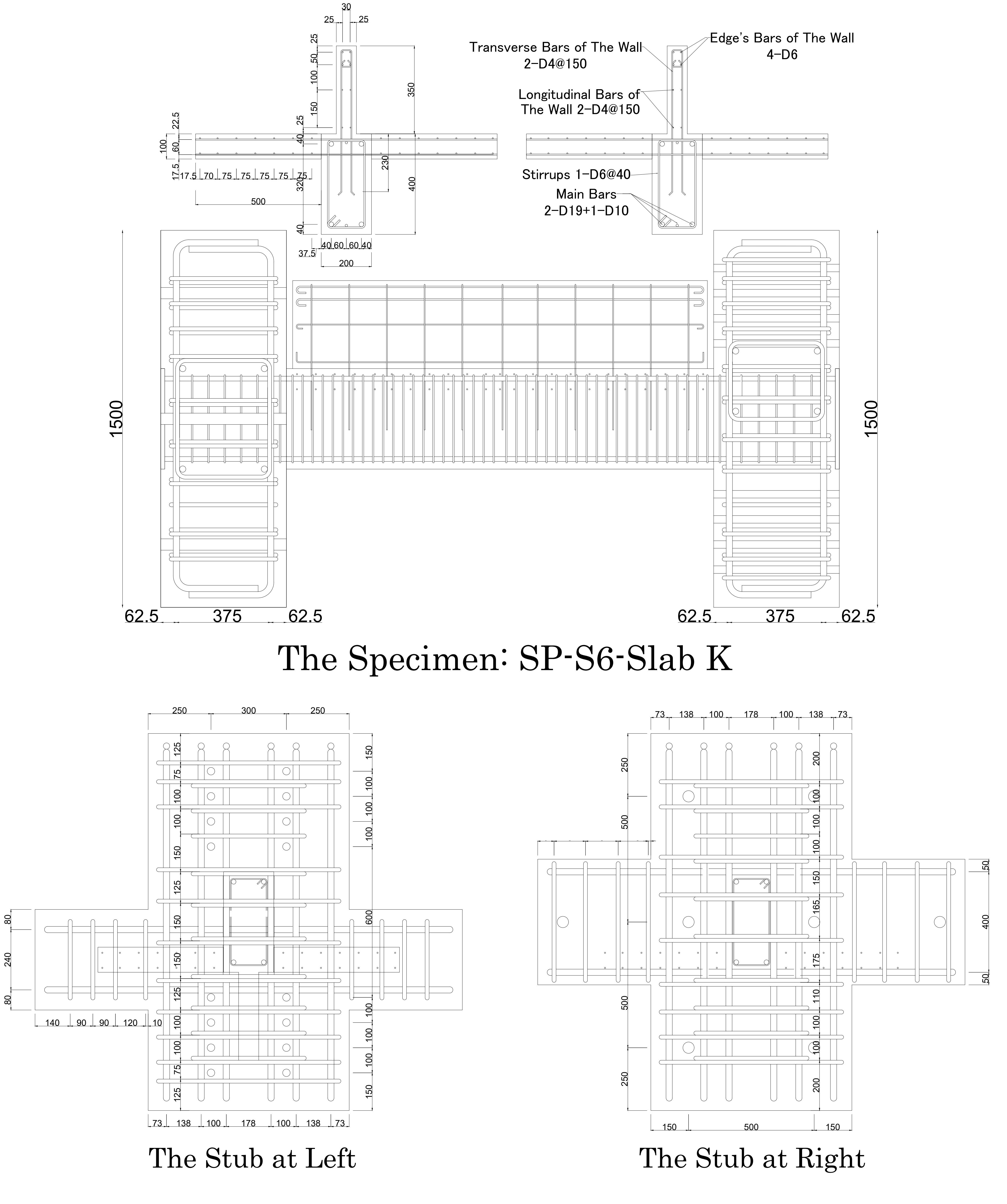

Fig(2.6) Dimensions and reinforcement details of SP-S5-Slab T

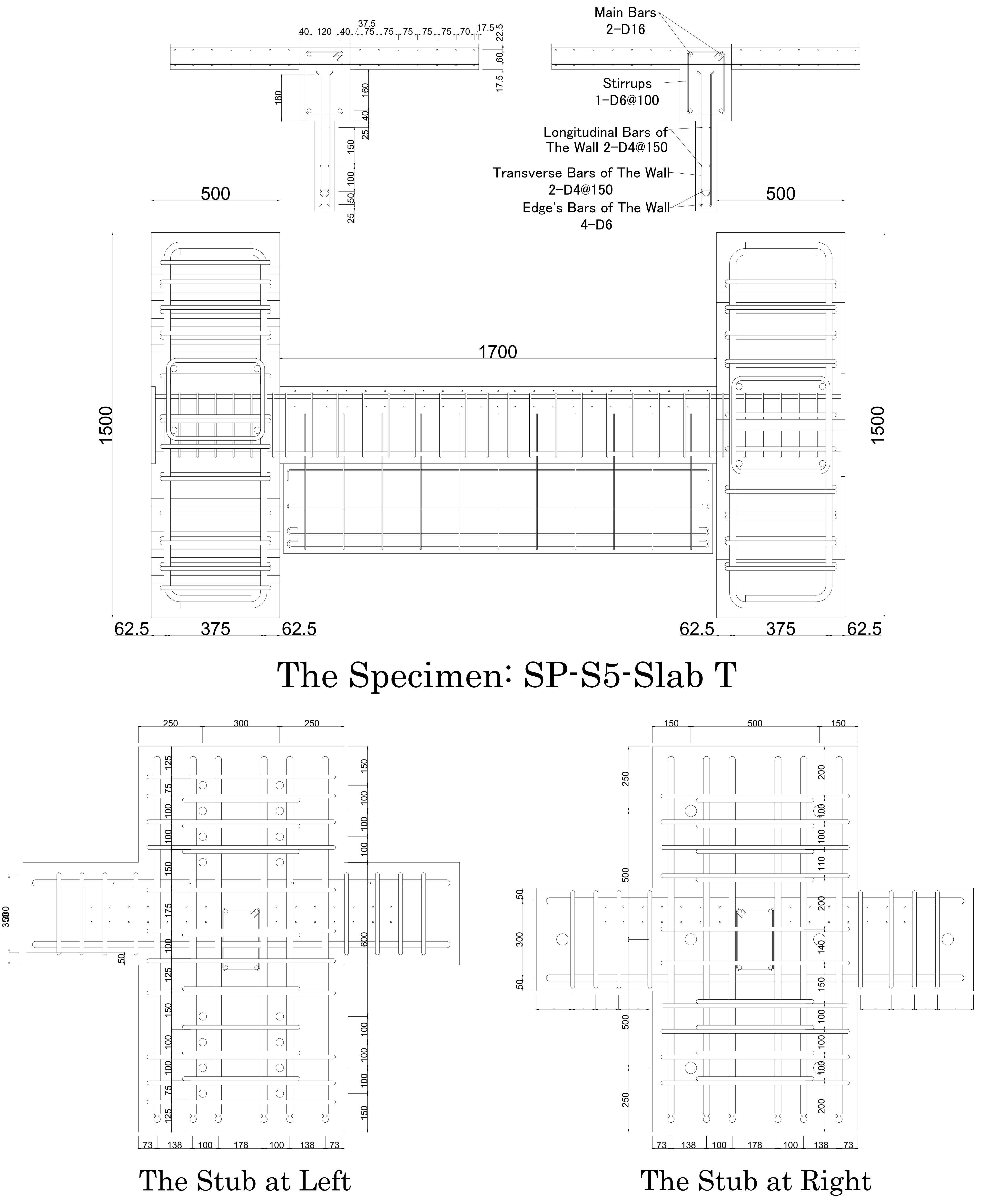

Fig(2.7) Reinforcement details of Slabs

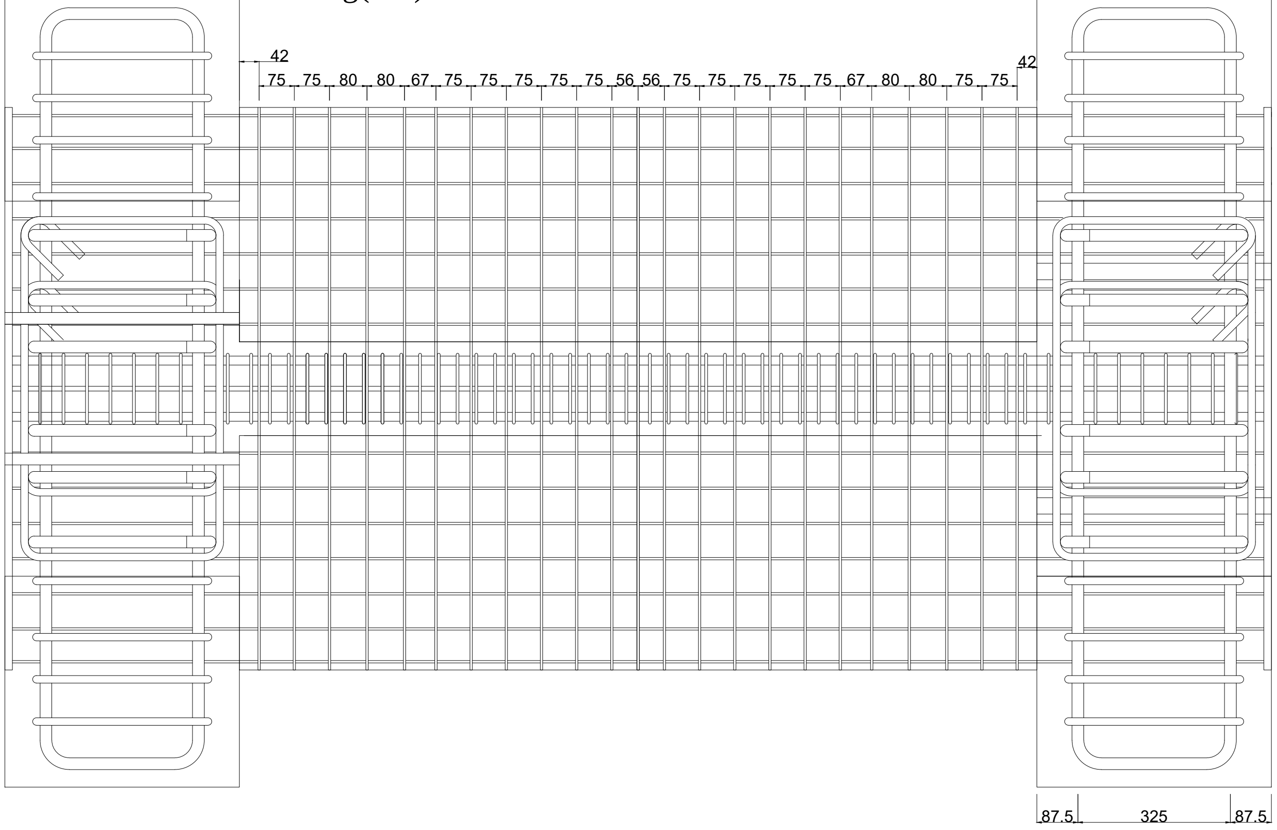

The Slab of Specimen SP-S6-Slab T

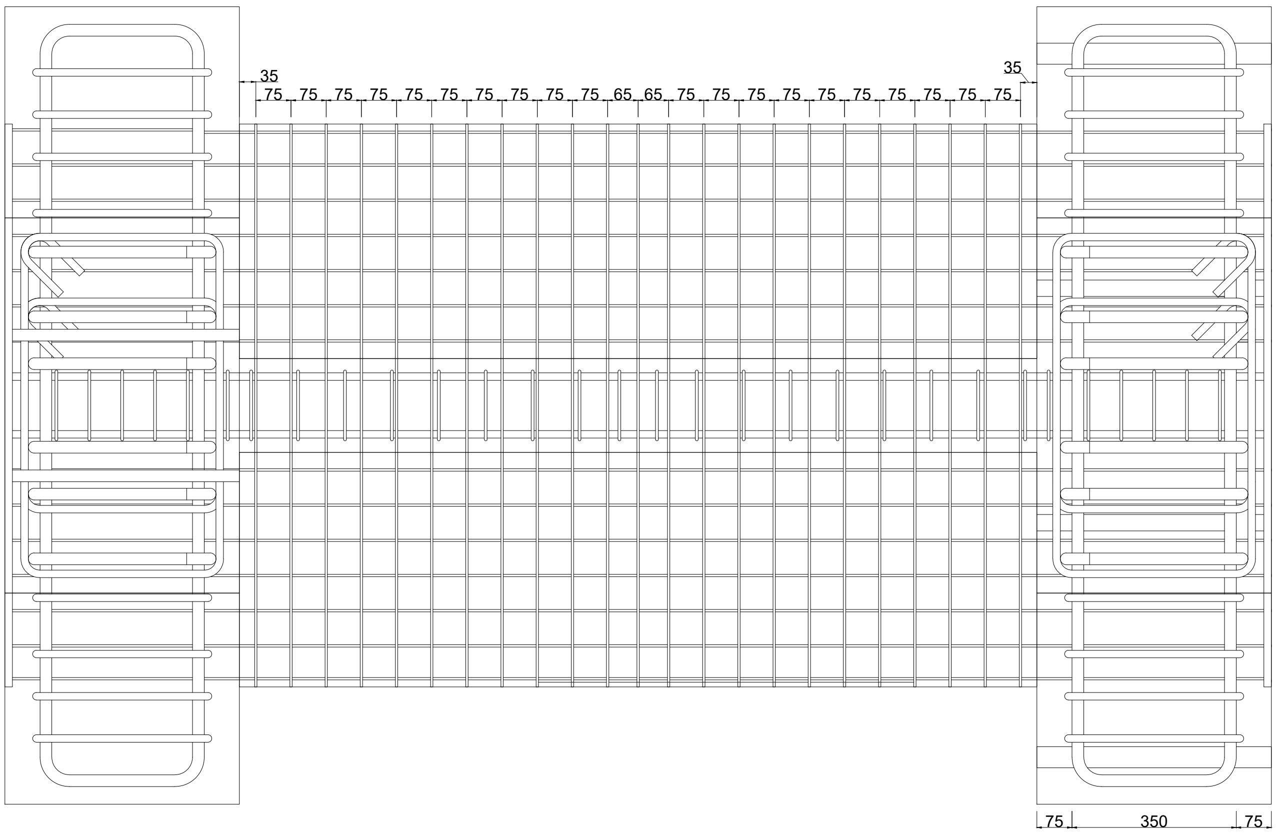

The Slab of Specimen SP-S5-Slab T

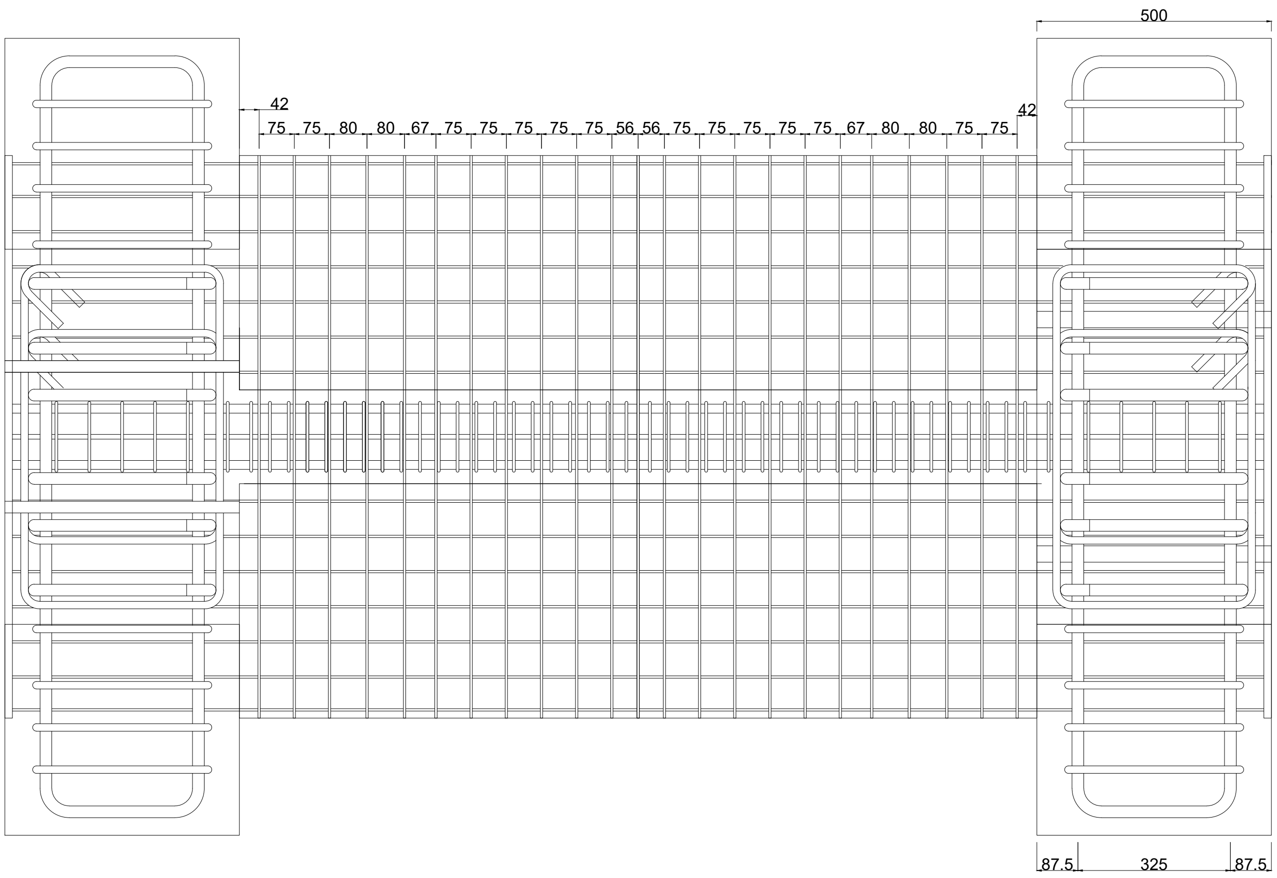

The Slab of Specimen SP-S6-Slab K

2.2 Estimation of Hysteresis Characteristics

2.2.1 Initial Stiffness

The initial elastic stiffness K_e was calculated by the following equations (7,14);

$$\frac{1}{K_e} = \frac{1}{K_f} + \frac{1}{K_s} \qquad \text{Eqn.2.2}$$

$$K_f = \frac{12 \cdot E_c \cdot I_e}{l^3} \qquad \text{Eqn.2.3}$$

$$K_s = \frac{G_c \cdot A}{k \cdot l} \qquad \text{Eqn.2.4}$$

$$G_c = \frac{E_c}{2 \cdot (1+v)} \qquad \text{Eqn.2.5}$$

Where:

K_f: Flexural stiffness (*N/mm*),

E_c: Elastic modulus of concrete (*N/mm²*),

I_e: Moment of inertia of un-cracked transformed section (*mm⁴*),

L: Length of beam (*mm*),

K_s: Shear stiffness (*N/mm*),

G_c: Shear modulus of concrete (*N/mm²*),

A: Cross sectional area (mm^2),

k Shape factor for shear deformation (*1.2*), and

v : Poisson's ratio of (*0.20*).

The initial stiffness was calculated using the observed elastic modulus of concrete and the clear span of beam.

2.2.2 Cracking Strength

Cracking moment M_{cr} was calculated on the basis of the observed splitting tensile strength of concrete σcr and the section modulus Ze of the un-cracked transformed section and given by(15):

$$M_{cr} = \sigma_{cr} \cdot Z_e = 0.56 \cdot \sqrt{\sigma_b} \cdot Z_e \qquad \text{Eqn.2.6}$$

And the cracking strength will be calculated:

$$Q_{cr} = 2 \cdot \frac{M_{cr}}{L} = 1.12 \cdot \sqrt{\sigma_b} \cdot Z_e \cdot L^{-1} \qquad \text{Eqn.2.7}$$

Where
σ_{cr}: Cracking tensile strength of concrete (*N/mm²*), and
Z_e: Section shape factor, taking into consideration the rebar of beam.

2.2.3 Yielding Strength

Yielding strength was calculated for rectangular section:

$$Q_y = 2 \cdot \frac{M_y}{L} = \frac{7 \cdot a_t \cdot \sigma_y \cdot d}{2 \cdot L} \qquad \text{Eqn.2.8}$$

Where:
M_y: Flexural moment at yielding (*kN*m)*,
a_t : Rebar sectional area of beam (*mm²*),
σ_y: Yielding strength of rebar (*N/mm²*), and
d : Effective depth of beam, the distance between the center of gravity of the tensile reinforcement and the extreme fiber of compressive zone (*mm*).

2.2.4 Stiffness Decreasing Factor α_y

Member end rotation at flexural yielding has been estimated by empirical stiffness degrading ratio α_y of secant stiffness at yielding to the initial stiffness. This empirical equation (15):

$$\alpha_y = \left\{0.043 + 1.64 \cdot n \cdot P_t + 0.043 \cdot \frac{a}{d}\right\} \cdot \left(\frac{d}{D}\right)^2 \qquad \text{Eqn.2.9}$$

Where:

n : Modular ratio of reinforcement to concrete (*Es/Ec*),

P_t: Tensile reinforcement ratio (*%*),

a/d: Shear span ratio, and

D: Depth of beam (*mm*).

2.3 Ultimate Flexural Strength

The ultimate flexural strength is calculated by the following (15):

$$M_u = 0.9 \cdot a_t \cdot \sigma_y \cdot d \qquad \text{Eqn.2.10}$$

$$Q_u = \frac{2 \cdot M_u}{L}$$

In case of slab, the effect of slab reinforcement was considered.

2.4 Ultimate Shear Strength

The ultimate shear strength is calculated by the following (15):

$$Q_{su} = \left\{ \frac{0.068 \cdot P_t^{0.23} \cdot (\sigma_b + 18)}{\frac{M}{Q \cdot d} + 0.12} + 0.85 \cdot \sqrt{P_w \cdot \sigma_{wy}} \right\} \cdot b \cdot j \qquad \text{Eqn.2.11}$$

Where:

F_c: Compressive strength of concrete (*N/mm²*),

P_w: Shear reinforcement ratio of the beam (*%*),

σ_{wy}: Yield strength of shear reinforcing bars (*N/mm²*),

b: Width of beam (*mm*), and

j: Distance between the centroids of the tension and compression portions, default value is (*7/8 · d*) (*mm*).

Table (2.3) shows the strengths and calculated characteristics of the hysteresis loops to each of studied beams.

Table 2.3 Strengths and characteristics of the hysteresis Q and R loops of studied beams

Beam	SP-S5	SP-S6	SP-S6-AR	SP-S6-Slab T	SP-S6-Slab K	SP-S5-Slab T
K0	27.96	64.86	60.71	123.35	138.52	66.41
Qcr	12.31	23.29	23.08	21.81	23.23	12.47
Qy	58.97	122.49	121.27	42.75	42.35	69.14
αy	0.221	0.226	0.231	0.112	0.111	0.115
Qu	60.66	125.99	124.73	136.82	138.89	71.12
Qsu	78.96	172.81	164.03	167.41	175.02	85.65

CHAPTER 3
MATERIALS PROPERTIES

- Compression Strength of Concrete
- Tensile Strength of Concrete
- Reinforcing Bars

3.1 Compression Strength of Concrete

Compression strength of Concrete is the most important characteristic of the concrete. And it effects on the other strength of concrete; shear and tension which increase by increasing the compression strength of concrete.

Experimentally, the compressive strength is determined by compression test on concrete specimens either cubes or cylinders until ultimate failure.

In the present research, cylinder specimens were used to determine the compressive strength of concrete experimentally according to Japanese standard. And the size of concrete specimens (100x 200) for diameter and height, respectively.

Two strain gauges attached on the cylinder concrete specimen to measure the strains along the loading. Where the compressive loading is increased gradually till the crushing of specimen.

Six concrete specimens were tested for each of studied beams, three were applied to axial loading to measure the compression strength and the others were applied to splitting tension test.

Figure (3.1) shows the illustrations of stress-strain relationship of concrete samples for each of studied beams.

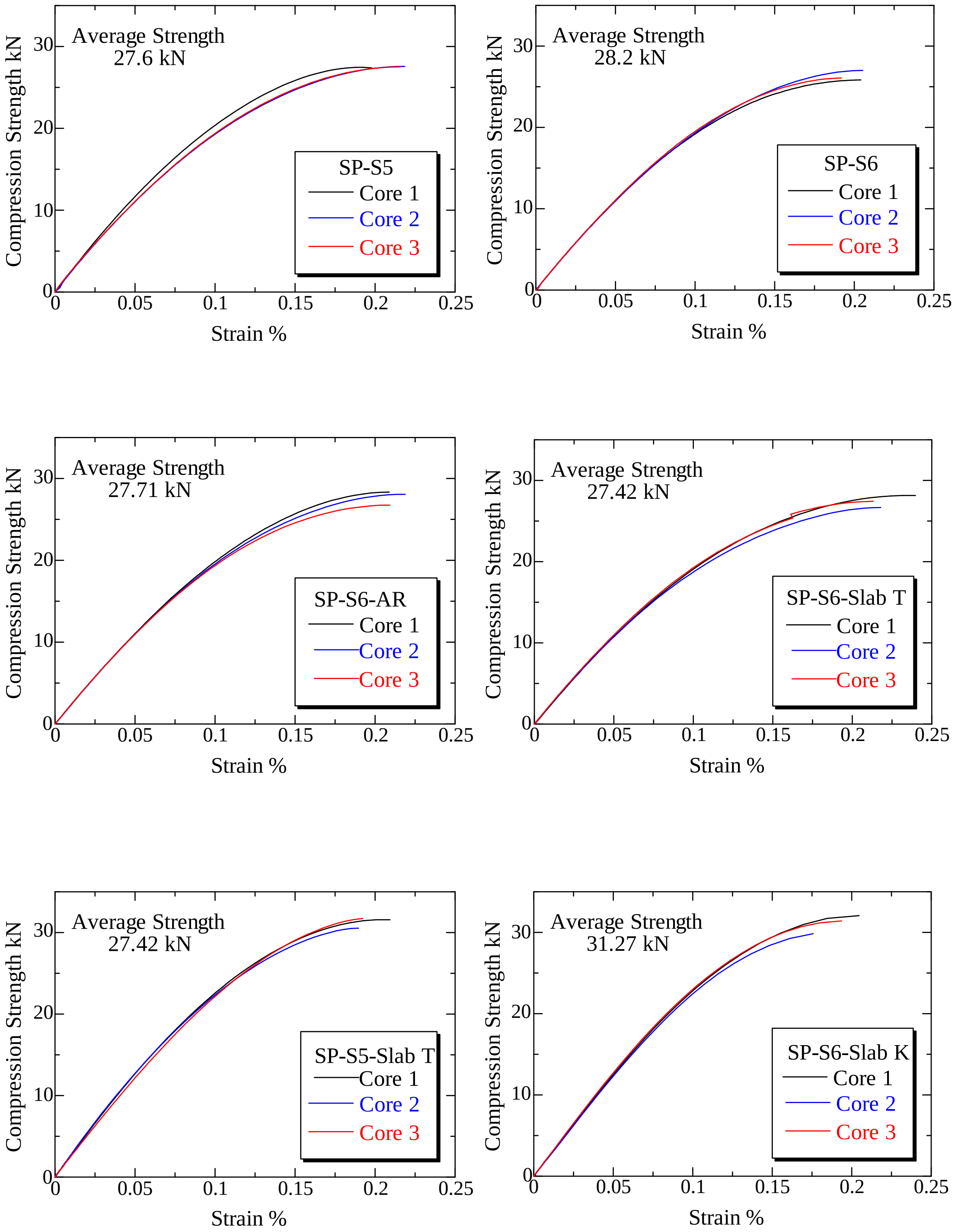

Fig (3.1) Stress-Strain relationship of concrete samples

3.2 Tensile Strength of Concrete

Although the compressive strength of concrete is the most important characteristic, the tensile strength is also important to know the developing of cracks along the loading. Even though, the tensile strength of concrete does not be considered in the design calculations of reinforced concrete structures.

Cracking of concrete occurs due to various reasons; shrinkage and tensile stresses caused by the loading.

Even though the tensile strength of concrete is lower than the compressive strength but it is important to be calculated. The tensile strength of concrete is determined by doing split cylinder test.

In the split cylinder test the concrete specimen size is (200 X 100 mm) where the 100 mm is the diameter and 200 mm is the height.

Figure (3.2) shows the spilt cylinder test.

And the tensile strength of concrete will be calculated by the following:

$$ft = \frac{2 \cdot P}{\pi \cdot D \cdot L} \qquad \text{Eqn.3.1}$$

Where:

P: Compression load at failure (*N*),

L: Length of cylinder (*mm*), and

D: Diameter of cylinder (*mm*).

The modulus of elasticity of concrete is calculated experimentally as the slope of the straight line at one third of compressive stress point.

In addition, the modulus is determined by the following equation (15) with $k_1 = k_2 = 1.0$ and $\gamma = 2.4$.

$$Ec = k_1 \cdot k_2 \cdot 3.35 \cdot 10^4 \cdot \left(\frac{\sigma_B}{60}\right)^{\frac{1}{3}} \cdot \left(\frac{\gamma}{2.4}\right)^2 \qquad \text{Eqn.3.2}$$

Where:

k_1: Factor representing type of coarse aggregates,

k_2: Factor representing kind of mineral admixture, σ_B: Observed compressive strength of concrete (*N/mm²*), and

γ: Unit density of concrete (*ton/m³*).

Table (3.1) shows the experimental mechanical properties of concrete for each of studied beams.

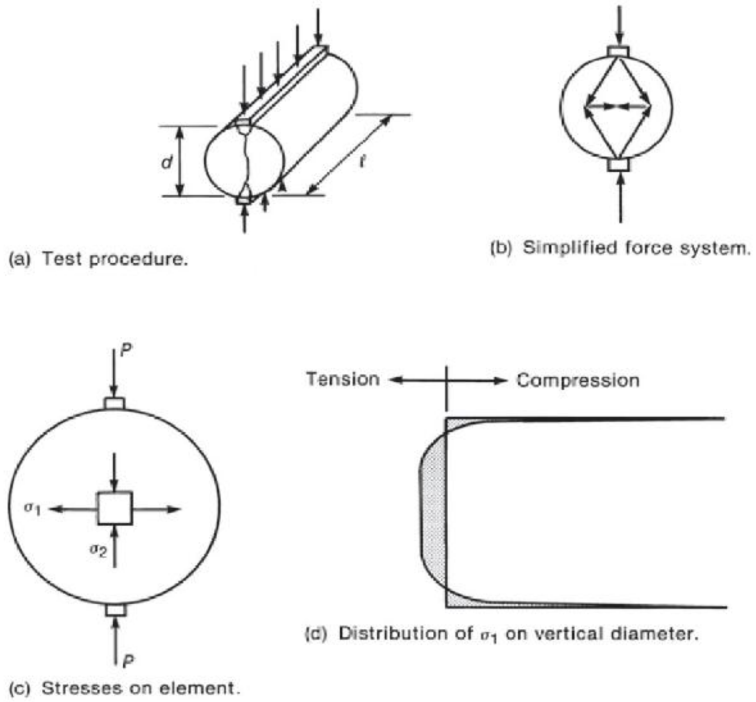

Fig (3.2) Split cylinder test[16]

Table 3.1 Mechanical properties of concrete (*N/mm²*).

Beam	SP-S5	SP-S6	SP-S6-AR	SP-S6-Slab T	SP-S6-Slab K	SP-S5-Slab T
F_C	27.6	28.2	27.71	27.42	31.095	31.27
F_t	2.5	2.39	2.39	2.16	2.40	2.47
Ec_{exp}	23049.0	22577.31	22400	22000	25905.93	25179.94
Ec_{cal}	23750.0	23920.88	23781.52	23698.27	24712.94	24759.21

3.3 Reinforcing Bars

Steel reinforcing bar is embedded in concrete to improve the overall strength of the concrete that surrounds it by providing tensile strength, complementing concrete's excellent compressive properties. Rebar also helps maintain structural integrity as concrete cracks from expansion and contraction cycles. The tensile strength of rebar steel and the tensile rebar-concrete bond strength are extremely important properties of rebar.

Figures (3.3, 3.4.a, 3.4.b, 3.5.a and 3.5.b) show graphically the stress-strain relationship of steel bars samples.

Table (3.2) shows the mechanical properties of reinforcing bars at each stage of research

Table 3.2 Mechanical properties of reinforcing bars

Steel Bar	E_s x 10^5 MPa			Yielding Strength MPa			Yielding Strain %		
	1st	2nd	3rd	1st	2nd	3rd	1st	2nd	3rd
D4	1.86	1.67	1.9	356.4	401.1	375.5	0.425*	0.233	0.380*
D5	-	1.83	1.98	-	372.8	369.3	-	0.417*	0.367*
D6	1.92	1.94	1.61	438.3	364.5	352.3	0.236	0.402*	0.398*
D10	-	1.91	1.75	-	368.2	380.8	-	0.203	0.311
D16	-	-	1.85	-	-	364.3	-	-	0.336
D19	1.96	1.92	1.83	383.9	380.4	390.2	0.209	0.218	0.324

*: 0.2% offset yield point (Proof Stress).

1st: First stage of research: SP-S5 and SP-S6.

2nd: Second stage of research: SP-S6-AR and SP-S6-Slab T.

3rd: Second stage of research: SP-S6-Slab K and SP-S5-Slab T.

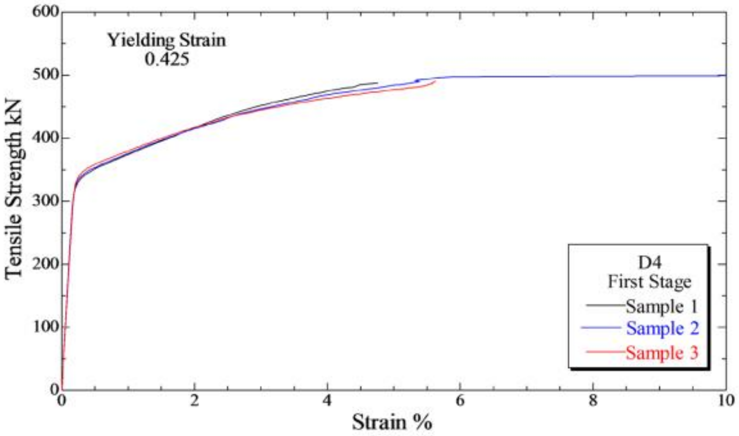

Diameter
D4
Yielding Strength
356.4 MPa
Yielding Strain%
0.425
Modulus of Elasticity
186000 MPa

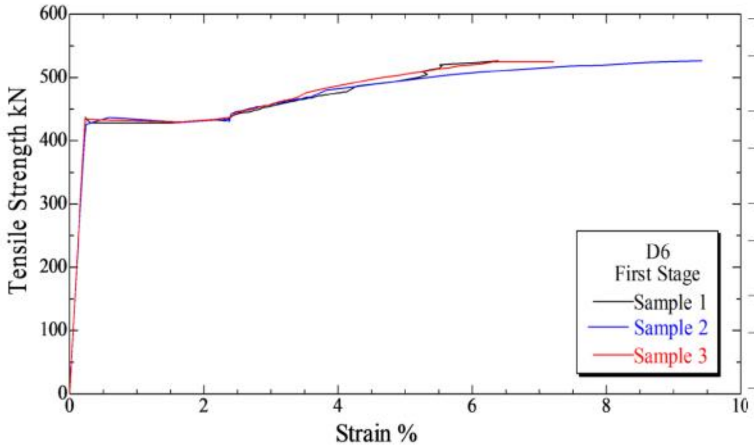

Diameter
D6
Yielding Strength
438.3 MPa
Yielding Strain%
0.236
Modulus of Elasticity
192000 MPa

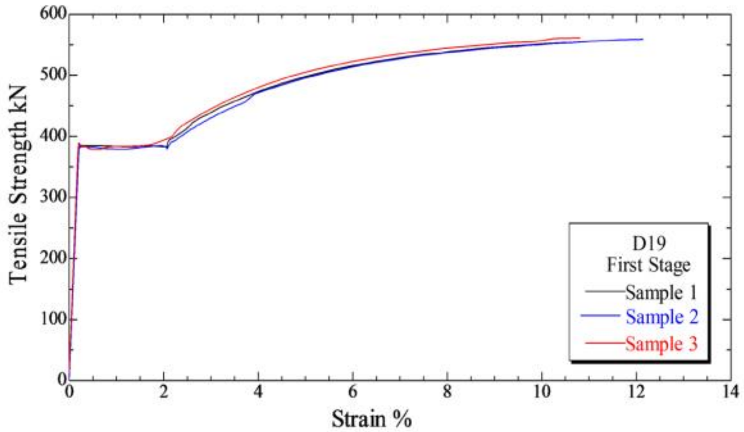

Diameter
D19
Yielding Strength
383.9 MPa
Yielding Strain%
0.209
Modulus of Elasticity
196000 MPa

Fig(3.3) Stress-Strain relationship of reinforcing bars for first stage of research

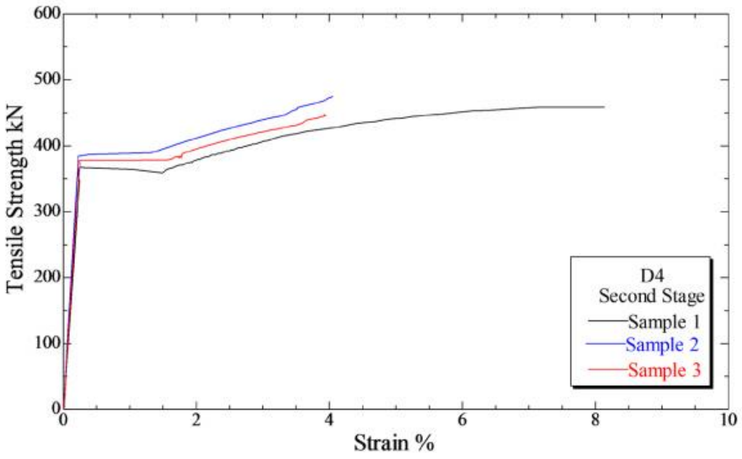

Diameter
D4
Yielding Strength
401.1 MPa
Yielding Strain%
0.233
Modulus of Elasticity
167000 MPa

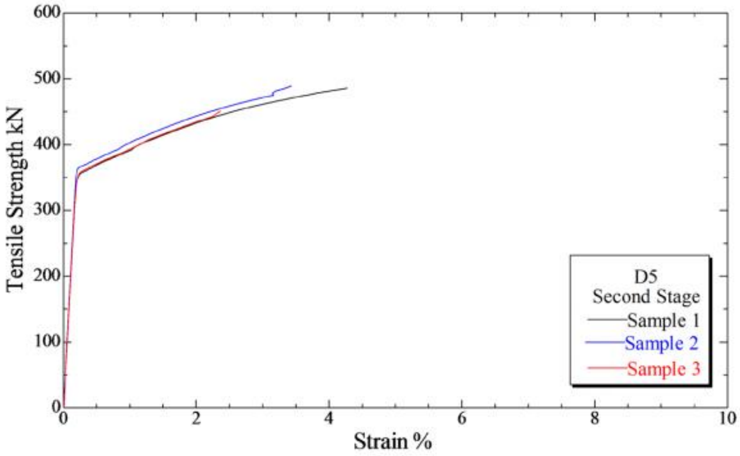

Diameter
D5
Yielding Strength
372.8 MPa
Yielding Strain%
0.417
Modulus of Elasticity
183000 MPa

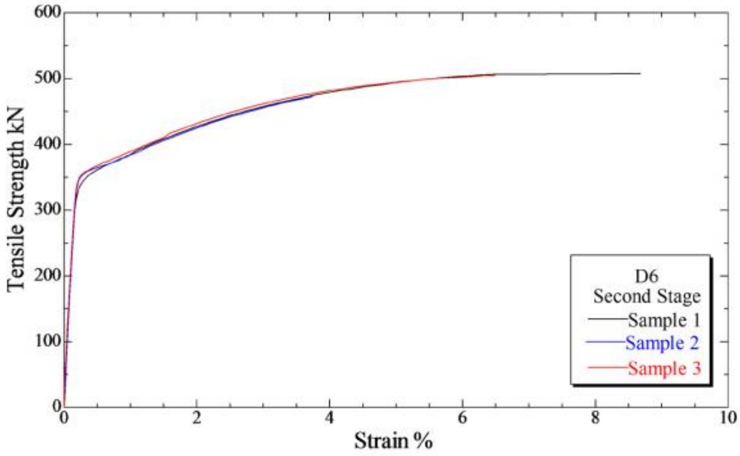

Diameter
D6
Yielding Strength
364.5 MPa
Yielding Strain%
0.402
Modulus of Elasticity
194000 MPa

Fig (3.4.a) Stress-Strain relationship of reinforcing bars for second stage of research

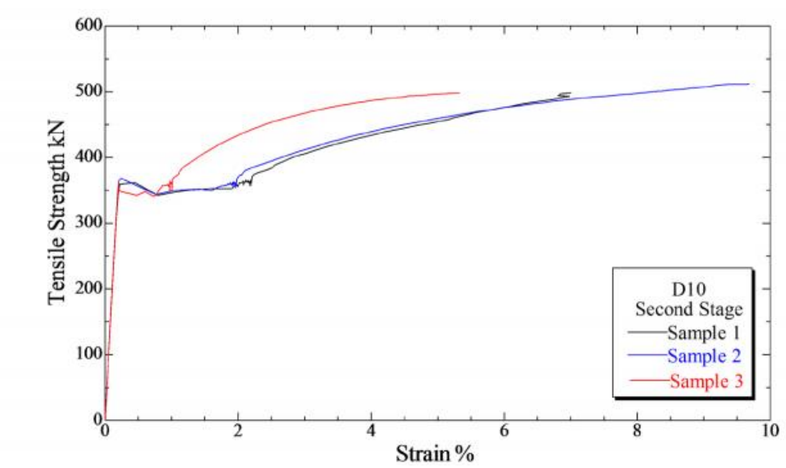

Diameter
D10
Yielding Strength
368.2 MPa
Yielding Strain%
0.203
Modulus of Elasticity
191000 MPa

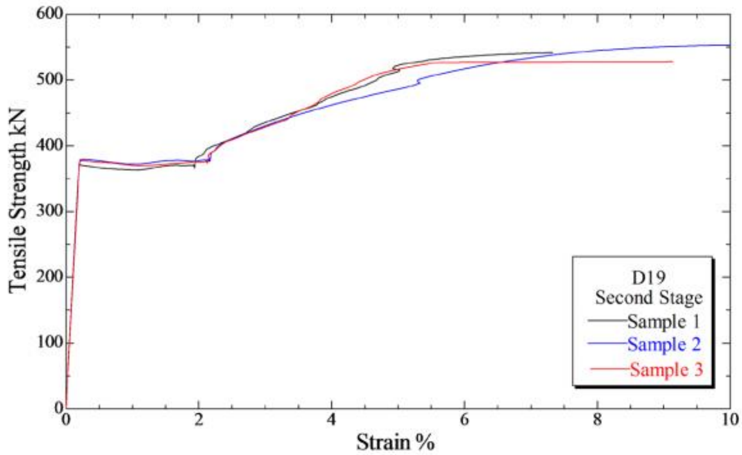

Diameter
D19
Yielding Strength
380.4 MPa
Yielding Strain%
0.218
Modulus of Elasticity
192000 MPa

Fig(3.4.b) Stress-Strain relationship of reinforcing bars for second stage of research

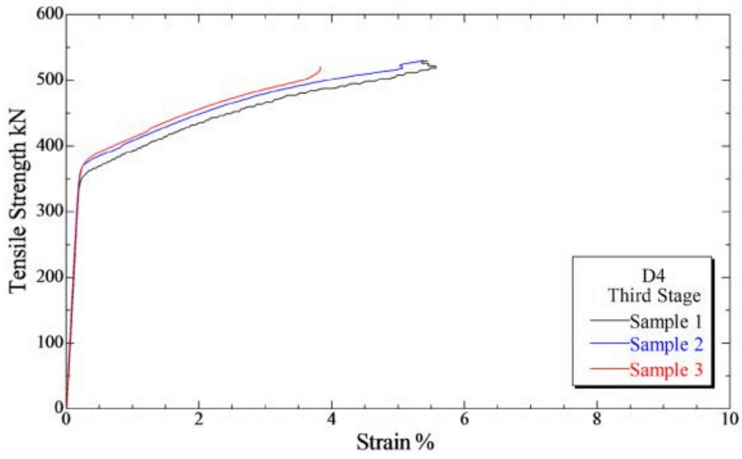

Diameter
D4
Yielding Strength
375.5 MPa
Yielding Strain%
0.380
Modulus of Elasticity
190000 MPa

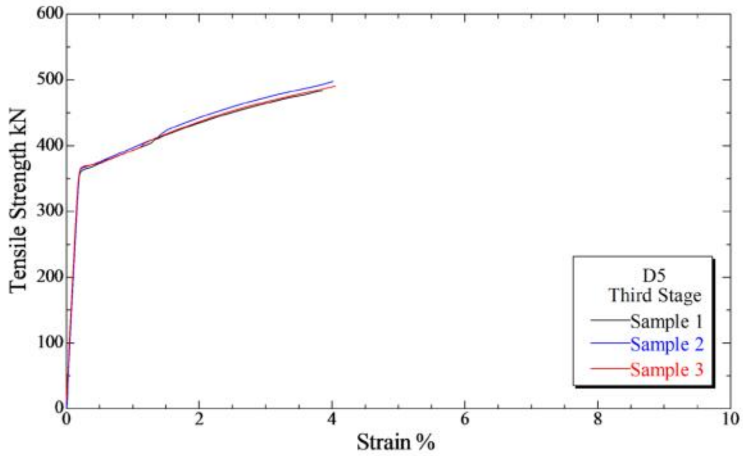

Diameter
D5
Yielding Strength
369.3 MPa
Yielding Strain%
0.367
Modulus of Elasticity
198000 MPa

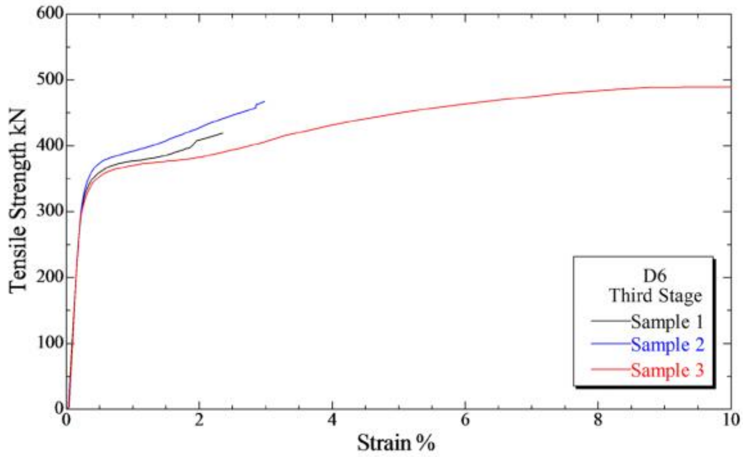

Diameter
D6
Yielding Strength
352.3 MPa
Yielding Strain%
0.398
Modulus of Elasticity
161000 MPa

Fig (3.5.a) Stress-Strain relationship of reinforcing bars for third stage of research

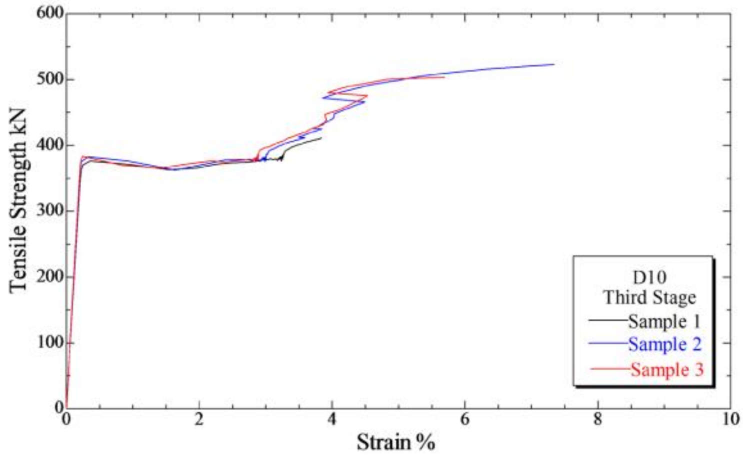

Diameter
D10
Yielding Strength
380.8 MPa
Yielding Strain%
0.311
Modulus of Elasticity
175000 MPa

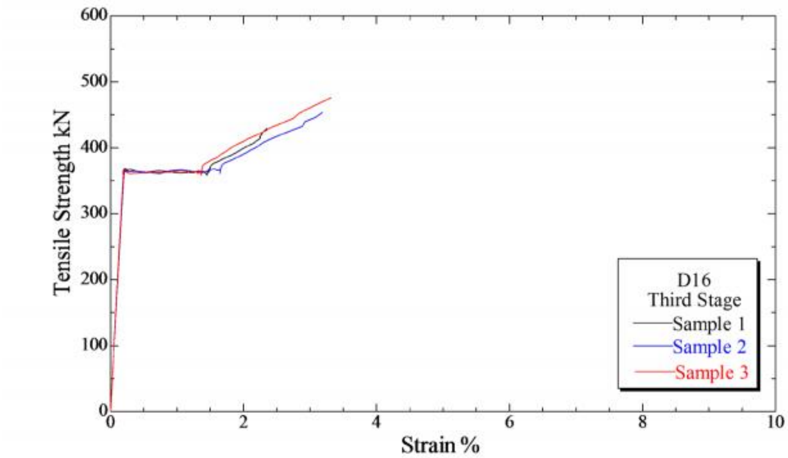

Diameter
D16
Yielding Strength
364.3 MPa
Yielding Strain%
0.336
Modulus of Elasticity
185000 MPa

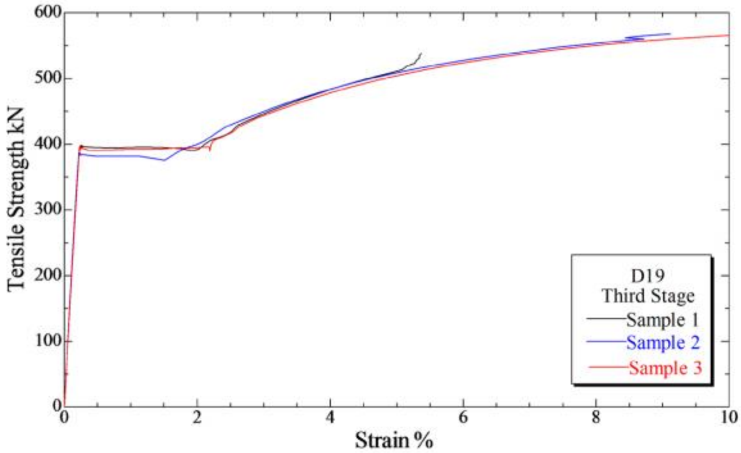

Diameter
D19
Yielding Strength
390.2 MPa
Yielding Strain%
0.324
Modulus of Elasticity
183000 MPa

Fig (3.5.b) Stress-Strain relationship of reinforcing bars for third stage of research

CHAPTER 4

THE EXPERIMENTAL WORK

- Preparation of Specimens
- Loading Apparatus

4.1 Preparing of Specimens

Stages of preparing each of the specimens before the experimental work:

- Adding strain gauges on the reinforcing bars in studied positions to record the hierarchy of strains of reinforcing bars.
- Drawing lines on the body of beam, wall and slab in the positions of reinforcing bars.
- Fixing displacement gauges in certain positions to measure flexural and shear displacement of beam. In addition, to measure the drift angle of specimen.
- Adding displacement transducers to measure the relative displacement between the two ends of beam.
- Two vertical hydraulic jacks were used to keep the upper support, upper stub, horizontal as possible during the loading.
- The lateral displacement was applied by horizontal hydraulic jack.

Figures (4.1) to (4.6) show the position of strain gauges attached on the reinforcing bars.

Figure (4.7) shows the strain transducers fixed on the rare face of beams.

The figures were added from SP-S5 to Sp-S5-Slab T and the last one shows the displacement transducers.

Fig(4.1) Positions of strain gauges attached on reinforcing bars of SP-S5

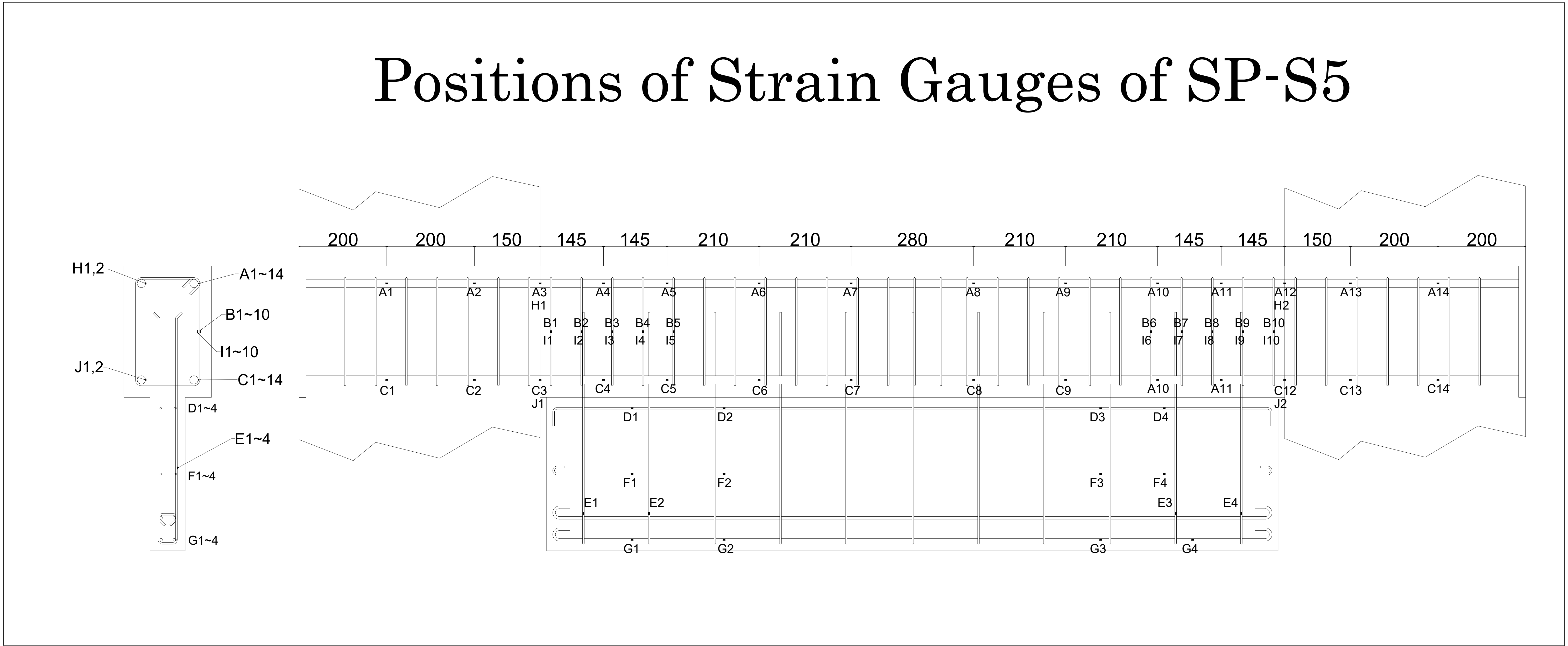

Fig(4.2) Positions of strain gauges attached on reinforcing bars of SP-S6

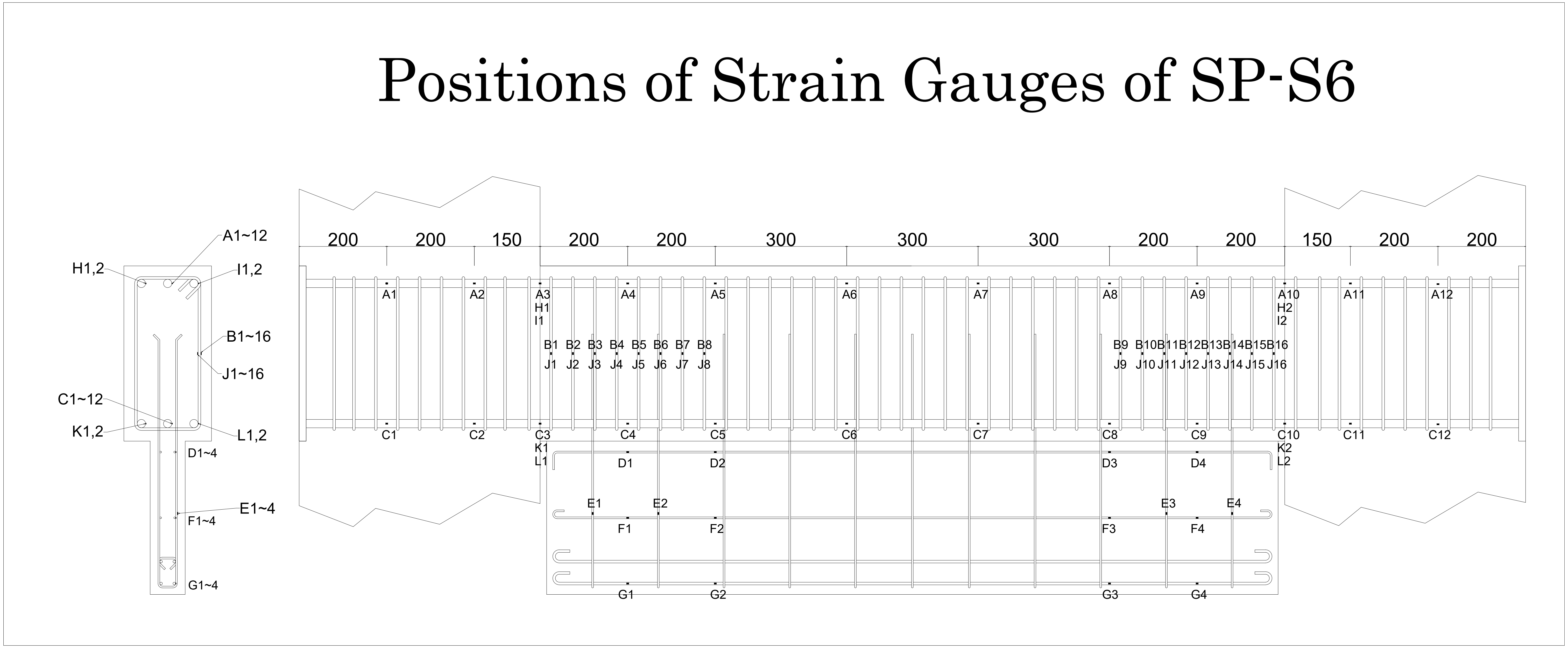

Fig(4.3) Positions of strain gauges attached on reinforcing bars of SP-S6-AR

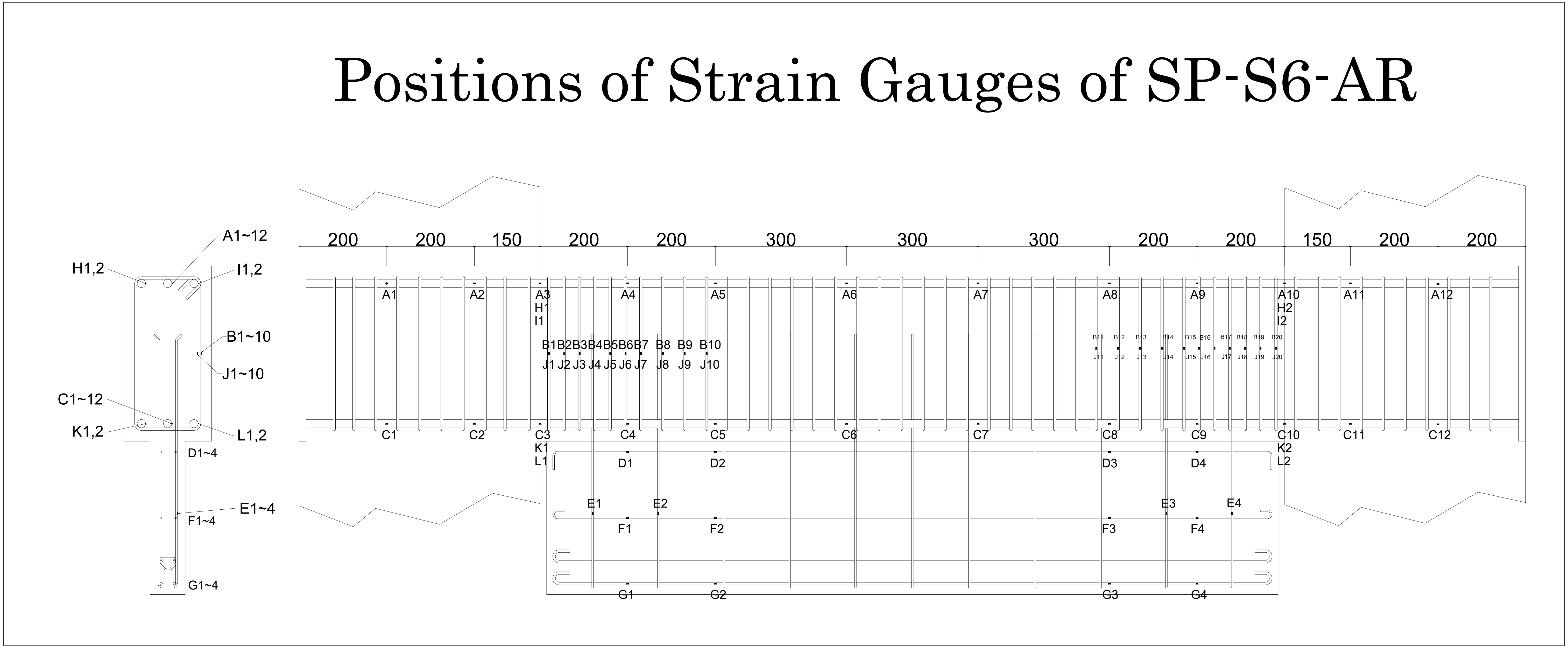

Positions of Strain Gauges of SP-S6-Slab T

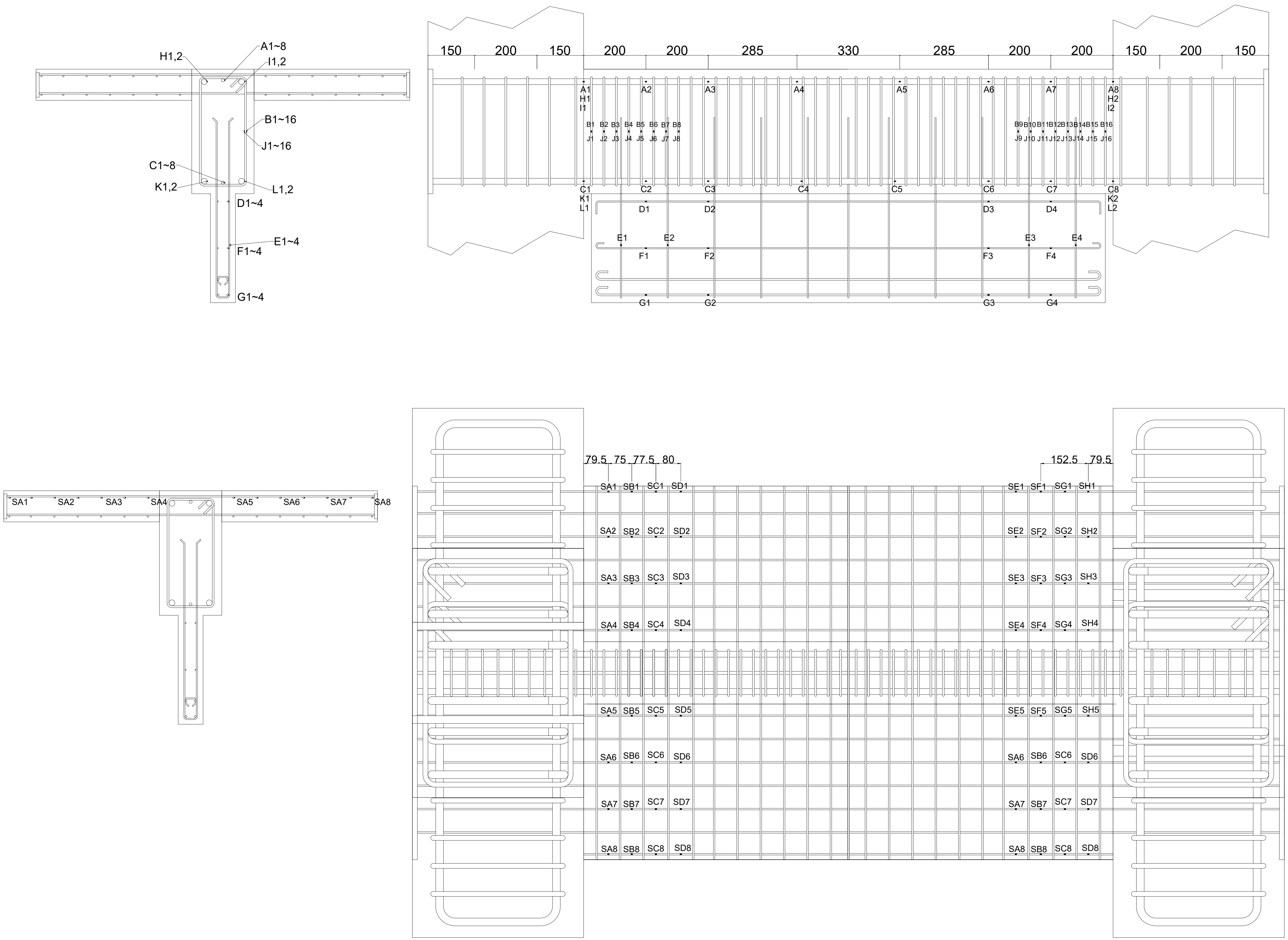

Fig(4.4) Positions of strain gauges attached on reinforcing bars of SP-S6-Slab T

Positions of Strain Gauges of SP-S6-Slab K

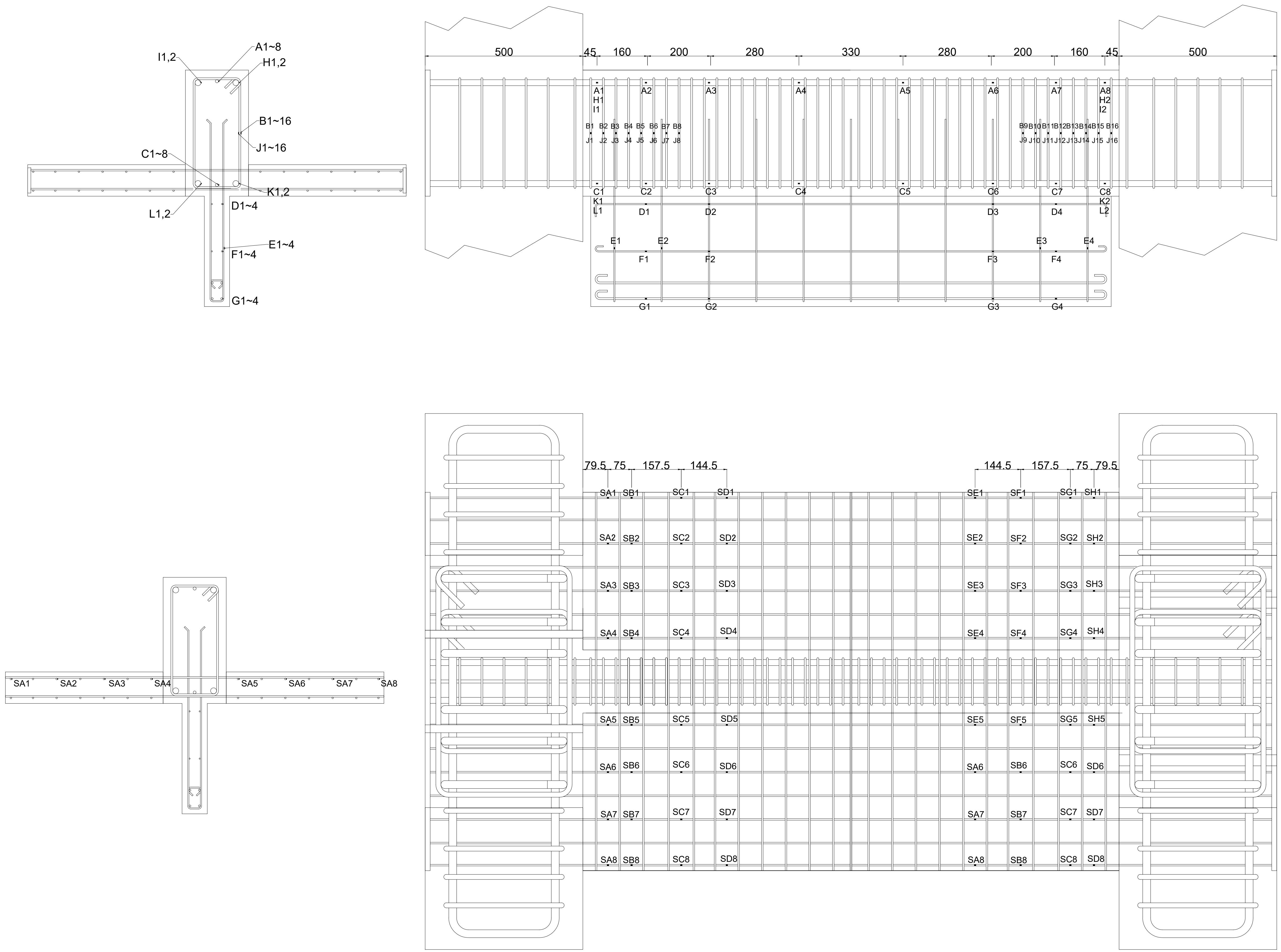

Fig(4.5) Positions of strain gauges attached on reinforcing bars of SP-S6-Slab K

Positions of Strain Gauges of SP-S5-Slab T

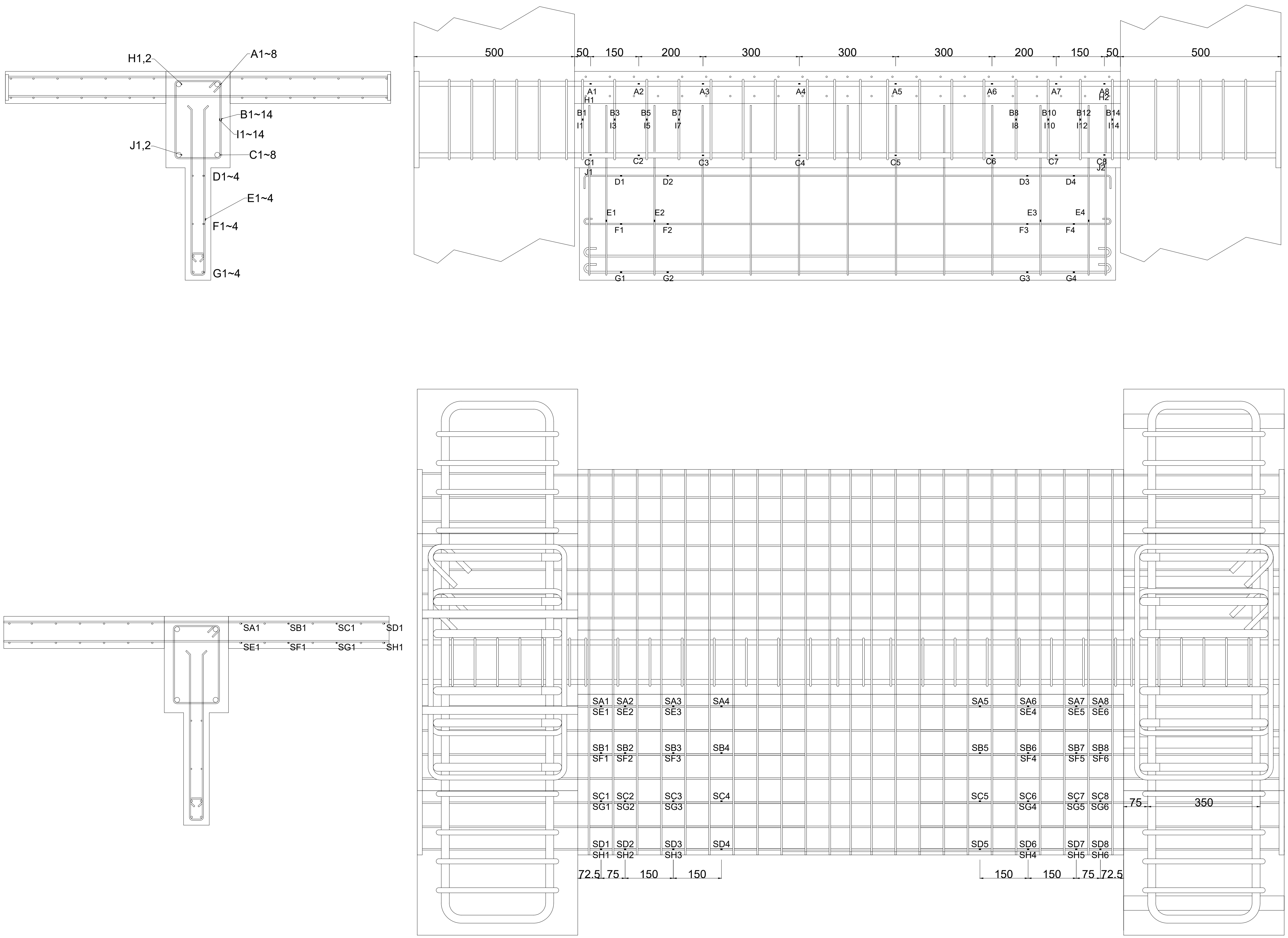

Fig(4.6) Positions of strain gauges attached on reinforcing bars of SP-S5-Slab T

Fig(4.7) Displacement gauges fixed on the rare face of beams

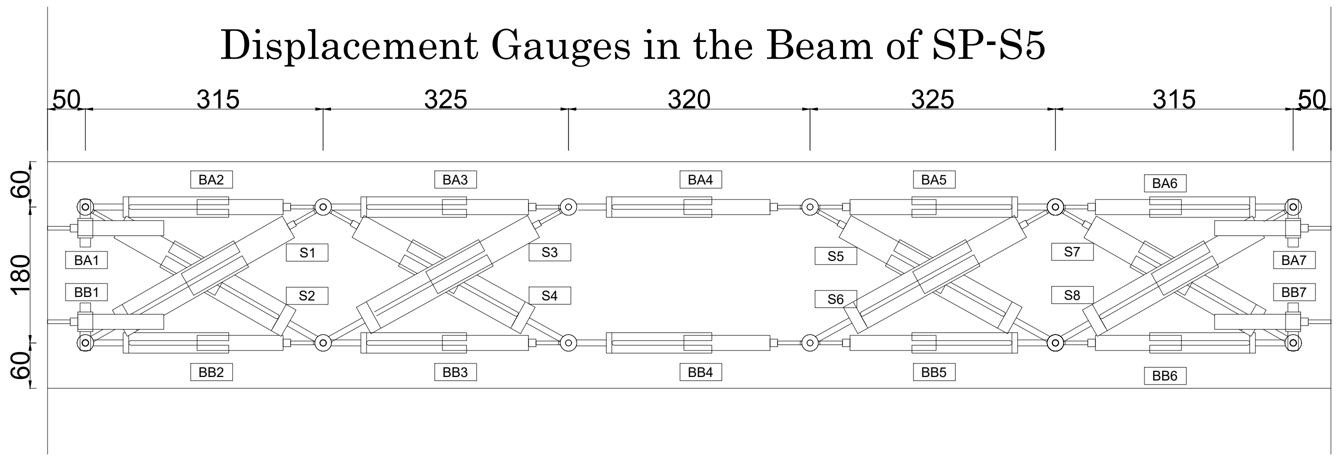

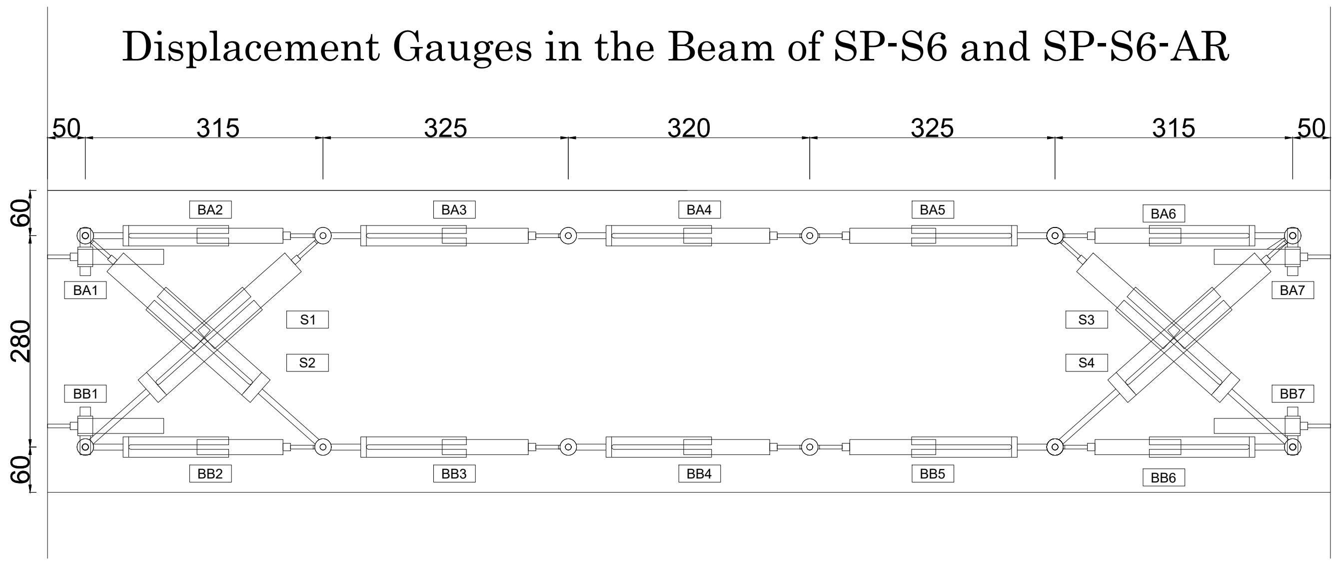

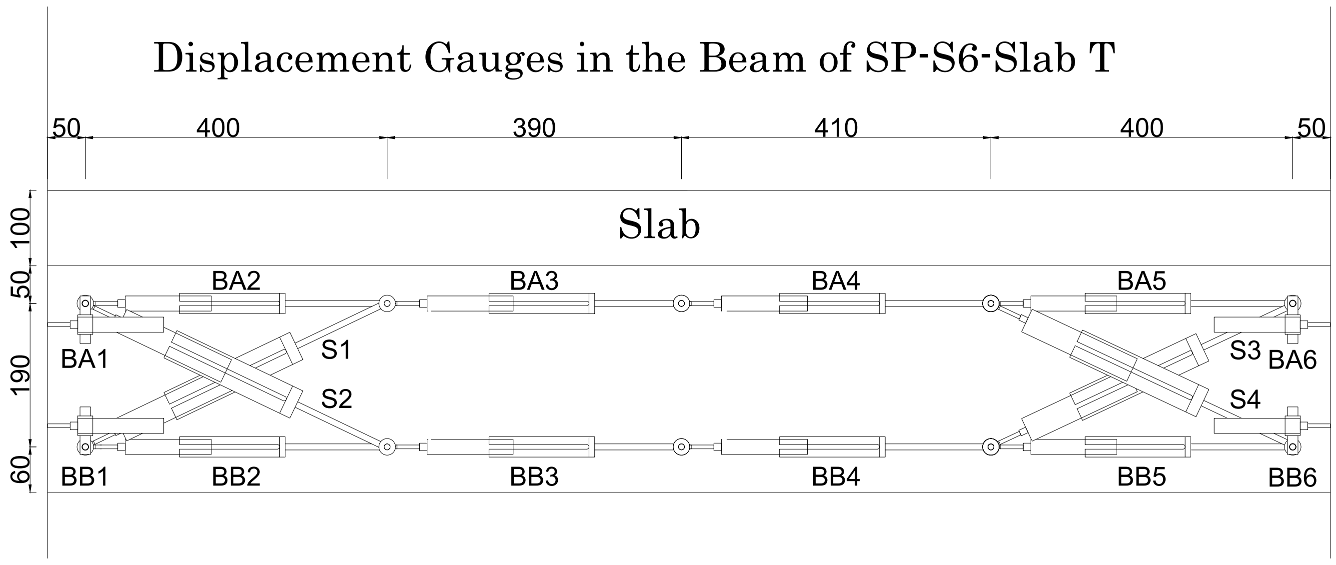

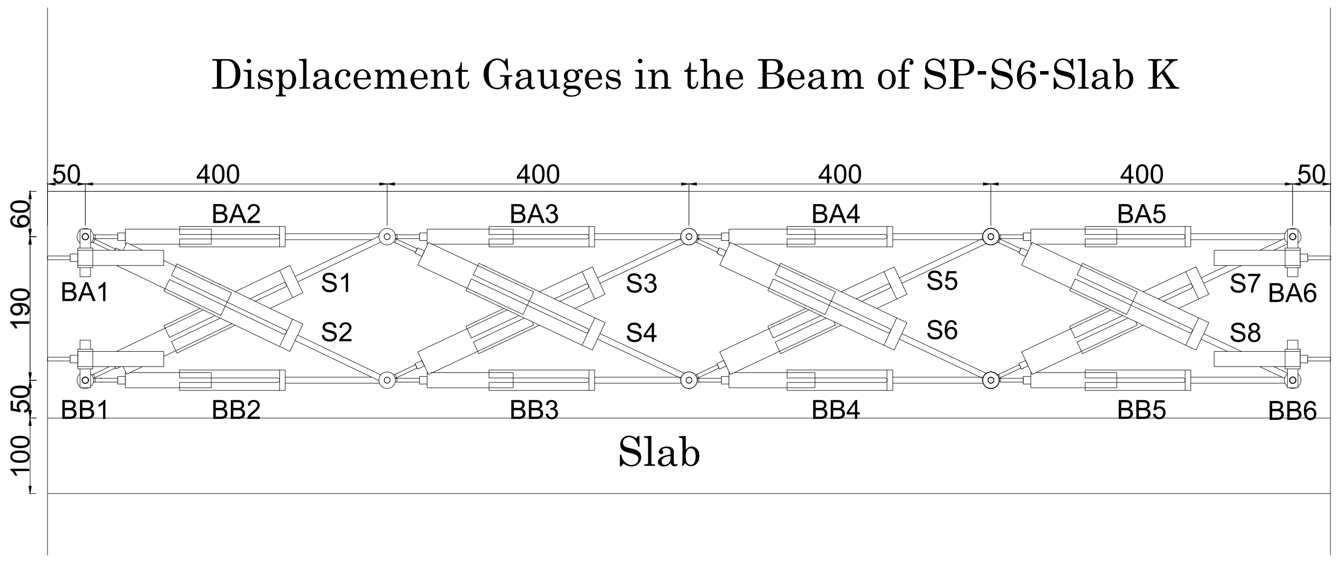

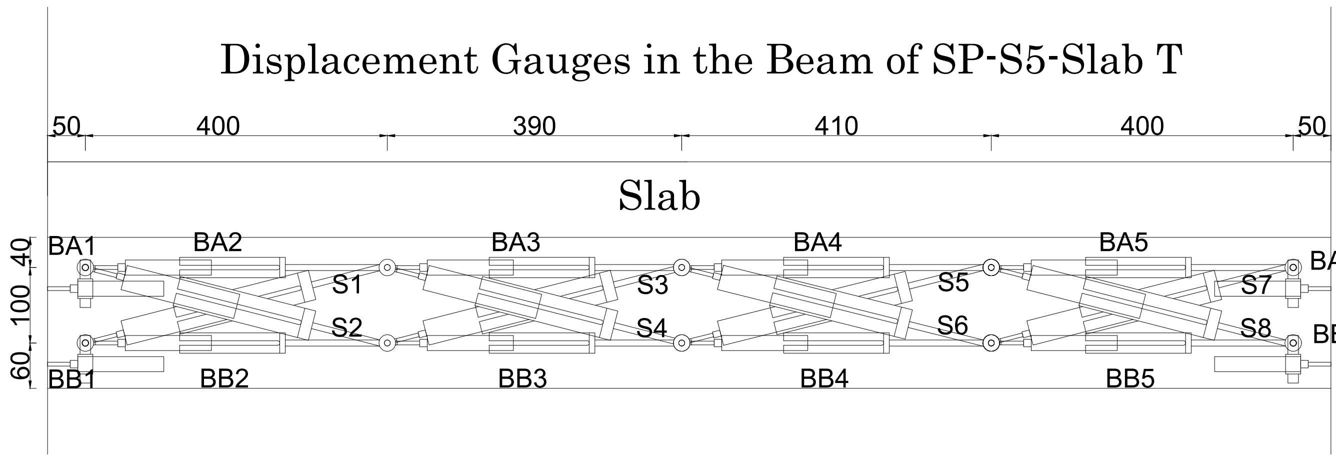

4.2 Loading Apparatus

The loading protocol, as shown in Figure (4.8), consists of the following stages: ± 50%Qcr, ± 100%Qcr once to each stage, ±1/800, ±1/400, ±1/200, ±1/100, ±1/50 twice to each stage, ±1/25 once and finally continuing the loading till failure or reaching the limit of horizontal hydraulic jack.

In case of beams with slabs, ± 100%Qcr, ± 200%Qcr instead of ± 50%Qcr, ± 100%Qcr.

Figure (4.9) shows the loading apparatus used in the experimental works.

Each of the specimens was placed vertically and the lateral displacement was applied horizontally on the upper stub and the stub at bottom was fixed to the ground.

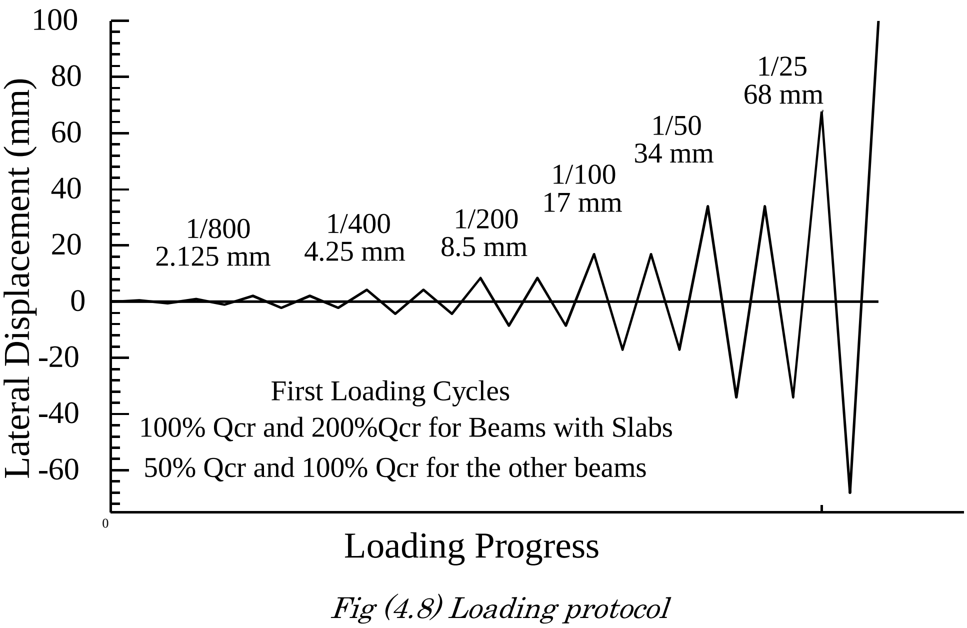

Fig (4.8) Loading protocol

Fig(4.8) Loading apparatus and position of studied beam during experimental work

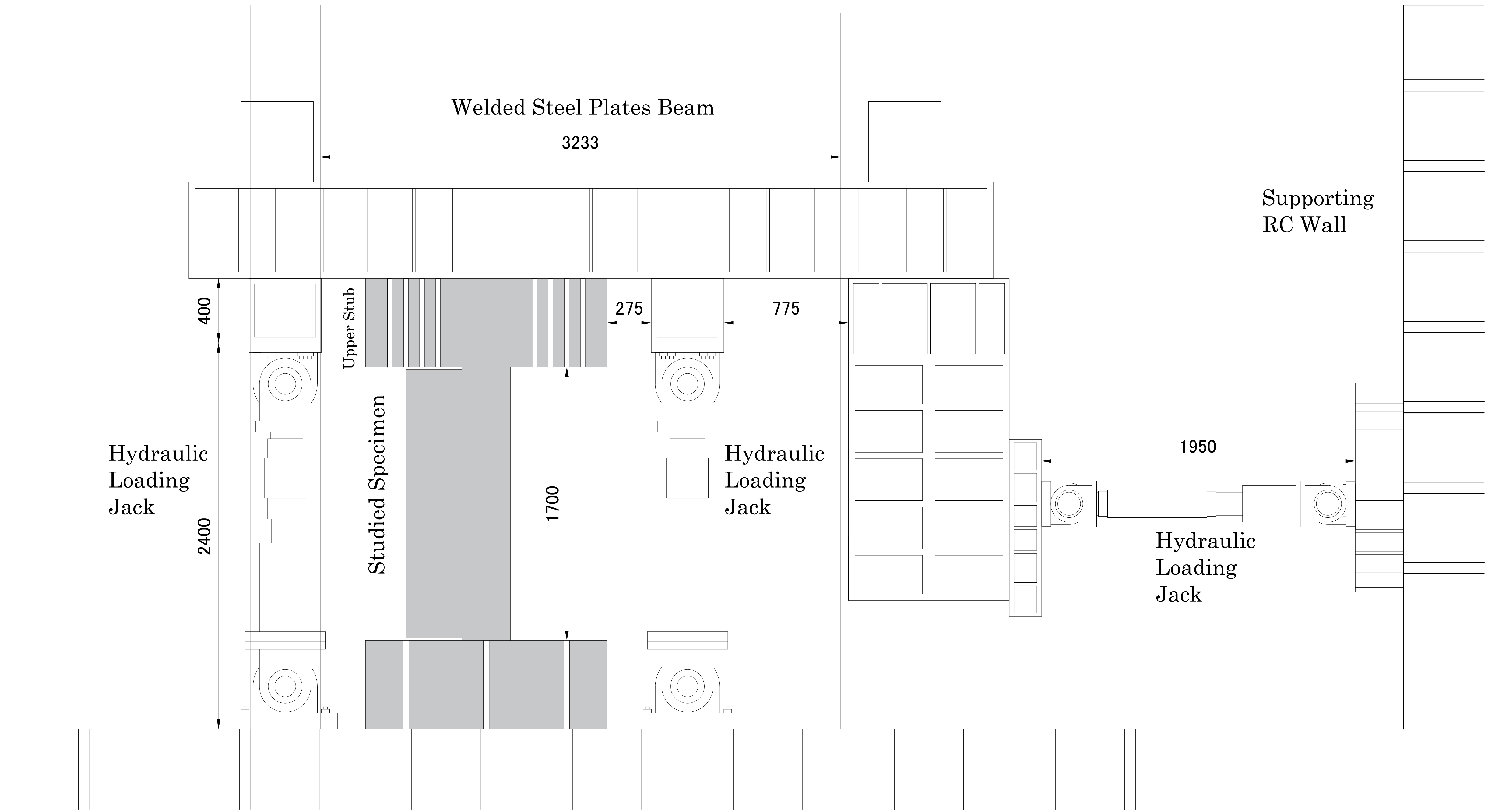

CHAPTER 5
THE EXPERIMENTAL RESULTS

- Failure Features
- The Hysteresis Loops of Shear Force and Drift Angle
- The Strength and Plastic Rotation Angle
- Readings of Reinforcement Strain Gauges
- Flexural and Shear Deformations
- The Dissipation Energy Capacity and the Equivalent Damping Factor.
- Shear Cracks Investigation

5.1 Failure Features

During the experimental work, the cracks were marked on each of the studied specimen after each loading peak.

The cracks patterns are illustrated with blue and red colors for positive loading direction and negative one, respectively.

The illustrations are shown in appendix B.

5.1.1 Failure Features of SP-S5

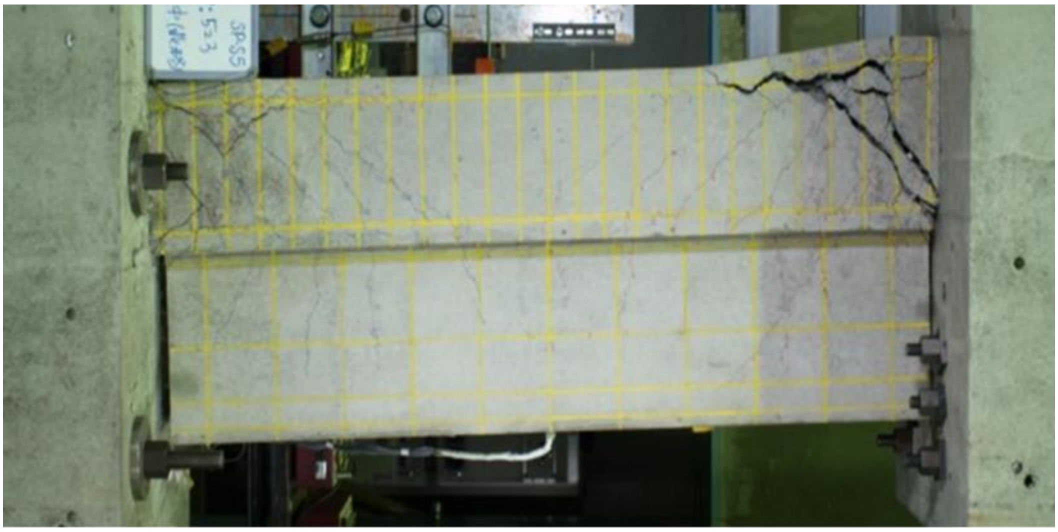

Fig (5.1) Failure features of SP-S5

The most obvious remarks during the experimental work:

- Some shear cracks extended from the beam to the wall from loading cycles of ± 1/200.
- Crushing of concrete occurred with degradation of strength where fracture of stirrup occurred after loading cycle -1/25.
- There was no cracks at the edge of wall, where the cracks crossed the longitudinal bars in wall only.

- Figure (5.2) shows the right part of beam at end of the experimental work. Wide shear cracks extend from the structural gap zone to the face of beam

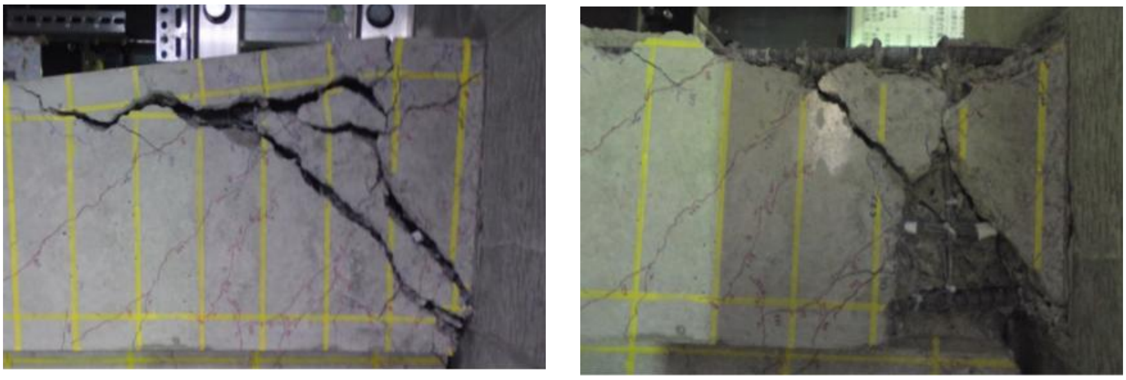

Fig (5.2) Splitting crack, wide shear cracks and crushing of concrete

with splitting crack along the longitudinal bars of beam can be clearly seen. In addition, crushing of the concrete in this part of beam occurred.

- At end of the experimental work and after removing the crushed concrete, one of the stirrups in the right part of beam was cut-off. Figure (5.3) shows the cut-off stirrup and its location which is the third stirrup at right.

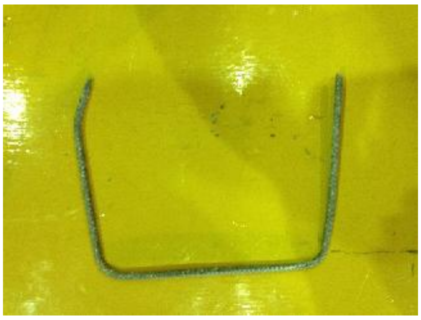

Fig (5.3) The cut-off stirrup and its location

5.1.2 Failure Features of Specimen SP-S6

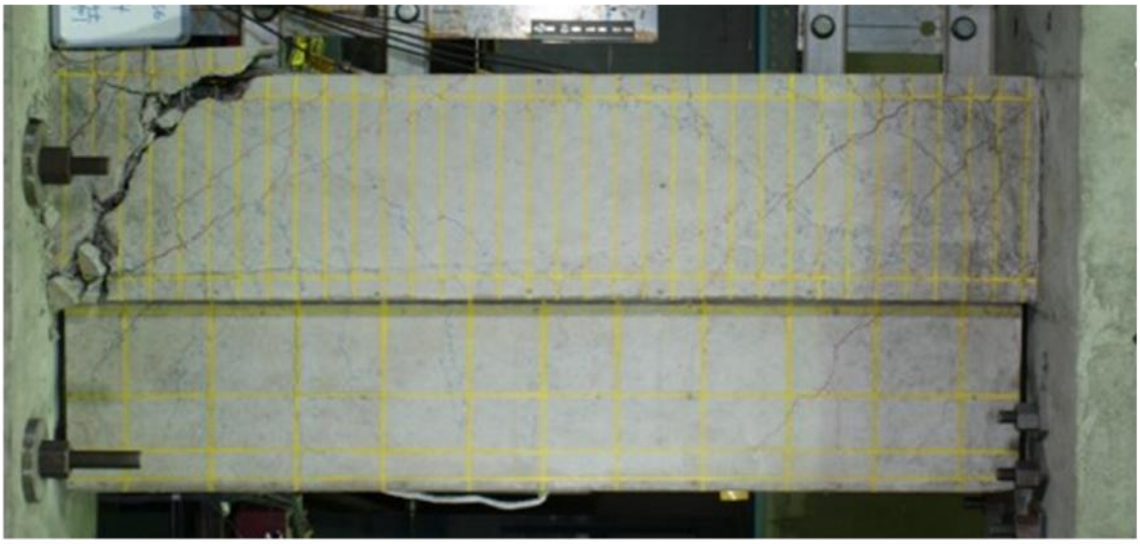

Fig (5.4) Failure features of SP-S6

The most obvious remarks during the experimental work:

- Diagonal cracks occurred obviously from 1/800(1) with extensions to the wall taking into consideration that the flexural cracks occurred in the beam early. Yielding of transverse reinforcement of beam occurred during loading cycle of -1/100(2).
- One of the stirrups left end of beam fractured. Figure (5.5) shows the location which is the third stirrup at left end of beam.
- Crushing of concrete and splitting of concrete cover with sliding between the faces of shear crack at left end of beam occurred as shown in Figure (5.6. a).
- Extended shear cracks in the beam and the wall were remarked at right end of SP-S6 beam, as shown in Figure (5.6. b).

➢

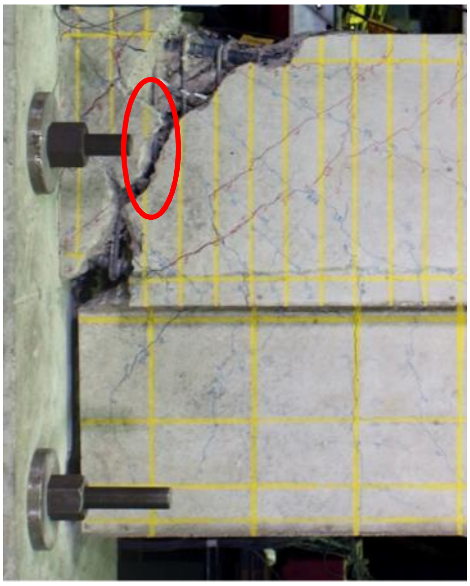

Fig (5.5) Fractured stirrup at left end of SP-S6

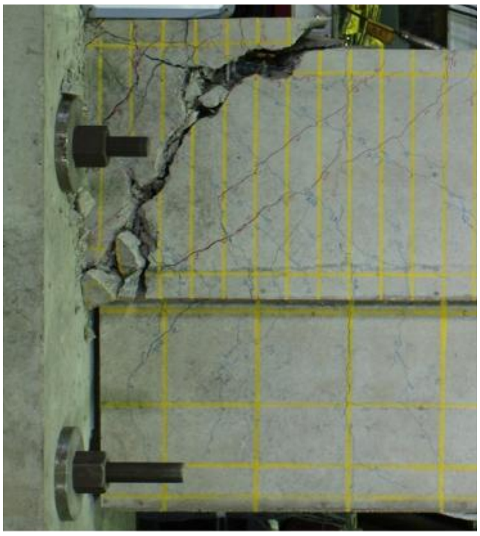

(a) Crushing of concrete and sliding between the faces of shear crack

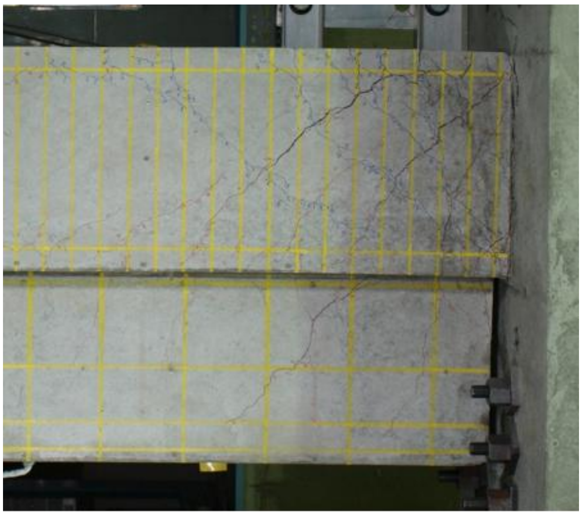

(b) Shear Cracks at right end of specimen

Fig (5.6) Failure features at right and left ends of SP-S6

5.1.3 Failure Features of Specimen SP-S6-AR

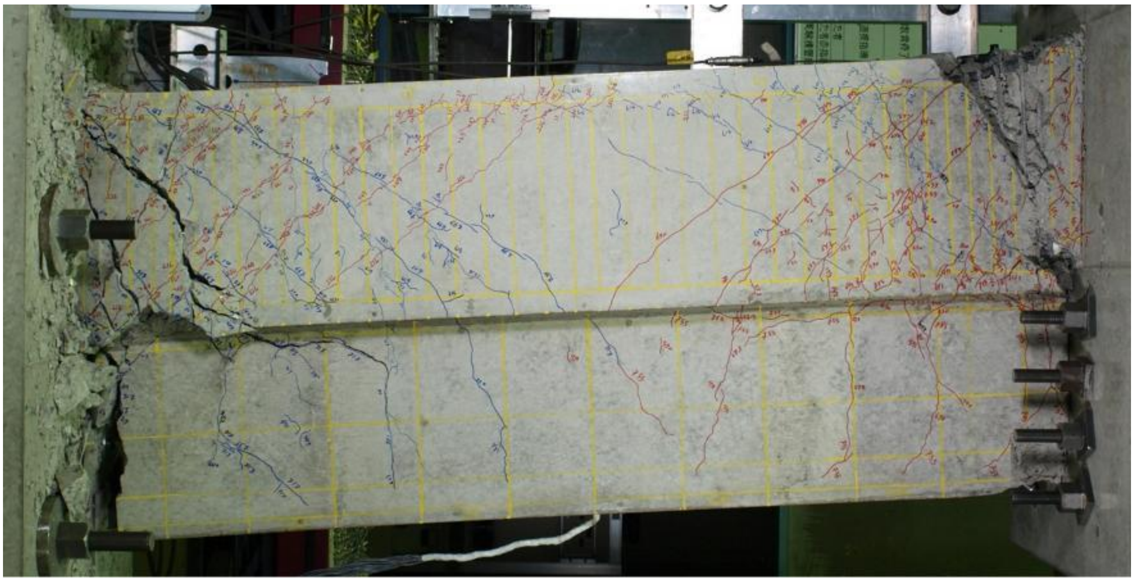

Fig (5.7) Failure features of SP-S6-AR

The most obvious remarks during the experimental work:

- Diagonal cracks formed at ends of specimen at 1/800. From 1/400, more diagonal cracks formed and extended to the wall. Widening of the cracks was remarkable from loading cycle of 1/50 and crushing of concrete at ends of the specimen during the last push-over loading cycle in positive loading direction.
- Some cracks extended to the wall and the length of cracks became larger toward the middle of beam, as shown in Figure (5.8).
- Crushing of concrete occurred at ends of beam as shown in Figure (5.9).
- Touching between the non-structural wall and the support at right occurred as shown in Figure (5.10).
- Sliding between the faces of shear crack at right end of beam occurred before the touching between the non-structural wall and the upper support as shown in Figure (5.11).

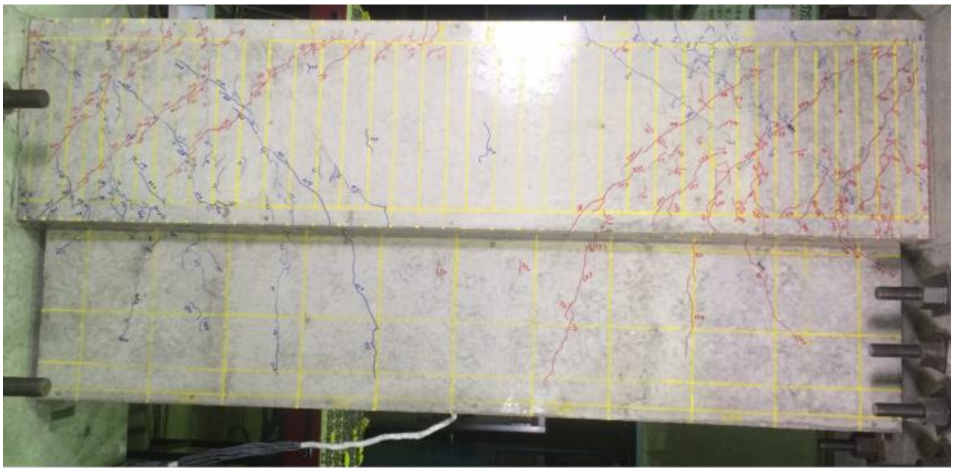

Fig (5.8) Extending the cracks to the wall at loading cycle of 1/100

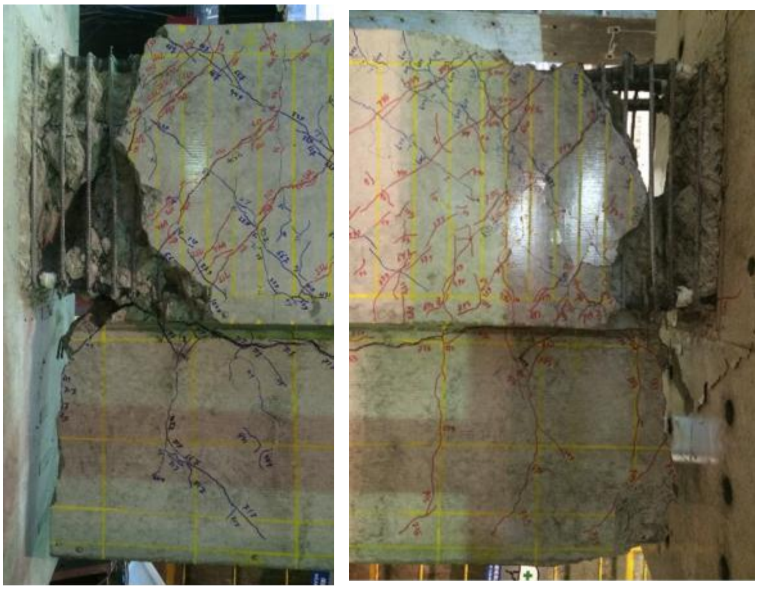

Fig (5.9) Crushing of concrete at right and left ends of SP-S6-AR

Fig (5.10) Touching between the non-structural wall and the support

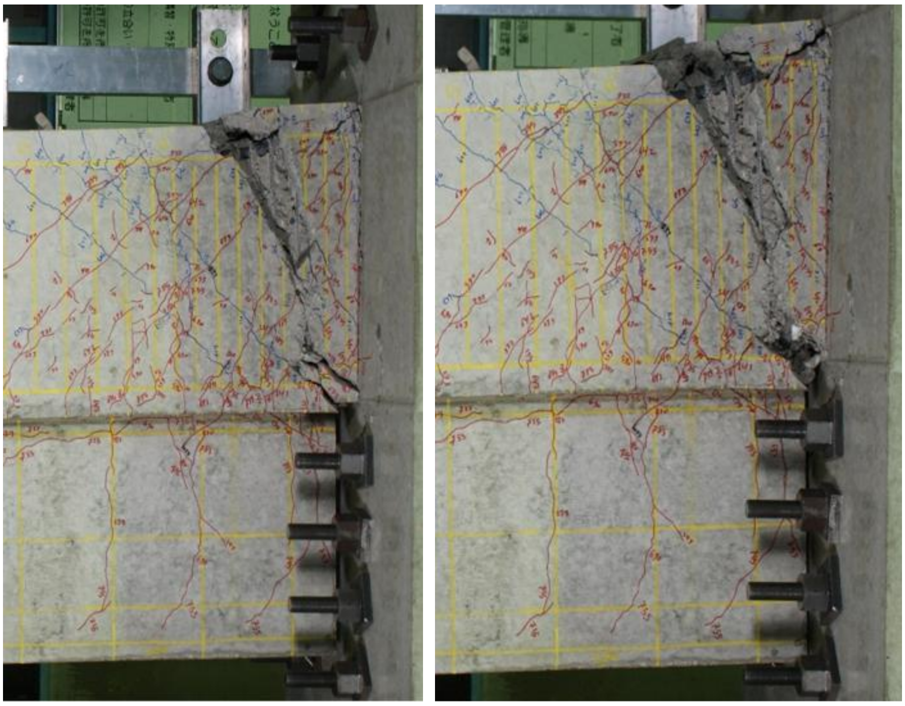

Fig (5.11) Sliding between the faces of shear crack at right end of beam

5.1.4 Failure Features of Specimen SP-S6-Slab T

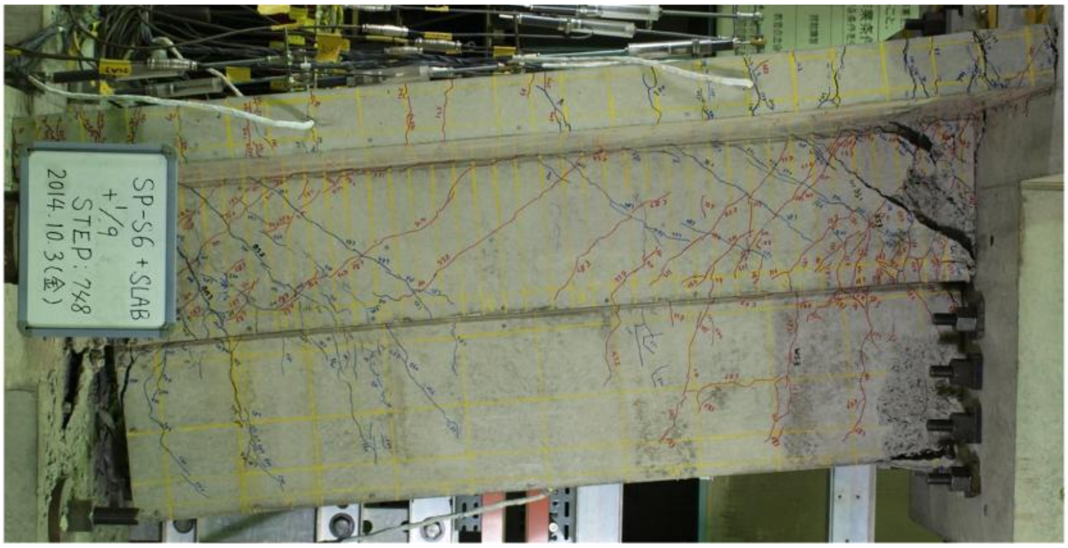

Fig (5.12) Failure features of SP-S6-Slab T

The most obvious remarks during the experimental work:

- Some cracks extended from the slab to the beam body as diagonal cracks as shown in Figure (5.13)
- Crushing of concrete occurred during the last push-over loading cycle as shown in Figure (5.14).

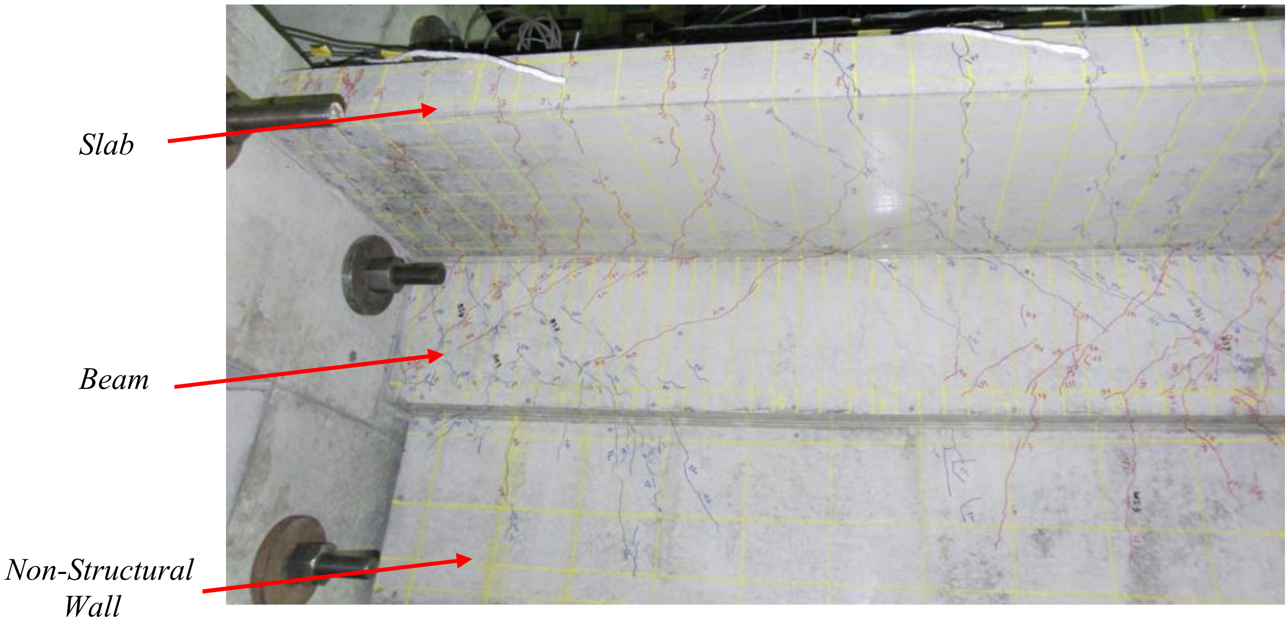

Fig (5.13) Diagonal cracks extended from the slab to beam body

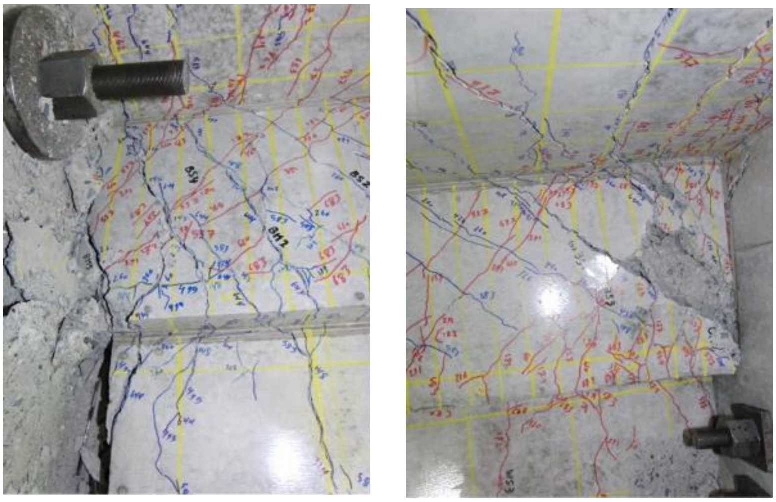

Fig (5.14) Crushing of concrete during last loading cycle

5.1.5 Failure Features of Specimen SP-S6-Slab K

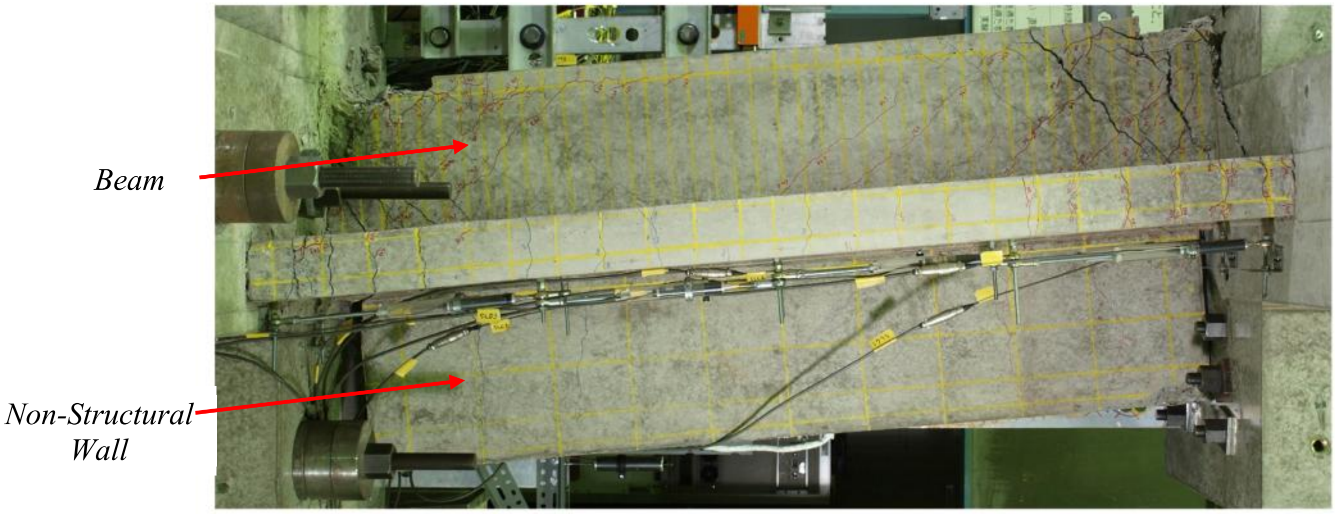

Fig (5.15) Failure features of SP-S6-Slab K

The most obvious remarks during the experimental work:

- Buckling of the longitudinal bars occurred, as shown in Figure (5.16).

Fig (5.16) Buckling of the longitudinal bars of beam

- Wide cracks and crushing of concrete were observed in the slab as shown in Figure (5.17).

Fig (5.17) Wide cracks with crushing of concrete in the slab

- Touching between the non-structural wall and one of the supports occurred. And crushing of concrete was observed at ends of beam as shown in Figure (5.18).

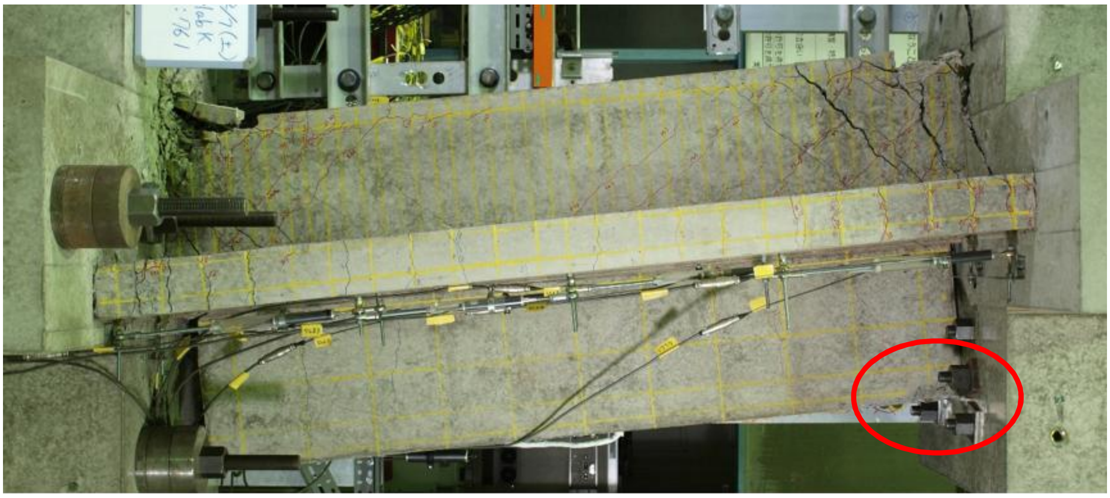

Fig (5.18) Touching between the non-structural wall and one of the supports with crushing of concrete at ends of the beam

5.1.6 Failure Features of Specimen SP-S5-Slab T

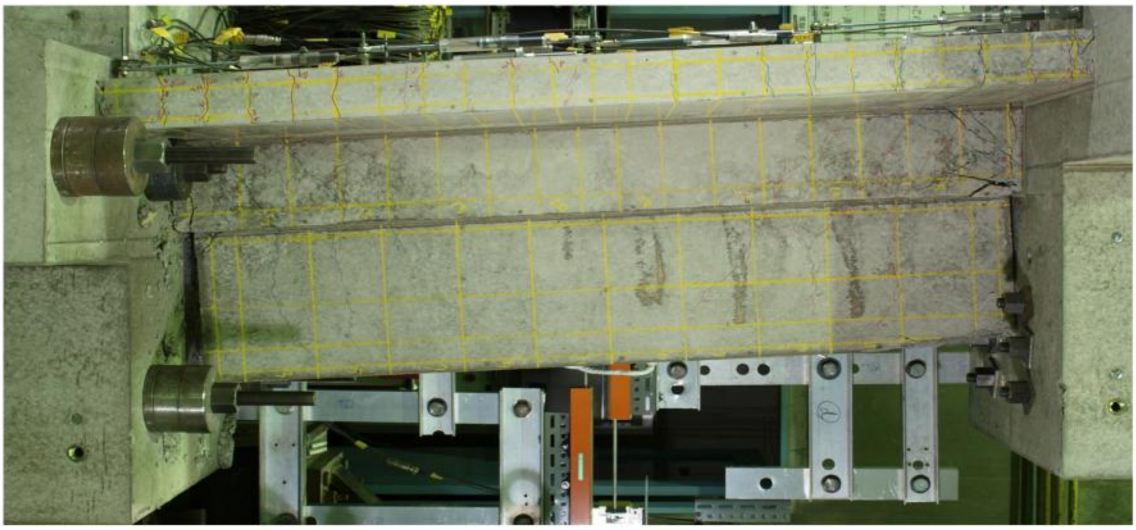

Fig (5.19) Failure features of SP-S5-Slab T

The most obvious remarks during the experimental work:

- Forming of cracks in the slab was obvious from loading cycle of 1/800.
- Forming diagonal crack in the beam during loading cycle of 1/400(2).
- Incline cracks were remarked in the slab from loading cycle of 1/200(1), as shown in Figure (5.20).
- Some cracks extended from the slab to the beam as diagonal cracks, as shown in Figure (5.21).
- Obvious widening of flexural cracks from loading cycle of 1/50 rad, as shown in Figure (5.21).
- During last push-over loading, crushing of concrete and touching between the wall and one of the supports occurred with widening in the cracks, as shown in Figure (5.23)

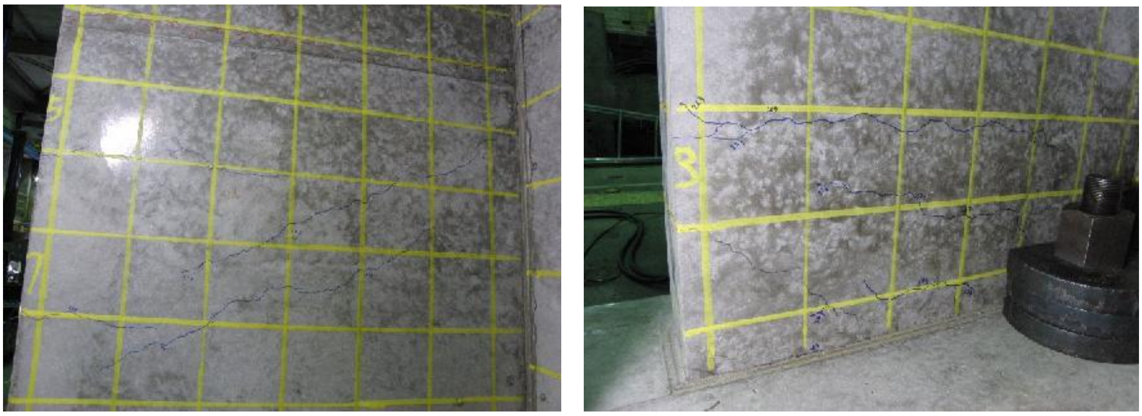

Fig (5.20) Incline cracks in the slab

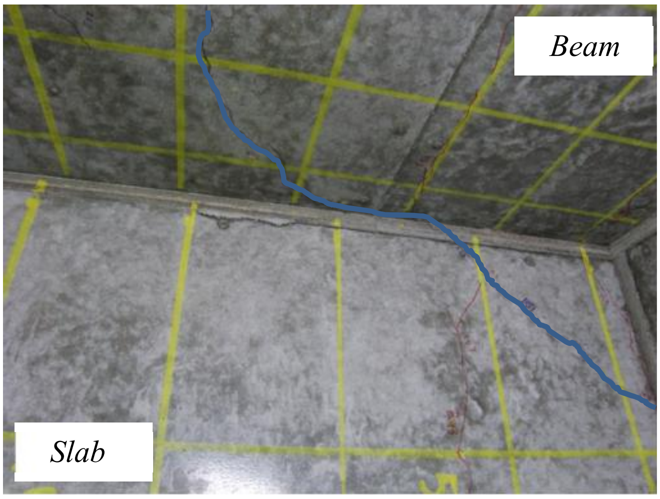

Fig(5.21) Extending cracks from the slab to the beam as diagonal cracks

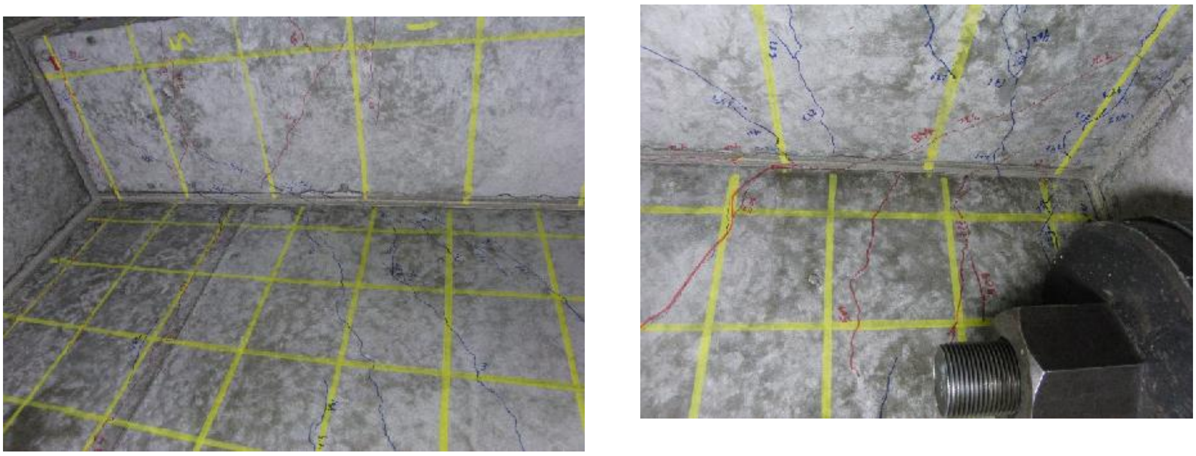

Fig (5.22) Widening of cracks from loading cycle of 1/50 rad

Fig (5.23) Crushing of concrete and touching between the wall and the stub with widening of cracks at last push-over loading

5.2 The Hysteresis loops of Shear Force and Drift Angle

5.2.1 Shear Force and Drift Angle of Specimen SP-S5

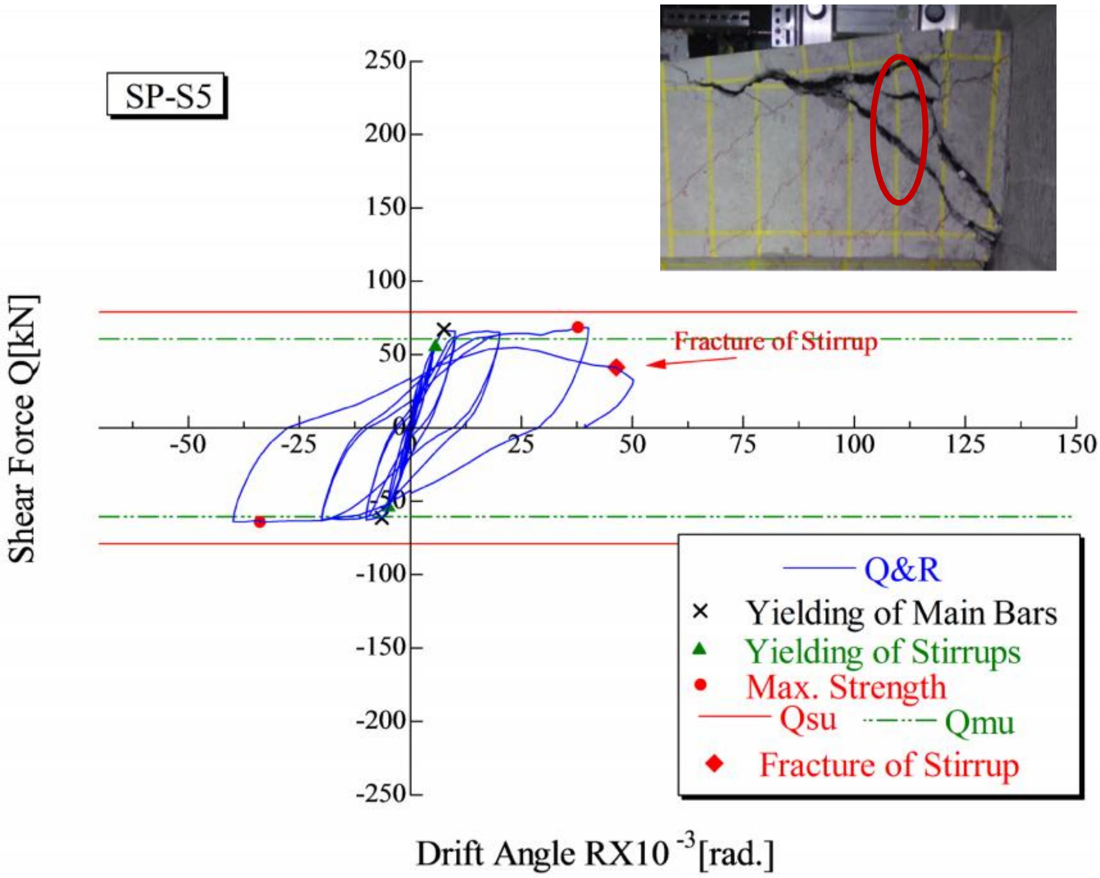

Fig (5.24) The experimental Q & R hysteresis loops of SP-S5

The maximum strength Q_{max} = 68.21 kN was reached at loading cycle of 1/25. The deformation capacity of SP-S5 beam was 1/25 rad. The longitudinal bars and stirrups yielded. And the stirrups yielded earlier, as shown in Figure (5.24). Fracture of stirrup was detected and followed by high degradation in strength after loading cycle of -1/25 rad, as shown in Figure (5.24), so the experiment was stopped. Yielding in the longitudinal bars of non-structural wall occurred at loading cycle of -1/25 rad.

5.2.2 Shear Force and Drift Angle of Specimen SP-S6

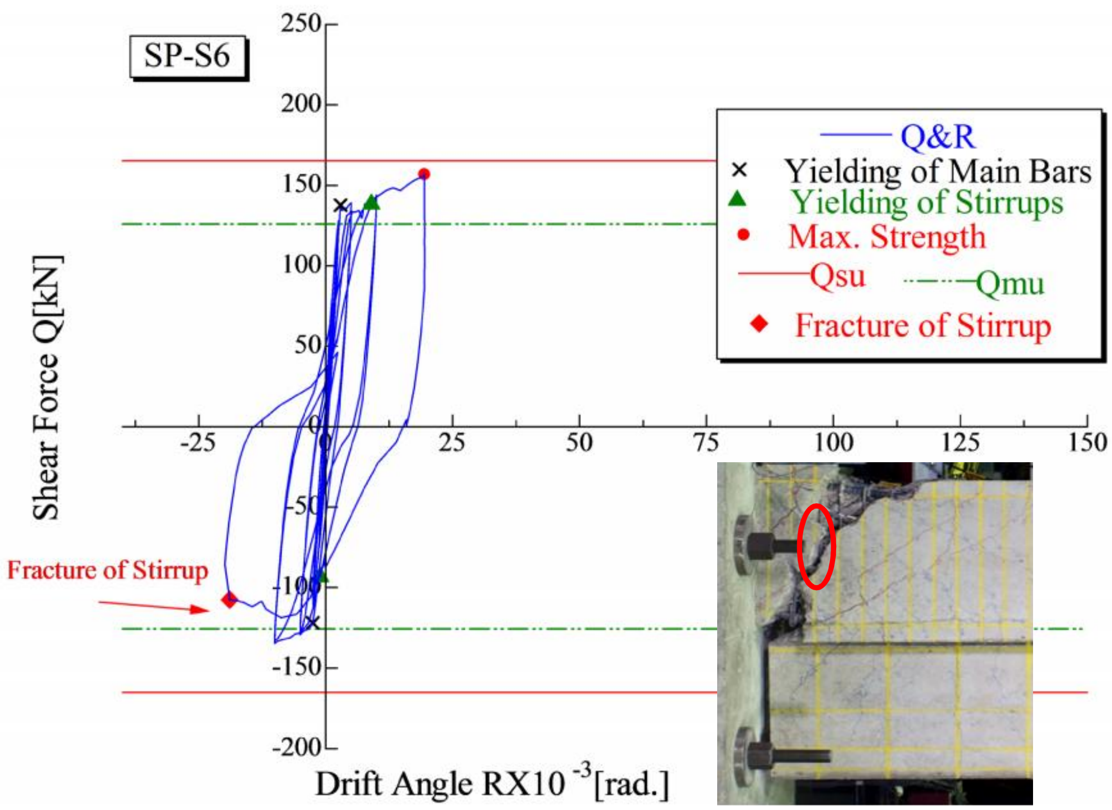

Fig (5.25) The experimental Q & R hysteresis loops of SP-S6

The maximum strength Q_{max} = 156.64 kN was reached at peak of loading cycle of 1/50. The deformation capacity of Sp-S6 was 1/50 rad. The longitudinal bars and stirrups of beam yielded, as shown in Figure (5.25). There is a slight degradation in the strength at loading cycle of -1/50 rad. Yielding in the longitudinal bars of non-structural wall occurred at loading cycle of 1/100 rad. Fracture of stirrup was detected as shown in Figure (5.25).

5.2.3 Shear Force and Drift Angle of Specimen SP-S6-AR

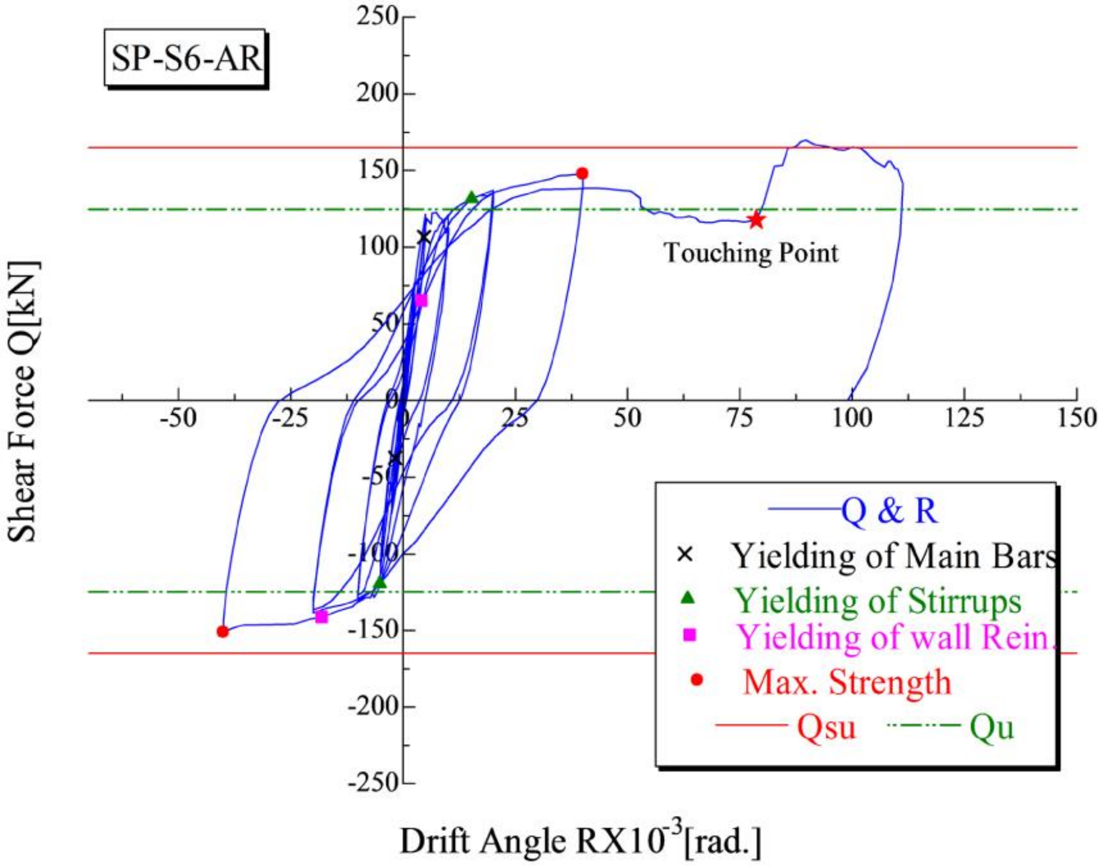

Fig (5,26) The experimental Q & R hysteresis loops of SP-S6-AR

The maximum strength Q_{max} =151.04 kN was reached at loading cycle of 1/25. The deformation capacity of was larger than 1/15 rad. Yielding of longitudinal bars and stirrups occurred. The loading was continued till reaching the limit of horizontal oil jacks. Touching between the non-structural wall and one of the supports was remarked by star in the Figure (5.26). More five stirrups yielded during the last push over loading cycle, where four stirrups yielded during the previous loading cycles from 1/50 rad.

5.2.4 Shear Force and Drift Angle of Specimen SP-S6-Slab T

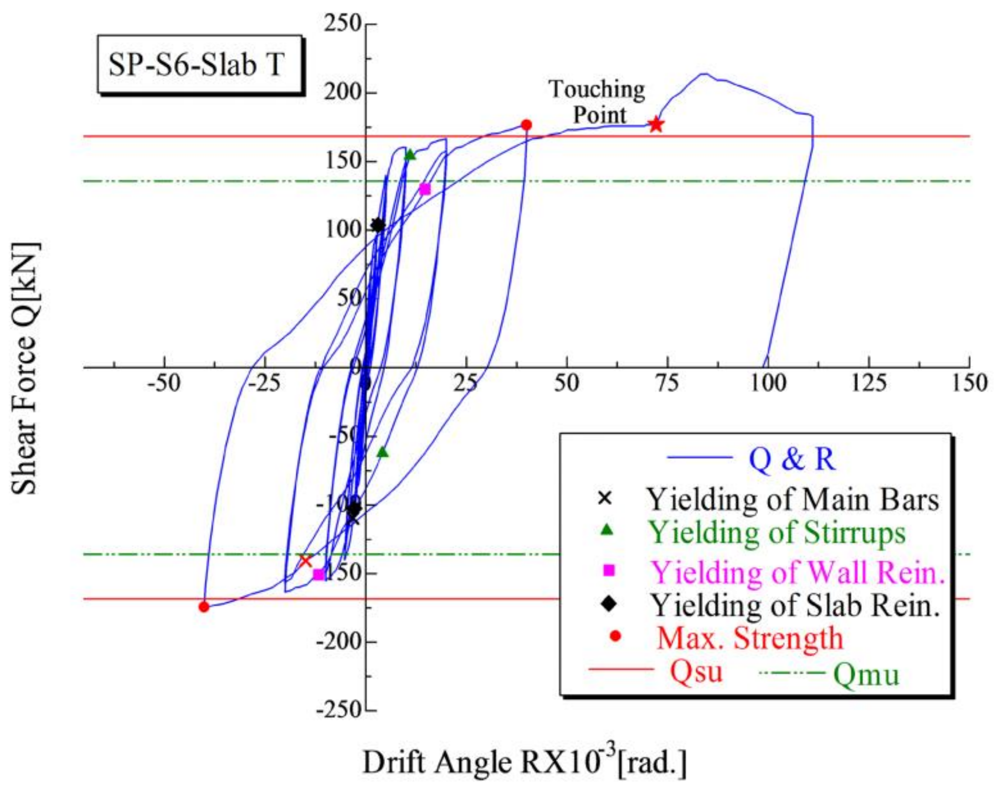

Fig (5.27)The experimental Q & R hysteresis loops of SP-S6-Slab T

The maximum strength Q_{max} =176.41 kN was reached at loading cycle of 1/25 in each direction of loading and it was higher than both design flexural strength and design shear strength. The deformation capacity of this beam was larger than 1/25 rad. Yielding of main bars of beam and slab, and stirrups occurred obviously, as shown in Figure (5.27). Touching between the wall and one of the supports occurred, as marked on the Figure (5.27). The loading was continued till reaching the limit of the horizontal hydraulic oil jack.

5.2.5 Shear Force and Drift Angle of Specimen SP-S6-Slab K

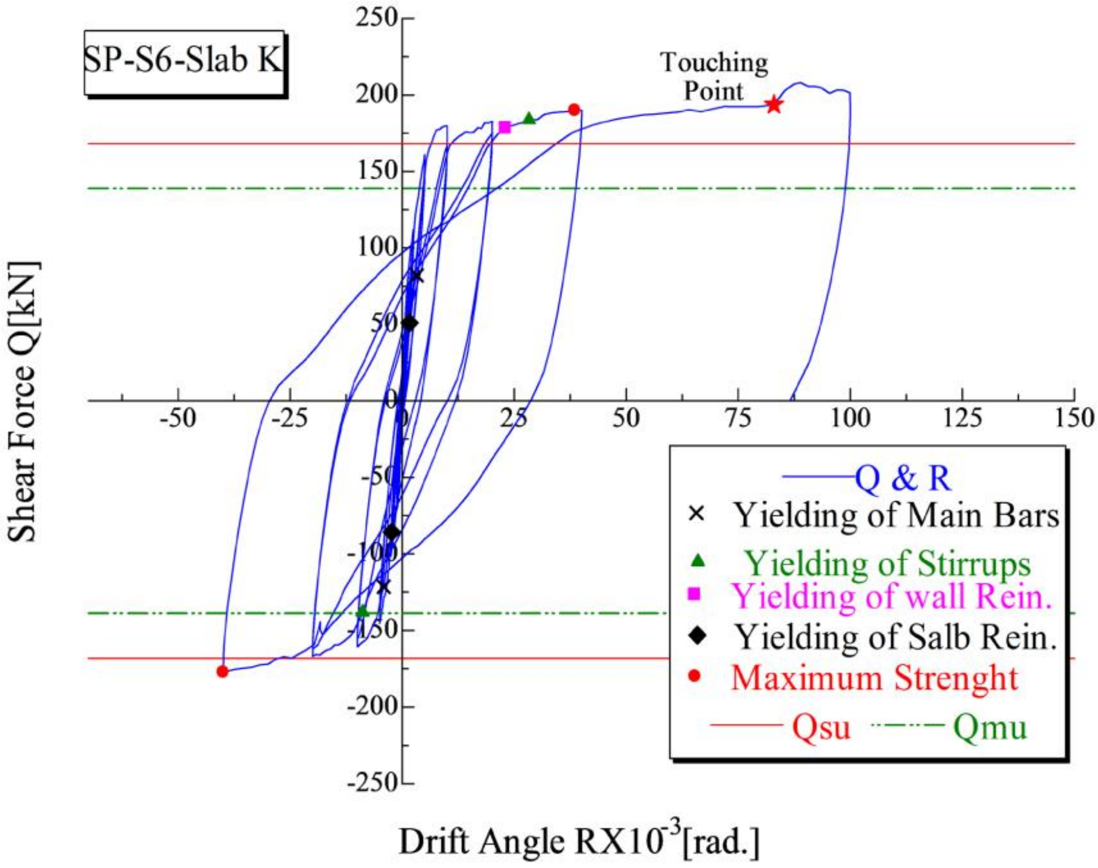

Fig (5.28) The experimental Q & R hysteresis loops of SP-S6-Slab K

The maximum strength Q_{max} =190.07 kN was reached at loading cycle of 1/25 in each direction of loading and it was higher than both design flexural strength and design shear strength. The deformation capacity of this beam was larger than 1/25 rad. Yielding of main bars of beam and slab, and stirrups occurred obviously, as shown in Figure (5.28). Touching between the wall and one of the supports occurred, as marked on the Figure (5.28). The loading was continued till reaching the limit of horizontal hydraulic oil jack.

5.2.6 Shear Force and Drift Angle of Specimen SP-S5-Slab T

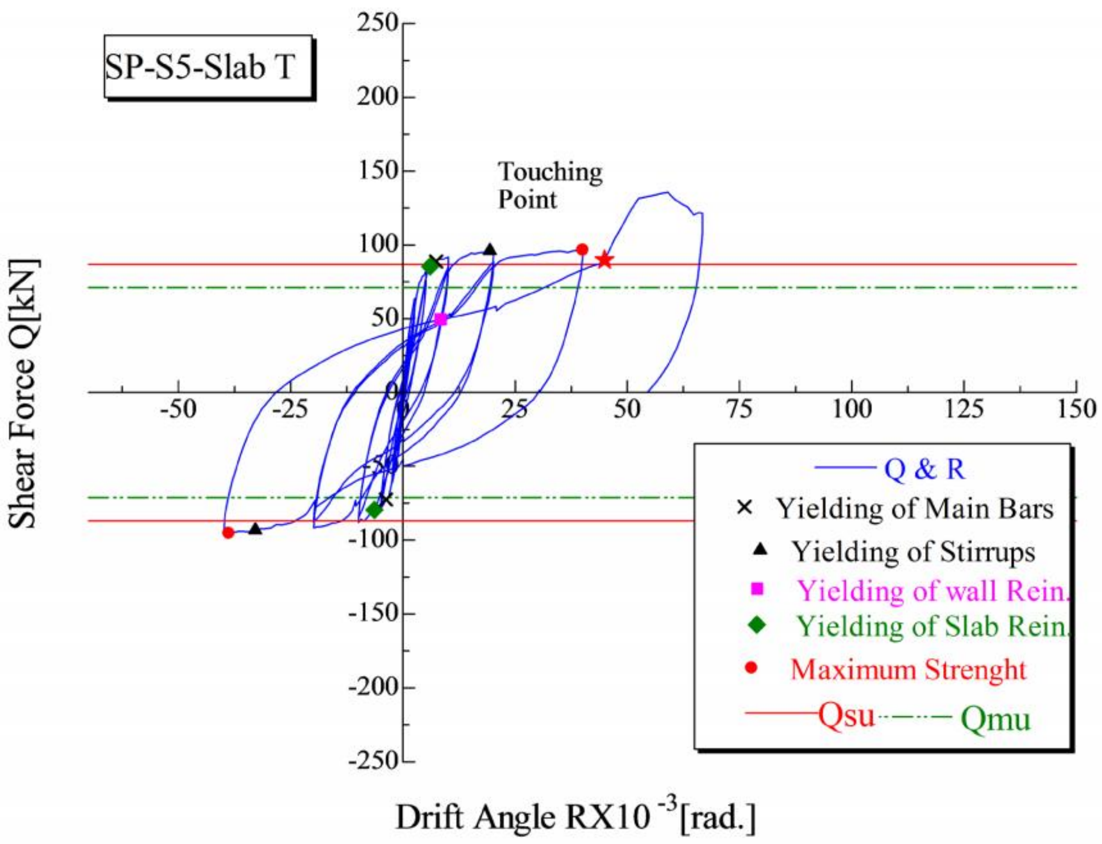

Fig (5.29) The experimental Q & R hysteresis loops of SP-S5-Slab T

The maximum strength Q_{max} =96.64 kN was reached at loading cycle of 1/25 in each direction of loading and it was higher than both design flexural strength and design shear strength. The deformation capacity of this beam was larger than 1/25 rad. Yielding of main bars of beam and slab, and stirrups occurred obviously, as shown in Figure (5.29). Touching between the wall and one of the supports occurred, as marked on the Figure (5.29). The loading was continued till reaching the limit of horizontal hydraulic oil jack.

5.3 The Strength and Plastic Rotation Angle

5.3.1 The Strength

Table 5.1 shows the experimental and calculated flexural and shear strength. The experimental strength is larger than the flexural strength by 10%, 20% and 30% in case of beams with slabs. Comparing with shear strength where it is less than the calculated shear strength for beams without slab and larger by 10% foe beams with slabs.

Table 5.1 Experimental and calculated flexural and shear strength (*kN*)

Specimen	Qexp.	Flexural Strength		Shear Strength	
		Qu	Qexp/Qu	Qsu	Qexp/Qsu
SP-S5	68.21	60.66	1.12	78.96	0.89
SP-S6	156.64	126.00	1.24	172.81	0.91
SP-S6-AR	151.04	124.74	1.21	164.03	0.92
SP-S6-Slab T	176.41	127.92	1.38	152.52	1.15
SP-S6-Slab K	190.07	136.81	1.39	167.41	1.13
SP-S5-Slab T	96.64	71.12	1.36	86.98	1.11

Another calculation to the shear strength based on the AIJ Guidelines [15], where the shear strength is taken the minimum value from all the values given below:

$$Vu = \mu \cdot P_w \cdot \sigma_{wy} \cdot b \cdot J_e + \left(\upsilon \cdot \sigma_B - \frac{5 \cdot P_w \cdot \sigma_{wy}}{\lambda} \right) \frac{b \cdot D}{2} tan\theta \qquad \text{Eqn.5.1}$$

$$Vu = \left\{ \left(\lambda \cdot \upsilon \cdot \sigma_B + P_w \cdot \sigma_{wy} \right) / 3 \right\} \cdot b \cdot J_e \qquad \text{Eqn.5.2}$$

$$Vu = \left\{ \left(\lambda \cdot \upsilon \cdot \sigma_B \right) / 2 \right\} \cdot b_e \cdot J_e \qquad \text{Eqn.5.3}$$

Where: $tan\theta = \sqrt{\left(\frac{L}{D} \right)^2 + 1} - \frac{L}{D}$, $\mu = 2 \cdot \left(1 - 10 \cdot R_p \right)$

$$\upsilon = \left(1 - 20 \cdot R_p\right) \cdot \left(0.7 - \frac{\sigma_B}{200}\right) \quad , \qquad \lambda = 1 - \frac{S}{2J_e} - \frac{b}{4J_e}$$

d: Effective depth of the tensile reinforcement (*mm*),

L: Length of beam (*mm*),

σ_B: Compression strength of concrete (N/mm^2),

P_w: Shear reinforcement ratio (*%*),

σ_{wy}: Yielding stress of shear reinforcement (N/mm^2),

b: Width of beam (*mm*),

s: Space of stirrups (*mm*), and j=7/8*d.

j_e, b_e: For rectangular section, were determined by the distance between the centers of horizontal legs of stirrup in same section, for the former, and between the vertical legs for the later.

In case of beam with slab, it was not determined exactly in AIJ guidelines [15].

be: the same for rectangular section, and

je: was proposed by the distance between the centers of compression rebar of beam to the center of upper tension rebar of slab.

Table (5.2) shows the experimental and calculated strengths of specimens.

Table 5.2 Experimental and calculated strength[15] kN

Specimen	Qexp.	Vu	Qexp./Vu	Qmu./Vu	Qsu./Vu
SP-S5	68.21	77.92	0.87	0.77	1.01
SP-S6	156.64	245.31	0.64	0.51	0.70
SP-S6-AR	151.04	274.32	0.55	0.45	0.59
SP-S6-Slab T	176.41	249.79	0.71	0.51	0.61
SP-S6-Slab K	190.07	261.25	0.72	0.52	0.64
SP-S5-Slab T	96.64	102.03	0.94	0.69	0.85

5.3.2 The Plastic Rotation Angle

The plastic rotation angle is calculated experimentally by subtracting the rotation angle at yielding from the ultimate rotation angle.

Bu using the equations Eqn. (5.1) to Eqn. (5.3), the plastic rotation angle is the value of R_p when $Q_{mu} = V_u$.

Figure (5.31) shows the details of calculation the plastic rotation angle depending on the equations of Vu depending on the inelastic displacement concept in AIJ guidelines 1999(15).

Table 5.3 Experimental and calculated plastic rotation angle Rp

Specimen	Ryexp	Ruexp	Rpexp	Rpcal	Rpexp/ Rpcal
SP-S5	0.0075	0.040	0.033	0.013	2.53
SP-S6	0.0020	0.020	0.018	0.032	0.56
SP-S6-AR	0.0052	0.063	0.057	0.036	1.58
SP-S6-Slab T	0.0036	0.072	0.068	0.030	2.26
SP-S6-Slab K	0.0041	0.069	0.065	0.031	2.09
SP-S5-Slab T	0.0037	0.040	0.036	0.018	2.00

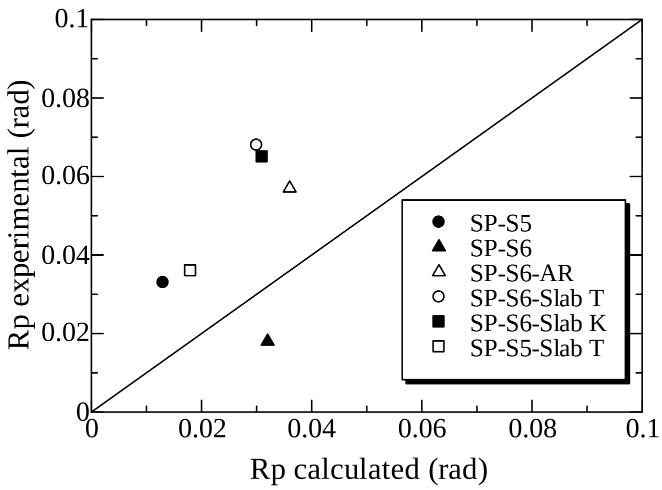

Fig (5.30) Comparison between calculated and experimental R_p

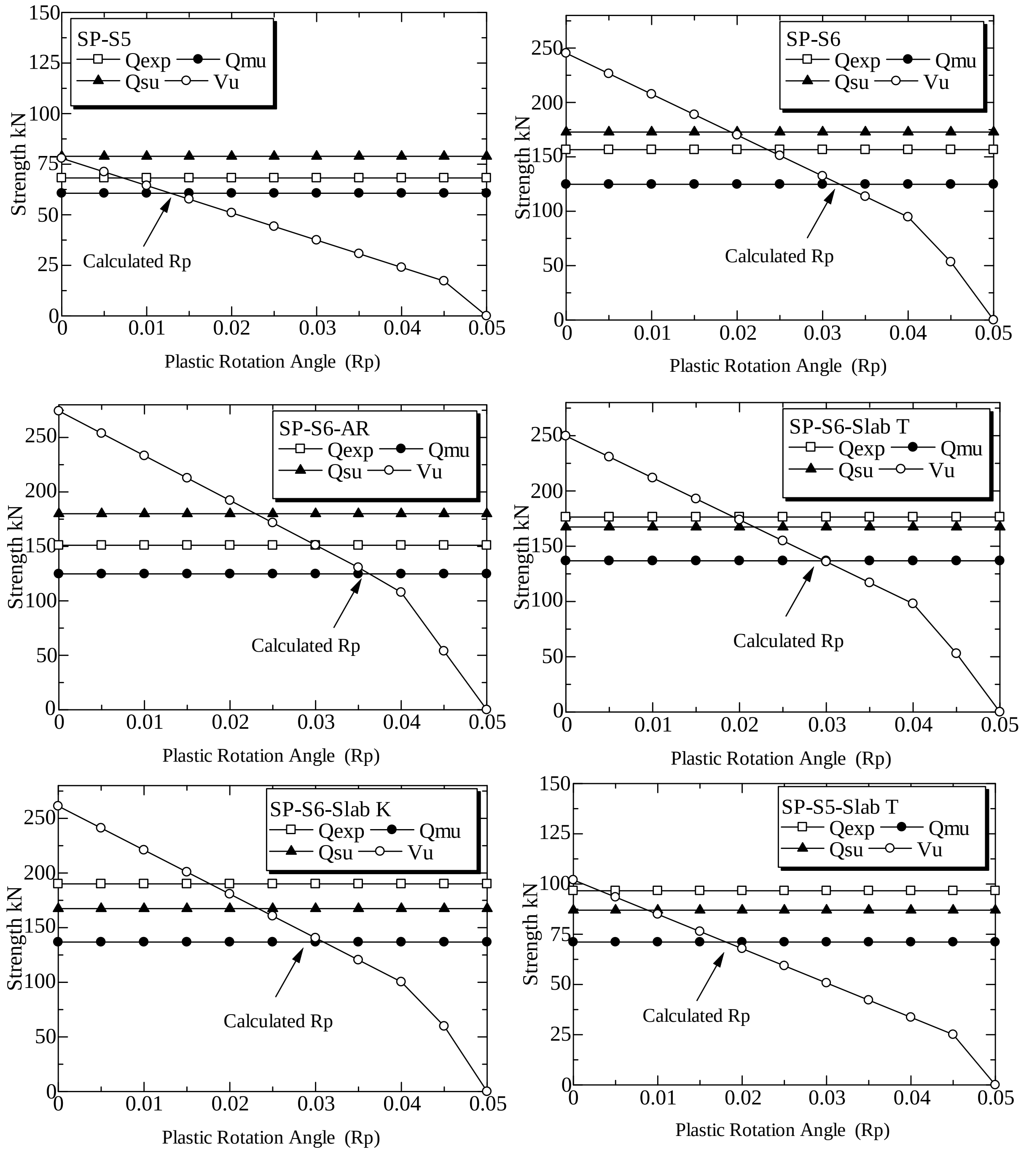

Fig (5.31) Calculated Rp depending on AIJ guidelines[15]

5.4 Readings of Strains Gauges of reinforcing Bars

The strains of reinforcement bars were recorded along the experimental works. Where strain gauges attached on the reinforcing bars were used for this purpose. Number of yielded stirrups and more details of yielding of reinforcing bars are shown in Tables (5.4.a) and (5.4.b).

Table 5.4.a Details of yielding of reinforcing bars

Specimen	Longitudinal Bars		Stirrups		Yielded Stirrups
	Q	R	Q	R	
SP-S5	67.10	1/100	55.14	1/100	6
SP-S6	94.91	1/200	-77.10	-1/100	2
SP-S6-AR	118.58	1/100	131.76	1/50	4
SP-S6-Slab T	116.63	1/200	118.58	1/50	4
SP-S6-Slab K	-121.50	-1/100	-138.10	-1/50	6
SP-S5-Slab T	-72.46	-1/200	96.13	1/50	2

Table 5.4.b Details of yielding of reinforcing bars

Specimen	Non-Structural Wall		Slab	
	Q	R	Q	R
SP-S5	-52.46	-1/25	No Slab	
SP-S6	138.83	1/100		
SP-S6-AR	64.90	1/25		
SP-S6-Slab T	-153.20	-1/50	144.40	1/100
SP-S6-Slab K	178.60	1/25	50.99	1/200
SP-S5-Slab T	49.28	1/25	85.40	1/100
* Yielding occurred from the mentioned values. ** Units: Q (kN), R (rad).				

Fig(5.32) Positions of strain gauges attached on reinforcing bars of SP-S5

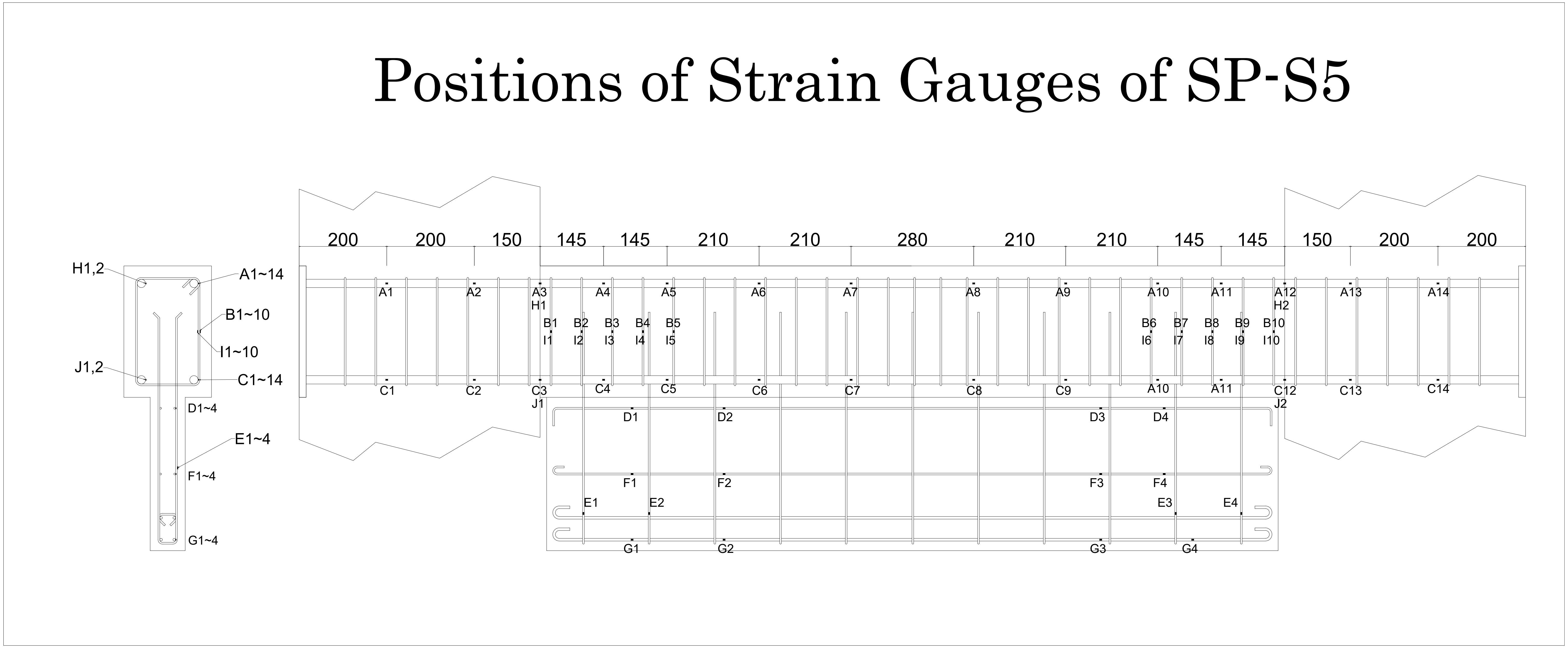

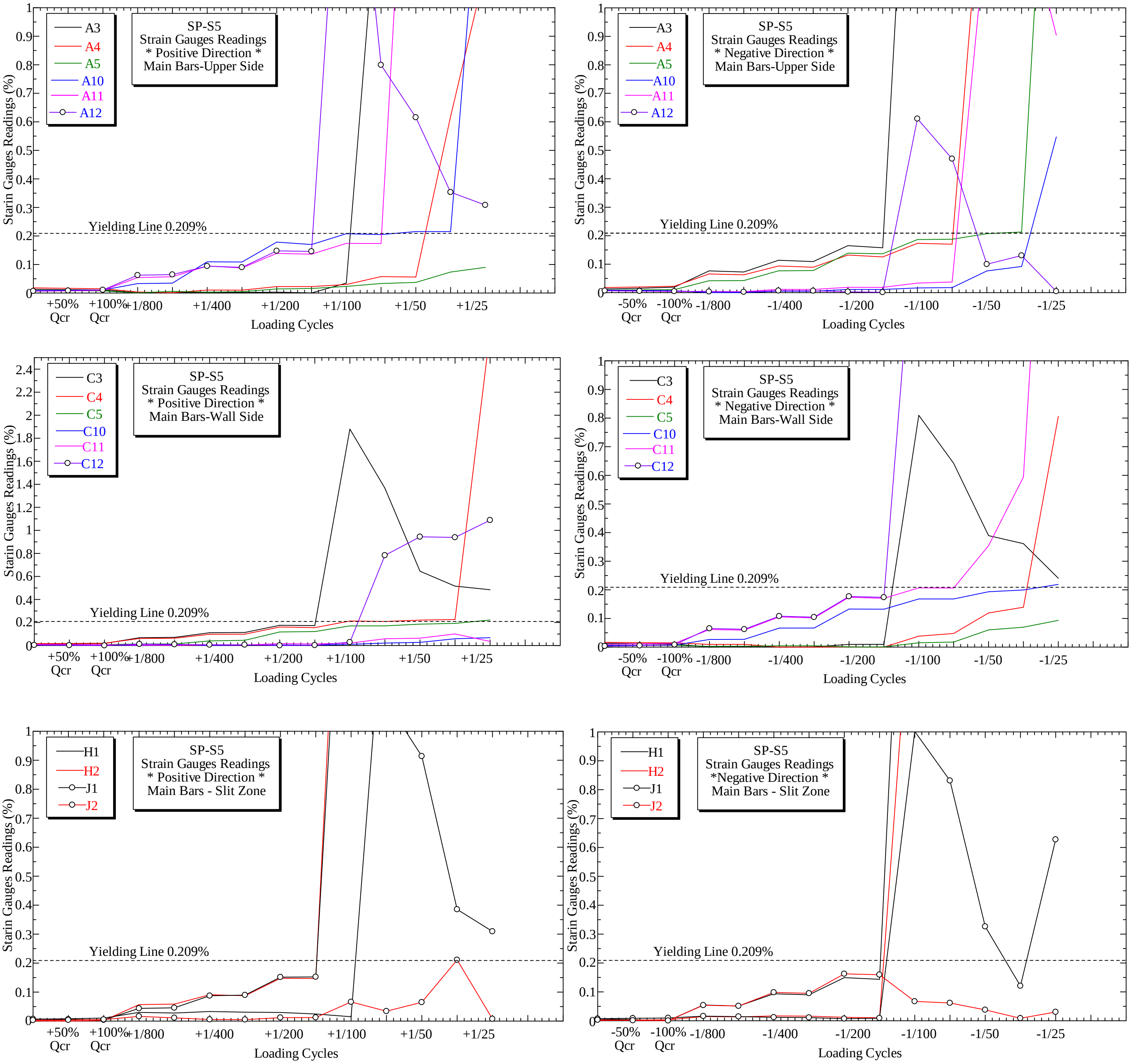

Fig (5.33.a) Readings of strain gauges of SP-S5

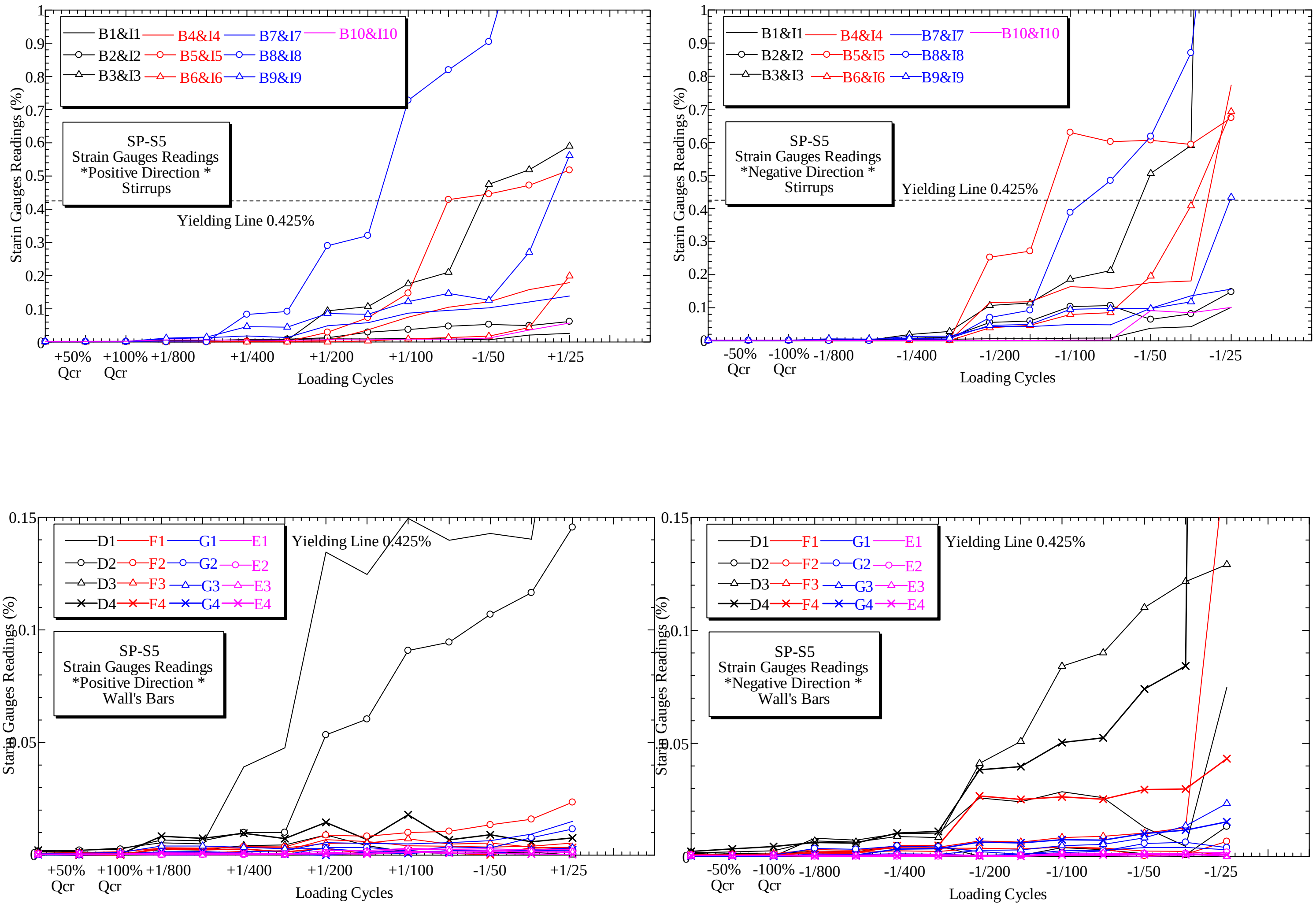

Fig (5.33.b) Readings of strain gauges of SP-S5

Fig(5.34) Positions of strain gauges attached on reinforcing bars of SP-S6

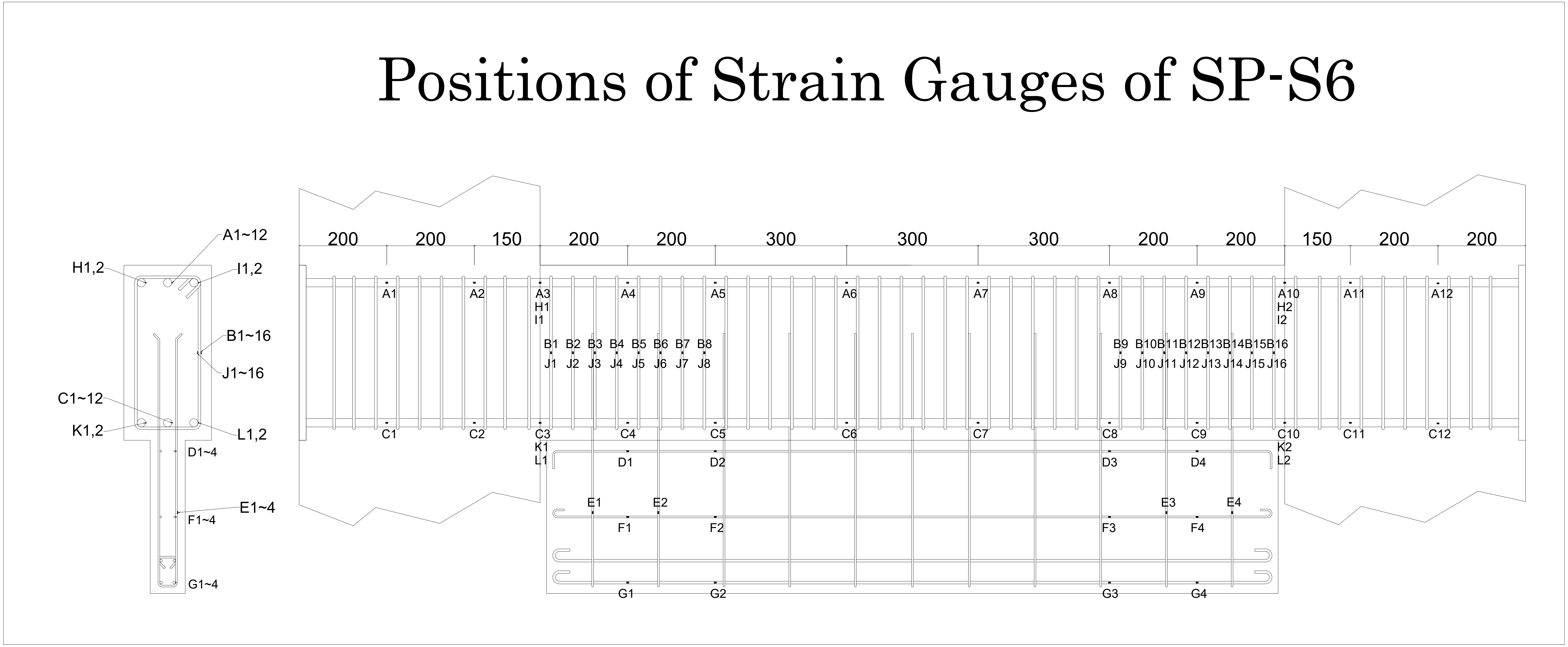

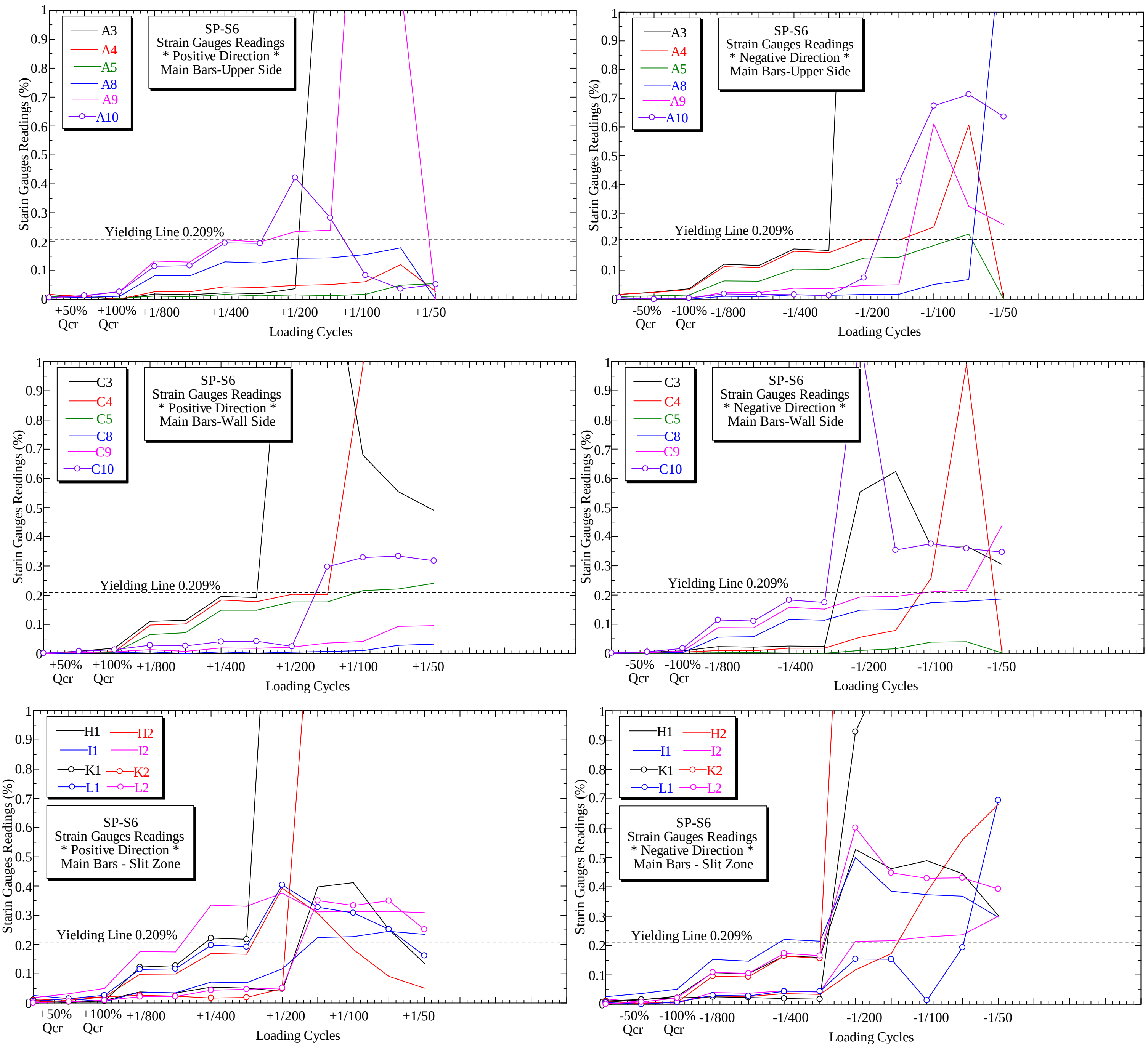

Fig (5.35.a) Readings of strain gauges of SP-S6

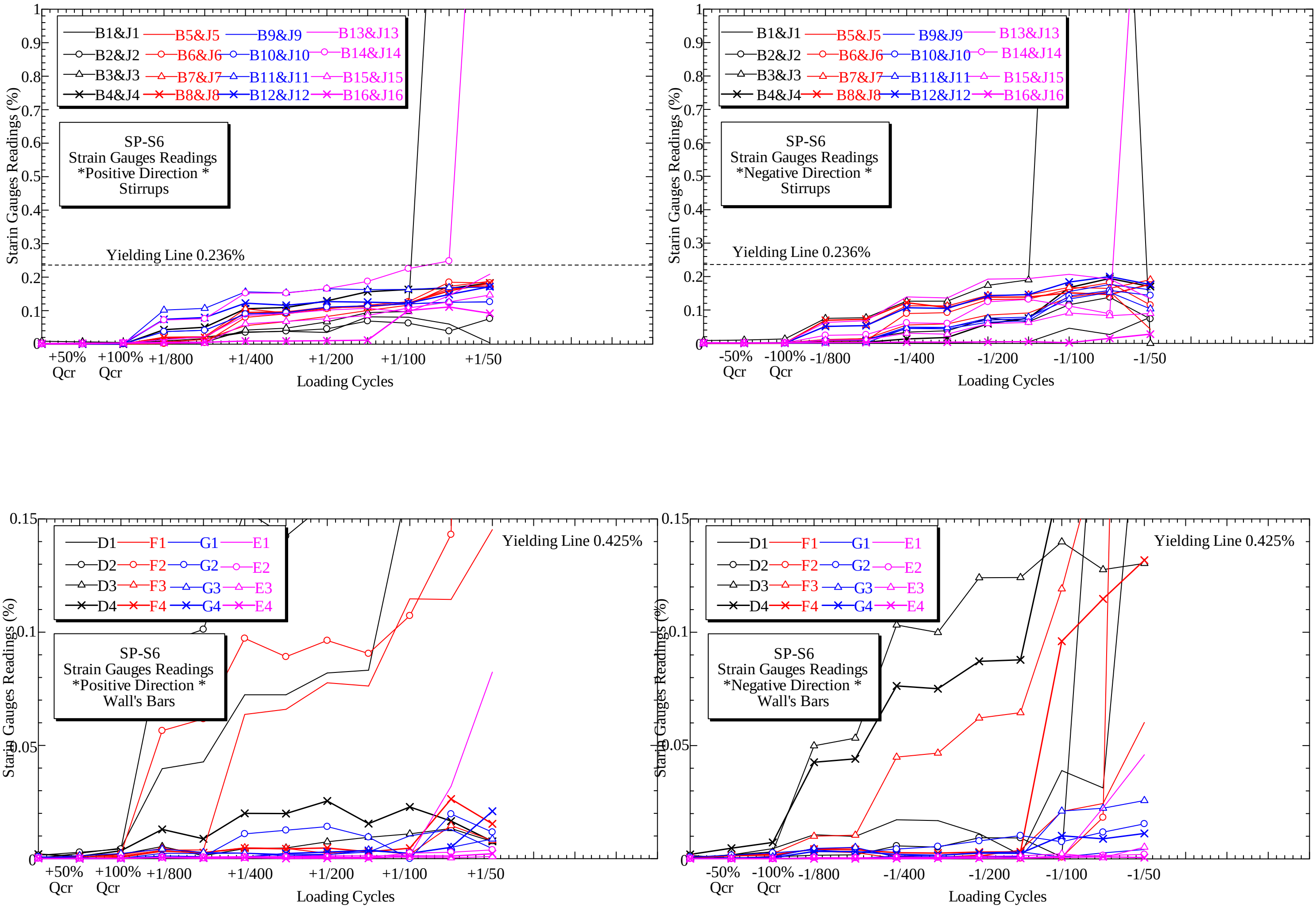

Fig (5.35.b) Readings of strain gauges of SP-S6

Fig(5.36) Positions of strain gauges attached on reinforcing bars of SP-S6-AR

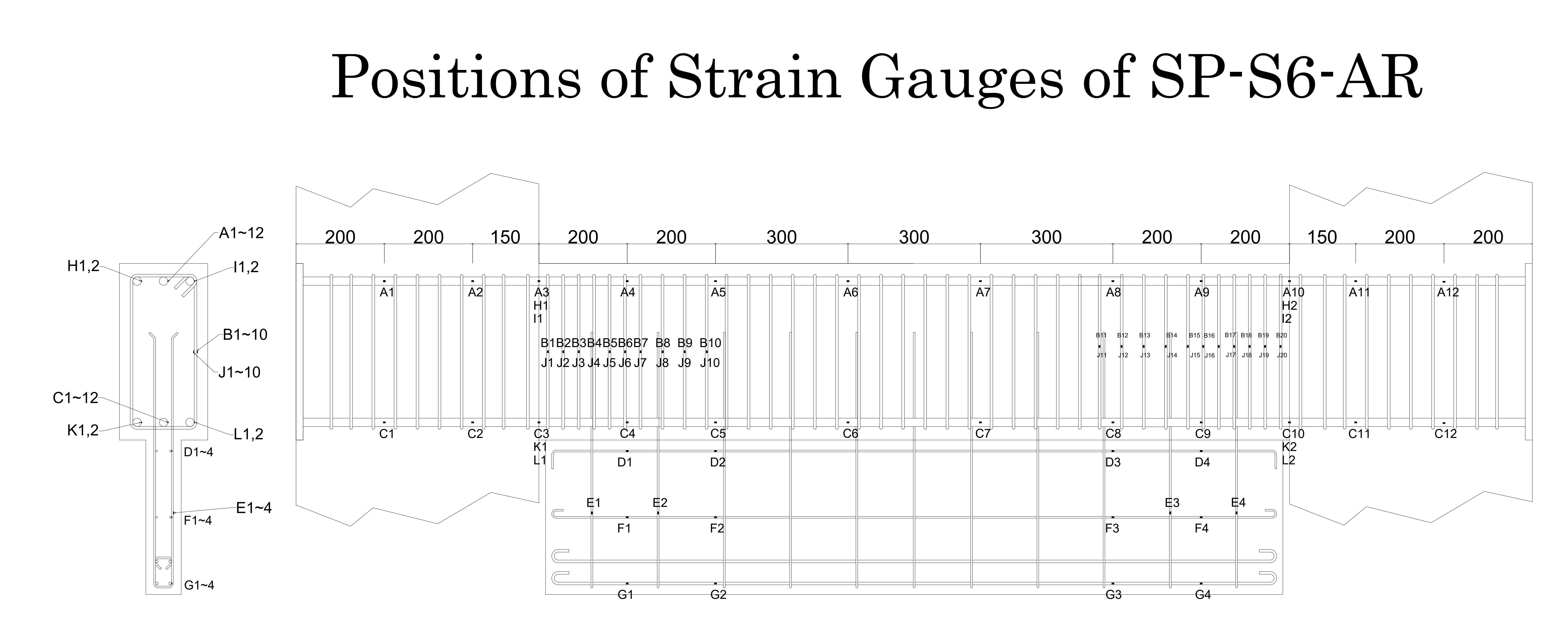

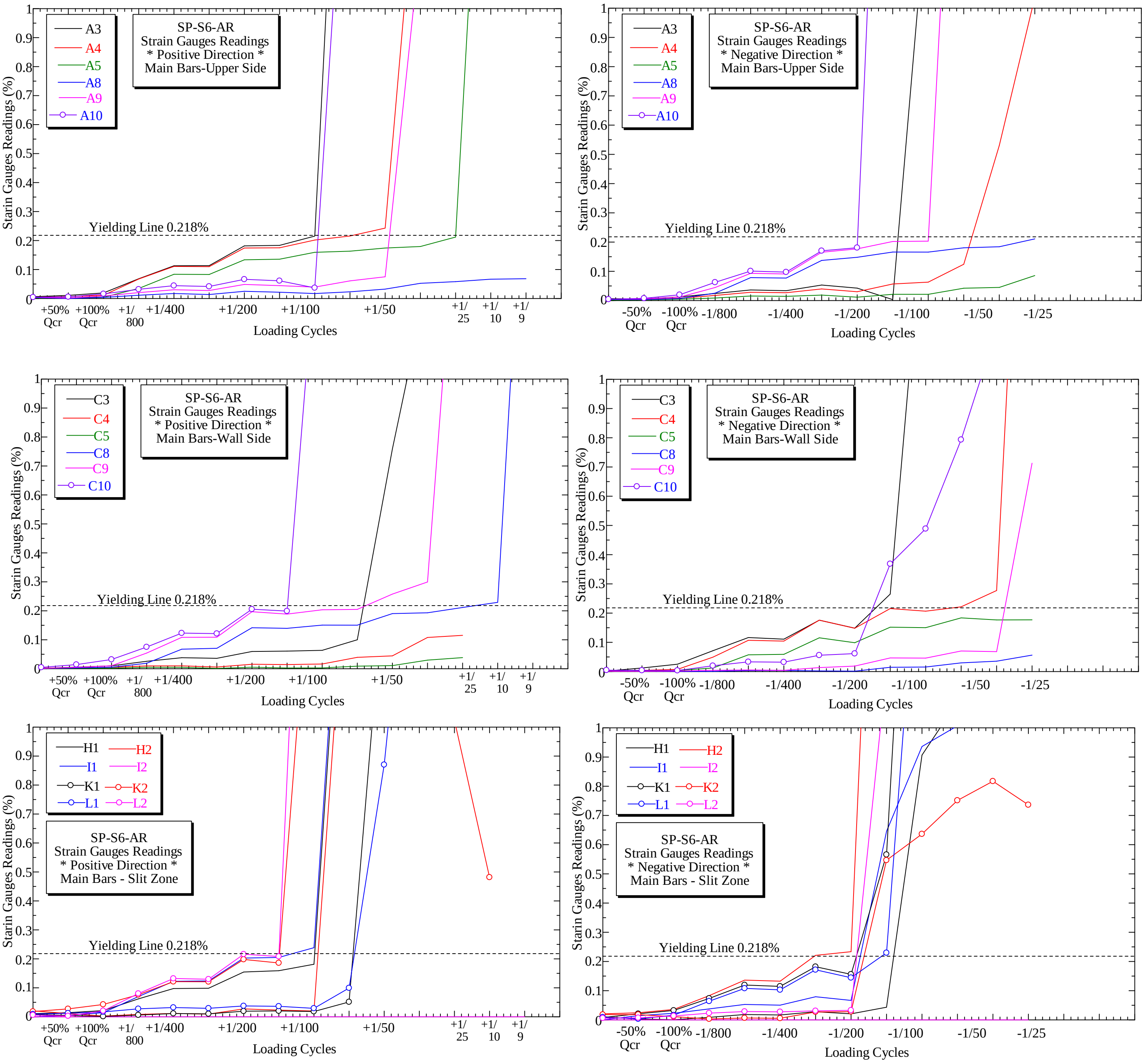

Fig (5.37.a) Readings of strain gauges of SP-S6-AR

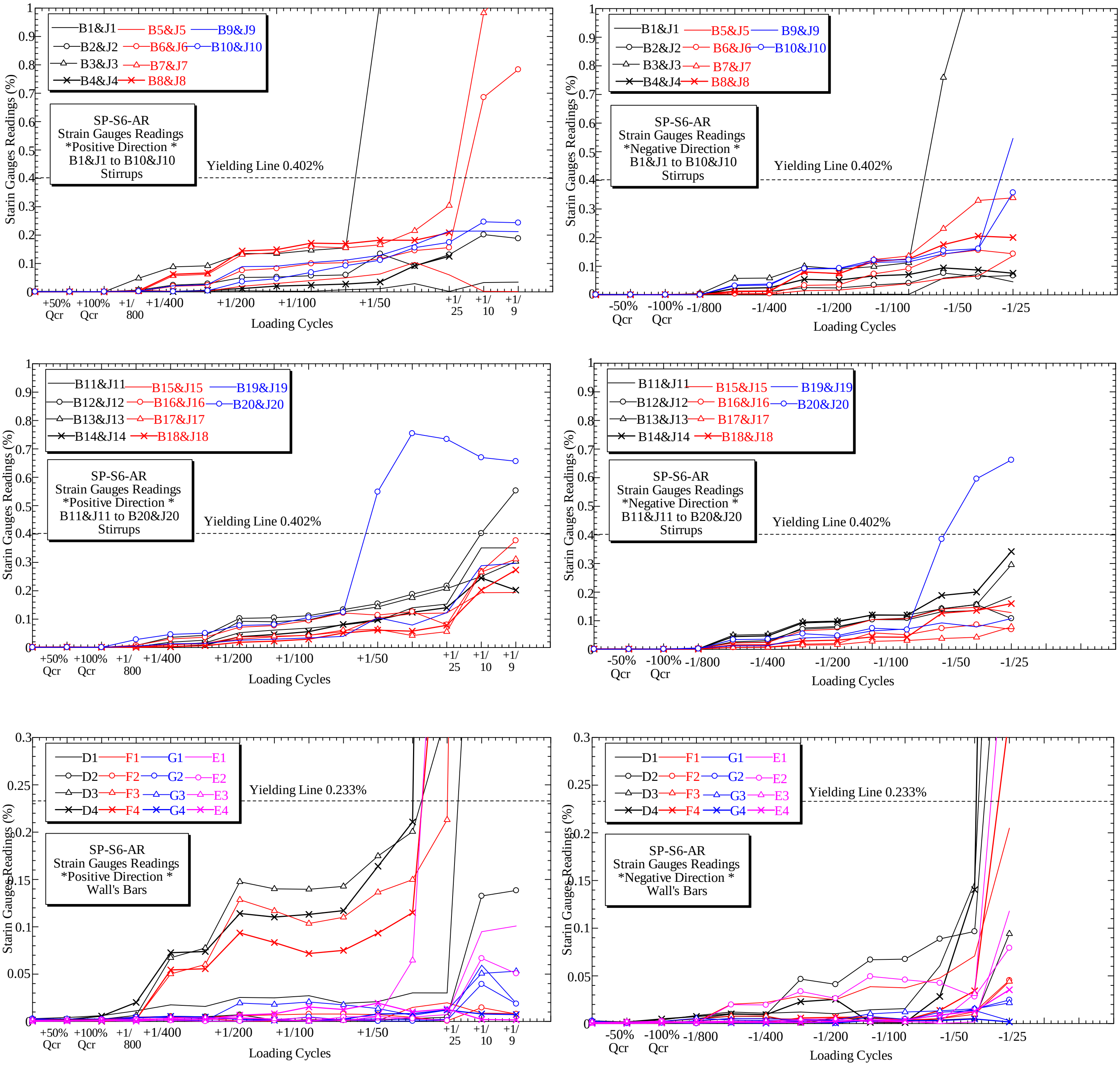

Fig (5.37.b) Readings of strain gauges of SP-S6-AR

Positions of Strain Gauges of SP-S6-Slab T

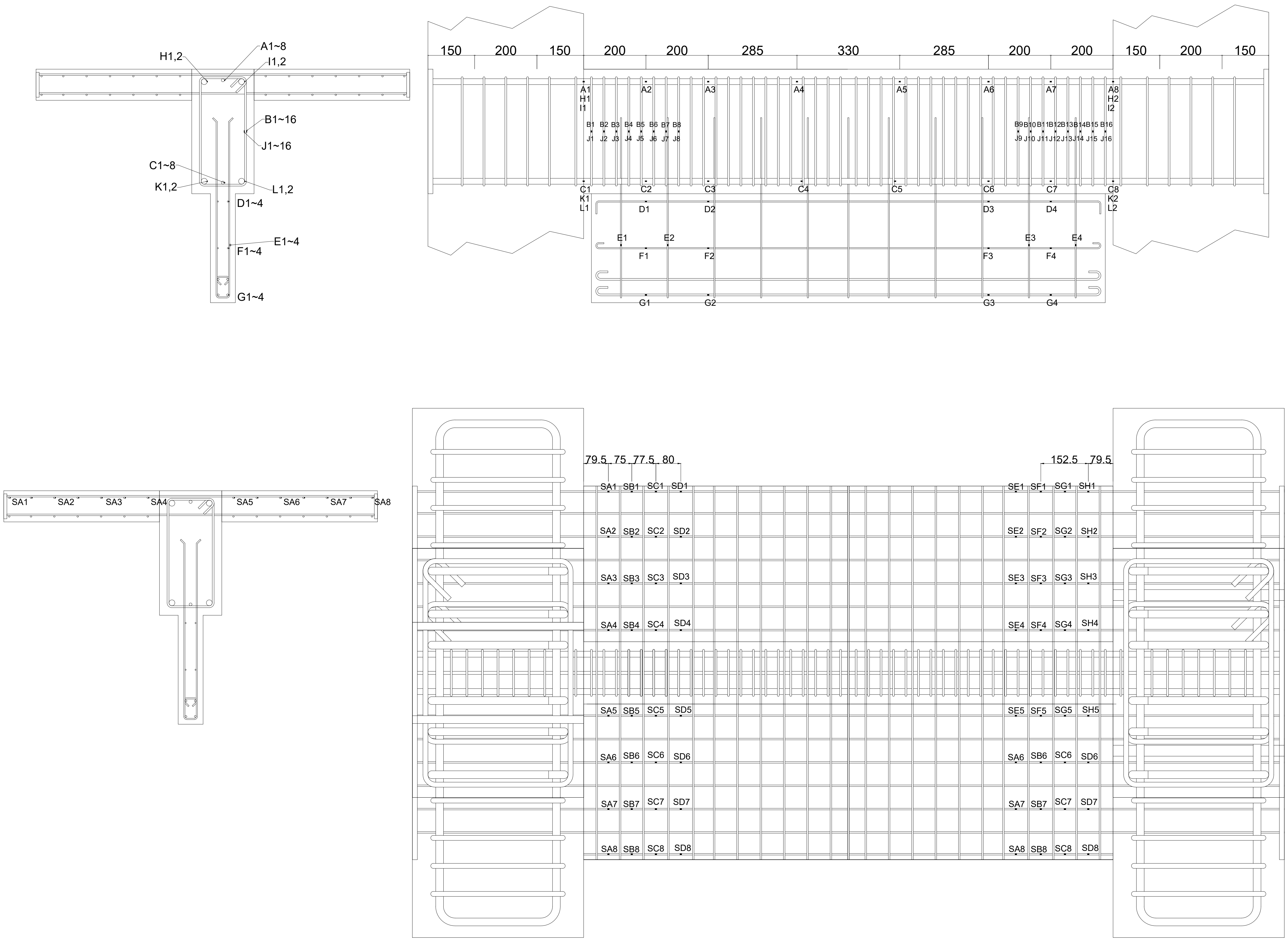

Fig(5.38) Positions of strain gauges attached on reinforcing bars of SP-S6-Slab T

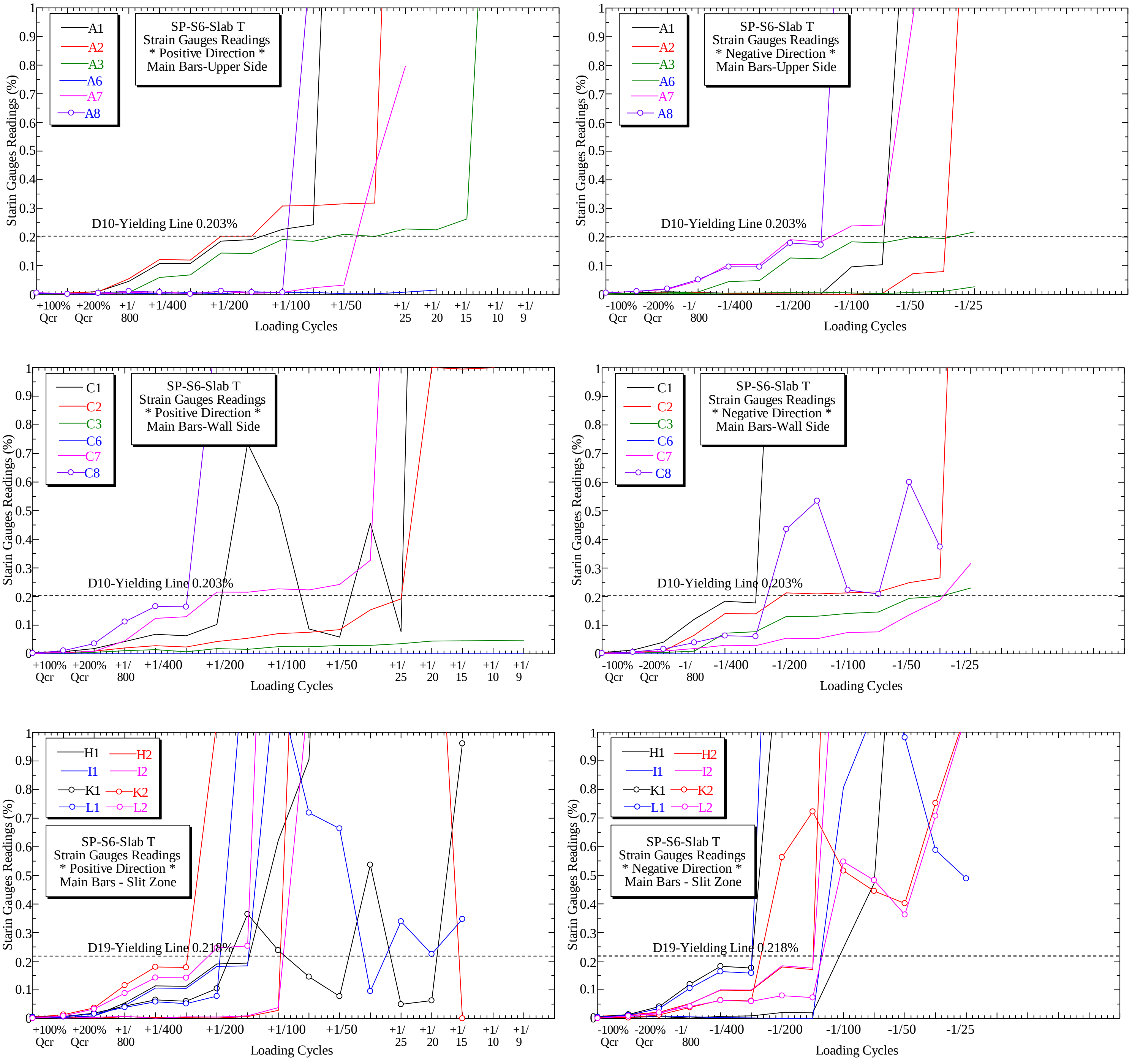

Fig (5.39.a) Readings of strain gauges of SP-S6-Slab T

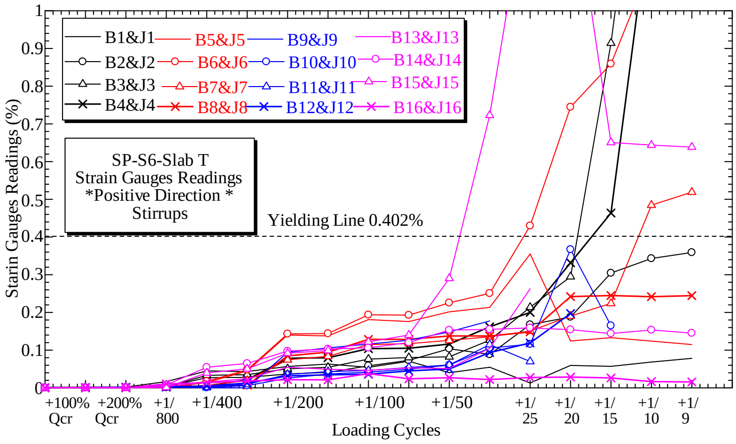

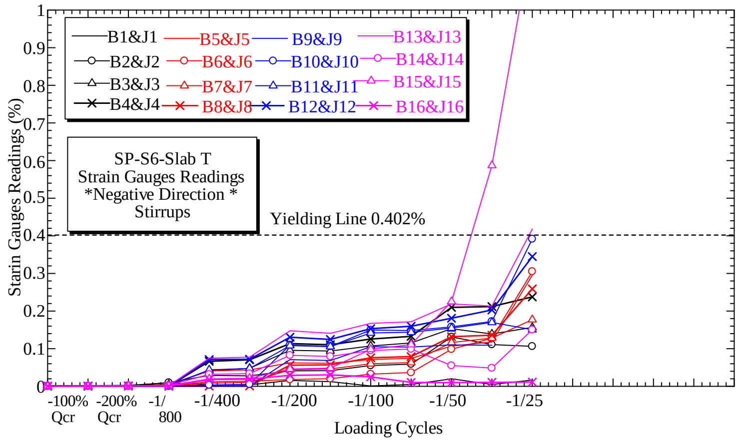

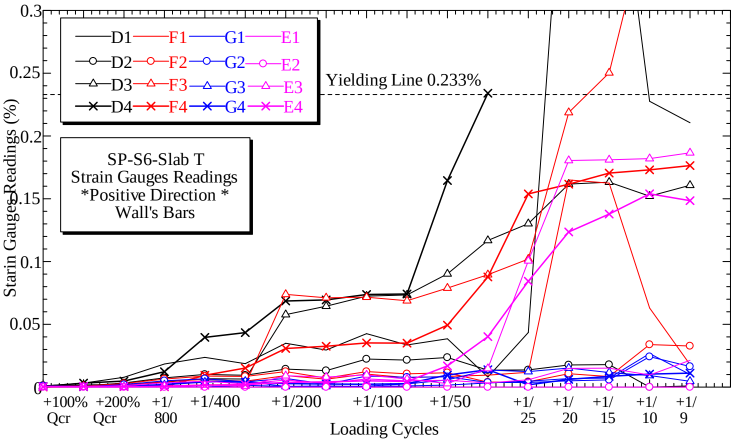

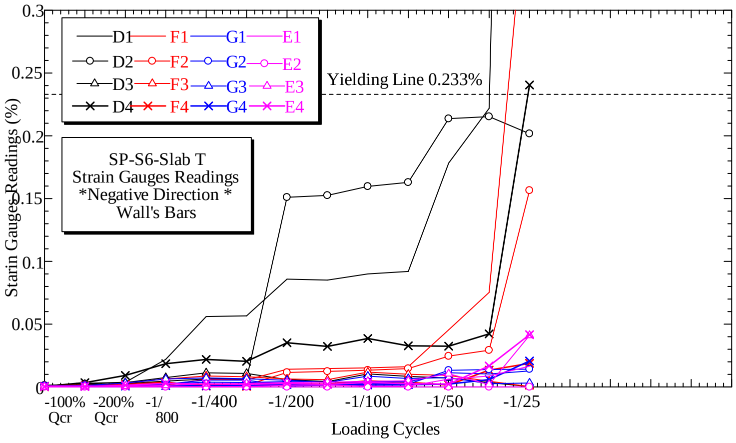

Fig (5.39.b) Readings of strain gauges of SP-S6-Slab T

Positions of Strain Gauges of SP-S6-Slab K

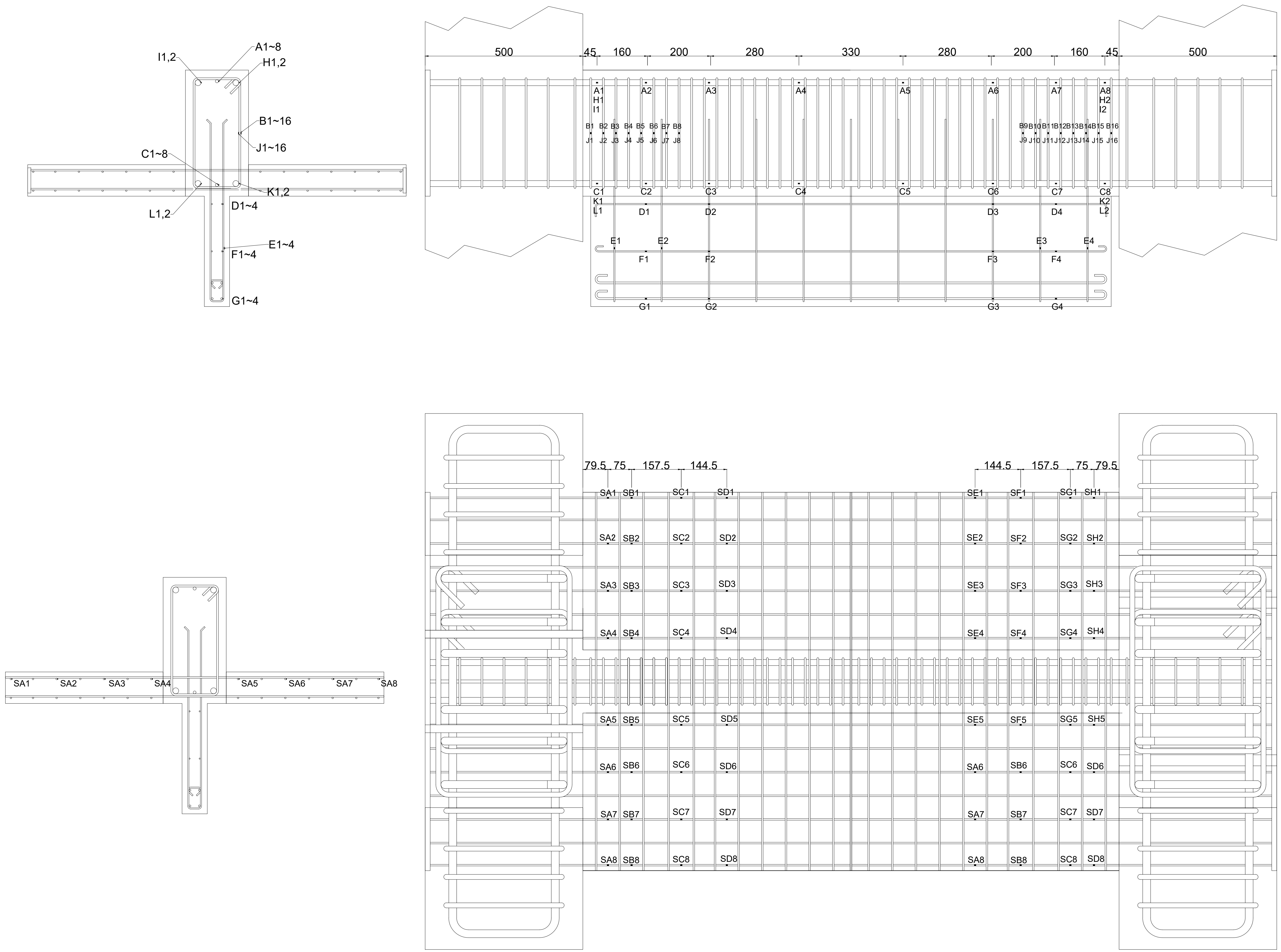

Fig(5.40) Positions of strain gauges attached on reinforcing bars of SP-S6-Slab K

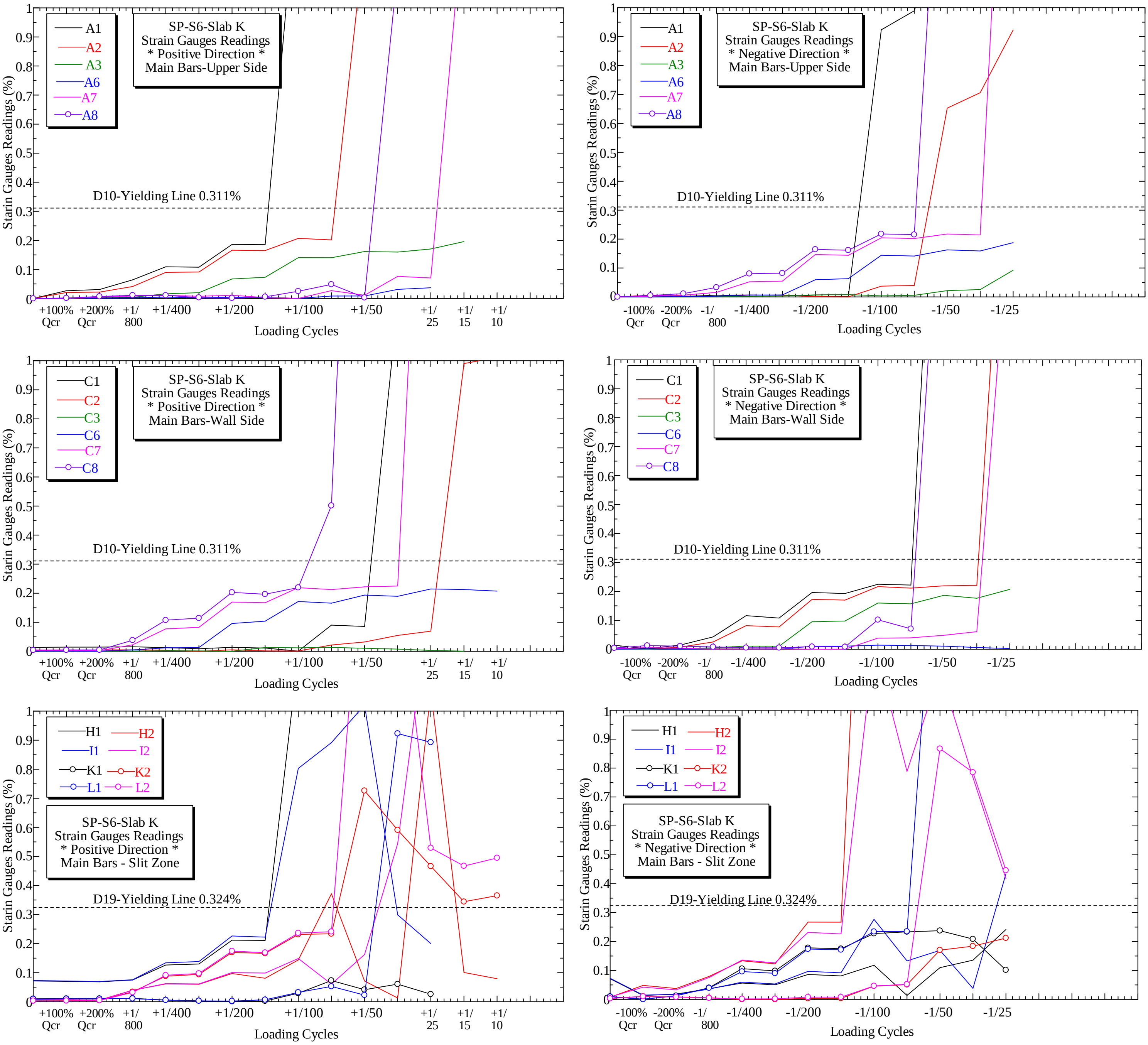

Fig (5.41.a) Readings of strain gauges of SP-S6-Slab K

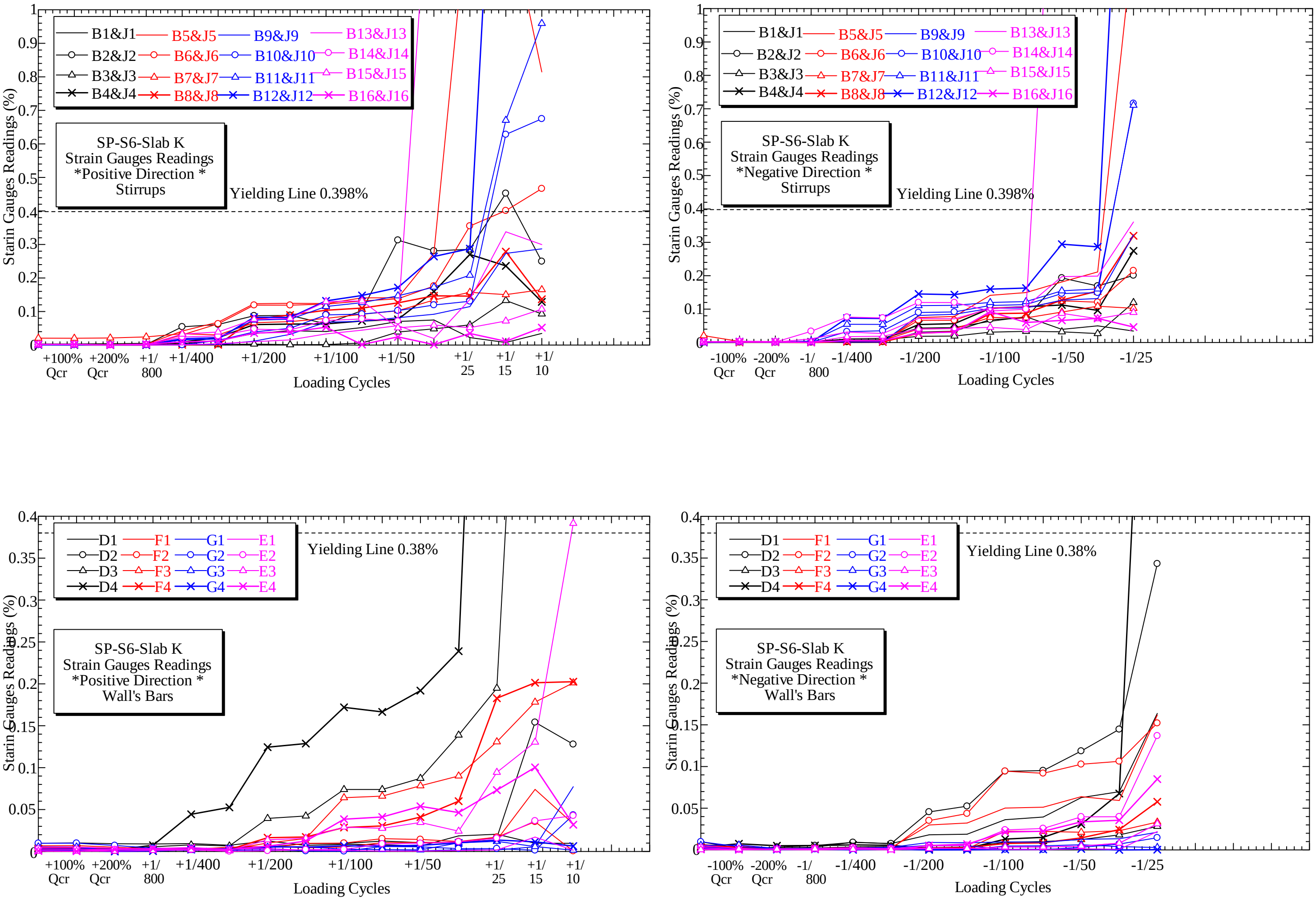

Fig (5.41.b) Readings of strain gauges of SP-S6-Slab K

Positions of Strain Gauges of SP-S5-Slab T

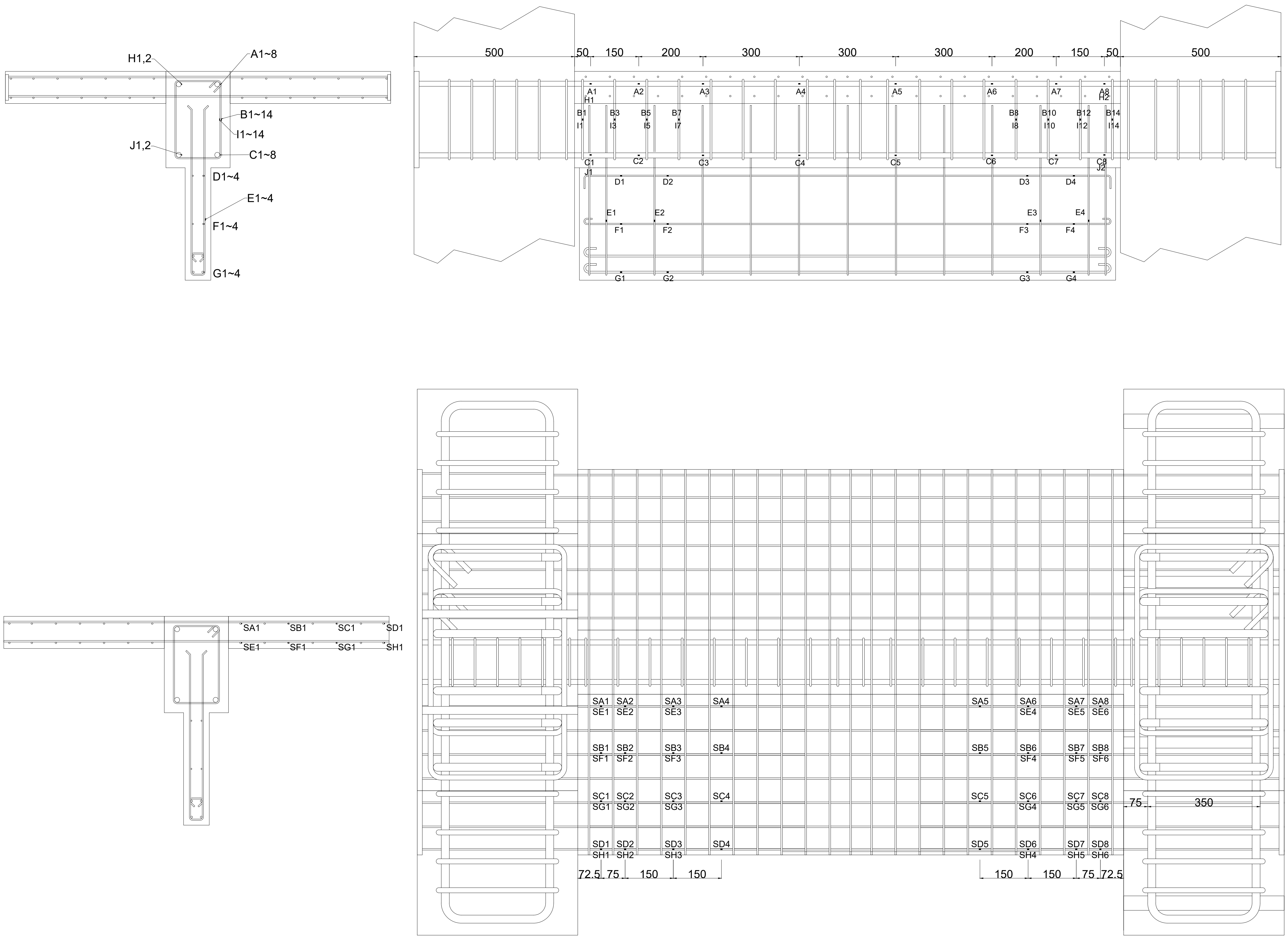

Fig(5.42) Positions of strain gauges attached on reinforcing bars of SP-S5-Slab T

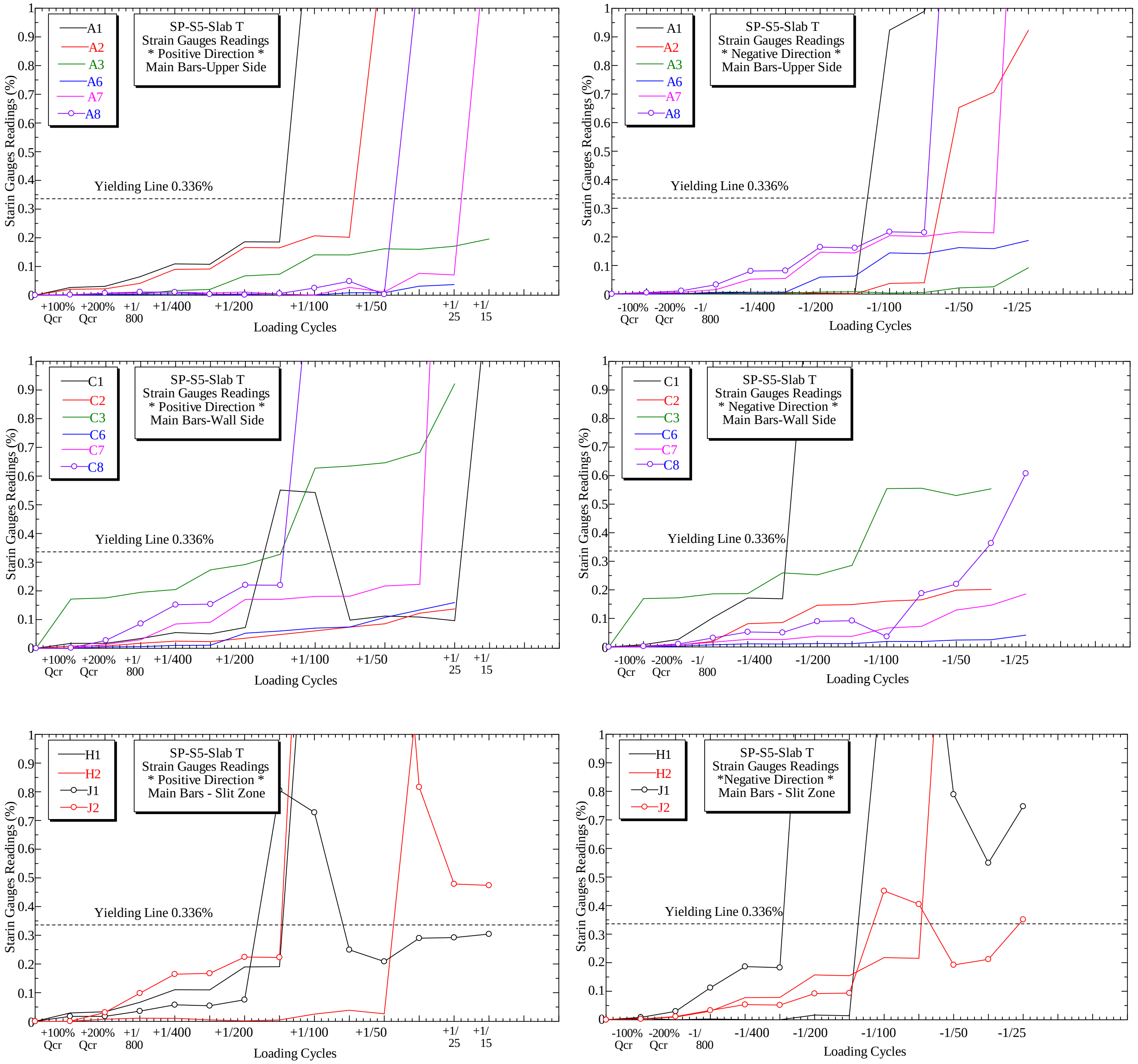

Fig (5.43.a) Readings of strain gauges of SP-S5-Slab T

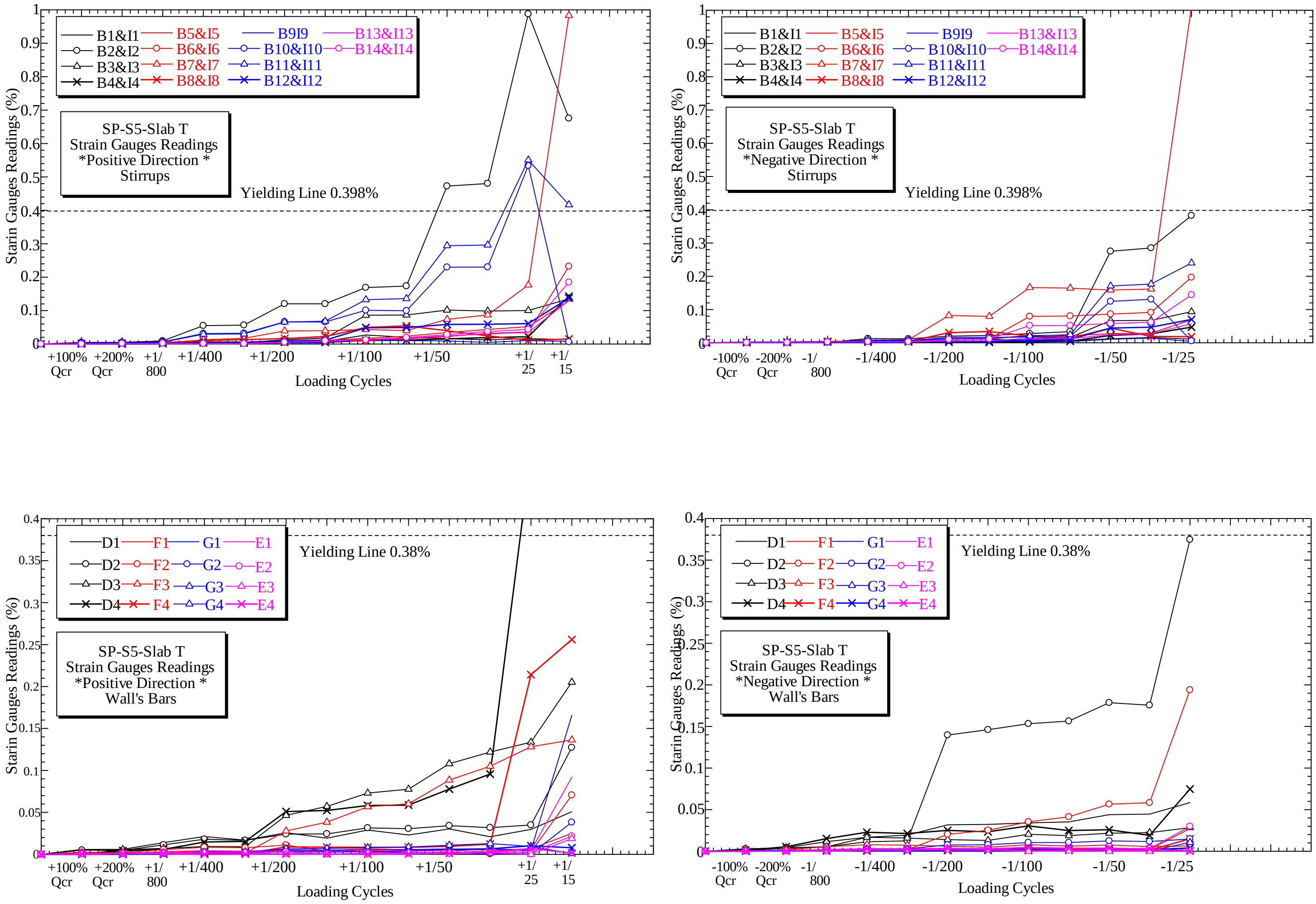

Fig (5.43.b) Readings of strain gauges of SP-S5-Slab T

5.5 Flexural and Shear Deformations

The flexural and shear deformations were able to be measured by using displacement gauges and displacement transducers fixed on the rare face of beam.

The beam was divided into zones, as shown in Figure (5.44) and the deformation were calculated to each zone, individually. Then the summation was calculated.

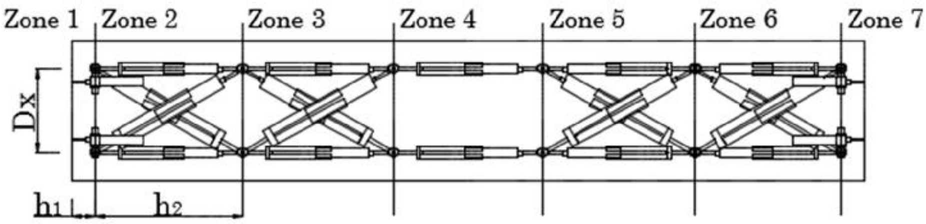

Fig (5.44) Dividing beam to zones to calculate the deformations

5.5.1 Flexural Deformations

The curvature of each zone was determined as the followings:

$$\ddot{}_{i} = \frac{{}_{i}\delta_{m1} - {}_{i}\delta_{m2}}{D_i * h} \qquad \text{Eqn.5.4}$$

The flexural displacement to the first zone at end of beam zone is measured as the following:

$$\delta_{f({}_1h)} = \iint {}_1\ddot{}\ dxdx = \int_0^{{}_1h} \left({}_1\ddot{}\ x\right)dx = \left[{}_1\ddot{}\ \frac{x^2}{2}\right]_0^{{}_1h} = {}_1\ddot{}\ \frac{{}_1h^2}{2} \qquad \text{Eqn. 5.5}$$

For the other zones in middle of beam, second zone:

$$\delta_{f({}_1h+{}_2h)} = \iint {}_1\ddot{}\ dxdx + \iint {}_2\ddot{}\ dxdx$$

$$= \delta_{f({}_1h)} + \int_{{}_1h}^{{}_2h+{}_1h} \left\{ {}_2\ddot{}\left(x - {}_1h\right) + {}_1\ddot{}\ {}_1h \right\} dx = \left[{}_2\ddot{}\ \frac{\left(x-{}_1h\right)^2}{2} + {}_1\ddot{}\ {}_1hx \right]_{{}_1h}^{{}_2h+{}_1h} = \delta_{f({}_1h)} + {}_2\ddot{}\ \frac{{}_2h^2}{2} + {}_1\ddot{}\ {}_1h\,{}_2h + \delta_{f({}_1h)}$$

Eqn.5.6

The total flexural displacement:

$$\delta_f = \delta_{f({}_1h+{}_2h+{}_3h+{}_4h)} + \delta_{f({}_5h+{}_6h+{}_7h)}$$ Eqn.5.7

Where:

$$\delta_{f({}_1h+{}_2h+{}_3h+{}_4h)} = {}_1\ddot{}\ \frac{{}_1h^2}{2} + {}_2\ddot{}\ \frac{{}_2h^2}{2} + {}_1\ddot{}\ {}_1h\,{}_2h + {}_3\ddot{}\ \frac{{}_3h^2}{2} + {}_2\ddot{}\ {}_2h\,{}_3h + {}_4\ddot{}\ \frac{{}_4h^2}{2} + {}_3\ddot{}\ {}_3h\,{}_4h$$

$$\delta_{f({}_5h+{}_6h+{}_7h)} = {}_7\ddot{}\ \frac{{}_7h^2}{2} + {}_6\ddot{}\ \frac{{}_6h^2}{2} + {}_7\ddot{}\ {}_7h\,{}_6h + {}_5\ddot{}\ \frac{{}_5h^2}{2} + {}_6\ddot{}\ {}_6h\,{}_5h$$

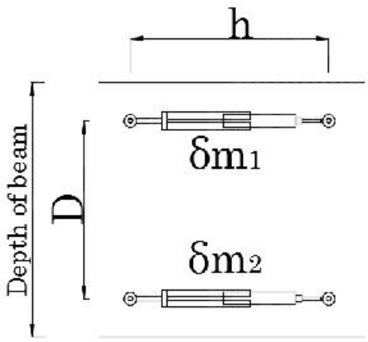

Fig (5.45) Details of calculating the flexural deformation

5.5.2 Shear Deformations

The shear displacements were measured by the inclined gauges, as shown in

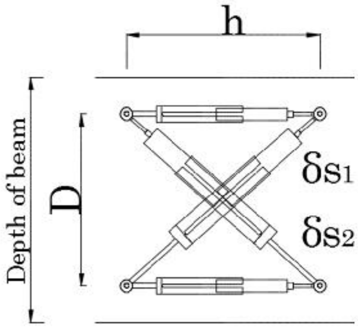

Fig (5.46) Details of calculating the shear deformation

Figure (5.46). The equations used in calculation of shear deformations:

$$(D_x + {}_i\delta_s)^2 + {}_ih^2 = \left(\sqrt{D_x^{\,2} + {}_ih^2} + {}_i\delta_{s1}\right)^2 \qquad \text{Eqn.5.8}$$

$$(D_x - {}_i\delta_s)^2 + {}_ih^2 = \left(\sqrt{D_x^{\,2} + {}_ih^2} + {}_i\delta_{s2}\right)^2 \qquad \text{Eqn.5.9}$$

$$4D_x \cdot {}_i\delta_s = \left(2\sqrt{D_x^{\,2} + {}_ih^2} + {}_i\delta_{s1} + {}_i\delta_{s2}\right)\left({}_i\delta_{s1} - {}_i\delta_{s2}\right) \qquad \text{Eqn.5.10}$$

$${}_i\delta_s = \frac{\sqrt{D_x^{\,2} + {}_ih^2}}{2D_x}\left({}_i\delta_{s1} - {}_i\delta_{s2}\right) \qquad \text{Eqn.5.11}$$

And total shear deformation will be:

$$\delta_s = {}_2\delta_s + {}_3\delta_s + {}_4\delta_s + {}_5\delta_s \qquad \text{Eqn.5.12}$$

Figures (5.47), (5.48) and (5.49) show the flexural and shear deformations of studied beams.

Shear deformations are larger than flexural deformations in case of:

SP-S5 and SP-S6 corresponded with the failure of these beams which is shear failure.

For the other beams, the flexural deformations are close to the shear deformation before touching where the failure is flexural failure.

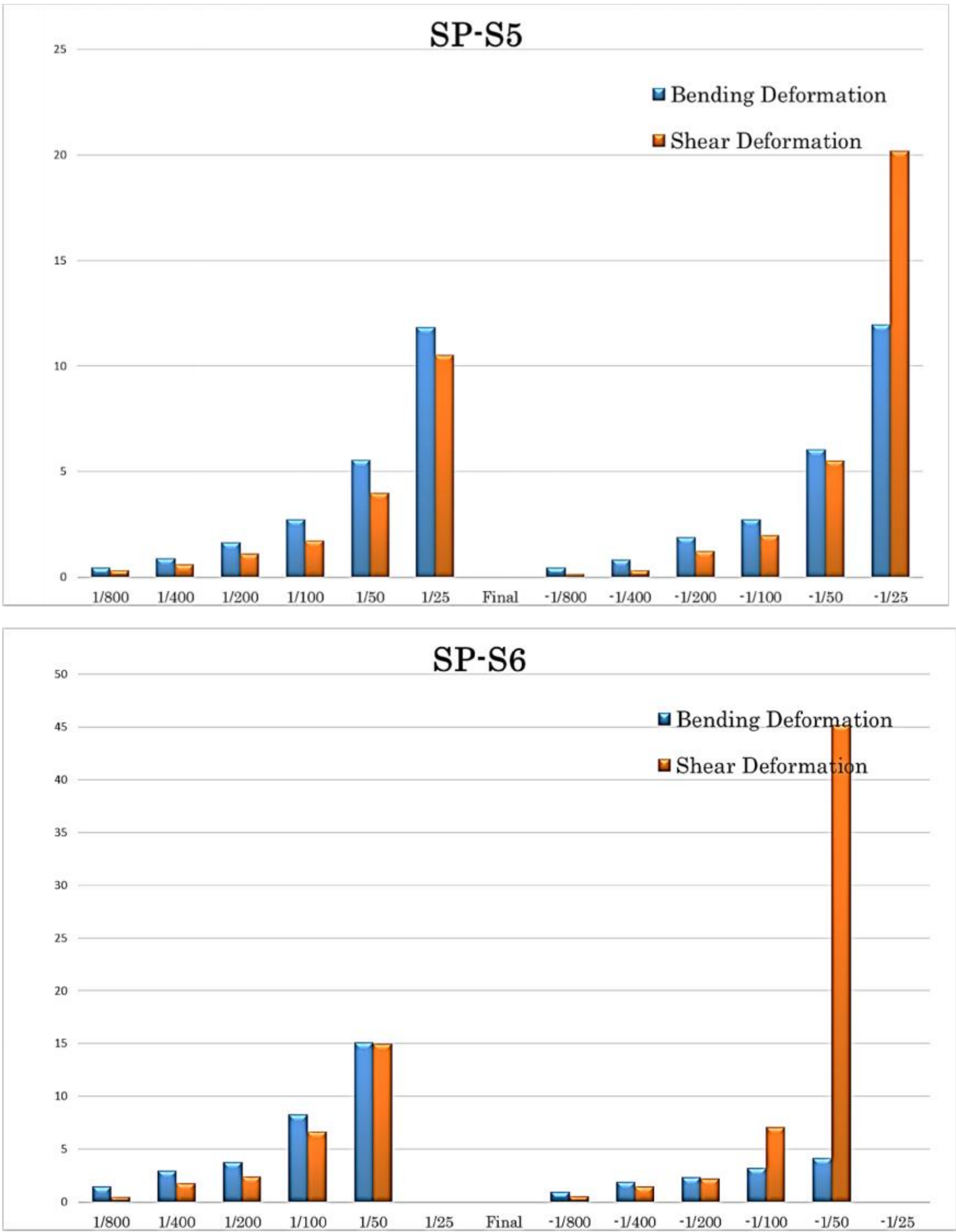

Fig (5.47) Flexural and shear deformations of SP-S5 and SP-S6

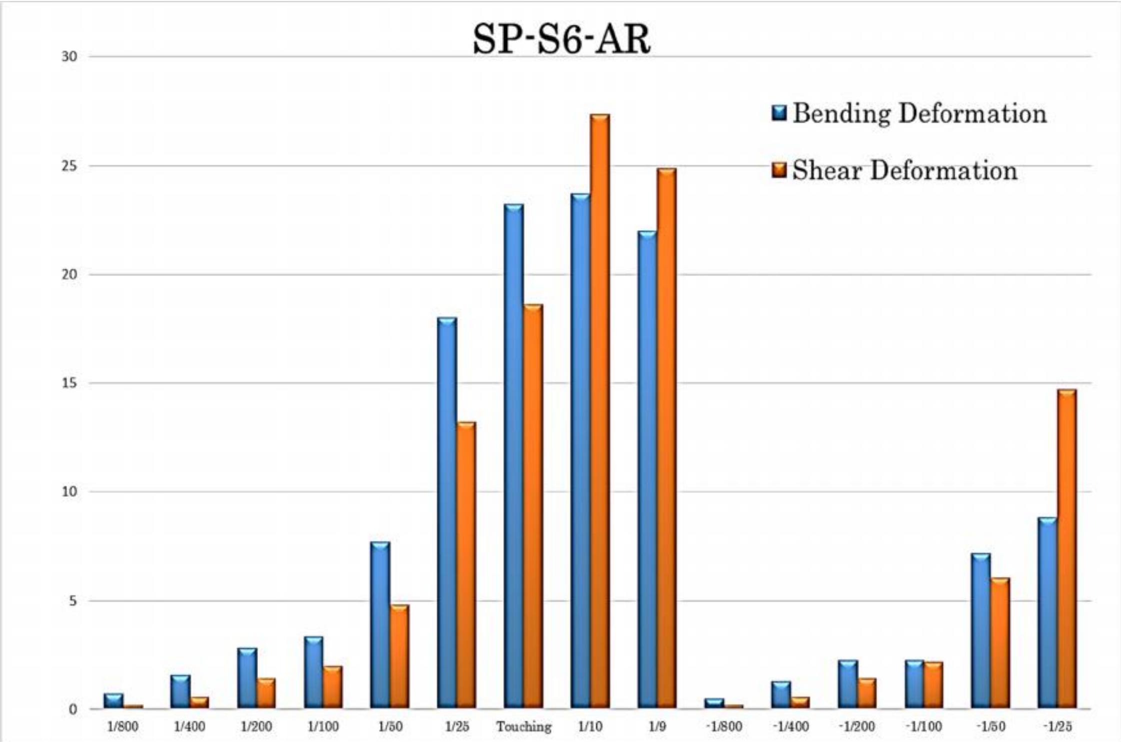

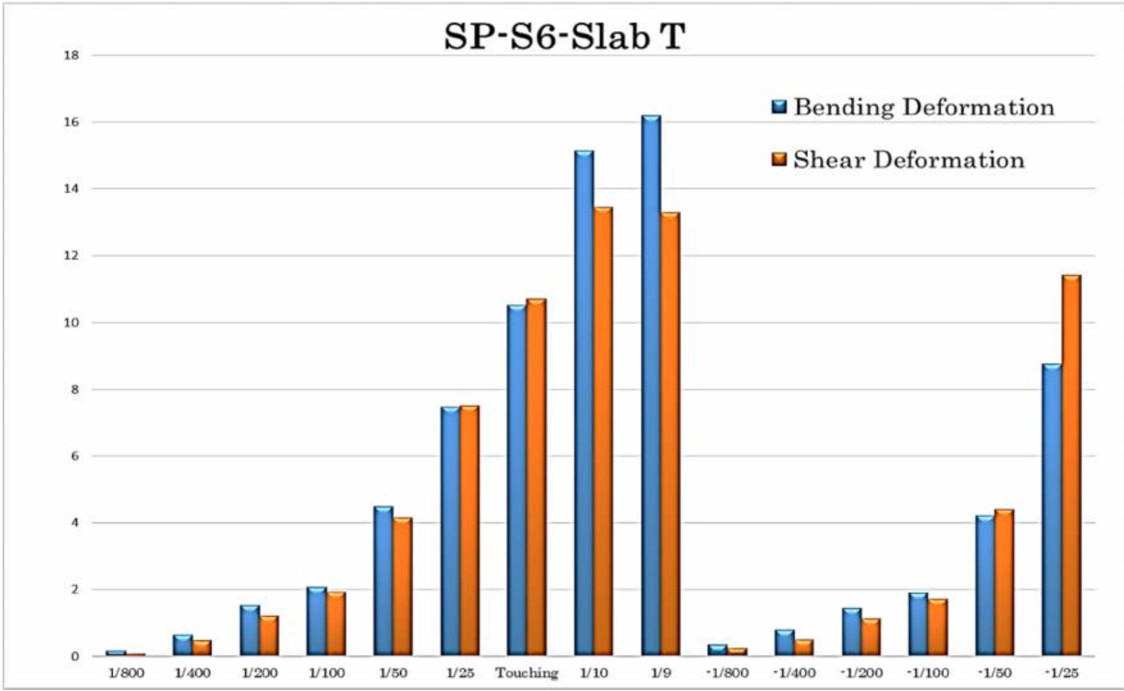

Fig (5.48) Flexural and shear deformations of SP-S6-AR and SP-S6-Slab T

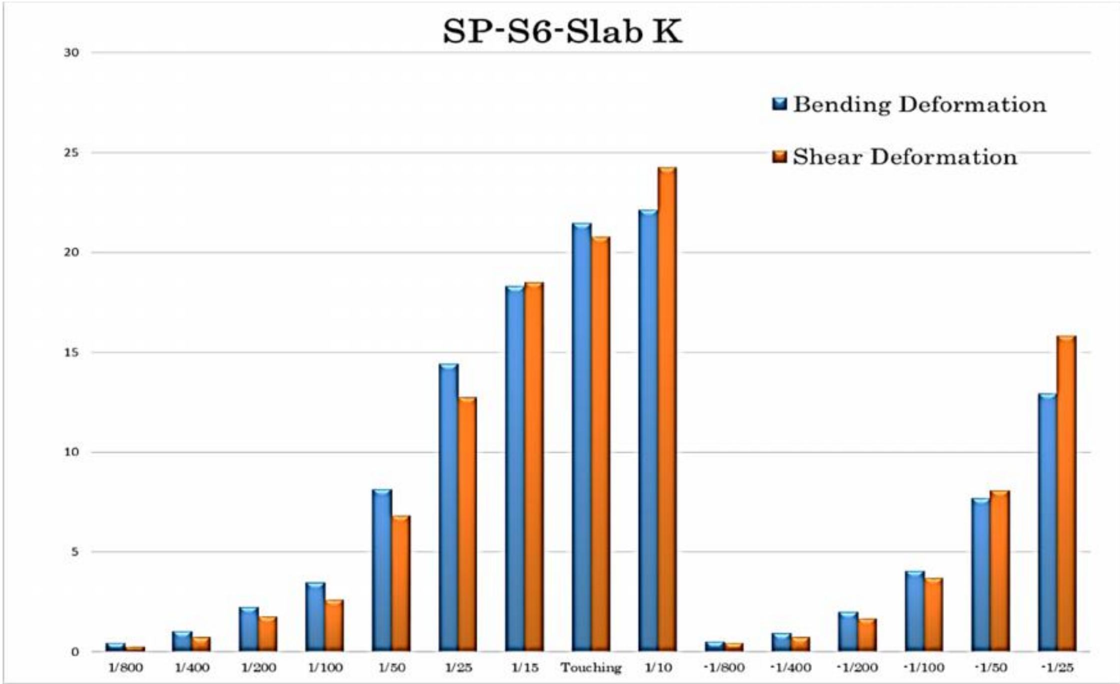

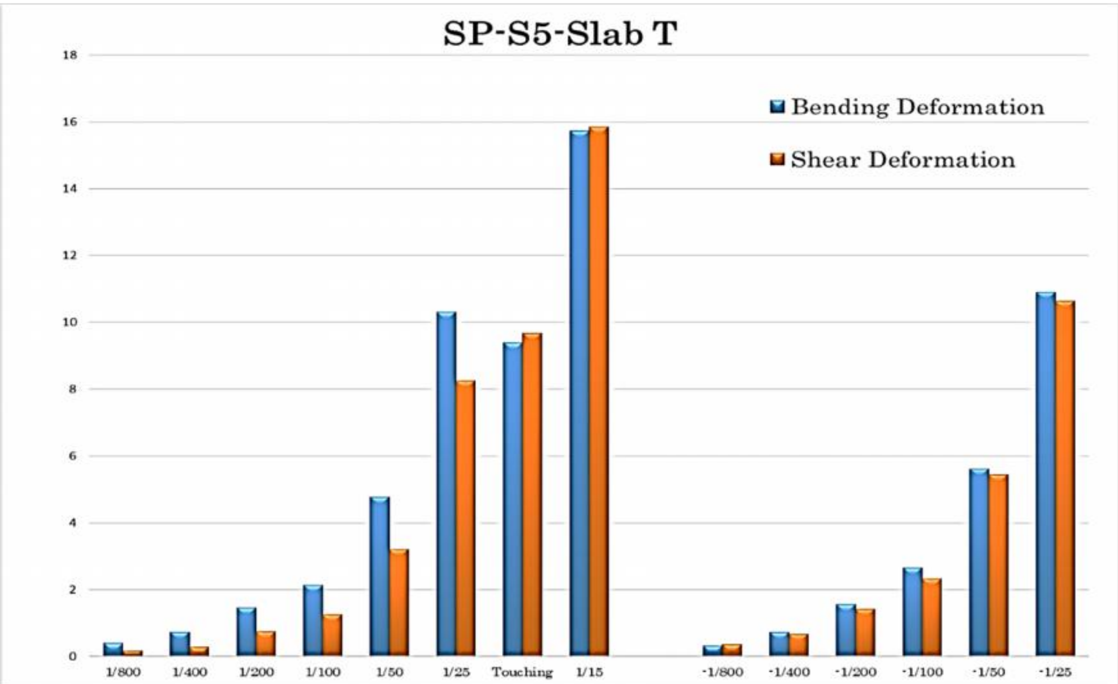

Fig (5.49) Flexural and shear deformations of SP-S6-Slab K and SP-S5-Slab T

5.6 Energy Dissipation and the Equivalent Damping Factor

One of the most important aspects of structural performance under seismic loading is the ability of the structure to adequately dissipate energy. The energy dissipated by the beams is taken as the area enclosed by the load-deflection curves. Though there are several criteria for evaluating beam performance, such as total number of cycles and rate of degradation, dissipation has been used most often. Hence, an evaluation of beam performance is first made based on the measured energy dissipation.

Figures (5.50) and (5.51) show the energy dissipation amount of each beam.

Figures (5.52) and (5.53) show the equivalent damping factor of each beam.

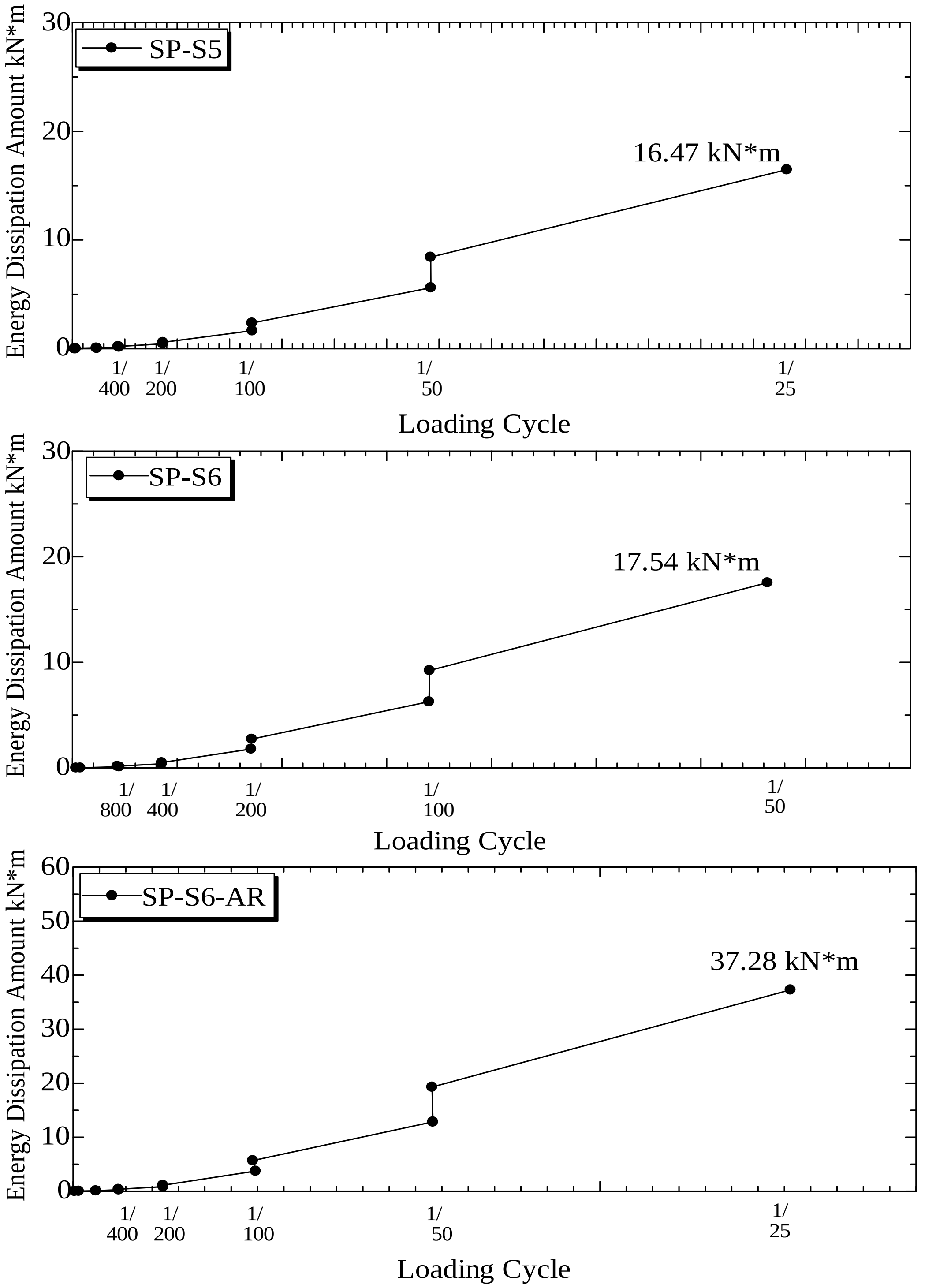

Fig (5.50) Energy dissipation amount of SP-S5, SP-S6 and SP-S6-AR

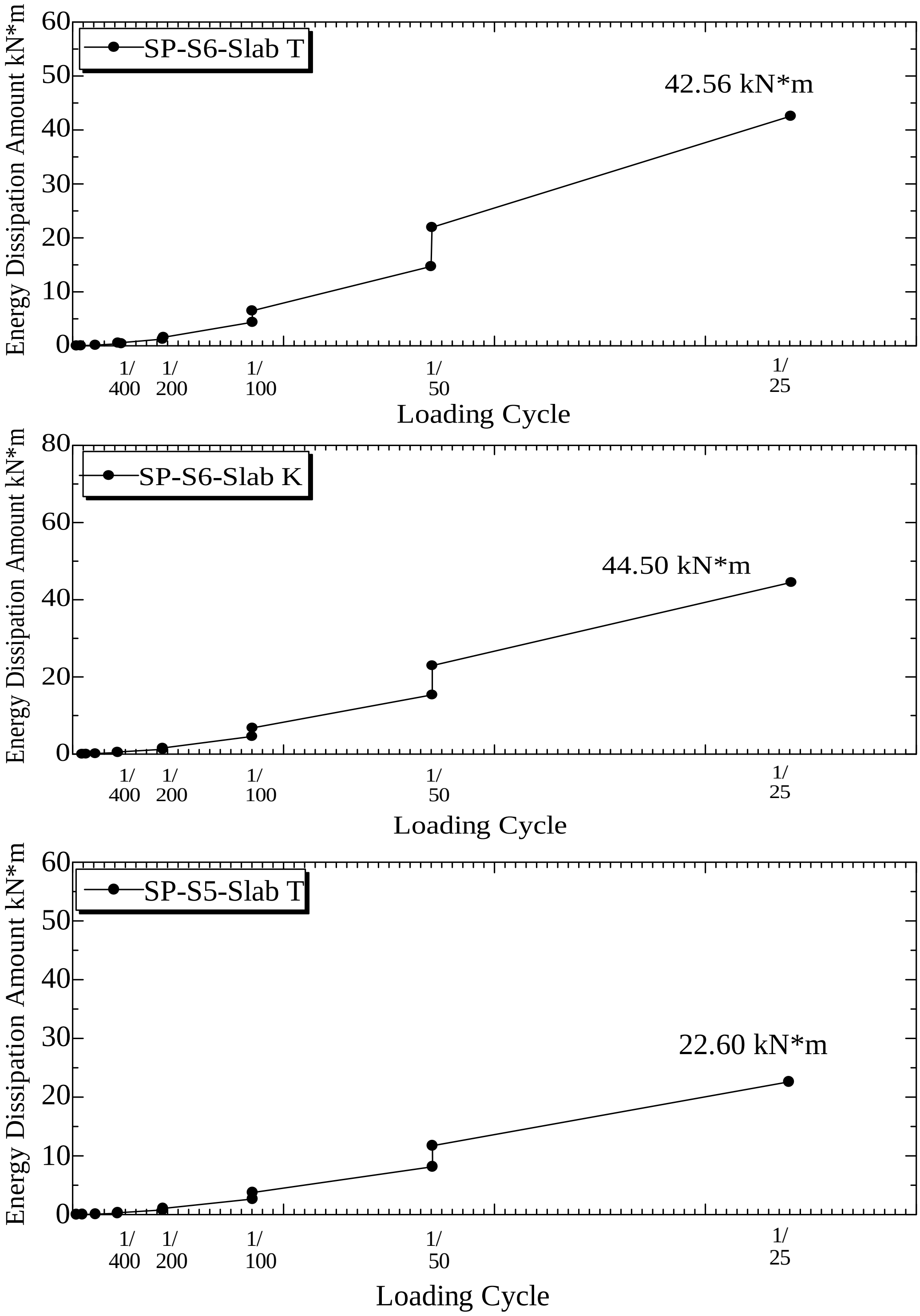

Fig (5.51) Energy dissipation amount of SP-S6-Slab T, SP-S6-Slab K and SP-S5-Slab T

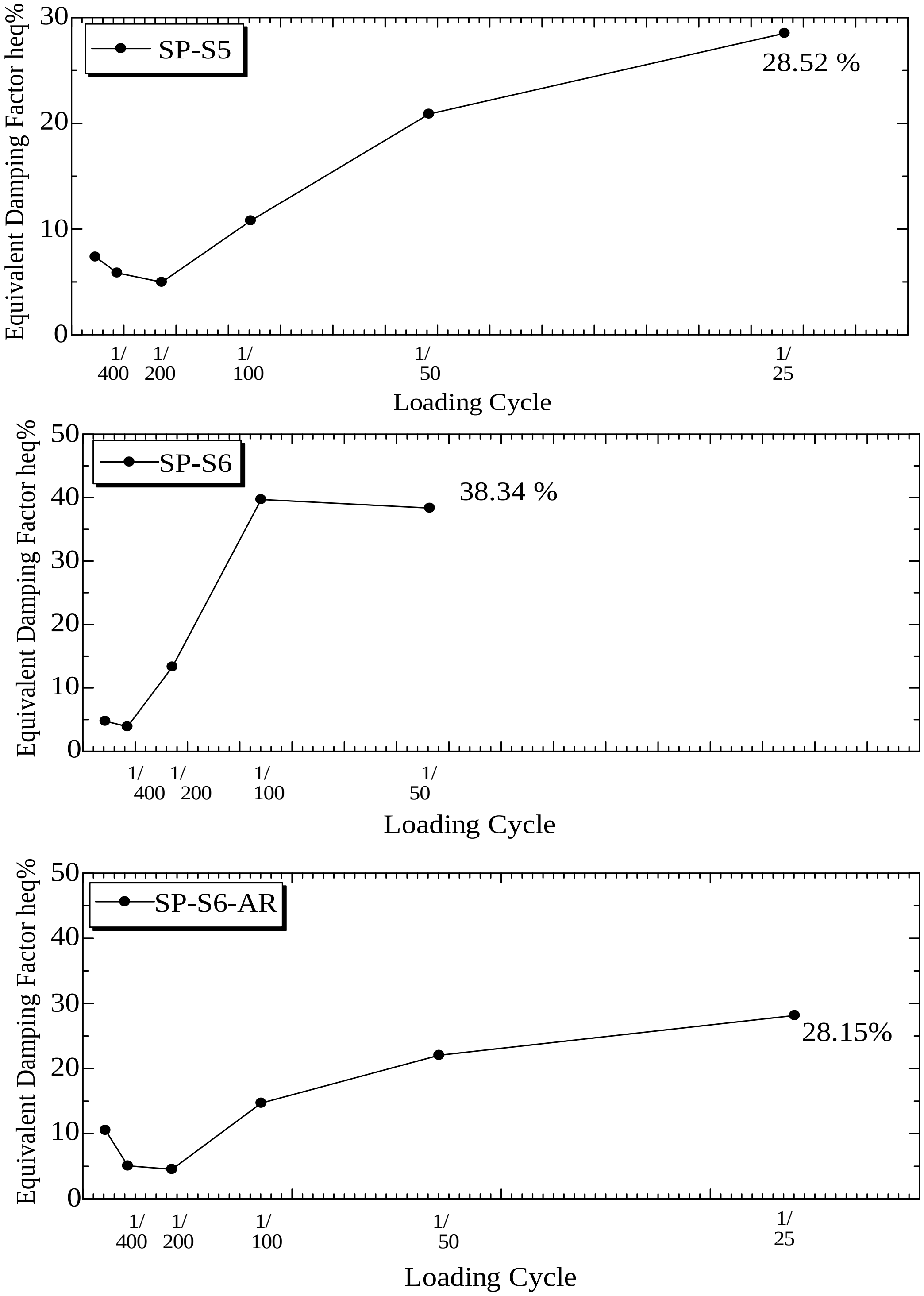

Fig (5.52) Equivalent damping factor of SP-S5, SP-S6 and SP-S6-AR

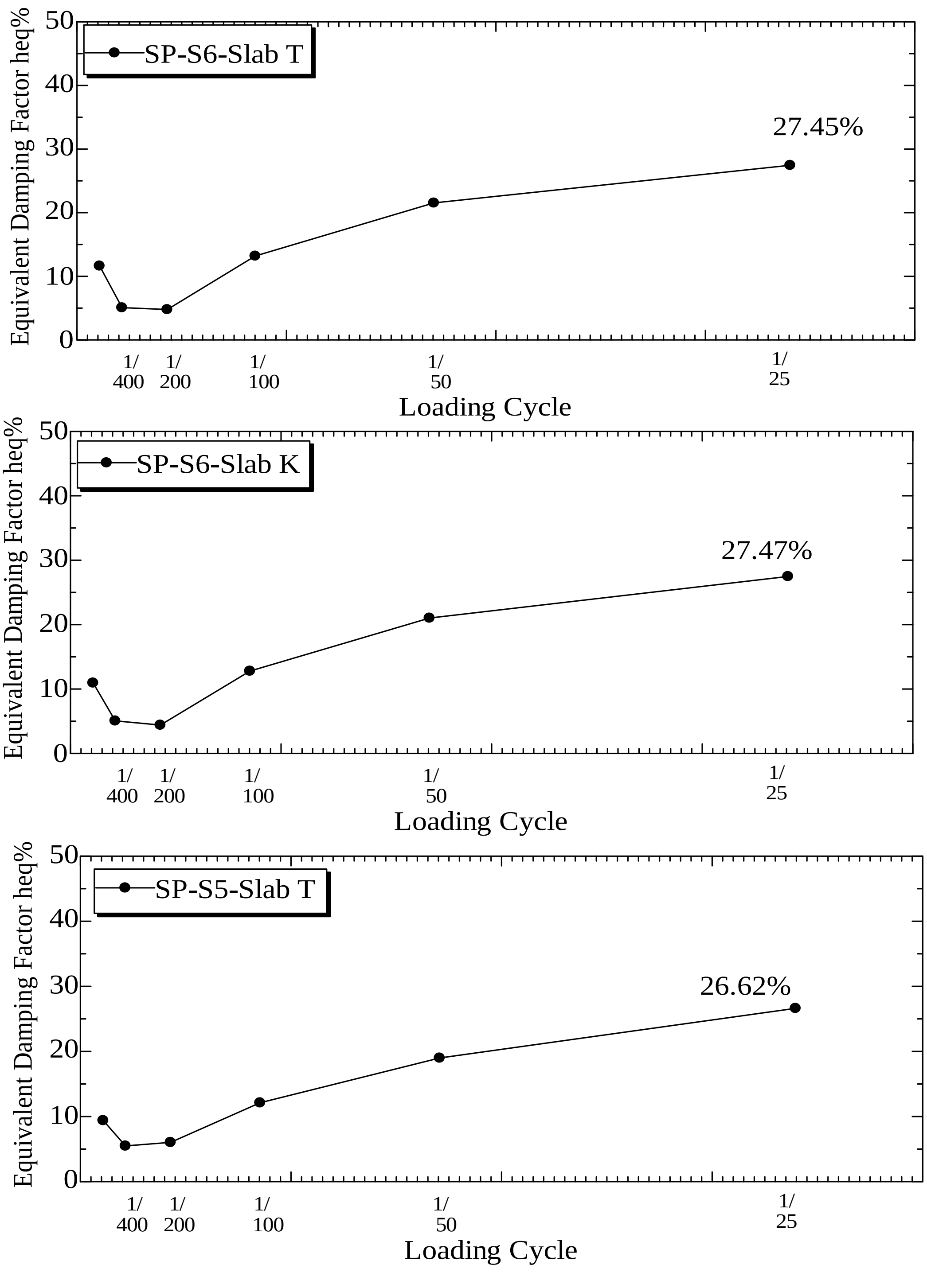

Fig (5.53) Equivalent damping factor of SP-S6-Slab T, SP-S6-Slab K and SP-S5-Slab T

5.7 Shear Cracks Investigation

5.7.1 Shear Cracks Characteristics

There are two types of shear cracks; shear cracks form diagonally in the body of structural member and cracks form as flexural cracks and then extend as diagonal shear cracks. The former is called shear cracks and the latter is called flexural-shear cracks.

There are many parameters effect on the shear cracks in RC beams and they were studied in previous researches as the following:

1)- The amount and arrangement of reinforcement at side face of beams were studied(17 ,18). The studied specimens were large size beams and controlling the flexural and shear cracks was studied. It was found out that the width of shear crack is higher than the width of flexural crack in the beams with 90 degree stirrups. Because the diagonal tensile stresses in the body of beam are higher than the tensile stresses in the longitudinal bars. In addition, because of the angle between the 90 degree stirrups and the diagonal shear cracks in the body of beam. In addition, the width of shear crack in case of beams with vertical stirrups is higher than beams with inclined stirrups in same conditions.

2)- The thickness of concrete cover was studied briefly (19,20).

3)- The influence of beam size was studied(21,22) by studying the shear-span ratio. It was found that beam size has an effect on the shear strength and failure mode of beam where the shear strength will decrease by increasing the depth of beam. And the spacing between the shear cracks in beam body will increase by increasing the size of beam (23,24,25).

4)- Amount of the longitudinal bars was studied(26,27,28). It was found that the longitudinal bars in the beam have an effect on the widening of shear cracks.

5)- Shear cracks widening was studied(29,30,31,32,33,34). It was found that widening of shear cracks is caused by many manners; elongation of horizontal and vertical legs of stirrups and slipping off the hook of stirrups.

5.7.2 Shear Cracks Angle

Shear cracks angles were marked and measured at each of the experimental works, as shown in Figure (5.54).

Table (5.5) shows the detailed values about the shear cracks angles and cracks projection.

Table 5.5 Shear cracks angles and shear reinforcement

Beam	SP-S5	SP-S6	S6-AR	S6-T	S6-K	S5-T
Projection	1.0	0.67	0.58	0.66	0.83	0.79
θ	45.00	34.00	30.43	33.52	40.00	38.33
τ	1.0	1.57	1.56	1.71	1.73	1.18
A_w	D4@70	D6@50	D6@35	D6@40	D6@40	D6@100
P_w%	0.20	0.64	0.91	0.79	0.79	0.32
Qsu/Qu	1.3	1.37	1.44	1.22	1.26	1.22

Where:

θ: Shear crack angle (rad), τ :Design shear stress(*N/mm²*),

A_w: Sectional area of stirrups (*mm²*), and P_w: Shear reinforcement ratio (*%*).

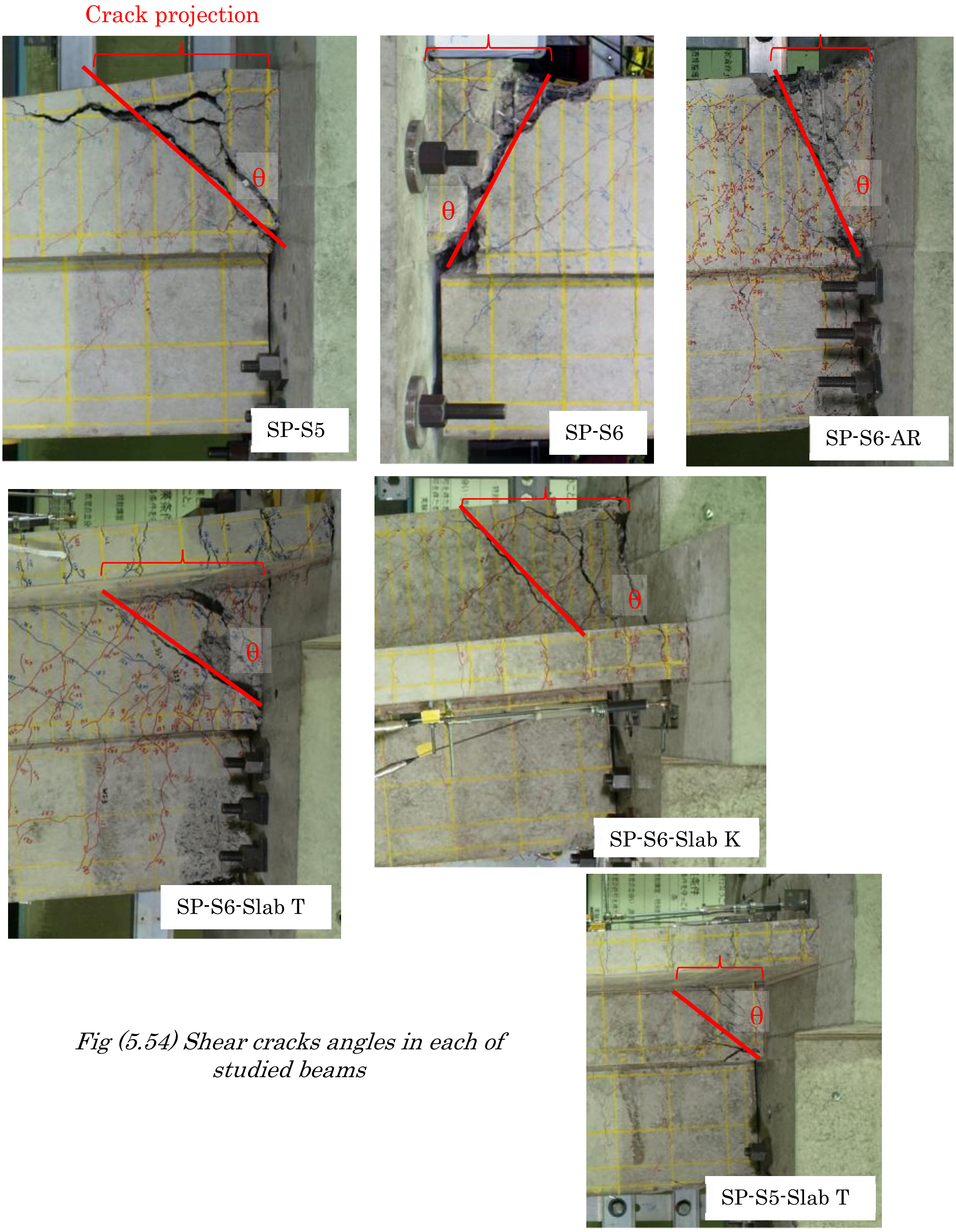

Fig (5.54) Shear cracks angles in each of studied beams

CHAPTER 6
THE ANALYTICAL STUDY

- Introduction
- Objective of the Analytical Study
- Modeling of Materials
- Details of the Analytical Study
- The Analytical Results

6.1 Introduction

The finite element method (FEM) can be considered as advanced step into accurate design and understanding of the structures in all different fields of life. Using the computers reinforces the finite element method by the speed and accuracy of calculations which makes the FEM essential and very helpful.

6.2 Objective of the Analytical Study

The main purpose of the current analytical study is to get the background of stresses distribution in the beam with non-structural walls. Which is needed strongly in the next step of research, the STM study.

6.3 Modeling of Materials

6.3.1 Concrete

The concrete was modeled using total strain model of cracks that are classified to the total strain model of distributed cracking model.

Total strain of crack model is divided into fixed crack model and rotation crack model, as shown in Figure (6.1).

In the fixed crack model, the axis of crack is determined once. And in the rotating crack model, the direction of crack rotates according to the changing of principle strains. The former was adopted in the analytical study.

Concrete before cracking has an isotropic properties, but it has anisotropic features since the cracking. The program deals with the characteristics of the later cracked concrete as orthotropic. Consequently, calculating the normal stress and shear stress from the cracked surface.

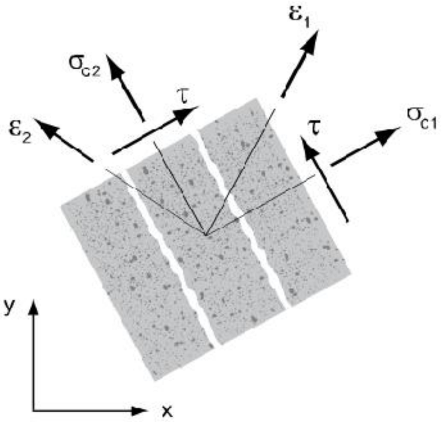

Fig. (6.1.a) Fixed crack model

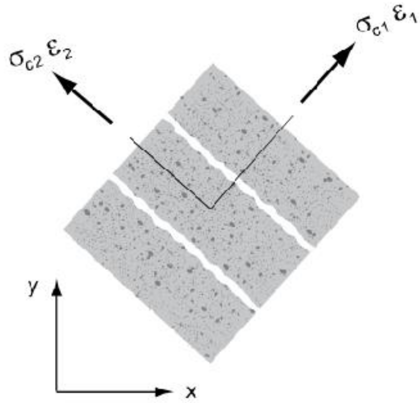

Fig. (6.1.b) Rotating crack model

Fig (6.1) Types of total strain of crack model

The following values should be defined for cracking analysis of total strain:

- Crack model type, fixed or rotating crack model,
- Mechanical properties of concrete, tensile behavior, compressive behavior, shear behavior, and horizontal crack effect.

These properties can be entered directly as numerical values from the user or using the values proposed in the standards. For instance, Young's modulus, Poisson's coefficient, tensile strength and compressive strength.

6.3.1.1 Compression Model of Total Strain Crack Model

Figure (6.2) shows the compression models of concrete provided in the software. And Thorenfeldt model was adopted in the analytical study.

Figure (6.3) shows the adopted strength curve of Thorenfeldt. And the curve equation(35) is as the following:

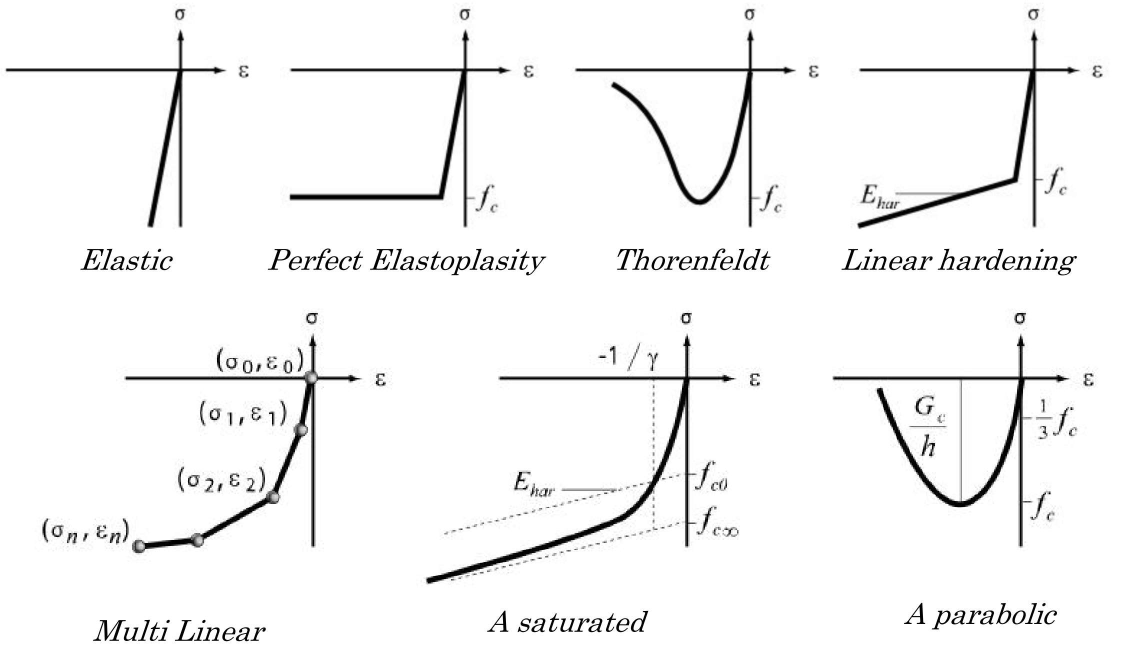

Fig (6.2) Compression models

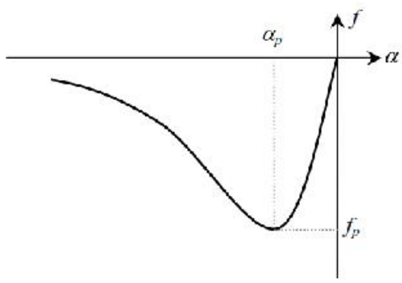

Fig (6.3) Thorenfeldt compression strength curve[35]

$$f = -f_p \frac{\alpha_i}{\alpha_p}\left(\frac{n}{n-1+\left(\frac{\alpha_i}{\alpha_p}\right)^{nk}} \right) \qquad \text{Eqn.6.1}$$

Where:

$n = 0.80 + \frac{f_{cc}}{17}$, F_{cc}: Compressive strength of concrete.

k=1 if $0 > \alpha > \alpha_p$, and $k = 0.67 + \frac{f_{cc}}{62}$ if $\alpha <= \alpha_p$.

6.3.1.2 Tensile Model of Total Strain Crack Model

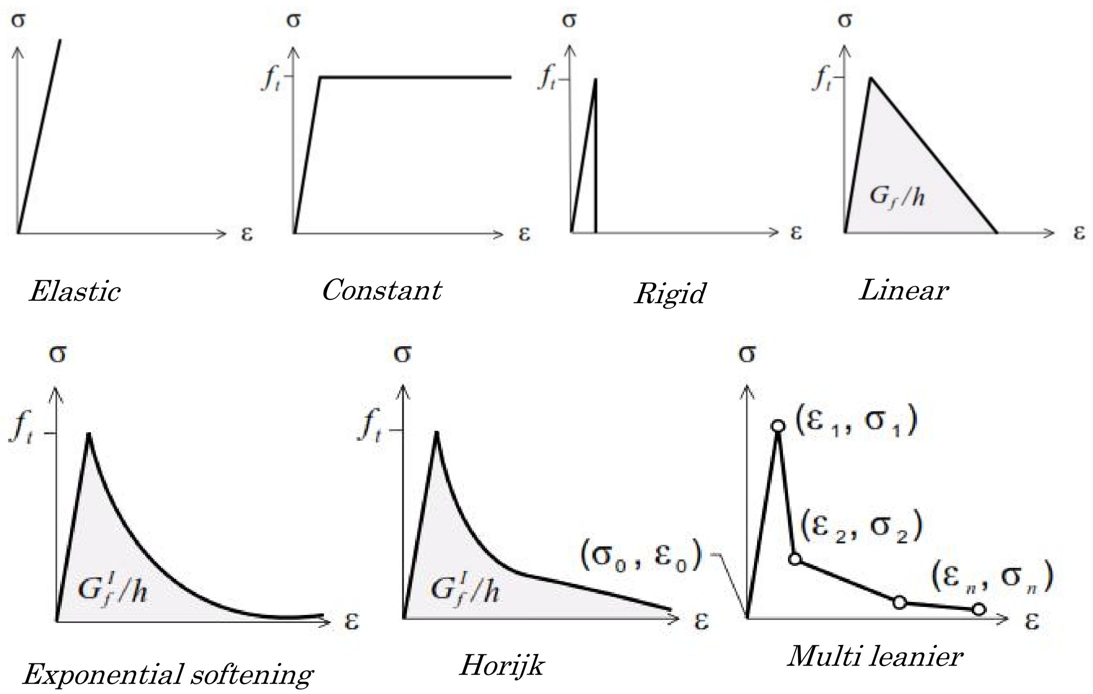

Fig (6.4) Tensile Models

Figure (6.4) shows the tension models (36,37,38) of concrete provided in the software. And Hordijk model was adopted in the analytical study.

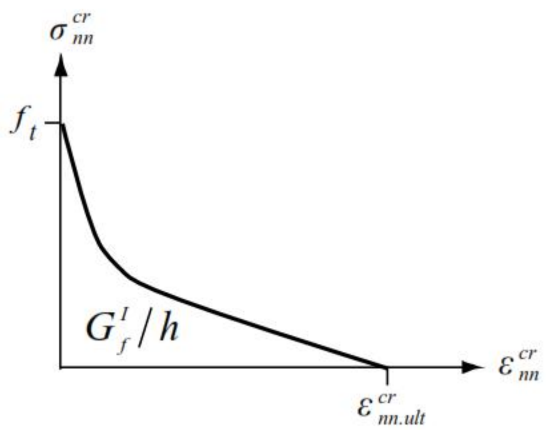

Fig (6.5) Hordijk tensile strength curve (37)

Figure (6.5) shows the adopted strength curve of Hordijk.

Fracture energy of concrete is calculated by the equation below:

$$G_f = G_{f0}\left(\frac{f_{cm}}{f_{cm0}}\right)^{0.7} \qquad \text{Eqn.6.2}$$

Where:

G_{f0} is calculated depending on the maximum size of aggregates, as shown in Table (6.1).F_{cm0}: is taken 10 *N/mm²*.

Table 6.1 Fracture energy of concrete

D_{max}(mm)	G_{f0}(J/m^2)
8	25
16	30
32	58

6.3.2 Reinforcing Bars

The reinforcing bars are consider as 1D elements, and there are two type of axial streeses are applied on the section of the reinforcement, tension and compression.

Bilinear Stress-Strain curve is used for modeling the reinforcement bars as shown in Figure (6.6).

The yield strength of steel bars is the main input data which is determined from the experimental tensile tests of samples of the steel bars.

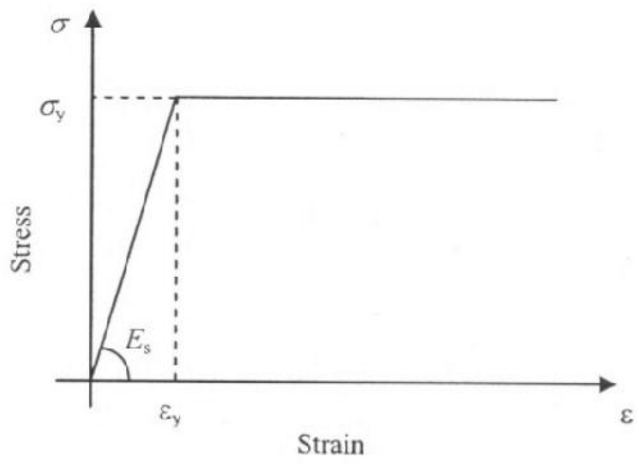

Fig (6.6) Bilinear Curve for modelling the reinforcing bars

6.4 Details of the Analytical Study

Meshing size of the model is 20 X 20 mm for the sections of wall and beam, and 50 mm for longitudinal mesh size of specimen except at the gaps which the size is half of gap width, 7.5 mm for SP-S5 and SP-S6 and 12.5 in case of SP-S6-AR. Figure (6.7) shows the mesh size of SP-S5 as an example.

Meshing size of the reinforcing bars is 20 mm as 1D elements.

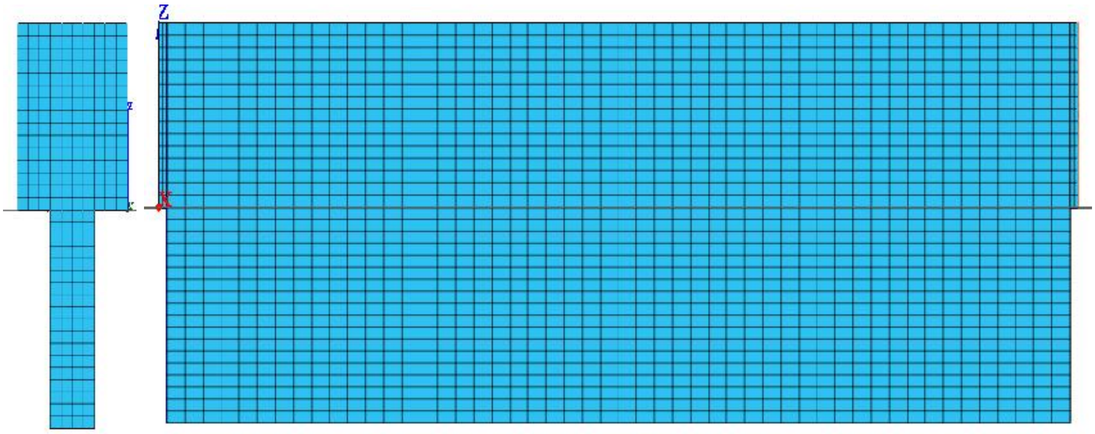

Fig (6.7) Mesh size of the analytical model

The weight of upper support is added as surface compression pressure on the same face of specimen where the specimen was placed vertically during the experimental work. Adopted models of concrete material are Thorenfeldt for compression and Hordijk for tension.

The mechanical properties of concrete and reinforcing bars were provided from the experimental tests of materials as explained previously in chapter of material properties.

Push-over analysis was done, and the maximum lateral displacement is the same of displacement of touching point between the wall and the stub, because the data will not be correct after the touching. Where it is (15*1700/350 ≈ 72 mm for SP-S5 and SP-S6, and 25*1700/350 ≈ 121 mm for SP-S6-AR.

End “A”, was modeled as fixed support.

End “B”, was modeled with: no rotation allowed and displacements allowed in axial direction and lateral displacement direction.

The arrow refers to the lateral displacement direction.

As shown in Figure (6.8), Z-direction is the lateral displacement direction and end “B” not allowed to move in X-direction.

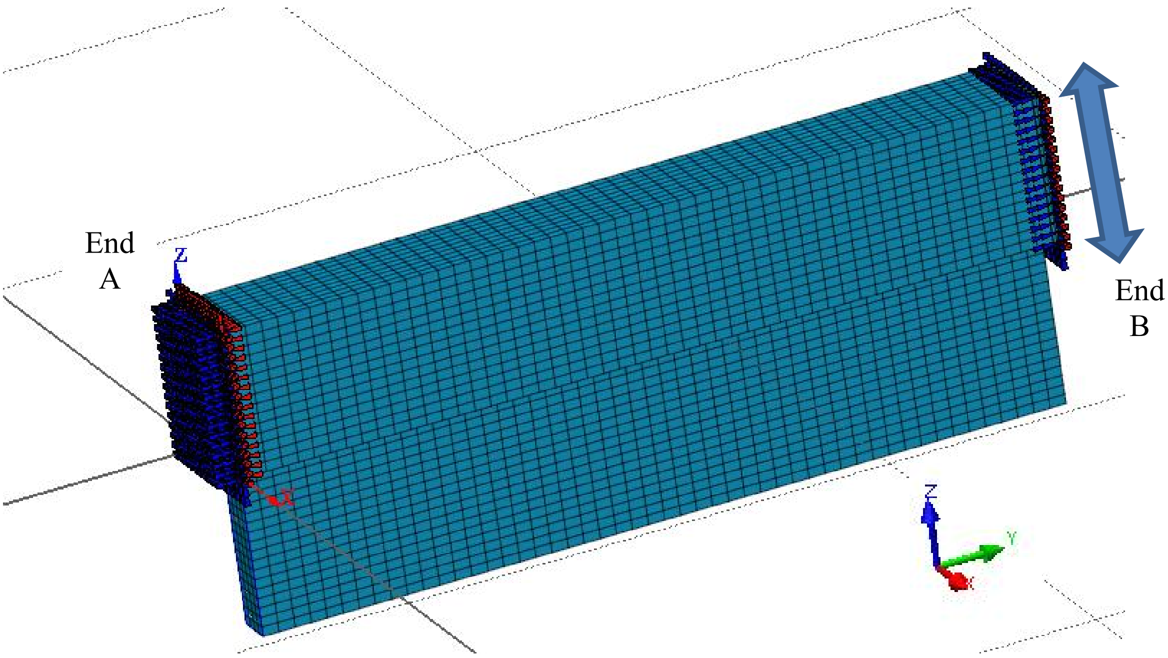

Fig (6.8) Loading direction and movement conditions of the two ends of specimen

6.5 The Analytical Results

6.5.1 Cracks Patterns

There is a correspondence between the cracks pattern analytically and the cracks pattern experimentally for each of specimens at end of experiment, SP-S5, Sp-S6 and Sp-S6-AR. As shown in Figures (6.9), (6.10)and (6.11).

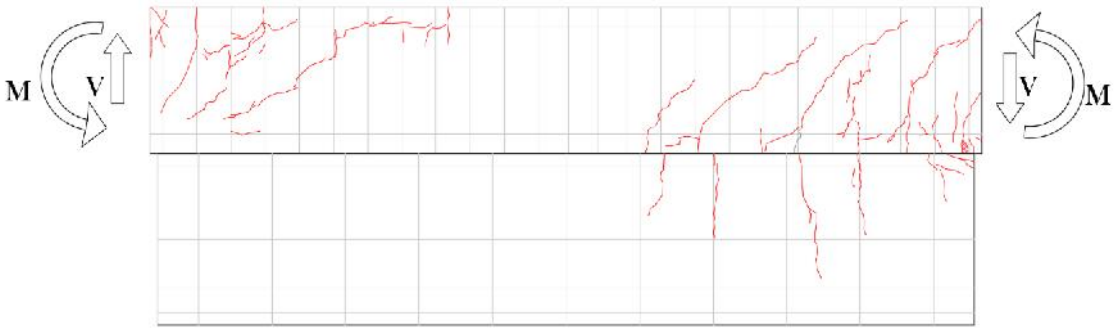

Fig (6.9.a) Experimental cracks pattern of SP-S5 for loading direction same to the analytical study

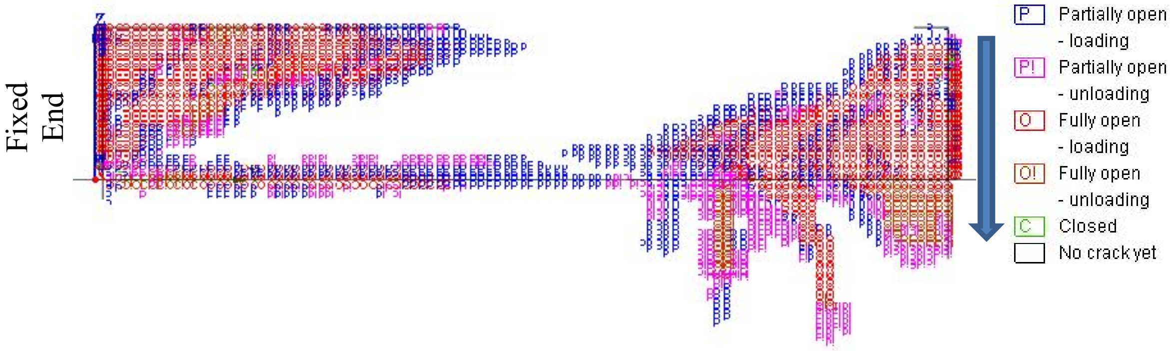

Fig (6.9.b) Analytical cracks pattern of SP-S5

Fig (6.9) Correspondence between the analytical cracks pattern and experimental cracks pattern of SP-S5

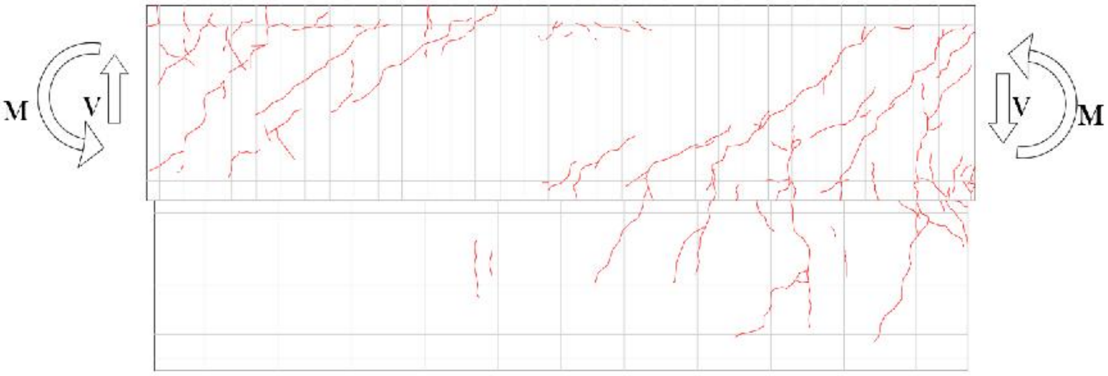

Fig (6.10.a) Experimental cracks pattern of SP-S6 for loading direction same to the analytical study

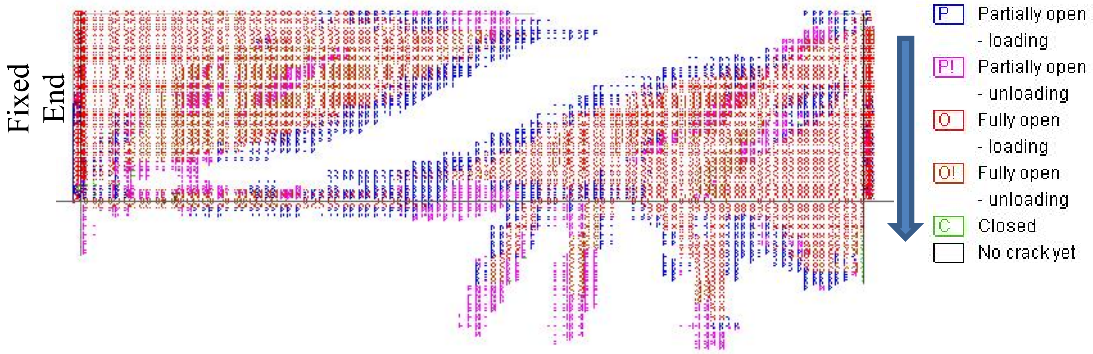

Fig (6.10.b) Analytical cracks pattern of SP-S6

Fig (6.10) Correspondence between the analytical cracks pattern and experimental cracks pattern of SP-S6

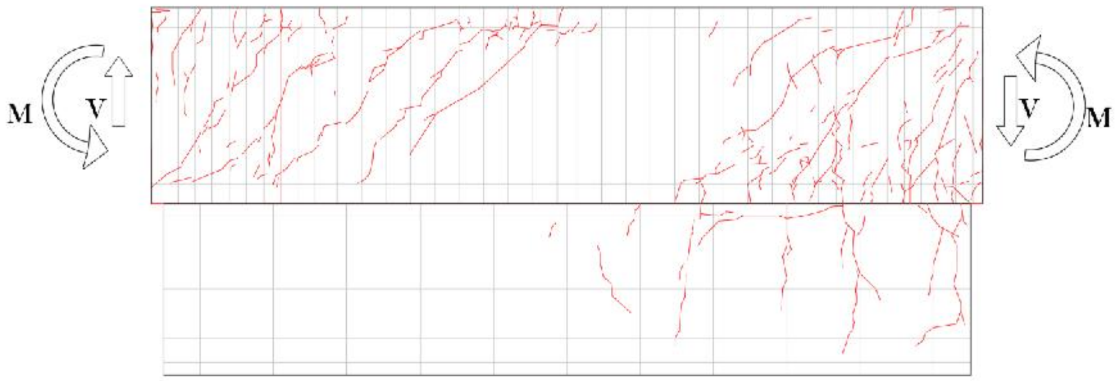

Fig (6.11.a) Experimental cracks pattern of SP-S6-AR for loading direction same to the analytical study

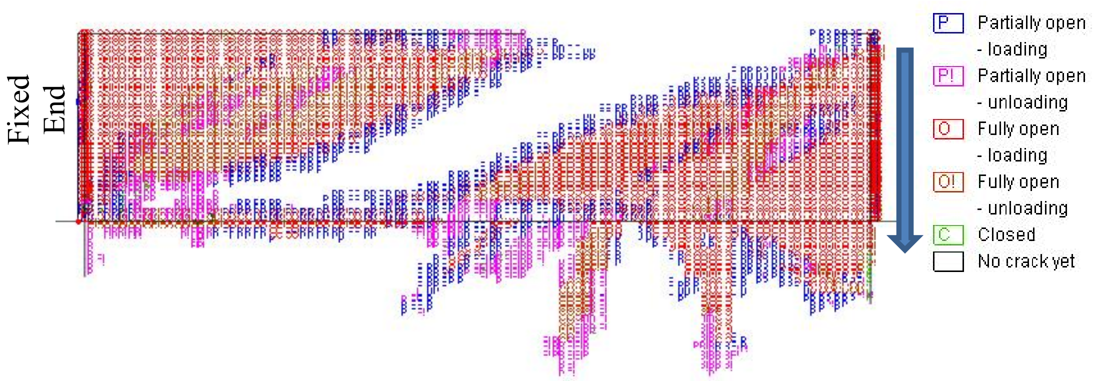

Fig (6.11.b) Analytical cracks pattern of SP-S6-AR

Fig (6.11) Correspondence between the analytical cracks pattern and experimental cracks pattern of SP-S6-AR

6.6.2 Shear Force and Lateral Displacement

The analytical and experimental Q and Displacement curves were illustrated in Figure (6.12) to each of SP-S5, SP-S6 and SP-S6-AR.

Yielding points positions of longitudinal bars and stirrups were shown on the figure.

Yielding of stirrups occurred before the longitudinal bars in SP-S5 in both analytical and experimental results.

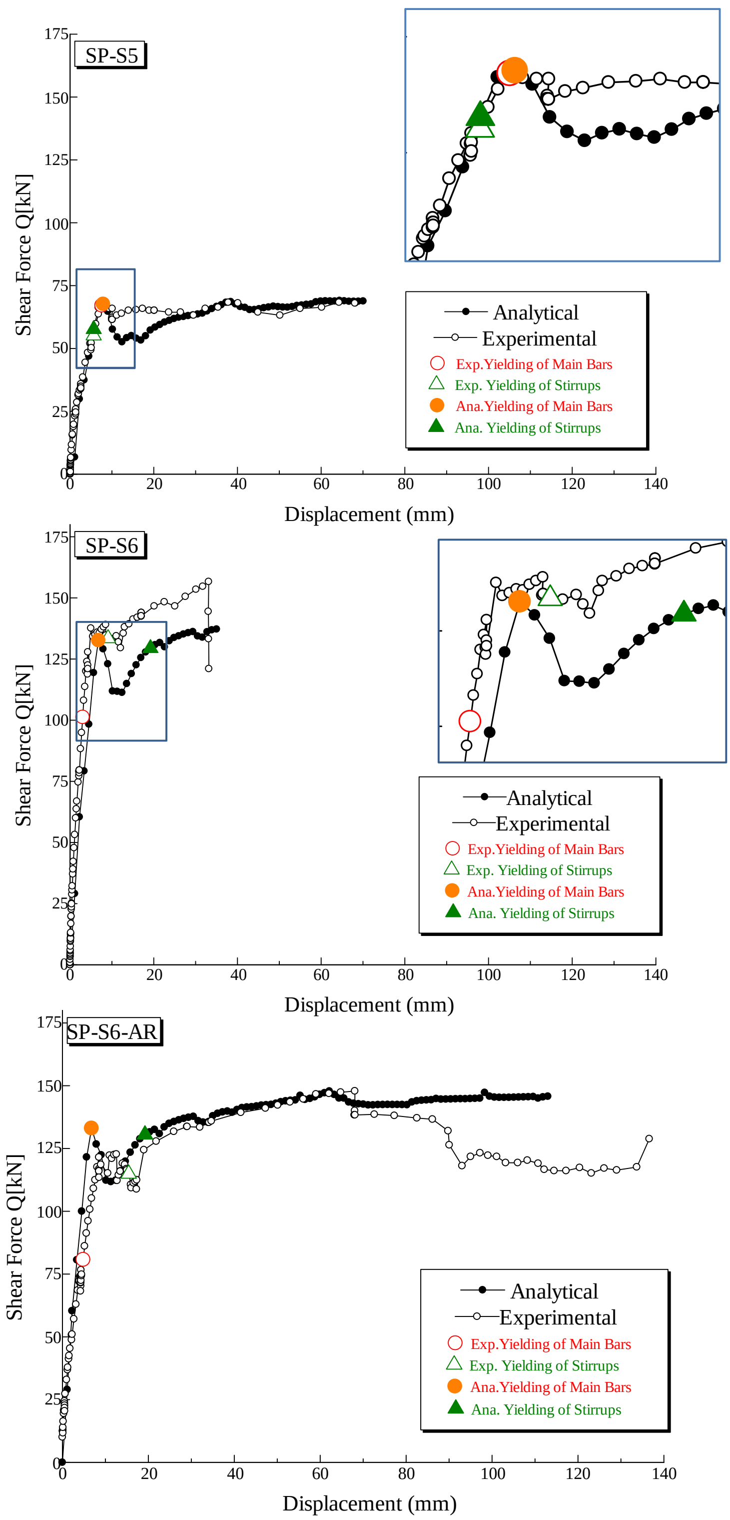

Fig (6.12) Q and Displacement analytically and experimentally

6.6.3 Tensile Stresses of Stirrups

By investigation the tensile stresses in the stirrups of each of specimens studied analytically, it is obvious that the tensile stresses were higher in the stirrups at end where the shear force direction toward the face of beam not toward the non-structural wall, as shown if Figure (6.13).

The arrows refer to the loading direction.

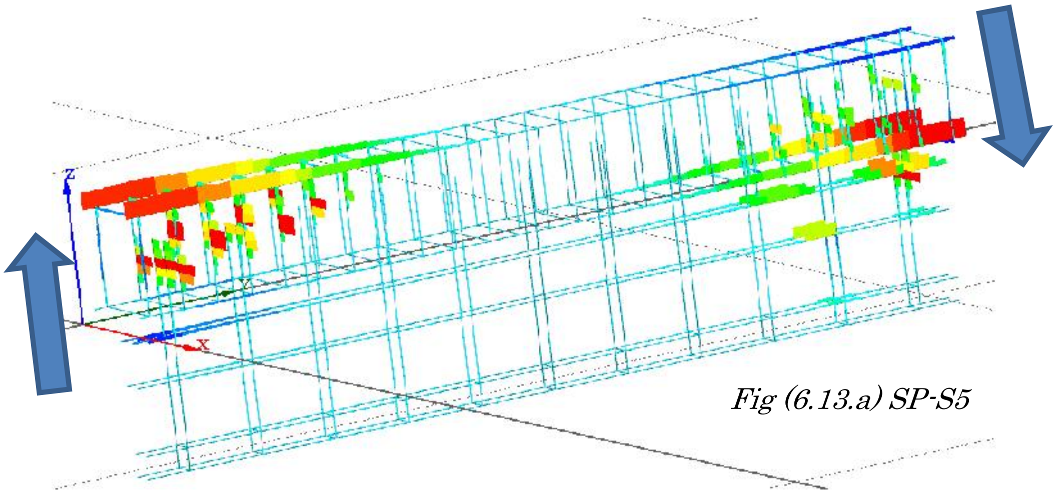

Fig (6.13.a) SP-S5

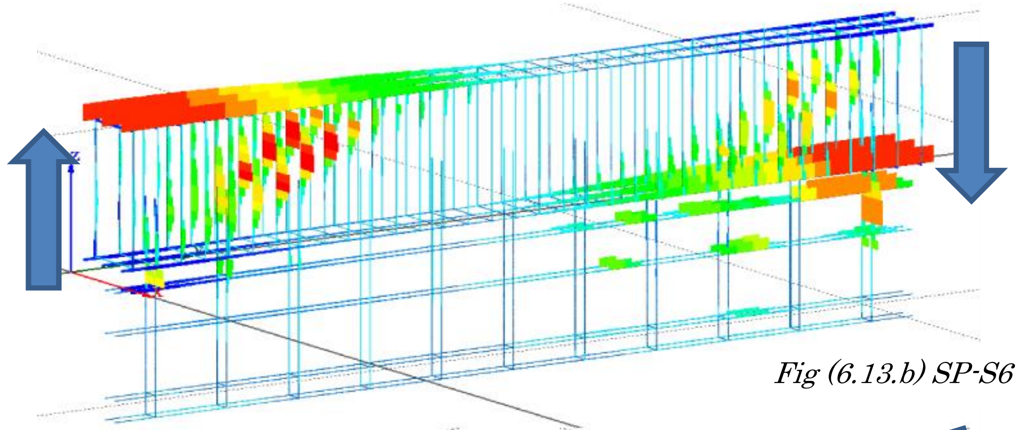

Fig (6.13.b) SP-S6

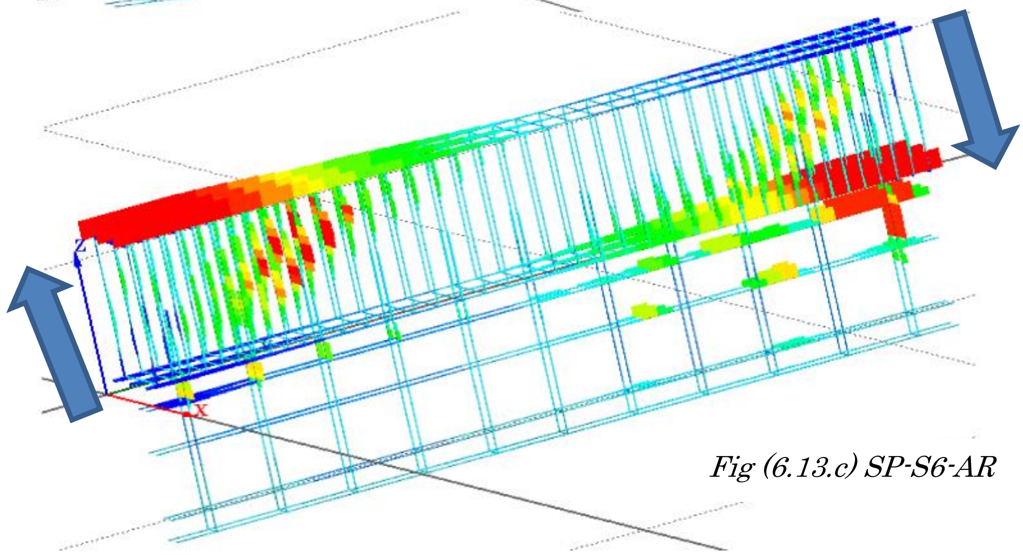

Fig (6.13.c) SP-S6-AR

Fig (6.13) Tensile stresses in the reinforcing bars of studied beams

6.6.4 Solid Stresses Distribution in the Concrete

Solid stresses were checked in a continuous plane in the beam and the wall. Figure (6.14) shows plane in the middle of specimen section which was studied. The results are shown in Figure (6.15) where yellow colour refers to compression stresses in concrete.

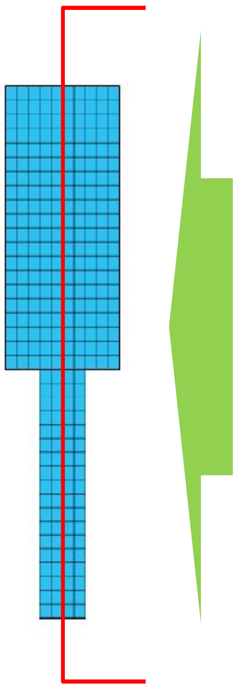

Fig (6.14) Studied plane in the models

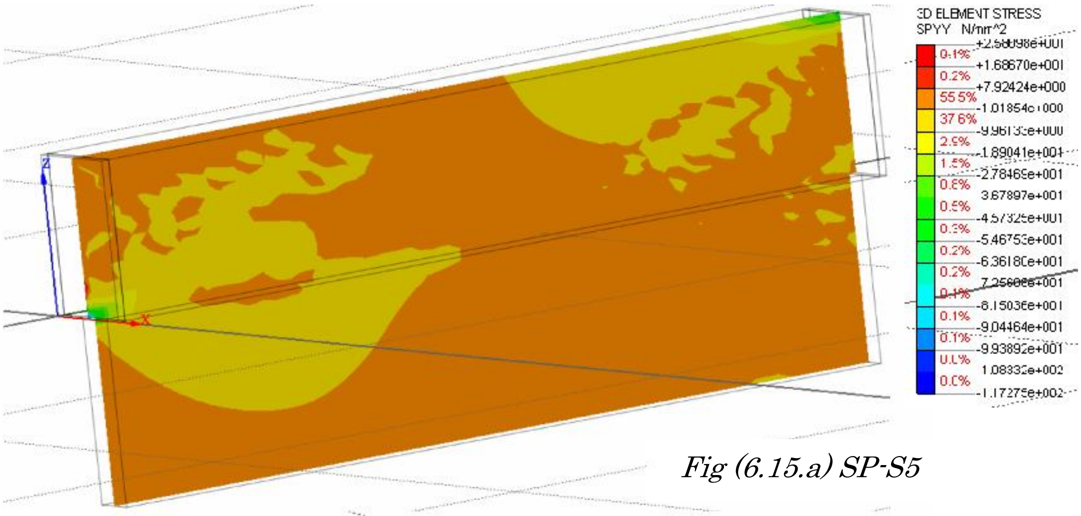

Fig (6.15.a) SP-S5

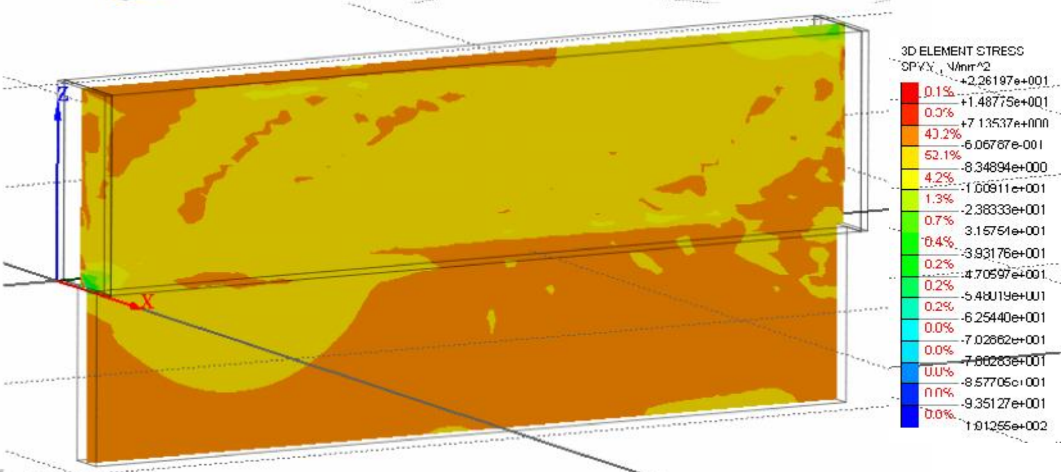

Fig (6.15.b) SP-S6

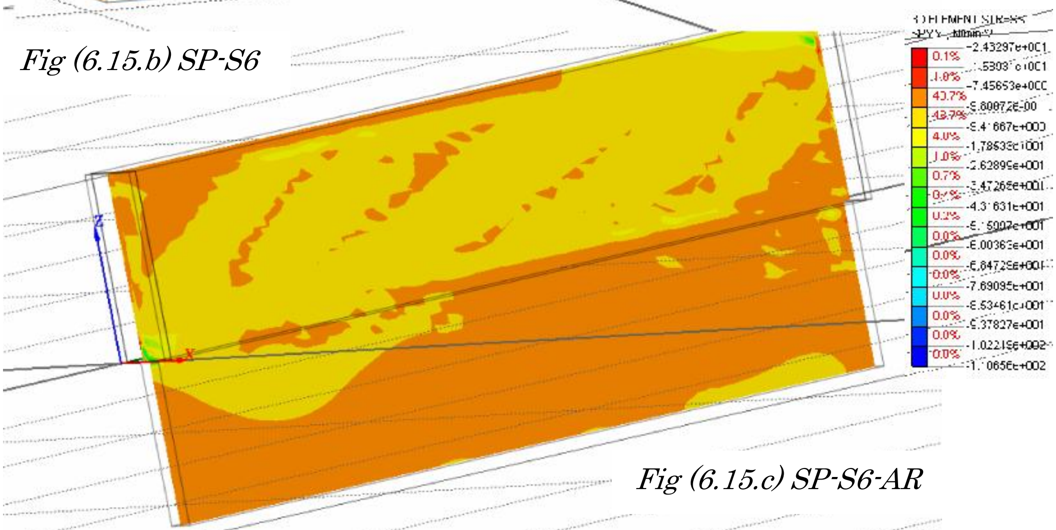

Fig (6.15.c) SP-S6-AR

Fig (6.15) Solid stresses in concrete of beam and wall

CHAPTER 7
THE STRUT-AND-TIE MODEL STUDY

- Background on Strut-and-Tie Modeling
- Elements of Strut-and-Tie Model
- The Proposed Model and Design Procedure
- Numerical Example

7.1 Background of the Strut-and-Tie Model

7.1.1 Overview

Principles of the strut and tie model, and a short review of its application is given according to SCHLAICH (1991)[(39)]. Internal stresses of RC structures are characterized by bending moments, axial and shear forces that are determined using well-known methods of the structural analysis. Connections between bending moments and deformations as well as distributions of stresses due to internal forces and moments are given on the base of a slightly modified elementary bending theory of bars which also takes the specific behavior of the structural concrete into account.

Bar forces acting at the struts and ties are the resultants of compressive and tensile stresses. The directions of struts have to be taken in the average direction of the trajectories of compressive stresses and located about the central lines of the pencils. The ties should follow the tensile stresses in the same way. Strut and tie modeling obviously provides the structural analyst with some freedom of choice that can be used to aim either at the safest or at the cheapest or at an otherwise optimized solution. For practical reasons (e.g. to produce a simpler replacement truss or to simplify the manufacturing of the reinforcement) one usually does not closely follow the principal and tensile stress directions. In this case it is necessary to consider the consequences of these deviations that is to check the equilibrium and to adjust the amount of reinforcement for taking into account its deviations from the principle directions. If modelling does not closely follow the stress-flows, it can cause incompatibilities in the corresponding strains that means, cracks and plastic deformations have to develop. It is well known that concrete has a low tensile strength and permits limited plastic compressive deformations. To avoid developing of wide cracks and exceeding plastic limit an additive reinforcement of two directions has to be used.

7.1.2 The Problem of Strut-and-Tie Model

The use of strut and tie models is strongly hampered by problems, not perfectly clarified so far, as follows:

Firstly, in order to determine whether principles used heretofore form a sufficient base to develop strut and tie models, which can properly model the real behaviour of structures, it is necessary to improve the adequateness of the modelling by refining the fundamental assumptions.

Questions connecting to this are as follows:

-What dense should a replacement truss be?

-What are the physical limits for constructing the truss?

-How does the reinforcement influence the truss?

-When using two strut and tie models for the same structures how can the load be split into parts born by each model?

-How have statically indeterminate strut and tie models to be correctly solved?

-How does a complicated cross-section influence the modelling?

Secondly, these are related to the accuracy of calculation. Connected to this one can ask:

-How does the deformation of strut and ties influence the action- effect of the truss elements?

-How can be compensated the neglecting of the compatibility condition for the changes in length of the fictitious bars?

-What is the minimal amount of reinforcement for assuring the sufficient ductility'?

-What kind of safety measures have to be used to avoid erroneous dimensioning?

-What kind of results do give the comparison between the calculated and the measured values?

-How does the bond change in nodes?

-How does the deviation of the strength of the concrete influence the results obtained by STMs?

7.1.3 The Influence of Cracks on the Strut-and-Tie Model

Cracks on a well-designed structure or structural element gradually appear as the intensity of the load increases, they are uniformly distributed and not concentrated in narrow strips of the structure, and their widths remain moderate in the service state of the structure.

It is impossible to avoid cracks at the level of load of service state, even in case of optimal design, however, crack widths and the crack pattern can be influenced in many ways (40,41,42). Factors influencing the crack pattern are as follows:

-the geometry and cross-section of the structure,

-the loads and their characteristics,

-the variance of strength of the concrete,

-the concrete covering the reinforcing bars,

-the temperature and the free motion hinder,

-the amount of reinforcement,

-the diameter of reinforcing bars,

-the distances of reinforcement,

-the direction of reinforcement (how it follows the direction of principal tensile stresses),

-the types of reinforcement (normal, prestressed or mixed),

-the bond and the anchorages.

At abrupt changes of the cross-section, so-called stress peaks develop. Here the maximum stresses can multiply exceed the average values calculated by usual methods. Steep changes in stresses especially in tensile stresses are hardly born by materials having a limited ductility like concrete. Around stress peaks, tensile stresses quickly increase and exceed the tensile strength of the concrete. Cracks arise, large deformation of the tensile reinforcement starts and plastic zones develop while other parts of the structure are in elastic range. The appearance of cracks that the equalizing of stresses has begun.

Cracks at stress peaks have a decisive influence on the load-bearing capacity of structures. These stress peaks form only small parts of the whole system of stresses and they can hardly be fit by any strut and tie model. However, disregarding them would be a bad mistake. Researches prove that unlike the other structural parts, where tensile forces can be conveniently covered by simple webs of orthogonal reinforcement, at stress peaks this method only gives a reduced-value solution.

Researches(43,44,45) have also shown that at places where stress peaks can develop the load bearing capacity can be increased by 20-30 % if reinforcing bars are put at right angles to the cracks. The solution can be improved by application of wedging, rounding up, that is, gradual and not abrupt changes of the cross-sections. These geometrical refinements also permit good possibilities to refine the reinforcement as well.

As previously mentioned, the reinforcement has a decisive effect on cracks. The correct direction of tensioned bars of strut and tie model around the stress peaks has a great importance because this gives a great influence on behaviour.

7.2 Members of Strut-and-Tie Model

7.2.1 Struts

The struts represent the members of STM which resist the compressive stresses. There are three types of struts:

a)- Prismatic struts, with constant cross section over the strut length. This type usually used along the compressive face of beam.

b)- Compression fan strut, where the sectional area of strut will increase from small area to large one. Usually this type is used at supports.

c)- Bottle-shaped strut, where the sectional area of strut increase from small area to larger area at middle of strut and then decrease to small area at the other end of strut. In this type, the tensile stresses in the middle of strut should be studied and necessary reinforcement grid will be needed. The bottle-shaped struts usually studied as prismatic struts.

Figure (7.1) shows the common types of struts.

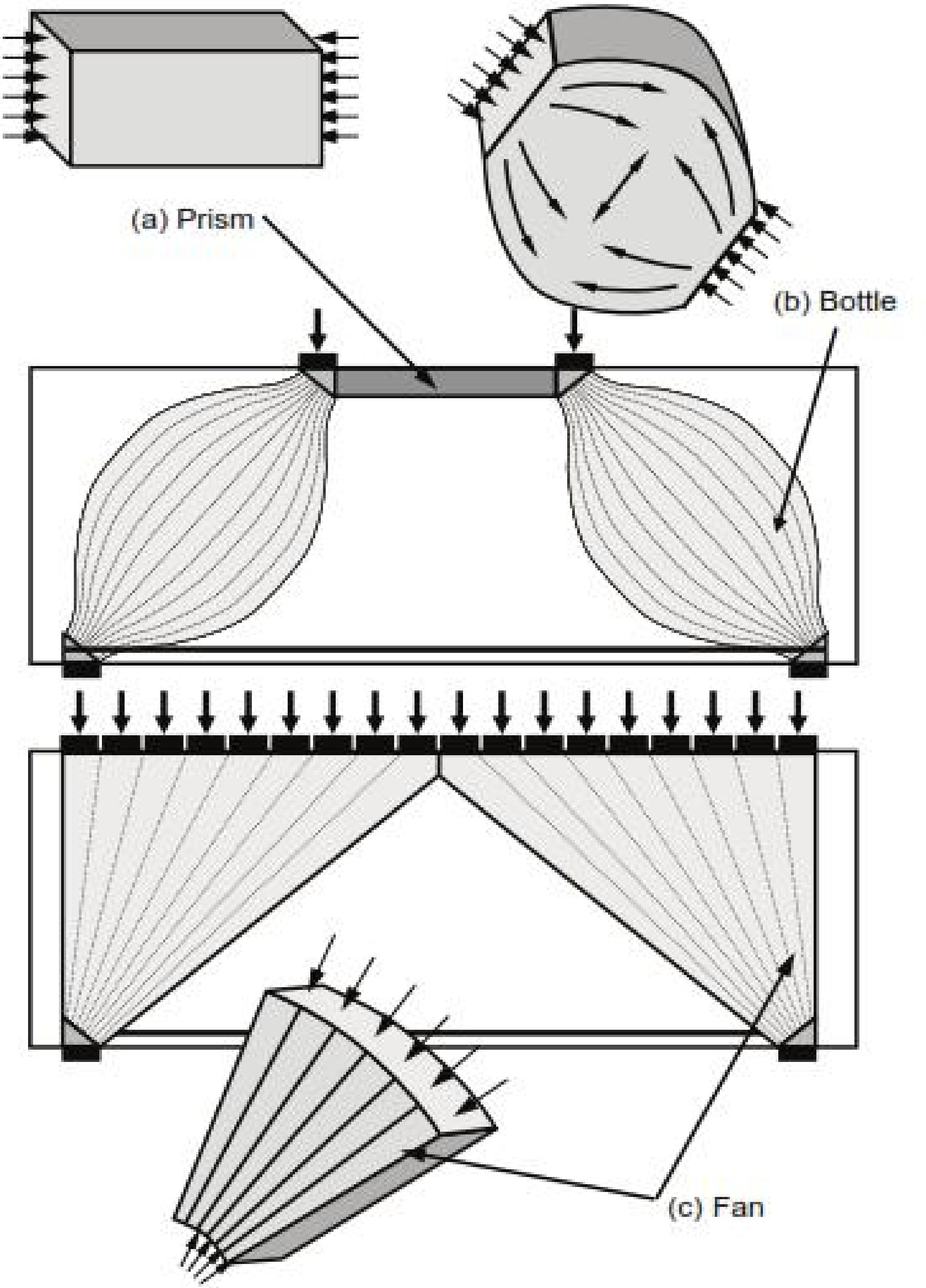

Fig(7.1) Common types of struts[46]

7.2.2 Ties

Ties are the member of STM which resist the tensile forces. Reinforcing bars in tension are represented by the ties. The vertical ties represent the stirrups and the longitudinal ties represent the longitudinal reinforcement in tension

7.2.3 Nodes

The STM consists of struts and ties and they intersect at nodes. There are three types of the nodes: CCC, CCT and CTT nodes. Where C refers to compression and T refers to tension. In the CCC node, it is expected to have the higher strength comparing to the other nodes due to the confinement by the compressive stresses. In the other types of nodes where tensile stresses are applied, the strength of node is less because the tensile stresses cause cracking in the nodal zone and as a result decreasing in the strength of node.

In designing the nodes there are two assumptions, hydrostatic nodes and non-hydrostatic nodes. In the former, there is no shear stresses at the nodal zone, and in the later, the shear stresses should be less than the shear strength of concrete.

Figure (7.2) shows the hydrostatic and non-hydrostatic nodes.

Figure (7.3) shows the stresses in each of hydrostatic nodes and non-hydroststic nodes.

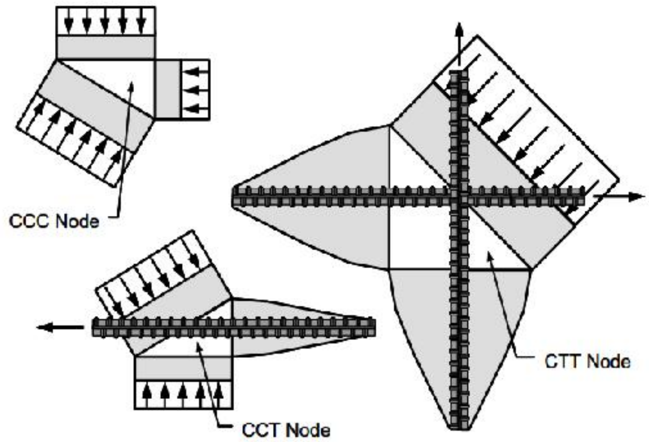

Fig (7.2) Schematic depictions of nodes (Thompson et al. 2003)[46]

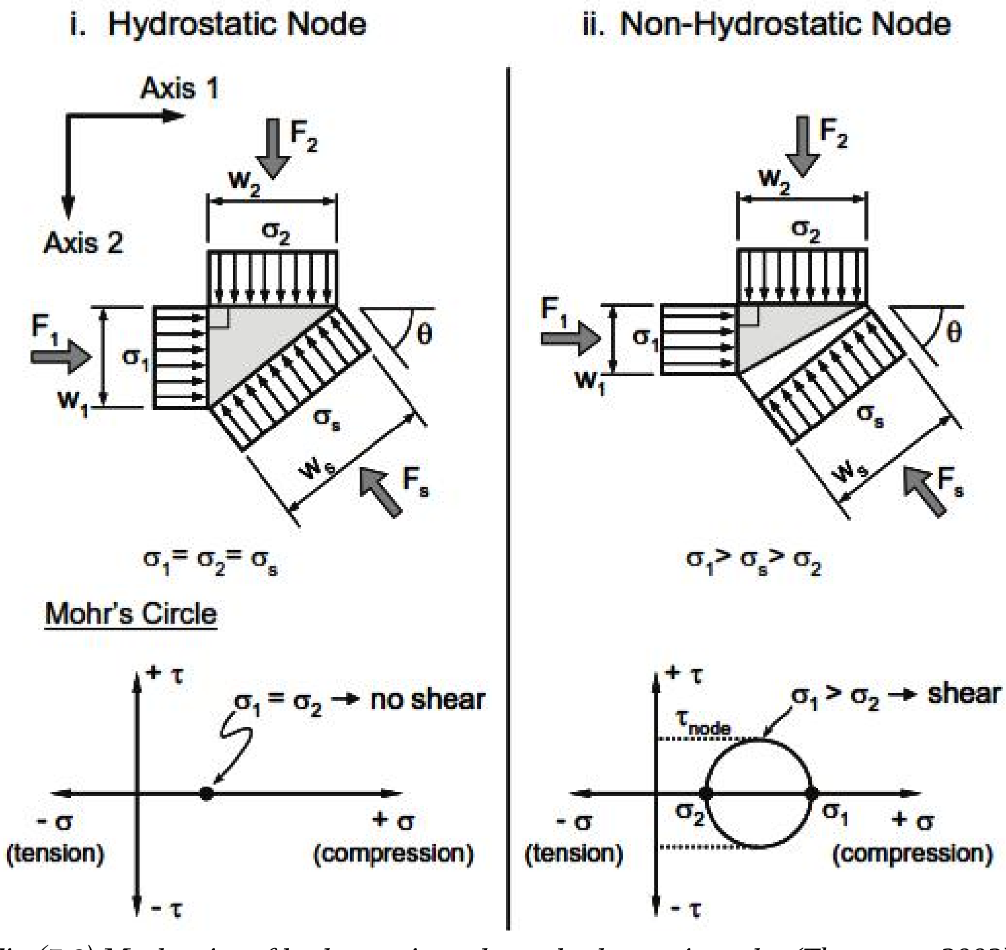

Fig (7.3) Mechanics of hydrostatic and non-hydrostatic nodes (Thompson 2002)[46]

7.3 The Proposed Model and Design Procedure

7.3.1 The Proposed Model

The beam without slab is considered in this study. Where the slab improved the seismic performance of the beam experimentally.

The proposed model relies on the forces distribution in the specimen, forces paths. The agreement of crack pattern is an important evidence of the stresses distribution.

To explain more about the proposed model, the specimens SP-S6, SP-S6-AR and SP-S5 were studied and compression between the experimental results and numerical results was done.

7.3.1.1 Strut-and-Tie Model of SP-S6

From the analytical study, the stresses distribution is necessary to know initially the forces paths in the specimen.

Figures (7.4) and (7.5) show the proposed STM model of specimen SP-S6, where dashed lines refer to members in compression and the solid lines refers to members in tension. It is corresponded with the crack patterns and the analytical results of FEM analysis.

The agreement of crack patterns is checked where the proposed positions of ties and struts are corresponded with the cracks patterns, the compression struts are parallel to the formed cracks and the ties are perpendicular to the cracks, approximately.

Fig(7.4) Cracks pattern and STM of SP-S6

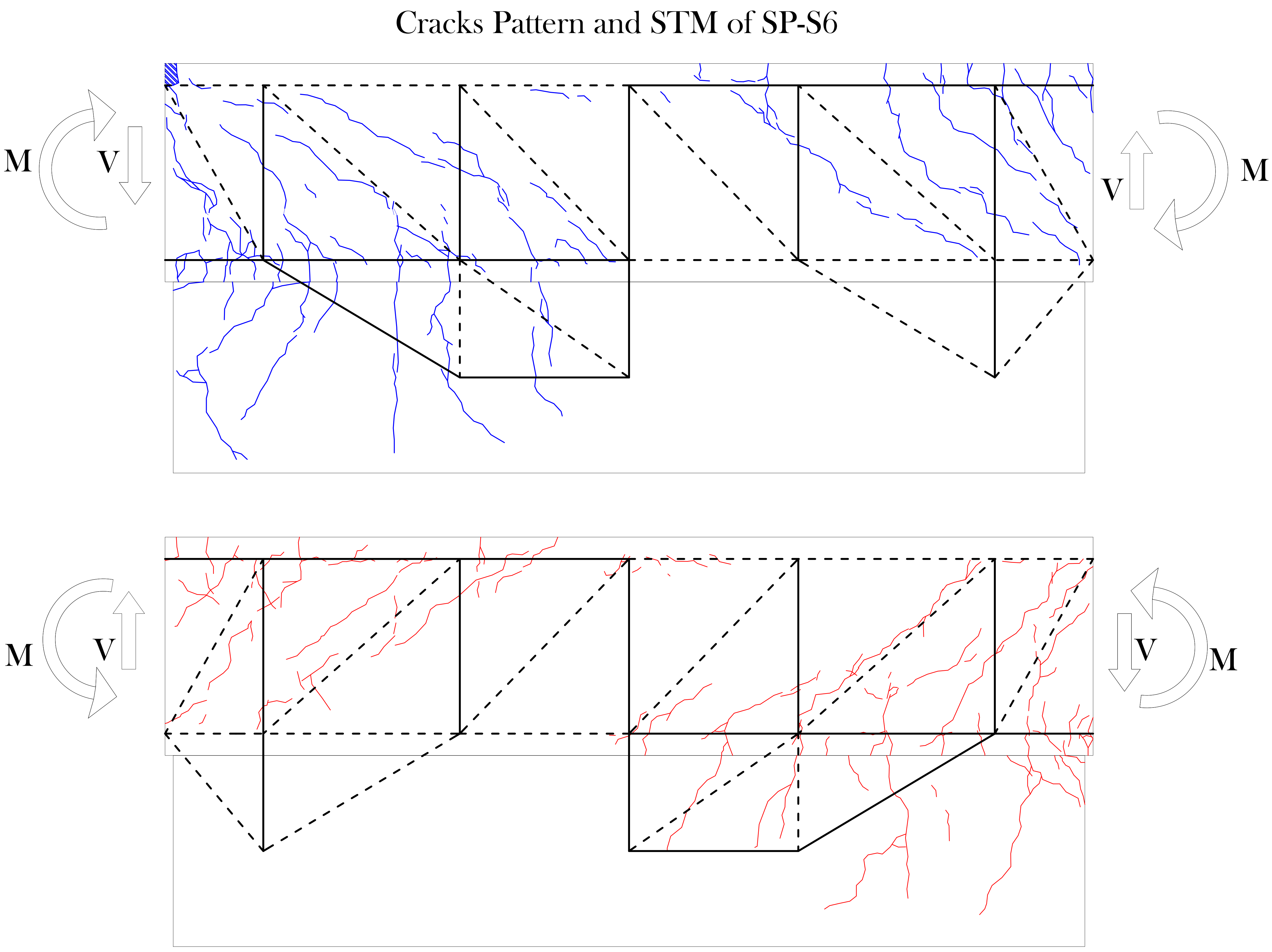

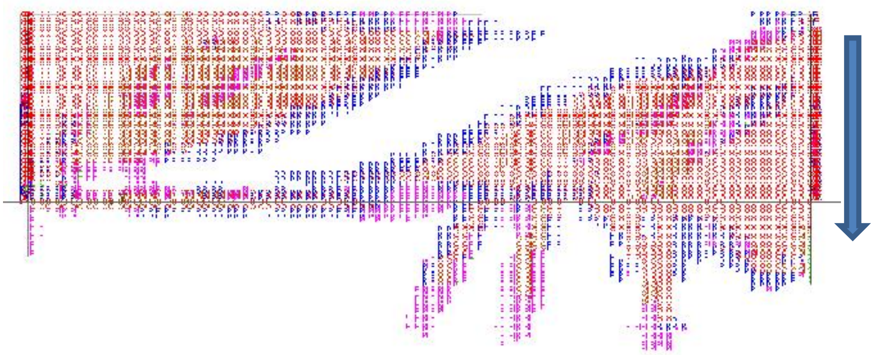

Fig (7.5.a) Cracks pattern analytically by FEM analysis of SP-S6

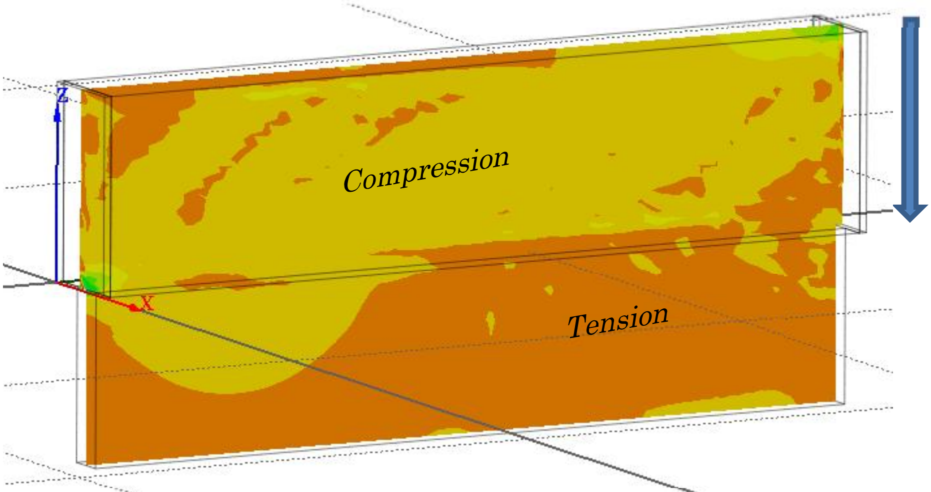

Fig (7.5.b) Solid stresses distribution by FEM analysis of SP-S6

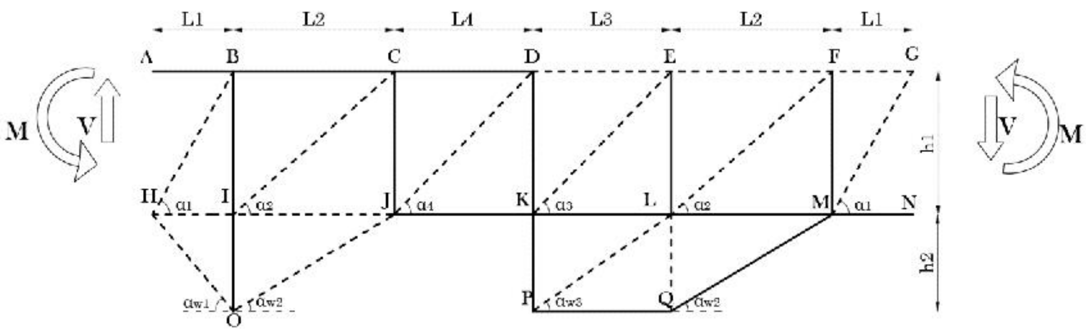

Fig (7.5.c) The analytical model of of SP-S6

Fig (7.5) Correspondence between the analytical results and proposed STM for SP-S6

7.3.1.2 Design Procedure of STM-S6

Figure (7.6) shows in details the analytical model of STM-S6.

The model is divided into zones as the followings:

The members “BI” and “FM”, each of them represents the tensile force in the stirrups distributed along “d” from the supports.

And the same assumption for the other vertical ties in the beam body, which means that the distance between the vertical ties was determined:

L_1= 0.5 * d = 0.5 * 360 = 180 mm.

L_2= d = 360 mm, $L_3 = L_4$ = 0.5 *(Length of beam – 2 * (L1 +L_2))

= 0.5*(1700- 2(180+360)) = 310 mm.

The angle between the strut and tie should not be less of 25 degree to prevent high strains in the reinforcement bars and to reduce the influence of wide cracks [27].

h_1: the centric distance between the compression bars and tension bars of beam,

h_1 = 400 - 2 * 40 = 320 mm.

h_2 : was proposed to consider the half of wall height as initial assumption,

h_2 = 0.5 * 350 + 40 = 215 mm.

The bending moment was applied as tension and compression forces, T and C, as shown in Figure (7.8).

$$C = T = V \cdot 0.5 \cdot L / h_1$$

V: the applied shear force (kN), and

L: Length of beam (mm).

Fig(7.6) Details of analytical model of STM-S6

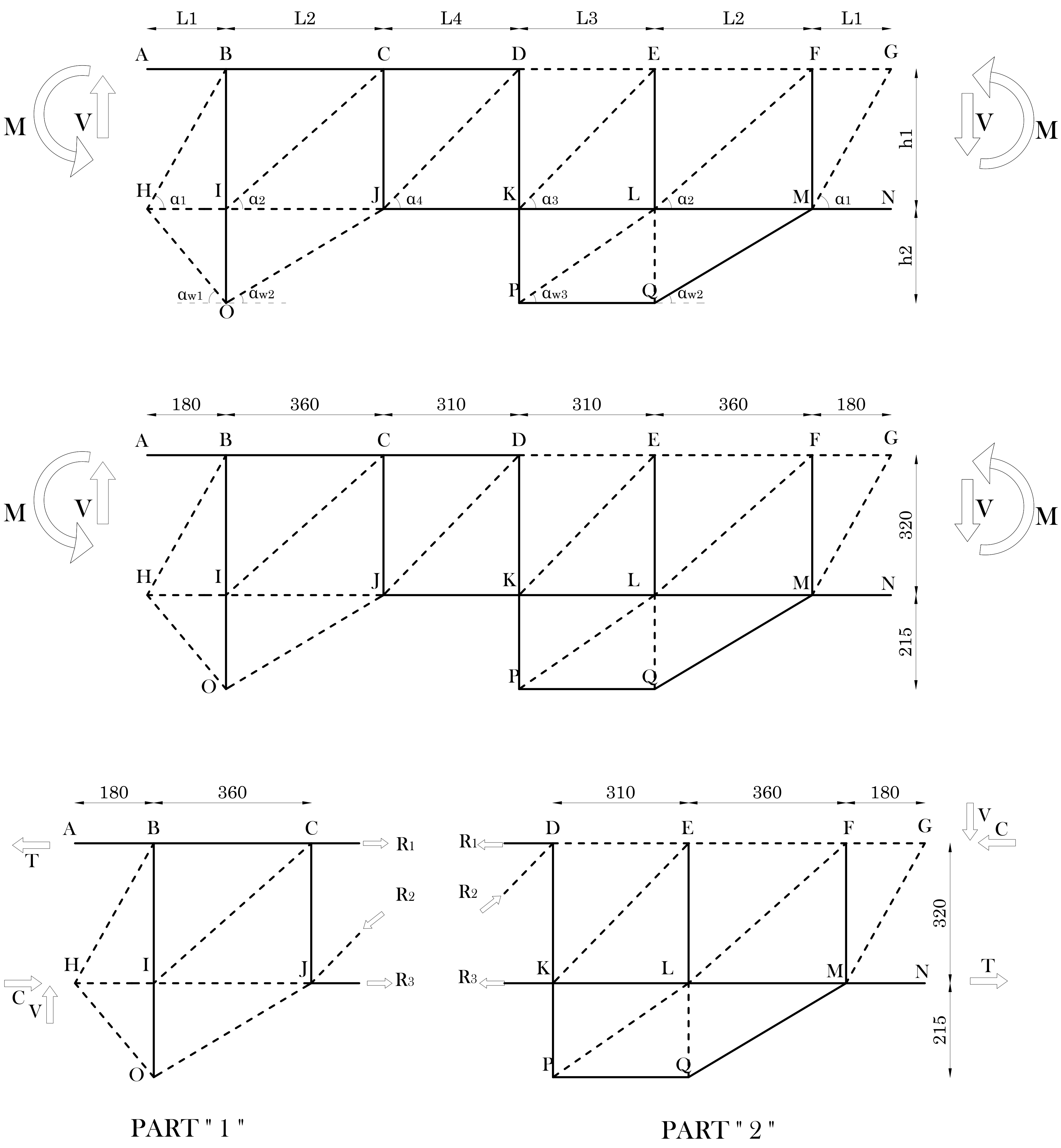

The Analytical Model of STM-S6

In general, STM-S6 is indeterminate to the second degree. To simplify the solution of it, it was divided into two parts and each part is determinate to first degree as shown in Figure (7.6).

Each of these parts was calculated individually.

For total model:

2 * n = 30 and M + R = 29 + 3 = 32, 2n< M + R (+2)

Virtual Work Method was applied in the analysis of each part of the truss, as the followings:

$$\sum_{1}^{n} \frac{{}_iP_0 \cdot {}_iP_1 \cdot {}_iL}{{}_iE_iA} \qquad \text{Eqn.7.1}$$

$$\sum_{1}^{n} \frac{{}_iP_1 \cdot {}_iP_1 \cdot {}_iL}{{}_iE_iA} \qquad \text{Eqn.7.2}$$

$$X = \frac{\sum_{1}^{n} \frac{{}_iP_0 \cdot {}_iP_1 \cdot {}_iL}{{}_iE_iA}}{\sum_{1}^{n} \frac{{}_iP_1 \cdot {}_iP_1 \cdot {}_iL}{{}_iE_iA}} \qquad \text{Eqn.7.3}$$

$${}_iN = {}_iP_0 + X \cdot {}_iP_1 \qquad \text{Eqn.7.7}$$

${}_iP_0$: The force in member " i " in the determinate truss after omitting one of the truss members,

${}_iP_1$: The force in member " i " in the truss after applying " 1 kN " instead of the omitted member and removing the external loads,

${}_iL$: Length of member " i ",

${}_iE_iA$: Axial stiffness of member " i ", and

${}_iN$: Final force in the member " i ".

Strength condition should be checked[47]:

$${}_iN \leq \varphi \cdot {}_iF_u \qquad \text{Eqn.7.8}$$

ϕ: Strength reduction factor (0.75). The purposes of the strength reduction factor φ are, according to ACI 318-05[47]:

(1) to allow for the probability of under-strength members due to variations in material strengths and dimensions,

(2) to allow for inaccuracies in the design equations,

(3) to reflect the degree of ductility and required reliability of the member under the load effects being considered, and

(4) to reflect the importance of the member in the structure.

${}_iF_u$: The nominal strength of member " i ". From ACI 318-05 the strength of struts, ties and nodes are determined as the following:

The nominal compressive strength of a strut without longitudinal reinforcement [47], F_{su} , shall be taken as the smaller value of

$$F_{su} = f_{su} \cdot A_{cs} \qquad \text{Eqn.7.9}$$

At the two ends of the strut.

A_{cs}: The cross-sectional area at one end of the strut, and

f_{su}: is the smaller of (a) and (b):

(a) the effective compressive strength of concrete in the strut[47]:

$$f_{su} = 0.85 \cdot \beta_s \cdot f'_c \qquad \text{Eqn.7.10}$$

Where the strength coefficient " $0.85 f'_c$ " represents the effective concrete strength under sustained compression.

$\beta_s = 1.0$ for strut with uniform cross-sectional area over its length, prismatic

$\beta_s = 0.85$ for strut with reinforcement grid,

$\beta_s = 0.7$ for strut with normal width cracks,

$\beta_s = 0.6$ for strut with wide width cracks,

(b) the effective compressive strength of concrete in the nodal zone[47]:

$$f_{su} = 0.85 \cdot \beta_n \cdot f'_c \qquad \text{Eqn.7.11}$$

$\beta_n = 1.0$ for CCC node,

$\beta_n = 0.8$ for CCT node, and

$\beta_n = 0.6$ for CTT node,

Figure (7.7) shows the types of nodes in strut-and-tie model.

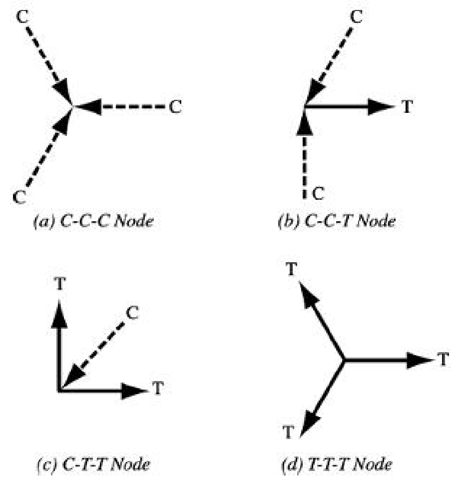

Fig (7.7) Classification of nodes

The use of compression reinforcement shall be permitted to increase the strength of a strut.

The nominal strength of a longitudinally reinforced strut [47] is:

$$F_{su} = f_{su} \cdot A_{cs} + A_s^{'} \cdot f_s^{'} \qquad \text{Eqn.7.12}$$

A'$_s$: Compressive strength in the strut,

f'_s: Stress in the compressive strength of the strut which will increase till yielding of compressive reinforcement.

The nominal strength of tie [47] shall be taken as:

$$F_{tu} = A_s \cdot f_y \qquad \text{Eqn.7.13}$$

The effective tie width assumed in design is considered in case of one layer of reinforcement as: the effective tie width can be taken as the diameter of the bars in the tie plus twice the cover to the surface of the bars.

The nominal strength of a nodal zone [47] shall be taken as:

$$F_{nu} = f_{nu} \cdot A_{cn} \qquad \text{Eqn.7.14}$$

f_{nu}: the effective compressive strength of concrete at the nodal zone[47] :

$$f_{nu} = 0.85 \cdot \beta_n \cdot f'_c \qquad \text{Eqn.7.15}$$

A_{cn} : is the smaller of (a) and (b)

(a) the area of the face of nodal zone on which ${}_iN$ acts, taken perpendicular to the line of action of ${}_iN$.

(b) the area of a section through the nodal zone, taken perpendicular to the line of action of the resultant force on the section.

Figure (7.8) shows the details of analysis model of part "1" of the total STM-S6.

Table (7.1) shows the equations of calculating part "1" of STM-S6.

Figure (7.9) shows the details of analysis model of part "2" of the total STM-S6.

Table (7.2) shows the equations of calculating part "2" of STM-S6.

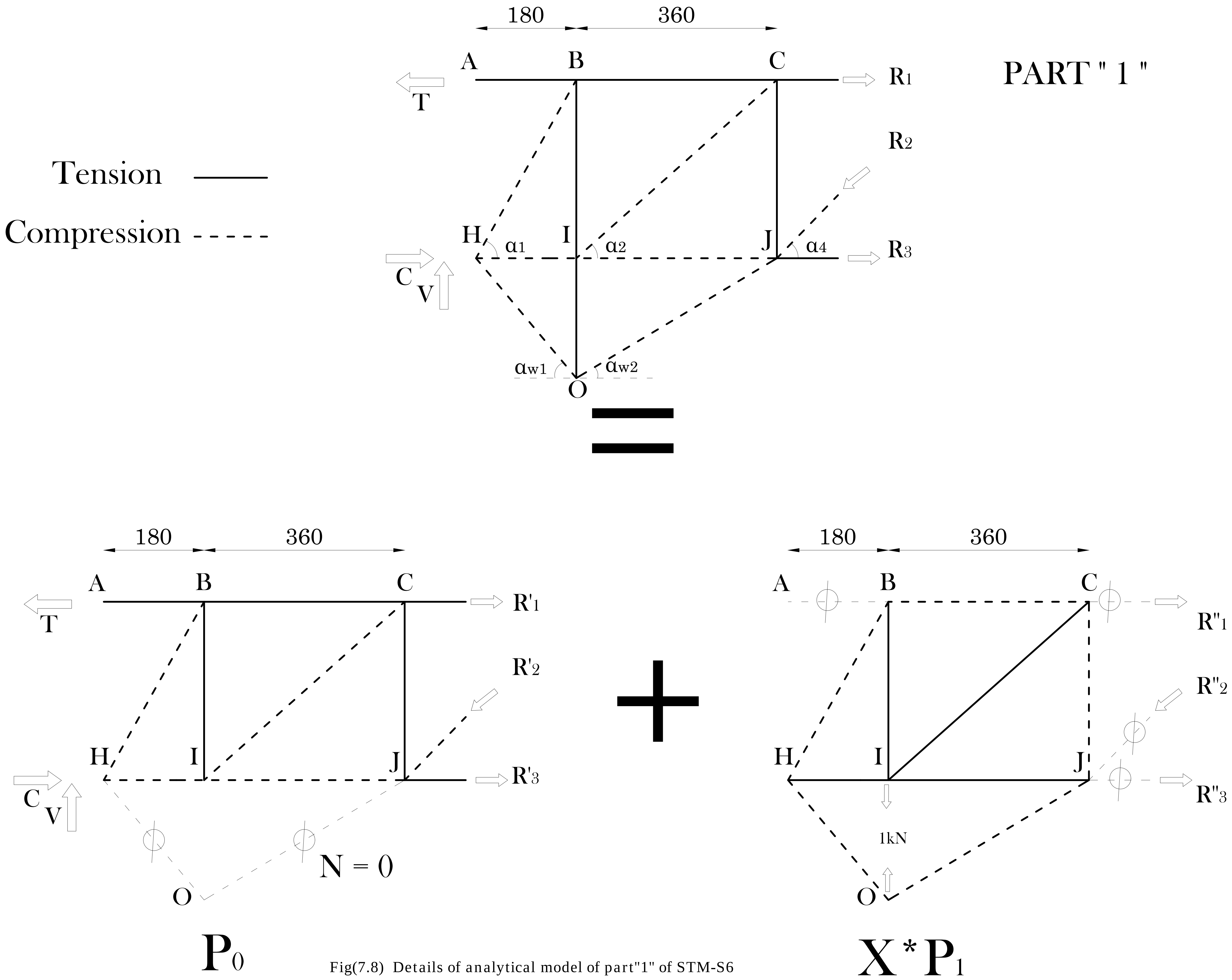

Fig(7.8) Details of analytical model of part"1" of STM-S6

Table 7.1 Equations of calculating the part "1" of STM-S6

P_0		P_1	
R'_1	$R'_3 - R'_2 \cdot cos(\alpha_4)$	R''_1	0
R'_2	$\frac{V}{sin(\alpha_4)}$	R''_2	0
R'_3	$-\frac{V \cdot (L_1 + L_2) - T \cdot h_1}{h_1}$	R''_3	0
AB	T	AB	0
BC	$AB - HB \cdot cos(\alpha_1)$	BC	$HB \cdot cos(\alpha_1)$
HI	$C - V \cdot cot(\alpha_1)$	HI	$HB \cdot cos(\alpha_1) + HO \cdot cos(\alpha_{w1})$
IJ	$R'_2 \cdot cos(\alpha_4) - R'_3$	IJ	$OJ \cdot cos(\alpha_{w2})$
BI	V	BI	$HB \cdot cos(\alpha_1)$
CJ	$IC \cdot cos(\alpha_2)$	CJ	$OJ \cdot cos(\alpha_{w2})$
IO	0	IO	1
HB	$\frac{V}{sin(\alpha_1)}$	HB	$HO \cdot \frac{\sin(\alpha_{w1})}{\sin(\alpha_1)}$
IC	$\frac{BI}{sin(\alpha_2)}$	IC	$\frac{CJ}{\sin(\alpha_2)}$
HO	0	HO	$\frac{1}{\cos(\alpha_{w1}) \cdot \tan(\alpha_{w2}) + \sin(\alpha_{w1})}$
OJ	0	OJ	$HO \cdot \frac{\cos(\alpha_{w1})}{\cos(\alpha_{w2})}$

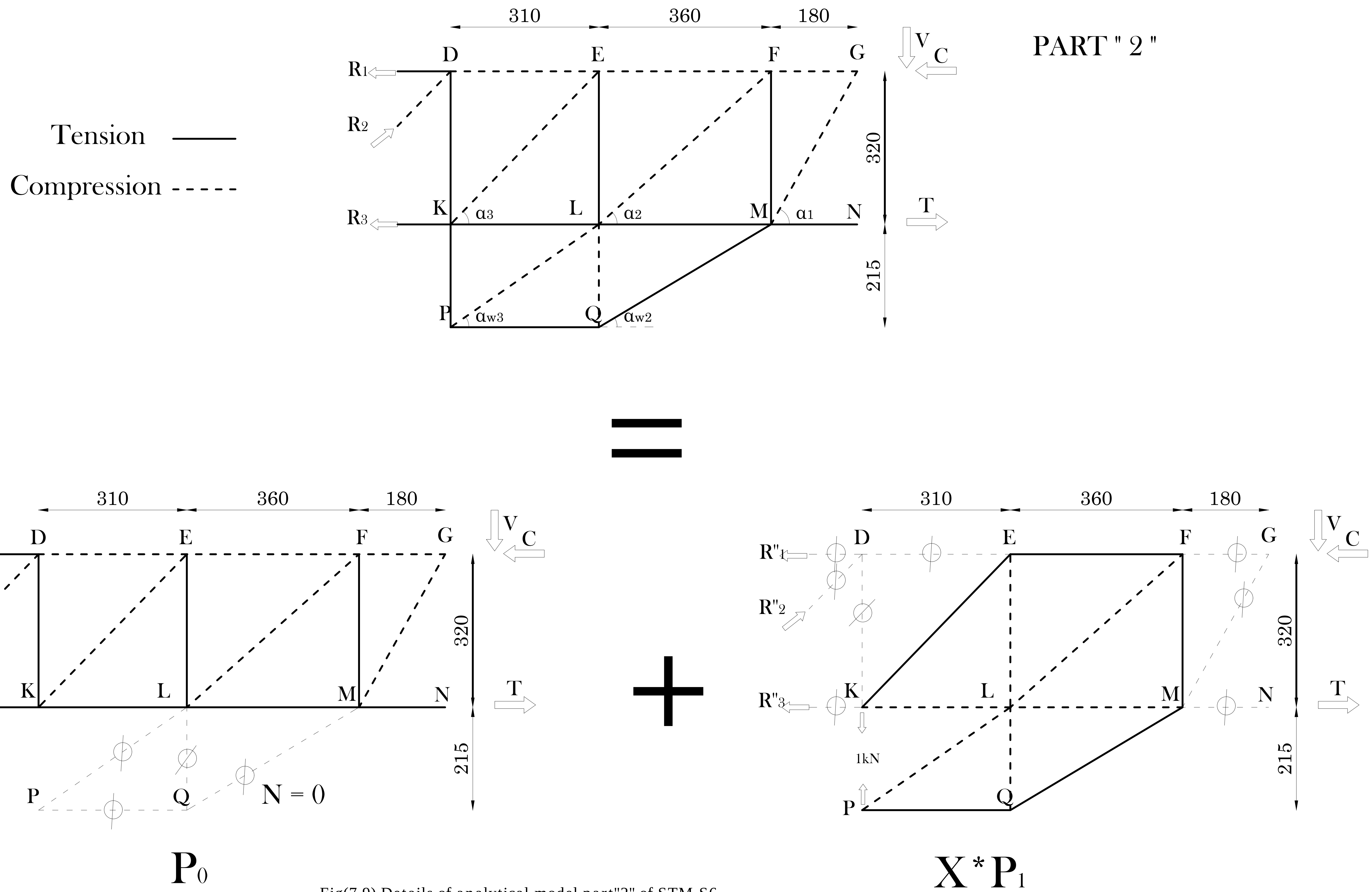

Fig(7.9) Details of analytical model part"2" of STM-S6

Table 7.2 Equations of calculating the part "2" of STM-S6

P_0		P_1	
R'$_1$	$R_3' - R_2' \cdot cos(\alpha_4)$	R"$_1$	0
R'$_2$	$\dfrac{V}{sin(\alpha_4)}$	R"$_2$	0
R'$_3$	$-\dfrac{V\cdot(L_1+L_2+L_3)-T\cdot h_1}{h_1}$	R"$_3$	0
DE	$R_1' + R_2' \cdot cos(\alpha_4)$	DE	0
EF	$AB + KE \cdot cos(\alpha_3)$	EF	$KE \cdot cos(\alpha_3)$
FG	$C - V \cdot cot(\alpha_1)$	FG	0
KL	$R_3' + KE \cdot cos(\alpha_3)$	KL	$KE \cdot cos(\alpha_3)$
LM	$T - V \cdot cot(\alpha_1)$	LM	$MQ \cdot cos(\alpha_5)$
PQ	0	PQ	$PL \cdot cos(\alpha_{w3})$
DK	$R_2' \cdot \sin(\alpha_4)$	DK	0
EL	$KE \cdot cos(\alpha_3)$	EL	$KE \cdot \sin(\alpha_3)$
FM	V	FM	$LF \cdot \sin(\alpha_2) = MQ \cdot \sin(\alpha_{w2})$
KP	0	KP	1
LQ	0	LQ	$KE \cdot \sin(\alpha_3)$
KE	$\dfrac{DK}{\sin(\alpha_3)}$	KE	$\dfrac{1}{\sin(\alpha_3)}$
LF	$\dfrac{EL}{\sin(\alpha_2)} = \dfrac{FG-EF}{\cos(\alpha_2)}$	LF	$\dfrac{EF}{\cos(\alpha_2)}$
MG	$\dfrac{V}{\sin(\alpha_1)}$	MG	0
PL	0	PL	$\dfrac{1}{\sin(\alpha_{w3})}$
MQ	0	MQ	$\dfrac{PQ}{\cos(\alpha_{w2})}$

To analyze the truss by Virtual Work Method, it is necessary to know the axial stiffness of members.

To calculate the axial stiffness,the truss members are classified to the following types:

A- Horizontal members in compression in beam without considering the compression reinforcement.

In this case, the compression force is less than the strength of strut without the compression bars. Modulus of elasticity will be considered for concrete only. Width of the strut will be calculated as twice of distance between the center of compression bars and the nearest face of beam.

B- Horizontal members in compression in beam with considering the compression reinforcement.

The compression force is higher than the strength of concrete strut, so the compression steel will contribute with concrete in resisting the compression force. The stress in the compression steel increases gradually till yielding.

Width of strut is constant, twice of distance between the center of compression bars and the nearest face of beam.

C- Horizontal members in tension in beam.

The horizontal members in tension in the beam represent the longitudinal bars of beam.

D- Inclined members in compression in beam.

Represent a concrete struts and the width is calculated depending on the strength of strut and nodal faces in nodal zones. And the other dimension of cross section is the width of beam.

E- Vertical members in tension in beam.

The vertical members in tension in the beam represent the stirrups of beam.

F- Horizontal members in tension in the non-structural wall.

The horizontal members in tension in the non-structural wall represent the longitudinal reinforcement of the wall.

G- Vertical members in tension in the non-structural wall.

The vertical members in tension in the non-structural wall represent the transverse reinforcement of the wall.

H- Vertical members in compression in the non-structural wall.

Represent a concrete struts and the width is calculated depending on the strength of strut and nodal faces in nodal zones. And the other dimension of cross section is the thickness of wall.

I- Inclined members in tension in the non-structural wall.

The longitudinal reinforcement was considered as the following:

$$A_{sI} = \frac{A_{sL}}{sin(\alpha_w)} \qquad \text{Eqn.7.16}$$

Where:

A_{sI}: The reinforcement of inclined member in tension of wall (mm^2),

A_{sL}: The longitudinal reinforcement of wall which is considered in the truss calculations (mm^2), and

α_w: The angle of inclined member in tension in the non-structural wall.

J- Inclined members in compression in the non-structural wall.

Represent a concrete struts and the width is calculated depending on the strength of strut and nodal faces in nodal zones. And the other dimension of cross section is the thickness of wall.

Calculation of concrete strut width relies on the strength of the strut itself and the strength of nodal face at each end of the strut.

Table (7.3) shows nodes types of STM-S6.

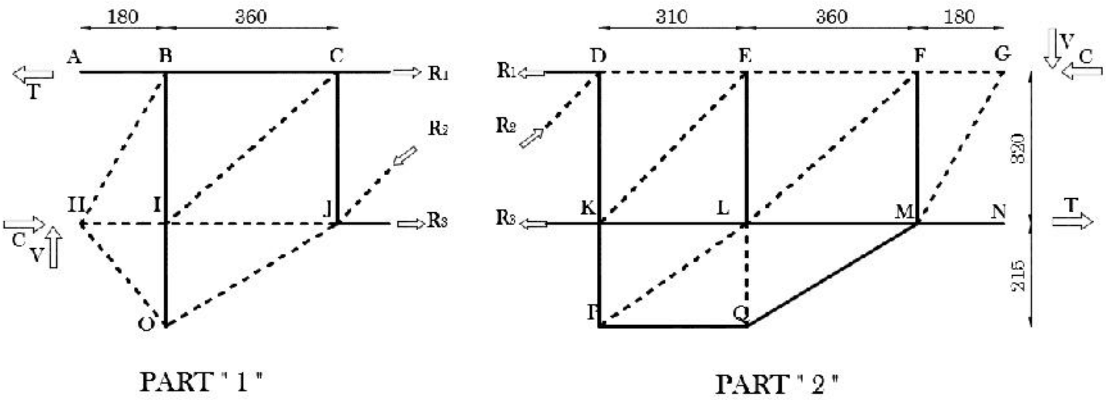

Fig (7.10) The analytical model STM-S6

Table 7.3 Nodes Types of STM-S6

Part "1"		Part "2"	
Node	Classification	Node	Classification
B	CTT	D	CTT
C	CTT	E	CCT
H	CCC	F	CCT
I	CTT	G	CCC
J	CTT	K	CTT
O	CCT	L	CTT
		M	CTT
		P	CTT
		Q	CTT

The details of numerical calculations are shown in the following tables:

Beam Section		Wall Section		Concrete Properties		Main Bars			
b	D	T	H	Ec	Fc	Es	As	Pt	Fy
200	400	80	350	22577	28.2	196000	861	0.011958	383.9

Wall's Bars							
Es	Number of H layers	AS	As-tot	Number of V layer	AS	As-tot	Fy
186000	2	14.05	56.2	2	14.05	56.2	356.4

Stirrups		
Es	Fy	Asw
192000	438.3	32

Dimensions mm							
h1	h2	L1	L2	L3	L4=L3	L	J
320	215	180	360	310	310	1700	320

Angles							
alpha1	>25	alpha2	>25	alpha3	>25	alpha4	>25
1.058407	OK	0.726642	OK	0.801270	OK	0.801270	OK

alpha W2	>25	alpha W3		alpha W1	
0.538375	OK	0.606383	OK	0.873775	OK

Strength		
Reinforcing Bars		
Wall		Main Bars
Long.	Trans.	
AS*FY	AS*FY	AS*FY
20029.68	20029.68	330537.9

Stirrups					
BI-FM					
Step	n	Hook	Pw %	AS	AS*Fyw
50	8	0	0.64OK	512	224409.6
CJ - EL					
Step	n	Hook	Pw %	AS	AS*Fyw
50	7	0	0.64OK	448	196358.4
DK					
Step	n	Hook	Pw %	AS	AS*Fyw
50	6	0	0.64OK	384	168307.2

Concrete	
Wall	Beam
0.85*Fc*	0.85*Fc*b
1917.6	4794

L4=L3=0.5*(1700-2*(L1+L2))
Considering the angle a6
additional zone will be add
this case L4=L3=(1700-2*(L1+L2))/3

Applied Forces		
V	C	T
156000	414375	414375

Tables of details of numerical calculations of STM-S6

PART "2"	P0					

Reactions

R1	R2	R3
151125	217197.5267	0

Horizontal Members

DE	EF	FG	KL	PQ	LM
0	151125	326625	151125	0	326625

Vertical Members

DK	EL	FM	LQ	KP
156000	156000	156000	0	0

Inclind Members

KE	LF	MG	PL	QM
217197.5267	234811.0943	178986.2076	0	0

P1

Reactions

R1	R2	R3
0	0	0

Horizontal Members

DE	EF	FG	KL	PQ	LM
0	0.96875	0	0.96875	1.441860465	1.441860465

Vertical Members

DK	EL	FM	LQ	KP
0	1	0.861111111	3.275389099	1

Inclind Members

KE	LF	MG	PL	QM
1.392291838	1.296143861	0	1.754697011	1.679426672

Modulus of Elasticity

Horizontal Members

DE	EF	FG	KL	PQ	LM
22577	22577	22577	196000	186000	196000

Vertical Members

DK	EL	FM	LQ	KP
192000	192000	192000	22577	186000

Inclind Members

KE	LF	MG	PL	QM
22577	22577	22577	22577	186000

Width of Struts

EF	FG	GH	MF	NG	OH	NS	RN
80	80	80	75.51019564	81.63367205	62.22577095	32	32

Axial Stiffness

Horizontal Members

DE	EF	FG	KL	PQ	LM
361232000	361232000	361232000	168756000	10453200	168756000

Vertical Members

DK	EL	FM	LQ	KP
75264000	87808000	100352000	57797120	2613300

Inclind Members

KE	LF	MG	PL	QM
340958737.4	368608682.8	280974246.2	57797120	20386896.26

Length of Members					
Horizontal Members					
DE	EF	FG	KL	PQ	LM
310	360	180	310	310	360
Vertical Members					
DK	EL	FM	LQ	KP	
320	320	320	215	215	
Inclind Members					
KE	LF	MG	PL	QM	
445.5333882	481.6637832	367.151195	377.2598574	419.3149175	

Each of (P0*P1*L/EA) and (P1*P1*L/EA) was calculated taking into considerat
members in tensiona and in compression

P0*P1*L/EA					
Horizontal Members					
DE	EF	FG	KL	PQ	LM
0	-0.145903031	0	-0.268936966	0	-1.004652651
Vertical Members					
DK	EL	FM	LQ	KP	
0	-0.56851312	-0.428358844	0	0	
Inclind Members					
KE	LF	MG	PL	QM	
-0.395151454	0.39769511	0	0	0	

P1*P1*L/EA					
Horizontal Members					
DE	EF	FG	KL	PQ	LM
0	9.35276E-07	0	1.72395E-06	6.16537E-05	4.43496E-06
Vertical Members					
DK	EL	FM	LQ	KP	
0	3.64431E-06	2.36452E-06	3.99078E-05	8.22715E-05	
Inclind Members					
KE	LF	MG	PL	QM	
2.53302E-06	2.19525E-06	0	2.00973E-05	5.80111E-05	

P0*P1*L/EA	-2.413820955	P1*P1*L/EA	0.000279773	X	8627.792522

	Final Axial Forces					
	Horizontal Members					
	DE	EF	FG	KL	PQ	LM
Force	0	159.483174	326.625	159.483174	12.44007294	339.0650729
strength	230.112	230.112	230.112	247.903425	15.02226	247.903425
	0	0.693067611	1.419417501	0.643327836	0.828109282	1.36773049
	Vertical Members					
	DK	EL	FM	LQ	KP	
Force	132.6	139.9336236	163.429488	28.25937758	8.627792522	
strength	126.2304	147.2688	168.3072	61.3632	20.02968	
	1.050460111	0.950191919	0.971018994	0.460526465	0.430750393	
	Inclind Members					
	KE	LF	MG	PL	QM	
Force	229.2099319	245.9939546	178.9862076	15.13916175	14.48974488	
strength	361.9958779	391.3518238	298.3103459	61.3632	39.06392379	
	0.633183817	0.628574954	0.6	0.24671402	0.370923949	

PART "1"

P0

Reactions

R1	R2	R3
151125	217197.5267	0

Horizontal Members

AB	BC		HI	IJ	
414375	326625		326625	151125	

Vertical Members

BI	CJ	IO	
156000	156000	0	

Inclind Members

HB	IC	HO	OJ	
178986.2076	234811.0943	0	0	

P1

Reactions

R1	R2	R3
0	0	0

Horizontal Members

AB	BC		HI	IJ	
0	0.375		0.933139535	0.558139535	

Vertical Members

BI	CJ	IO	
0.666666667	0.333333333	1	

Inclind Members

HB	IC	HO	OJ	
0.764898323	0.501733107	0.869462009	0.650100647	

Modulus of Elastisity

Horizontal Members

AB	BC		HI	IJ	
196000	196000		22577	22577	

Vertical Members

BI	CJ	IO	
192000	192000	192000	

Inclind Members

HB	IC	HO	OJ	
22577	22577	22577	22577	

Width of Struts

HI	IJ		HB	IC		OH	OJ
80	80		62.22577095	81.63367205		10	10

Axial Stiffness

Horizontal Members

AB	BC		HI	IJ	
168756000	168756000		361232000	361232000	

Vertical Members

BI	CJ	IO	
98304000	86016000	73728000	

Inclind Members

HB	IC	HO	OJ	
280974246.2	368608682.8	45154000	18061600	

Length of Members					
Horizontal Members					
AB	BC		HI	IJ	
180	360		180	360	

Vertical Members			
BI	CJ	IO	
320	320	215	

Inclind Members				
HB	IC	HO	OJ	
367.151195	481.6637832	280.4014979	419.3149175	

Each of (P0*P1*L/EA) and (P1*P1*L/EA) was calculated taking into consideration the
in tensiona and in compression

P0*P1*L/EA					
Horizontal Members					
AB	BC		HI	IJ	
0	-0.26129071		-0.151873605	-0.084061161	

Vertical Members			
BI	CJ	IO	
0.338541667	-0.193452381	0	

Inclind Members				
HB	IC	HO	OJ	
0.178896443	-0.153946494	0	0	

P1*P1*L/EA					
Horizontal Members					
AB	BC		HI	IJ	
0	2.99989E-07		4.3389E-07	3.10457E-07	

Vertical Members			
BI	CJ	IO	
1.44676E-06	4.1336E-07	2.91612E-06	

Inclind Members				
HB	IC	HO	OJ	
7.64515E-07	3.28946E-07	4.69446E-06	9.81172E-06	

P0*P1*L/EA	-0.327186241	P1*P1*L/EA	2.14202E-05	X	15274.64457

	Final Axial Forces					
	Horizontal Members					
	AB	BC		HI	IJ	
Force	414.375	332.3529917		340.8783747	159.650383	
strength	247.903425	247.903425		383.52	383.52	
	1.67151785	1.340655103		0.88881512	0.416276551	

	Vertical Members			
	BI	CJ	IO	
Force	191.1105608	161.0915482	17.56584126	
strength	168.3072	147.2688	20.02968	
	1.135486544	1.09386067	0.876990609	

	Inclind Members				
	HB	IC	HO	OJ	
Force	190.6697576	242.4748892	13.28072315	9.930056321	
strength	298.3103459	391.3518238	19.176	19.176	
	0.639165755	0.619582878	0.692570043	0.517837731	

Figure (7.11) shows the numerical results of STM-S6.The values in Figure (7.11) are the values of (force / strength) of each member.

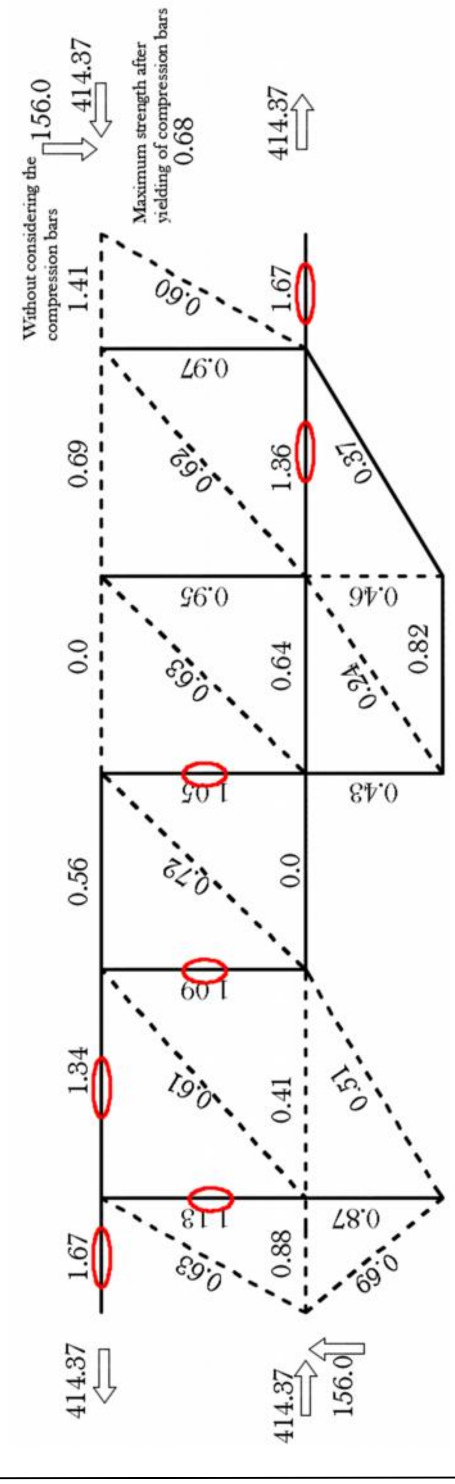

Fig (7.11) The analytical results of STM-S6

7.3.1.3 Numerical Results of STM-S6-AR

The specimen SP-S6-AR was modeled using the same model of SP-S6. Considering the difference is in the materials properties and the arrangement of stirrups. Where the two specimens, SP-S6 and SP-S6-AR, were designed and constructed in different stages of research.

The details of numerical calculations of STM-S6-AR are shown in followings tables.

Beam Section		Wall Section		Concrete Propertie		Main Bars			
b	D	T	H	Ec	Fc	Es	As	Pt	Fy
200	400	80	350	22400	27.71	192000	861	0.011958	380.4

Wall's Bars								
Es	Number of H layers		AS	As-tot	Number of V layer	AS	As-tot	Fy
167000	2		14.05	56.2	2	14.05	56.2	401.1

Stirrups		
Es	Fy	Asw
194000	364.5	32

Dimensions mm								
h1	h2	L1	L2	L3	L4=L3	L	J	
320	215	180	360	310	310	1700	320	

Angles							
alpha1	>25	alpha2	>25	alpha3	>25	alpha4	>25
1.058407	OK	0.726642	OK	0.801270	OK	0.801270	OK

alpha W2	>25	alpha W3		alpha W1	
0.538375	OK	0.606383	OK	0.873775	OK

Strength		
Reinforcing Bars		
Wall		Main Bars
Long.	Trans.	
AS*FY	AS*FY	AS*FY
22541.82	22541.82	327524.4

Stirrups					
BI-FM					
Step	n	Hook	Pw %	AS	AS*Fyw
35	11	0	0.914286 OK	704	256608
CJ - EL					
Step	n	Hook	Pw %	AS	AS*Fyw
50	7	0	0.64 OK	448	163296
DK					
Step	n	Hook	Pw %	AS	AS*Fyw
50	6	0	0.64 OK	384	139968

Concrete	
Wall	Beam
0.85*Fc*T	0.85*Fc*b
1884.28	4710.7

L4=L3=0.5*(1700-2*(L1+L2))
Considering the angle a6
additional zone will be add
this case L4=L3=(1700-2*(L1+L2))/3

Applied Forces		
V	C	T
152000	403750	403750

Tables of details of numerical calculations of STM-S6-AR

PART "2"	P0					

Reactions		
R1	R2	R3
147250	211628.3594	0

Horizontal Members					
DE	EF	FG	KL	PQ	LM
0	147250	318250	147250	0	318250

Vertical Members				
DK	EL	FM	LQ	KP
152000	152000	152000	0	0

Inclind Members				
KE	LF	MG	PL	QM
211628.3594	228790.297	174396.8176	0	0

P1

Reactions		
R1	R2	R3
0	0	0

Horizontal Members					
DE	EF	FG	KL	PQ	LM
0	0.96875	0	0.96875	1.441860465	1.441860465

Vertical Members				
DK	EL	FM	LQ	KP
0	1	0.861111111	3.275389099	1

Inclind Members				
KE	LF	MG	PL	QM
1.392291838	1.296143861	0	1.754697011	1.679426672

Modulus of Elastisity

Horizontal Members					
DE	EF	FG	KL	PQ	LM
22400	22400	22400	192000	167000	192000

Vertical Members				
DK	EL	FM	LQ	KP
194000	194000	194000	22400	167000

Inclind Members				
KE	LF	MG	PL	QM
22400	22400	22400	22400	167000

Width of Struts

EF	FG	GH	MF	NG	OH	NS	RN
80	80	80	74.87505728	80.94702733	61.70237177	32	32

Axial Stiffness

Horizontal Members					
DE	EF	FG	KL	PQ	LM
358400000	358400000	358400000	165312000	9385400	165312000

Vertical Members				
DK	EL	FM	LQ	KP
73728000	86016000	135168000	57344000	2346350

Inclind Members				
KE	LF	MG	PL	QM
335440256.6	362642682.5	276426625.6	57344000	18304363.84

Length of Members					
Horizontal Members					
DE	EF	FG	KL	PQ	LM
310	360	180	310	310	360

Vertical Members				
DK	EL	FM	LQ	KP
320	320	320	215	215

Inclind Members				
KE	LF	MG	PL	QM
445.5333882	481.6637832	367.151195	377.2598574	419.3149175

Each of (P0*P1*L/EA) and (P1*P1*L/EA) was calculated taking into considerat
members in tensiona and in compression

P0*P1*L/EA					
Horizontal Members					
DE	EF	FG	KL	PQ	LM
0	-0.143285261	0	-0.267500336	0	-0.999285917

Vertical Members				
DK	EL	FM	LQ	KP
0	-0.56547619	-0.309869529	0	0

Inclind Members				
KE	LF	MG	PL	QM
-0.391353495	0.393872703	0	0	0

P1*P1*L/EA					
Horizontal Members					
DE	EF	FG	KL	PQ	LM
0	9.42666E-07	0	1.75987E-06	6.86682E-05	4.52736E-06

Vertical Members				
DK	EL	FM	LQ	KP
0	3.72024E-06	1.75547E-06	4.02232E-05	9.16317E-05

Inclind Members				
KE	LF	MG	PL	QM
2.57469E-06	2.23137E-06	0	2.02561E-05	6.46112E-05

P0*P1*L/EA	-2.282898025	P1*P1*L/EA	0.000302902	X	7536.754124

	Final Axial Forces					
	Horizontal Members					
	DE	EF	FG	KL	PQ	LM
Force	0	154.5512306	318.25	154.5512306	10.86694781	329.1169478
strength	226.1136	226.1136	226.1136	245.6433	16.906365	245.6433
	0	0.683511432	1.407478365	0.62916933	0.642772578	1.339816506

	Vertical Members				
	DK	EL	FM	LQ	KP
Force	129.2	135.606241	158.4899827	24.6858023	7.536754124
strength	104.976	122.472	192.456	60.29696	22.54182
	1.230757506	1.107242807	0.823512817	0.409403763	0.334345413

	Inclind Members				
	KE	LF	MG	PL	QM
Force	222.1217206	238.5590146	174.3968176	13.22471994	12.6574259
strength	352.7139323	381.3171617	290.6613627	60.29696	43.96335531
	0.629750345	0.625618353	0.6	0.219326479	0.28790855

PART "1"

P0

Reactions

R1	R2	R3
147250	211628.3594	0

Horizontal Members

AB	BC		HI	IJ	
403750	318250		318250	147250	

Vertical Members

BI	CJ	IO	
152000	152000	0	

Inclind Members

HB	IC	HO	OJ	
174396.8176	228790.297	0	0	

P1

Reactions

R1	R2	R3
0	0	0

Horizontal Members

AB	BC		HI	IJ	
0	0.375		0.933139535	0.558139535	

Vertical Members

BI	CJ	IO	
0.666666667	0.333333333	1	

Inclind Members

HB	IC	HO	OJ	
0.764898323	0.501733107	0.869462009	0.650100647	

Modulus of Elastisity

Horizontal Members

AB	BC		HI	IJ	
192000	192000		22400	22400	

Vertical Members

BI	CJ	IO	
194000	194000	194000	

Inclind Members

HB	IC	HO	OJ	
22400	22400	22400	22400	

Width of Struts

HI	IJ		HB	IC		OH	OJ
80	80		61.70237177	80.94702733		32	32

Axial Stiffness

Horizontal Members

AB	BC		HI	IJ	
165312000	165312000		358400000	358400000	

Vertical Members

BI	CJ	IO	
136576000	86912000	74496000	

Inclind Members

HB	IC	HO	OJ	
276426625.6	362642682.5	143360000	57344000	

Length of Members

Horizontal Members

AB	BC		HI	IJ	
180	360		180	360	

Vertical Members

BI	CJ	IO	
320	320	215	

Inclind Members

HB	IC	HO	OJ	
367.151195	481.6637832	280.4014979	419.3149175	

Each of (P0*P1*L/EA) and (P1*P1*L/EA) was calculated taking into consideration the in tensiona and in compression

P0*P1*L/EA

Horizontal Members

AB	BC		HI	IJ	
0	-0.259894926		-0.149148712	-0.082552949	

Vertical Members

BI	CJ	IO	
0.237425804	-0.186548846	0	

Inclind Members

HB	IC	HO	OJ	
0.177176998	-0.152466853	0	0	

P1*P1*L/EA

Horizontal Members

AB	BC		HI	IJ	
0	3.06239E-07		4.37318E-07	3.1291E-07	

Vertical Members

BI	CJ	IO	
1.04134E-06	4.09098E-07	2.88606E-06	

Inclind Members

HB	IC	HO	OJ	
7.77092E-07	3.34357E-07	1.47861E-06	3.09039E-06	

P0*P1*L/EA	-0.416009483	P1*P1*L/EA	1.10734E-05	X	37568.29561

Final Axial Forces

Horizontal Members

	AB	BC		HI	IJ	
Force	403.75	332.3381109		353.3064619	168.218351	
strength	245.6433	245.6433		376.856	376.856	
	1.643643446	1.352929678		0.937510513	0.446373021	

Vertical Members

	BI	CJ	IO	
Force	203.60236	123.3920739	16.90573302	
strength	192.456	122.472	22.54182	
	1.057916407	1.007512525	0.749971964	

Inclind Members

	HB	IC	HO	OJ	
Force	203.1327439	247.6395547	32.66420577	24.42317329	
strength	290.6613627	381.3171617	60.29696	60.29696	
	0.698863936	0.649431968	0.541722265	0.40504817	

Figure (7.12) shows the numerical results of STM-S6-AR.

The values in Figure (7.12) are the values of (force / strength) of each member.

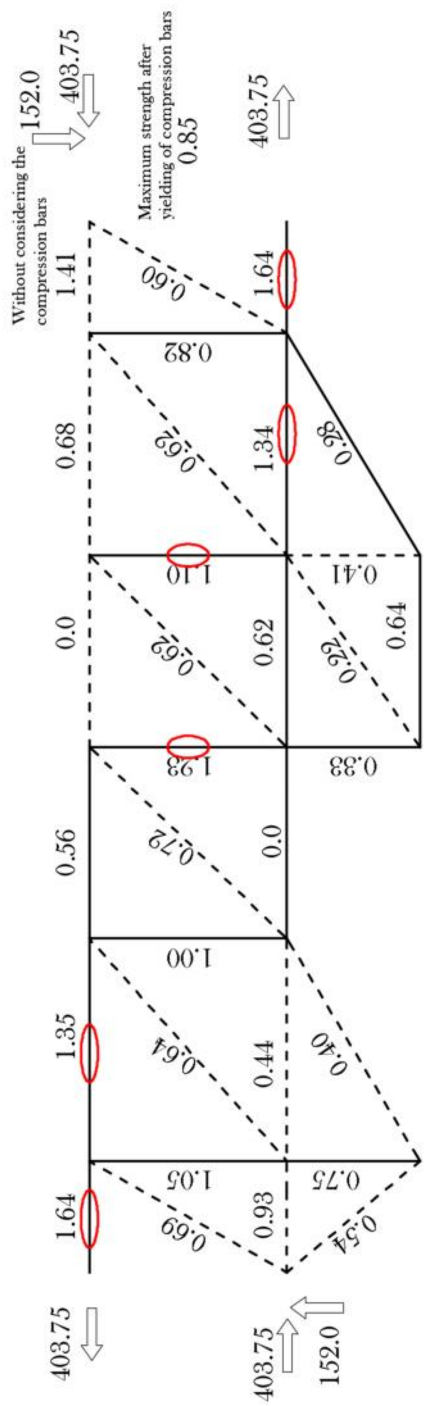

Fig (7.12) The analytical results of STM-S6-AR

7.3.1.4 Parametric Study of Shear reinforcement to each of STM-S6 and STM-S6-AR

By increasing of shear reinforcement ratio in STM-S6 to get the ratio for safe design, the force values in the members will change as a result due to changing of axial stiffness of vertical ties.

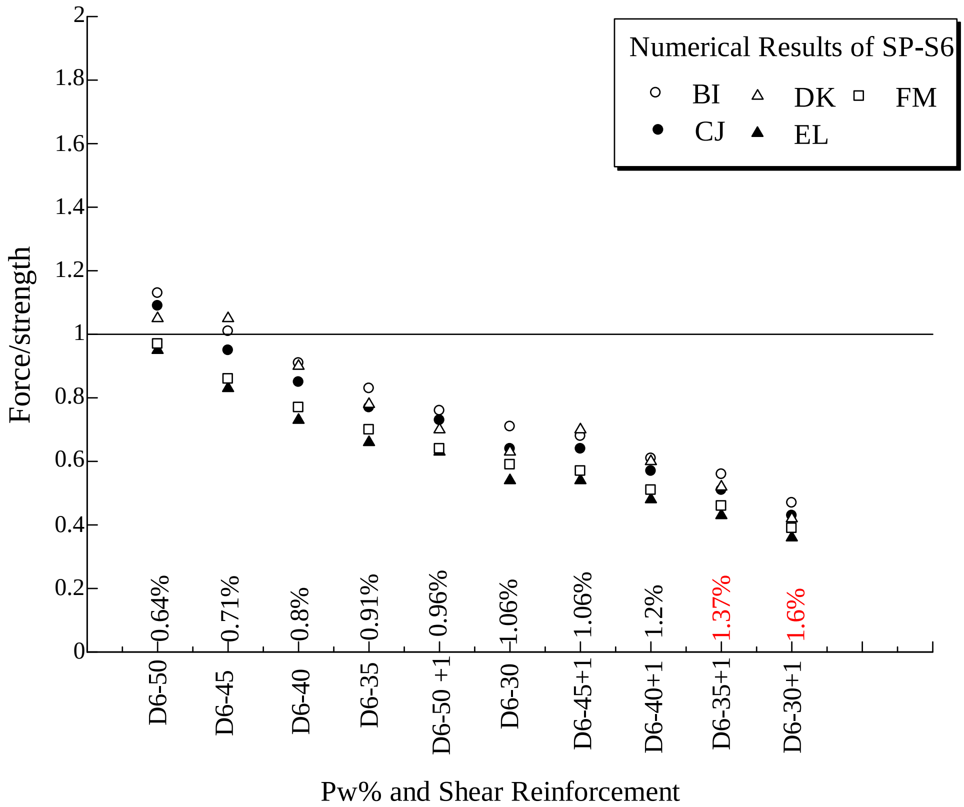

Fig (7.13) Parametric study of the shear reinforcement of SP-S6

Figure (7.13) shows the values of (force / strength) of vertical ties of STM-S6. By increasing the shear reinforcement ratio, (force / strength) will decrease as a result. The designer can choose the proper amount of shear reinforcement to prevent shear failure of specimen.

From Figure (7.12), for shear reinforcement D6@35 at ends of beam, the design is safe and for the other parts of beam where shear reinforcement was kept D6@50, the ties in middle of the beam were not safe. However, this design may be considered to be safe where the plastic hinge regions are safe and by considering the strength reduction factor of stirrups (0.75).

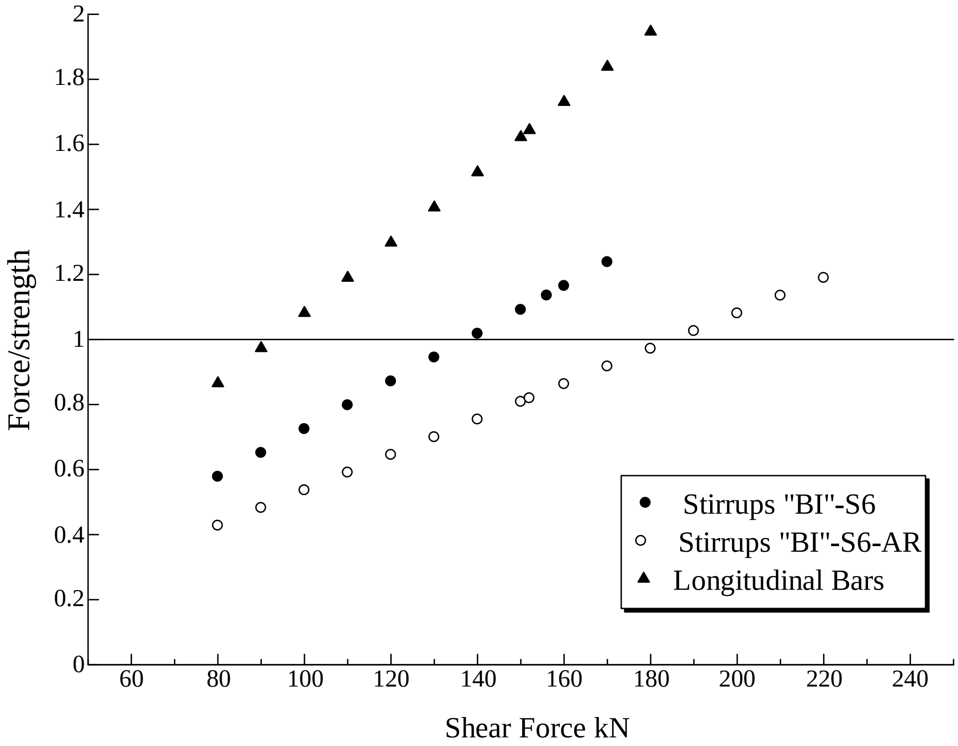

Fig (7.14) Numerical yielding of main bars and stirrups in S6 and S6-AR

From Figure (7.14), it is obvious that the yielding in stirrups at plastic hinge region "BI" occurred after yielding of main bars as same of experimental results of both SP-S6 and SP-S6-AR. In addition, yielding of stirrups "BI" will occurred in STM-S6-AR at higher shear force comparing with STM-S6.

7.3.1.5 Parametric Study of considered height of non-structural wall

Figure (7.15) shows the influence of changing the height of non-structural wall. By increasing the angle between the strut and tie from 25 degree to 65 degree, the limits of height of wall can be calculated.

It is obvious that there is no important influence of the considered height of

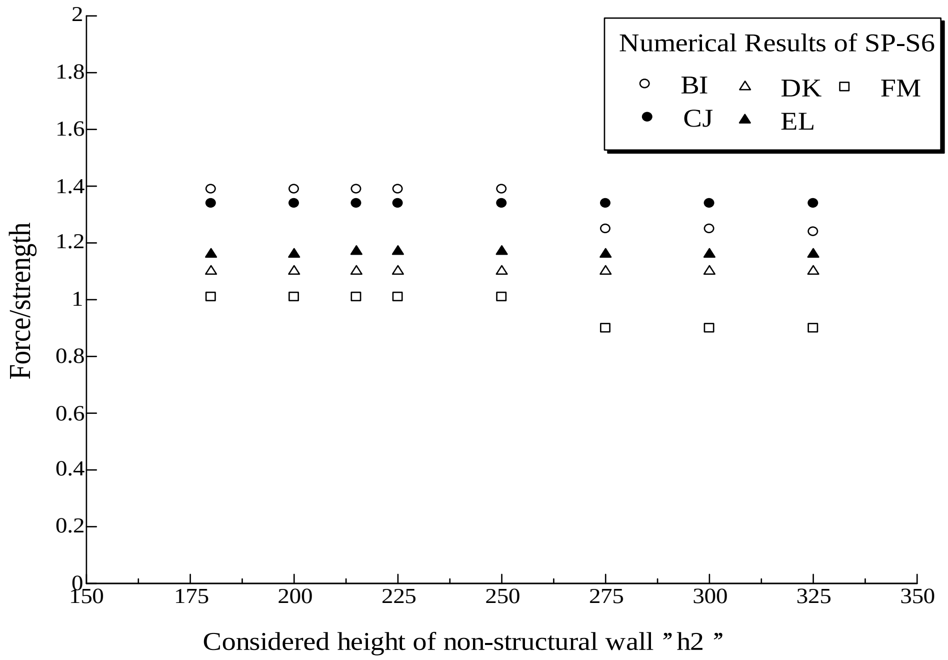

Fig (7.15) Influence of changing height of non-structural wall

wall on the (force/strength) of vertical ties.

In the numerical study, half of height of the wall was considered:

$$h_2 = 0.5 \cdot H + 40 = 0.5 \cdot 350 + 40 = 215mm$$

Where:

H: height of the wall 350 mm, and

40 mm refers to the distance between the face of beam and center of tensile reinforcement.

7.4 Numerical Example

7.4.1 STM-S5

The specimen SP-S5 was modeled using the proposed STM as STM-S5.
Figure (7.16) shows the analytical model of SP-S5.
The following tables show the details of numerical calculations of STM-S5.
Figure (7.17) shows the numerical results of STM-S6-AR.
The values in Figure (7.17) are the values of (force / strength) of each member.
The truss is indeterminate to the second degree. It was divided into two parts each of them is indeterminate to the first degree. The analysis was done using Virtual Work Method.

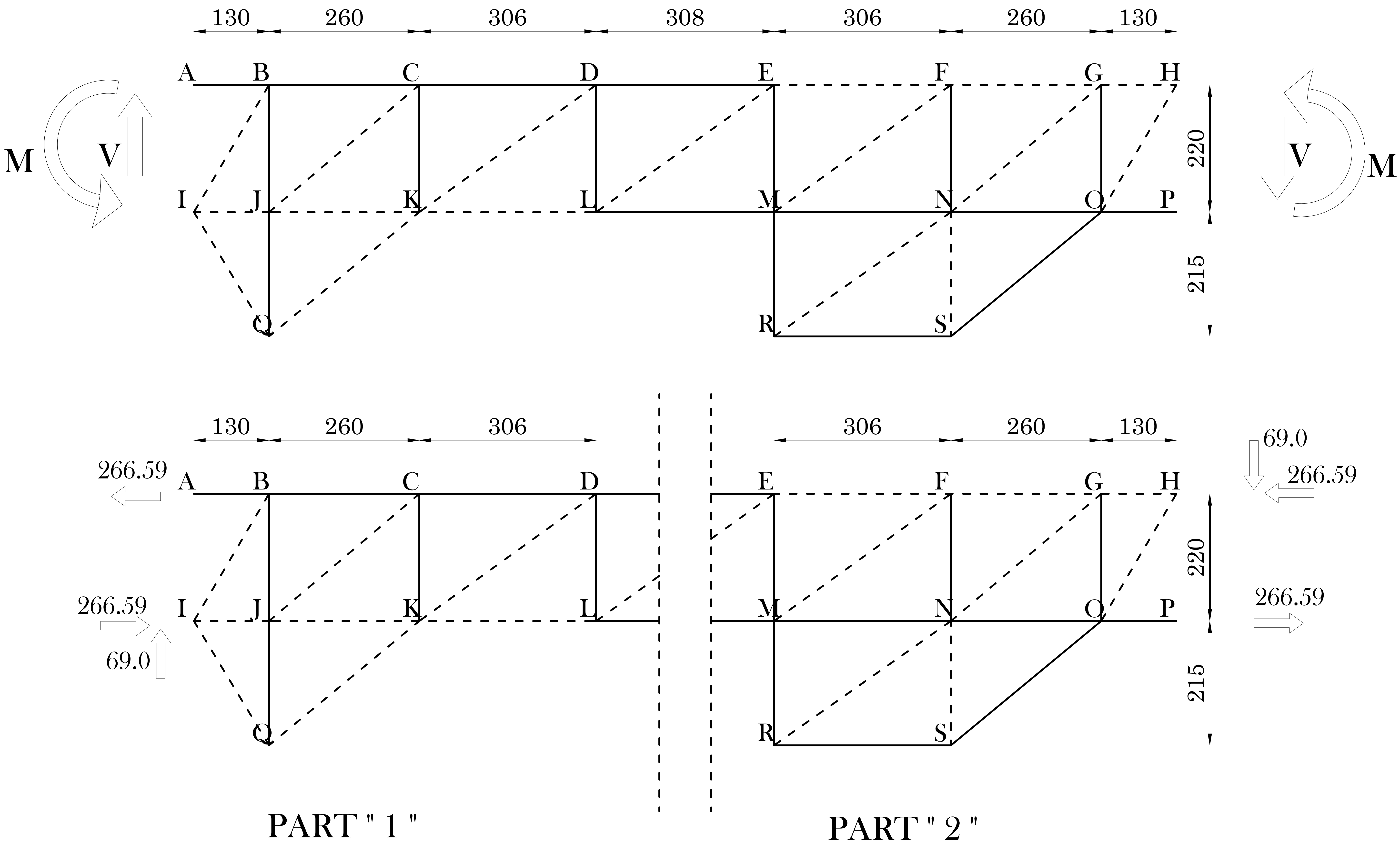

The Analytical Model of SP-S5

Beam Section		Wall Section		Concrete Propertie		Main Bars			
b	D	T	H	Ec	Fc	Es	As	Pt	Fy
200	300	80	350	23049	27.6	196000	570	0.010962	383

Wall's Bars									
Es	Number of H layers		AS	As-tot	Number of V layer		AS	As-tot	Fy
186000	2		14.05	56.2	2		14.05	56.2	356.4

Stirrups		
Es	Fy	Asw
186000	356.4	14.05

Dimensions mm									
h1	h2	L1	L2	L3	L4=L3	L	J		
220	215	130	260	306.6667	306.6667	1700	220		

Angles							
alpha1	>25	alpha2	>25	alpha3	>25	alpha4	>25
1.037088	OK	0.702257	OK	0.622303	OK	0.622303	OK

alpha W2	>25	alpha W3		alpha W1	
0.690943	OK	0.611455	OK	1.026964	OK

Strength		
Reinforcing Bars		
Wall		Main Bars
Long.	Trans.	
AS*FY	AS*FY	AS*FY
20029.68	20029.68	218310

Stirrups					
BJ					
Step	n	Hook	Pw %	AS	AS*Fyw
70	4	0	0.200714OK	112.4	40059.36
CK					
Step	n	Hook	Pw %	AS	AS*Fyw
70	5	0	0.200714OK	140.5	50074.2
DL					
Step	n	Hook	Pw %	AS	AS*Fyw
70	5	0	0.200714OK	140.5	50074.2

Concrete	
Wall	Beam
0.85*Fc*T	0.85*Fc*b
1876.8	4692

L4=L3=0.5*(1700-2*(L1+L2))
Considering the angle a6
additional zone will be add
this case L4=L3=(1700-2*(L1+L2))/3

Applied Forces		
V	C	T
69000	266590.9091	266590.9

Tables of details of numerical calculations of STM-S5

PART "1"

P0

Reactions

R1	R2	R3
48090.90909	118372.0497	48090.90909

Horizontal Members

AB	BC	CD	IJ	JK	KL
266590.9091	225818.1818	144272.7273	225818.1818	144272.7273	48090.90909

Vertical Members

BJ	CK	DL	JQ
69000	69000	69000	0

Inclind Members

IB	JC	KD	IQ	QK
80146.21195	106820.6963	118372.0497	0	0

P1

Reactions

R1	R2	R3
0	0	0

Horizontal Members

AB	BC	CD	IJ	JK	KL
0	0.393939394	0	0.797040169	0.403100775	0

Vertical Members

BJ	CK	DL	JQ
0.666666667	0.333333333	0	1

Inclind Members

IB	JC	KD	IQ	QK
0.774359536	0.516042011	0	0.779060126	0.52306916

Modulus of Elastisity

Horizontal Members

AB	BC	CD	IJ-CONC	JK-CONC	KL-CONC
196000	196000	196000	23049	23049	23049

Vertical Members

BJ	CK	DL	JQ
186000	186000	186000	186000

Inclind Members

IB	JC	KD	IQ	QK
23049	23049	23049	23049	23049

Width of Struts

IJ	JK	KL	IB	JC	KD	IQ	QK
80	80	80	28.46910058	37.94426552	42.04747432	10	10

Axial Stiffness

Horizontal Members

AB	BC	CD	IJ	JK	KL
111720000	111720000	111720000	368784000	368784000	368784000

Vertical Members

BJ	CK	DL	JQ
20906400	26133000	26133000	10453200

Inclind Members

IB	JC	KD	IQ	QK
131236859.8	174915475.2	193830447.1	18439200	18439200

Length of Members

Horizontal Members					
AB	BC	CD	IJ	JK	KL
130	260	306.6666667	130	260	306.6666667

Vertical Members			
BJ	CK	DL	JQ
220	220	220	215

Inclind Members				
IB	JC	KD	IQ	QK
255.5386468	340.5877273	377.4181295	251.2468905	337.3796082

Each of (P0*P1*L/EA) and (P1*P1*L/EA) was calculated taking into consideration the
in tensiona and in compression

P0*P1*L/EA

Horizontal Members					
AB	BC	CD	IJ	JK	KL
0	-0.207028788	0	-0.063446899	-0.041001444	0

Vertical Members			
BJ	CK	DL	JQ
0.484062297	-0.193624919	0	0

Inclind Members				
IB	JC	KD	IQ	QK
0.120844367	-0.107334966	0	0	0

P1*P1*L/EA

Horizontal Members					
AB	BC	CD	IJ	JK	KL
0	3.61161E-07	0	2.2394E-07	1.14559E-07	0

Vertical Members			
BJ	CK	DL	JQ
4.67693E-06	9.35386E-07	0	2.05679E-05

Inclind Members				
IB	JC	KD	IQ	QK
1.16758E-06	5.18526E-07	0	8.26991E-06	5.00605E-06

P0*P1*L/EA	-0.007530352	P1*P1*L/EA	4.18419E-05	X	179.9715532

Final Axial Forces

	Horizontal Members					
	AB	BC	CD	IJ	JK	KL
Force	266.5909091	225.8890797	144.2727273	225.9616264	144.3452739	48.09090909
strength	163.7325	163.7325	163.7325	225.216	225.216	225.216
	1.628210093	1.379622736	0.881148992	1.003310717	0.640919268	0.213532383

	Vertical Members			
	BJ	CK	DL	JQ
Force	79.48797819	79.4189891	79.35	0.179971553
strength	30.04452	37.55565	37.55565	15.02226
	2.645673094	2.114701492	2.112864509	0.011980325

	Inclind Members				
	IB	JC	KD	IQ	QK
Force	80.28557463	106.9135692	118.3720497	0.140208661	0.094137569
strength	133.5770199	178.0344938	197.2867495	11.2608	11.2608
	0.601043313	0.600521657	0.6	0.012451039	0.008359759

PART "2"	P0						

Reactions

R1	R2	R3
48090.90909	118372.0497	48090.90909

Horizontal Members

EF	FG	GH	MN	RS	NO	OP
48090.90909	144272.7273	225818.1818	144272.7273	0	225818.1818	266590.9

Vertical Members

EM	FN	GO	NS	MR
69000	69000	69000	0	0

Inclind Members

MF	NG	OH	RN	SO
118372.0497	106820.6963	80146.21195	0	0

P1

Reactions

R1	R2	R3
0	0	0

Horizontal Members

EF	FG	GH	MN	RS	NO
0	1.393939394	0	1.393939394	1.426356589	1.426356589

Vertical Members

EM	FN	GO	NS	MR
0	1	1.179487179	2.90438352	1

Inclind Members

MF	NG	OH	RN	SO
1.715536952	1.825994808	0	1.741979655	1.850860104

Modulus of Elastisity

Horizontal Members

EF	FG	GH	MN	RS	NO
23049	23049	23049	196000	186000	196000

Vertical Members

EM	FN	GO	NS	MR
186000	186000	186000	23049	186000

Inclind Members

MF	NG	OH	RN	SO
23049	23049	23049	23049	186000

Width of Struts

EF	FG	GH	MF	NG	OH	NS	RN
80	80	80	42.04747432	37.94426552	28.46910058	32	32

Axial Stiffness

Horizontal Members

EF	FG	GH	MN	RS	NO
368784000	368784000	368784000	111720000	10453200	111720000

Vertical Members

EM	FN	GO	NS	MR
27538000	27538000	22030400	59005440	2613300

Inclind Members

MF	NG	OH	RN	SO
193830447.1	174915475.2	131236859.8	59005440	16403239.63

Length of Members					
Horizontal Members					
EF	FG	GH	MN	RS	NO
306.6666667	260	130	306.6666667	306.6666667	260
Vertical Members					
EM	FN	GO	NS	MR	
220	220	220	215	215	
Inclind Members					
MF	NG	OH	RN	SO	
377.4181295	340.5877273	255.5386468	374.5256259	337.3796082	

Each of (P0*P1*L/EA) and (P1*P1*L/EA) was calculated taking into considerat
members in tensiona and in compression

P0*P1*L/EA					
Horizontal Members					
EF	FG	GH	MN	RS	NO
0	-0.141784714	0	-0.552031397	0	-0.749599762
Vertical Members					
EM	FN	GO	NS	MR	
0	-0.551238289	-0.812723118	0	0	
Inclind Members					
MF	NG	OH	RN	SO	
-0.395412146	0.37980065	0	0	0	

P1*P1*L/EA					
Horizontal Members					
EF	FG	GH	MN	RS	NO
0	1.3699E-06	0	5.33364E-06	5.96861E-05	4.73477E-06
Vertical Members					
EM	FN	GO	NS	MR	
0	7.98896E-06	1.38927E-05	3.07365E-05	8.22715E-05	
Inclind Members					
MF	NG	OH	RN	SO	
5.73061E-06	6.49232E-06	0	1.92609E-05	7.0459E-05	

P0*P1*L/EA	-2.822988776	P1*P1*L/EA	0.000307957	X	9166.832502

	Final Axial Forces						
	Horizontal Members						
	EF	FG	GH	MN	RS	NO	OP
Force	48.09090909	157.0507362	225.8181818	157.0507362	13.07517194	238.8933538	266.5909
strength	375.36	375.36	375.36	163.7325	15.02226	163.7325	163.7325
	0.12811943	0.418400299	0.601604278	0.959190974	0.870386476	1.459046639	1.62821
	Vertical Members						
	EM	FN	GO	NS	MR		
Force	65.55	74.25849088	75.82155334	26.62399725	9.166832502		
strength	37.55565	37.55565	30.04452	60.0576	15.02226		
	1.745409812	1.977292122	2.52364003	0.443307712	0.610216605		
	Inclind Members						
	MF	NG	OH	RN	SO		
Force	134.0980896	123.5592849	80.14621195	15.96843572	16.96652456		
strength	197.2867495	178.0344938	133.5770199	60.0576	31.43072367		
	0.679711587	0.694018795	0.6	0.265885345	0.539806997		

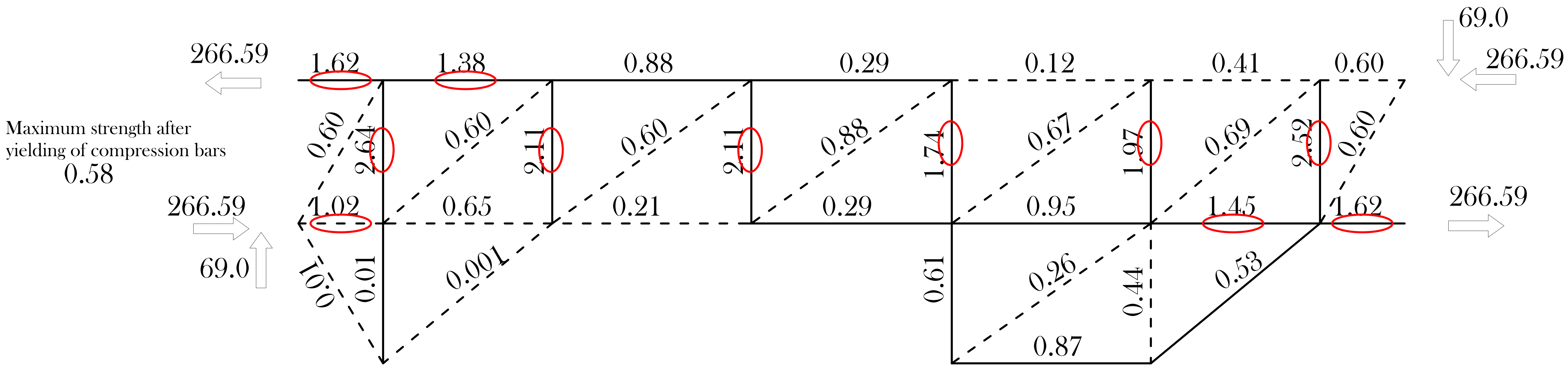

The Analytical Results of STM-S5

7.4.2 STM-S5-AR

The following tables show the details of numerical calculations of STM-S5. Figure (7.18) shows the numerical results model of SP-S5-AR. Where the shear reinforcement was increased to be D6@70 mm. The mechanical properties of the stirrups were same of in SP-S6.

Beam Section		Wall Section		Concrete Properties		Main Bars			
b	D	T	H	Ec	Fc	Es	As	Pt	Fy
200	300	80	350	23049	27.6	196000	570	0.010962	383

Wall's Bars							
Es	Number of H layers	AS	As-tot	Number of V layer	AS	As-tot	Fy
186000	2	14.05	56.2	2	14.05	56.2	356.4

Stirrups		
Es	Fy	Asw
192000	438.3	32

Dimensions mm									
h1	h2	L1	L2	L3	L4=L3	L	J		
220	215	130	260	306.6667	306.6667	1700	220		

Angles							
alpha1	>25	alpha2	>25	alpha3	>25	alpha4	>25
1.037088	OK	0.702257	OK	0.622303	OK	0.622303	OK

alpha W2	>25	alpha W3		alpha W1	
0.690943	OK	0.611455	OK	1.026964	OK

Strength		
Reinforcing Bars		
Wall		Main Bars
Long.	Trans.	
AS*FY	AS*FY	AS*FY
20029.68	20029.68	218310

Stirrups					
BJ					
Step	n	Hook	Pw %	AS	AS*Fyw
70	4	0	0.457143OK	256	112204.8
CK					
Step	n	Hook	Pw %	AS	AS*Fyw
70	5	0	0.457143OK	320	140256
DL					
Step	n	Hook	Pw %	AS	AS*Fyw
70	5	0	0.457143OK	320	140256

Concrete	
Wall	Beam
0.85*Fc*	0.85*Fc*b
1876.8	4692

L4=L3=0.5*(1700-2*(L1+L2))
Considering the angle a6
additional zone will be add
this case L4=L3=(1700-
2*(L1+L2))/3

Applied Forces		
V	C	T
69000	266590.9091	266590.9

Tables of details of numerical calculations of STM-S5-AR

PART "1"	P0					
	Reactions					
	R1	R2	R3			
	48090.90909	118372.0497	48090.90909			
	Horizontal Members					
	AB	BC	CD	IJ	JK	KL
	266590.9091	225818.1818	144272.7273	225818.1818	144272.7273	48090.90909
	Vertical Members					
	BJ	CK	DL	JQ		
	69000	69000	69000	0		
	Inclind Members					
	IB	JC	KD	IQ	QK	
	80146.21195	106820.6963	118372.0497	0	0	

P1					
Reactions					
R1	R2	R3			
0	0	0			
Horizontal Members					
AB	BC	CD	IJ	JK	KL
0	0.393939394	0	0.797040169	0.403100775	0
Vertical Members					
BJ	CK	DL	JQ		
0.666666667	0.333333333	0	1		
Inclind Members					
IB	JC	KD	IQ	QK	
0.774359536	0.516042011	0	0.779060126	0.52306916	

Modulus of Elastisity					
Horizontal Members					
AB	BC	CD	IJ-CONC	JK-CONC	KL-CONC
196000	196000	196000	23049	23049	23049
Vertical Members					
BJ	CK	DL	JQ		
192000	192000	192000	186000		
Inclind Members					
IB	JC	KD	IQ	QK	
23049	23049	23049	23049	23049	

Width of Struts							
IJ	JK	KL	IB	JC	KD	IQ	QK
80	80	80	28.46910058	37.94426552	42.04747432	10	10

Axial Stiffness					
Horizontal Members					
AB	BC	CD	IJ	JK	KL
111720000	111720000	111720000	368784000	368784000	368784000
Vertical Members					
BJ	CK	DL	JQ		
49152000	61440000	61440000	10453200		
Inclind Members					
IB	JC	KD	IQ	QK	
131236859.8	174915475.2	193830447.1	18439200	18439200	

Length of Members

Horizontal Members					
AB	BC	CD	IJ	JK	KL
130	260	306.6666667	130	260	306.6666667

Vertical Members			
BJ	CK	DL	JQ
220	220	220	215

Inclind Members				
IB	JC	KD	IQ	QK
255.5386468	340.5877273	377.4181295	251.2468905	337.3796082

Each of (P0*P1*L/EA) and (P1*P1*L/EA) was calculated taking into consideration the
in tensiona and in compression

P0*P1*L/EA

Horizontal Members					
AB	BC	CD	IJ	JK	KL
0	-0.207028788	0	-0.063446899	-0.041001444	0

Vertical Members			
BJ	CK	DL	JQ
0.205891927	-0.082356771	0	0

Inclind Members				
IB	JC	KD	IQ	QK
0.120844367	-0.107334966	0	0	0

P1*P1*L/EA

Horizontal Members					
AB	BC	CD	IJ	JK	KL
0	3.61161E-07	0	2.2394E-07	1.14559E-07	0

Vertical Members			
BJ	CK	DL	JQ
1.98929E-06	3.97859E-07	0	2.05679E-05

Inclind Members				
IB	JC	KD	IQ	QK
1.16758E-06	5.18526E-07	0	8.26991E-06	5.00605E-06

P0*P1*L/EA	-0.174432573	P1*P1*L/EA	3.86167E-05	X	4517.020132

Final Axial Forces

	Horizontal Members					
	AB	BC	CD	IJ	JK	KL
Force	266.5909091	227.597614	144.2727273	229.4184283	146.0935416	48.09090909
strength	163.7325	163.7325	163.7325	225.216	225.216	225.216
	1.628210093	1.390057649	0.881148992	1.018659546	0.648681895	0.213532383

	Vertical Members			
	BJ	CK	DL	JQ
Force	82.81304877	81.08152438	79.35	4.517020132
strength	84.1536	105.192	105.192	15.02226
	0.984070186	0.770795539	0.75433493	0.300688454

	Inclind Members				
	IB	JC	KD	IQ	QK
Force	83.64400956	109.1516684	118.3720497	3.519030272	2.362713926
strength	133.5770199	178.0344938	197.2867495	11.2608	11.2608
	0.626185624	0.613092812	0.6	0.312502688	0.209817591

PART "2"

P0

Reactions		
R1	R2	R3
48090.90909	118372.0497	48090.90909

Horizontal Members						
EF	FG	GH	MN	RS	NO	OP
48090.90909	144272.7273	225818.1818	144272.7273	0	225818.1818	266590.9

Vertical Members				
EM	FN	GO	NS	MR
69000	69000	69000	0	0

Inclind Members				
MF	NG	OH	RN	SO
118372.0497	106820.6963	80146.21195	0	0

P1

Reactions		
R1	R2	R3
0	0	0

Horizontal Members					
EF	FG	GH	MN	RS	NO
0	1.393939394	0	1.393939394	1.426356589	1.426356589

Vertical Members				
EM	FN	GO	NS	MR
0	1	1.179487179	2.90438352	1

Inclind Members				
MF	NG	OH	RN	SO
1.715536952	1.825994808	0	1.741979655	1.850860104

Modulus of Elastisity

Horizontal Members					
EF	FG	GH	MN	RS	NO
23049	23049	23049	196000	186000	196000

Vertical Members				
EM	FN	GO	NS	MR
192000	192000	192000	23049	186000

Inclind Members				
MF	NG	OH	RN	SO
23049	23049	23049	23049	186000

Width of Struts

EF	FG	GH	MF	NG	OH	NS	RN
80	80	80	42.04747432	37.94426552	28.46910058	10	10

Axial Stiffness

Horizontal Members					
EF	FG	GH	MN	RS	NO
368784000	368784000	368784000	111720000	10453200	111720000

Vertical Members				
EM	FN	GO	NS	MR
62720000	62720000	50176000	18439200	2613300

Inclind Members				
MF	NG	OH	RN	SO
193830447.1	174915475.2	131236859.8	18439200	16403239.63

Length of Members					
Horizontal Members					
EF	FG	GH	MN	RS	NO
306.6666667	260	130	306.6666667	306.6666667	260

Vertical Members				
EM	FN	GO	NS	MR
220	220	220	215	215

Inclind Members				
MF	NG	OH	RN	SO
377.4181295	340.5877273	255.5386468	374.5256259	337.3796082

Each of (P0*P1*L/EA) and (P1*P1*L/EA) was calculated taking into considerat
members in tensiona and in compression

P0*P1*L/EA					
Horizontal Members					
EF	FG	GH	MN	RS	NO
0	-0.141784714	0	-0.552031397	0	-0.749599762

Vertical Members				
EM	FN	GO	NS	MR
0	-0.242028061	-0.356836244	0	0

Inclind Members				
MF	NG	OH	RN	SO
-0.395412146	0.37980065	0	0	0

P1*P1*L/EA					
Horizontal Members					
EF	FG	GH	MN	RS	NO
0	1.3699E-06	0	5.33364E-06	5.96861E-05	4.73477E-06

Vertical Members				
EM	FN	GO	NS	MR
0	3.50765E-06	6.09976E-06	9.83568E-05	8.22715E-05

Inclind Members				
MF	NG	OH	RN	SO
5.73061E-06	6.49232E-06	0	6.16347E-05	7.0459E-05

P0*P1*L/EA	-2.057891674	P1*P1*L/EA	0.000405677	X	5072.737257

	Final Axial Forces						
	Horizontal Members						
	EF	FG	GH	MN	RS	NO	OP
Force	48.09090909	151.3438156	225.8181818	151.3438156	7.235532212	233.053714	266.5909
strength	375.36	375.36	375.36	163.7325	15.02226	163.7325	163.7325
	0.12811943	0.40319644	0.601604278	0.924335826	0.48165404	1.423380905	1.62821

	Vertical Members				
	EM	FN	GO	NS	MR
Force	65.55	70.36910039	71.23406713	14.73317449	5.072737257
strength	105.192	105.192	84.1536	18.768	15.02226
	0.623146247	0.66895867	0.846476765	0.785015691	0.337681365

	Inclind Members				
	MF	NG	OH	RN	SO
Force	127.0745179	116.0834882	80.14621195	8.836605099	9.38892701
strength	197.2867495	178.0344938	133.5770199	18.768	31.43072367
	0.644110759	0.652028074	0.6	0.470833605	0.29871813

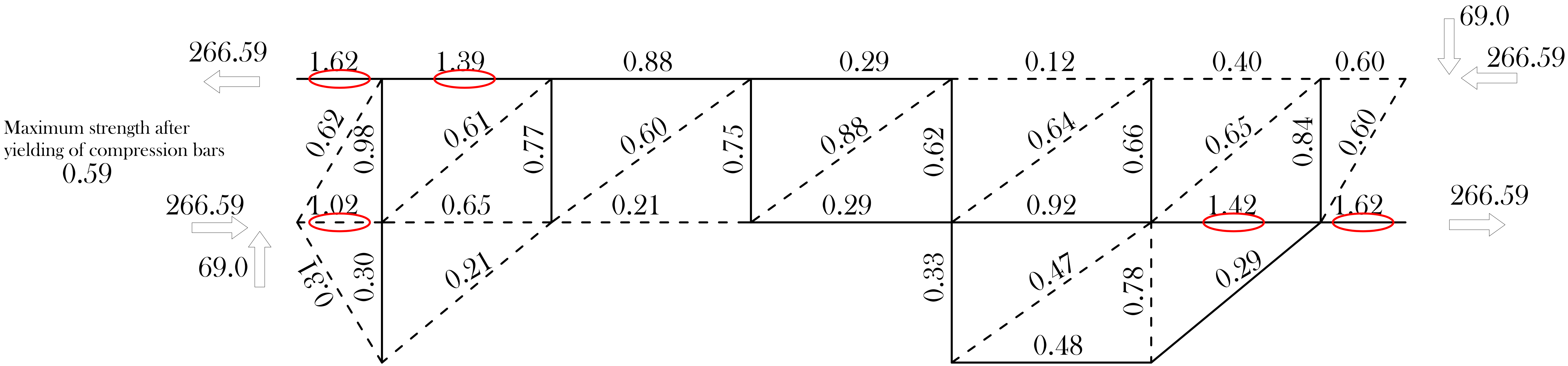

The Analytical Results of STM-S5-AR

7.4.3 Parametric Study of the shear Reinforcement to each of STM-S5 and STM-S5-AR

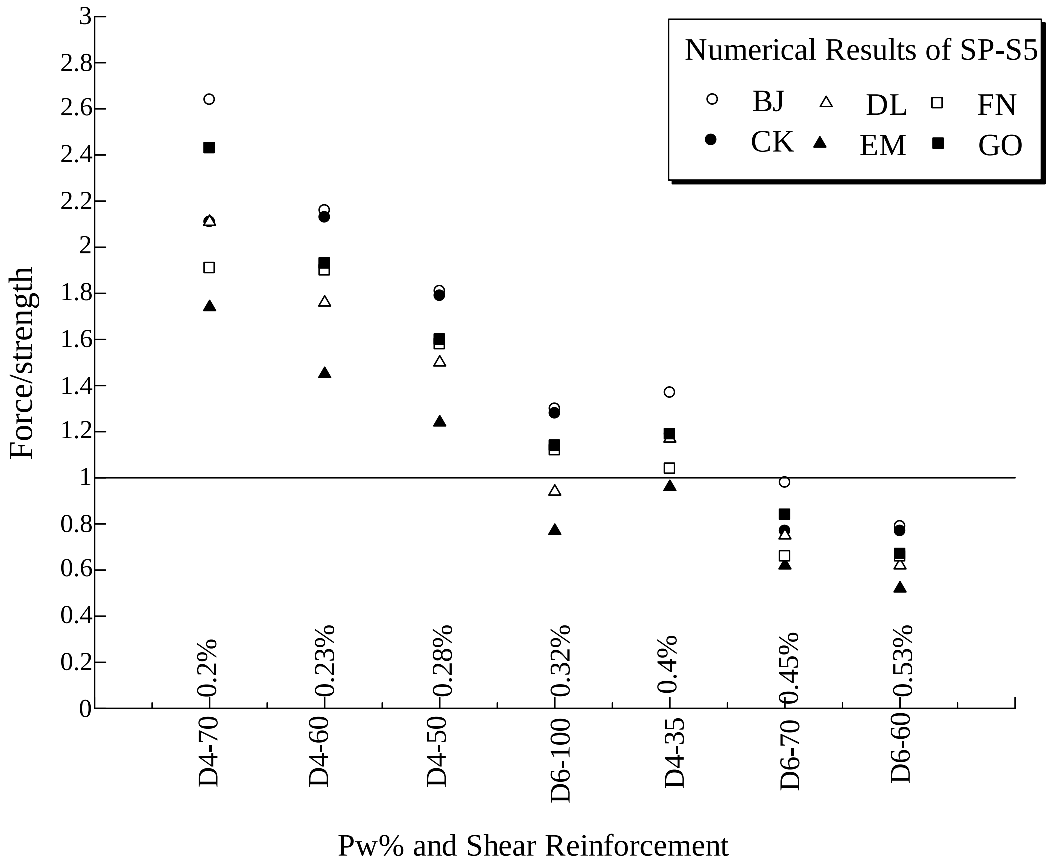

Fig (7.19) Parametric study of the shear reinforcement of SP-S5

Figure (7.19) shows the values of (force / strength) of vertical ties of STM-S5. By increasing the shear reinforcement ratio, (force / strength) will decrease as a result. The designer can choose the proper amount of shear reinforcement to prevent shear failure of specimen.

For shear reinforcement D6@70 for all parts of beam is enough for safe design for SP-S5.

CHAPTER 8
CONCLUSIONS AND FUTURE WORK

- Conclusions
- Future Work

8.1 Conclusions

RC beams with non-structural walls at one side of beam with structural gaps were studied. The influence of the walls on the seismic behavior of beams should not be neglected according the experimental works done on this field of research. The Japanese codes did not determine a specific method for designing these beams and left it up to the designer.

Six beams with different situations were studied and significant experimental results were summarized below:

1)- High tension forces in the stirrups at plastic hinge regions when the loading direction is toward beam face. The lateral enforced displacement was applied as cyclic loading in two directions in same plain; (a) toward the beam face and (b) toward the wall side as shown in Figure (8.1).

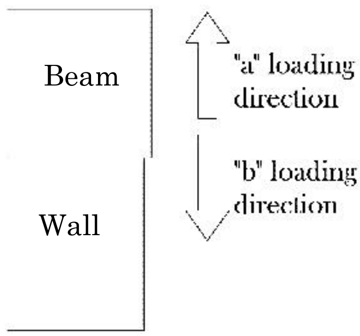

Fig (8.1) Loading directions

The tensile stresses in stirrups at plastic hinge region were higher in case of "a" loading direction.

Each of experimental, analytical and numerical results referred to this important result.

2)- By decreasing the shear span ratio, shear failure occurred. In previous researches, the beam length is 2500 mm and in the current research the same beam was restudied after decreasing the shear span ratio, shear margin.

In the two beams yielding of stirrups occurred but the failure was flexural failure for the beam with length 2500 mm and brittle shear failure in the same beam after decreasing the shear span ratio. The shear span ratio was decreased by shortening the length of beam and increasing the depth of beam, individually. In the former beam, the failure occurred after loading cycle of 1/25 rad where large degradation of strength occurred.

In the later beam, quick forming and propagation of cracks was remarked and the failure occurred at loading cycle of 1/50 rad.

3)- Fracture of stirrups was remarked in two beams and deterioration in the strength occurred immediately after the fracture.

4)- By increasing the amount of shear reinforcement in the plastic hinge region, the seismic performance of the beam improved; large deformation capacity, higher than 1/15 rad, and flexural failure of specimen.

5)- Beams with slab were studied in different situations of slab and wall, hanging and standing walls. The seismic performance improved; large deformation capacity and flexural failure of specimen comparing with the same beams without slabs; shear failure and smaller deformation capacity.

6)- By studying the plastic rotation angle depending on shear strength equation in AIJ guidelines, inelastic displacement concept, it was found that not all cases of beams will be in the safe side of design. Where one of the studied beams was not.

7)- Strut and tie model was proposed to get a safe design of these beams. American code ACI 318-05 was adopted in the designing. Two beam were checked and the numerical results were close to the experimental ones.

8)- The propose model gives the amount of shear reinforcement needed for safe design of RC beams with non-structural wall at one side of beams with structural gaps.

8.2 Future Work

Improving the proposed model by applying lateral displacement instead of the lateral forces. And by knowing the sections of truss members, calculating the deformations of model will be achieved using stiffness matrix concept.

APPENDIX A

THE EXPERIMENTAL RESULTS OF SPECIMENS OF PREVIOUS RESEARCHES

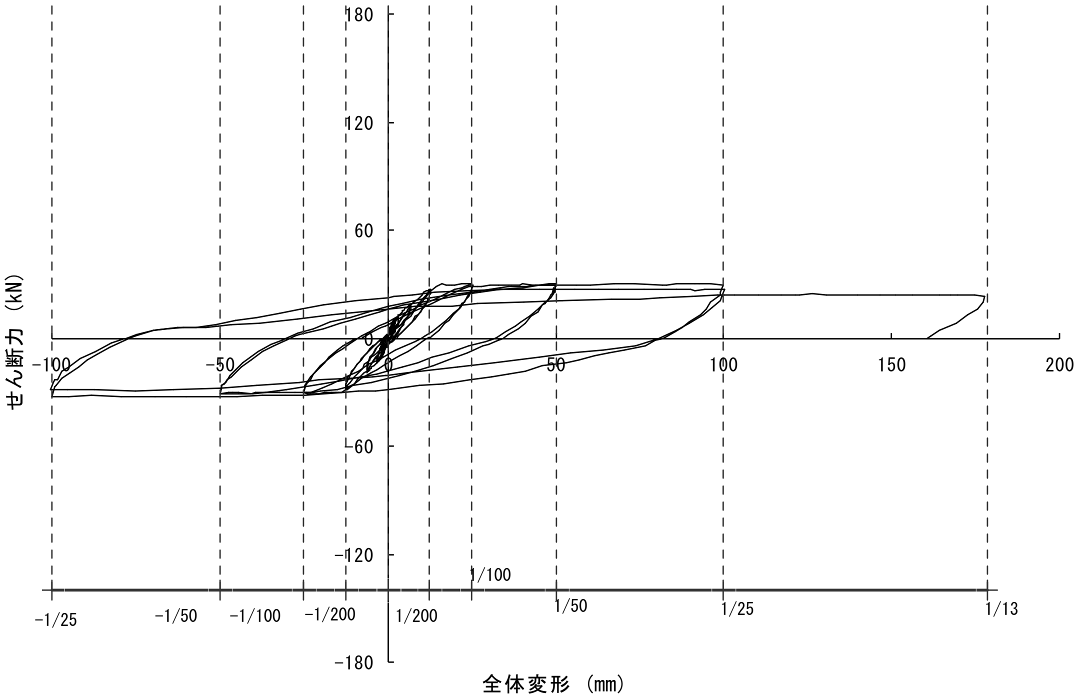

Fig (A.1) Shear force and drift angle of SP-B1

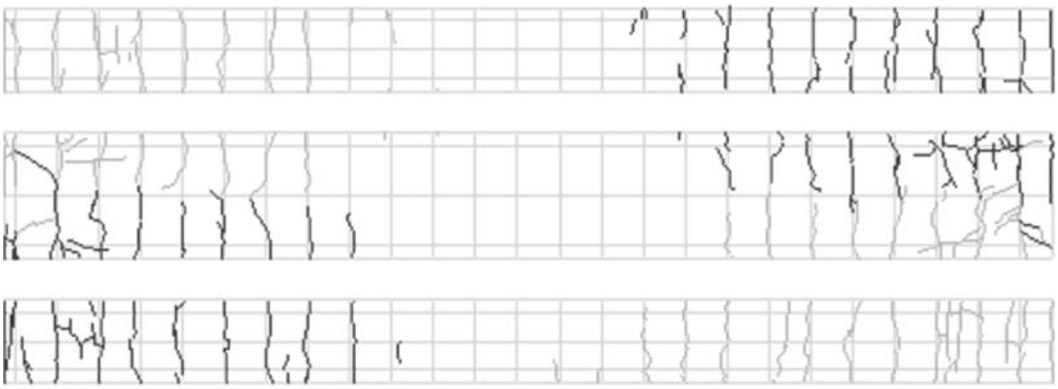

Fig (A.2) Cracks pattern of SP-B1

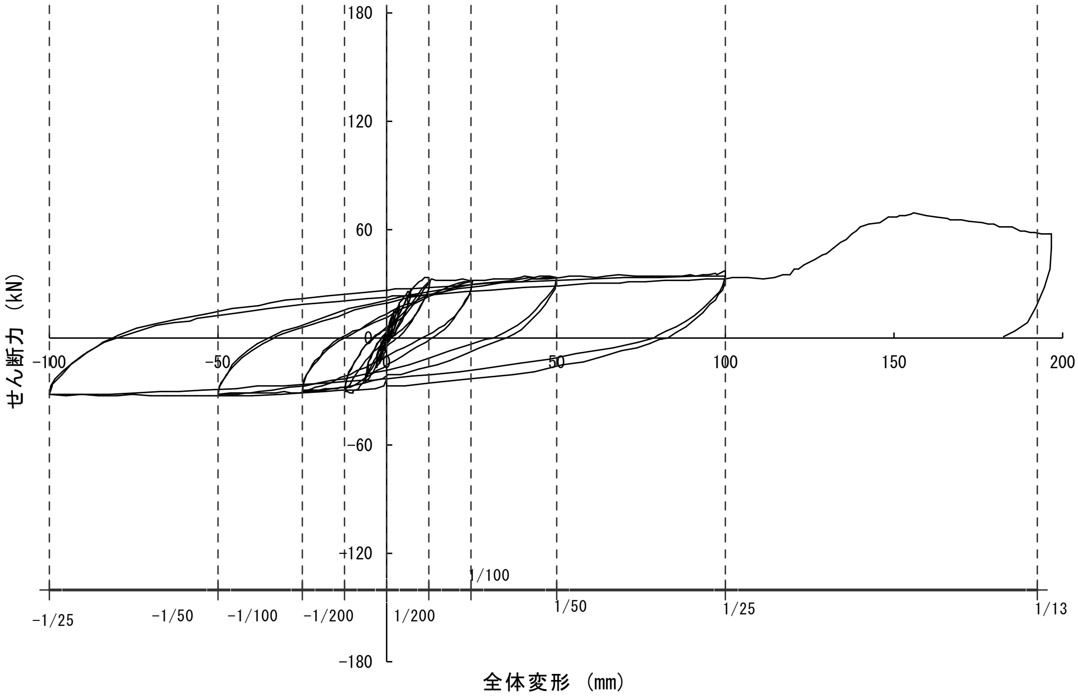

Fig (A.3) Shear force and drift angle of SP-S1

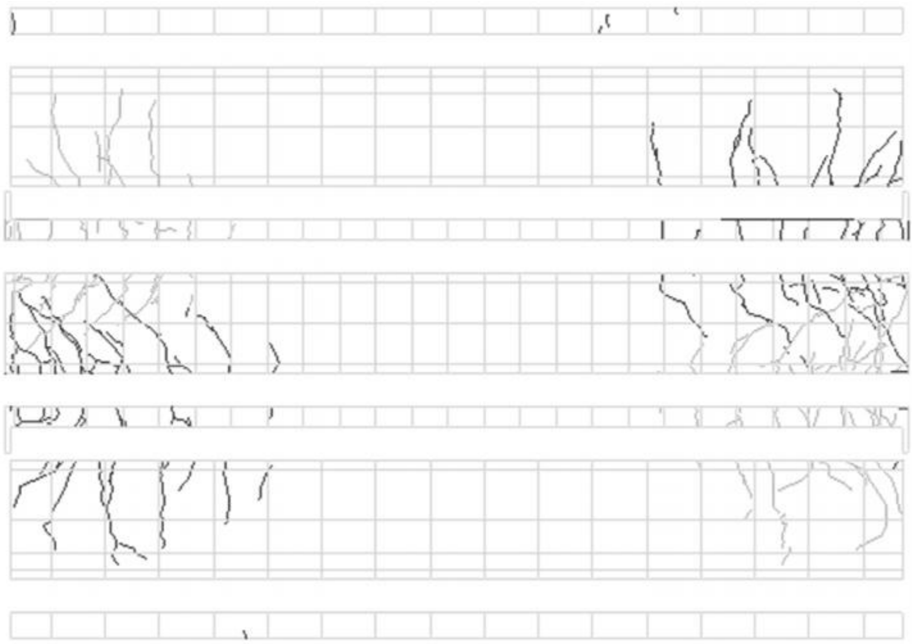

Fig (A.4) Cracks pattern of SP-S1

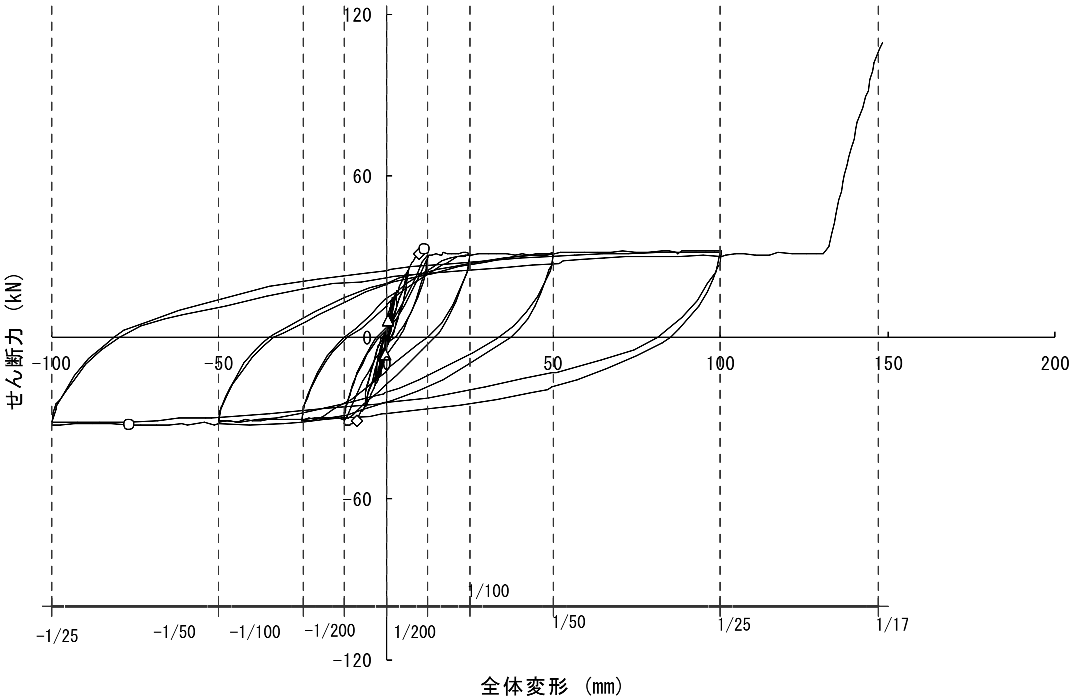

Fig (A.5) Shear force and drift angle of SP-S2

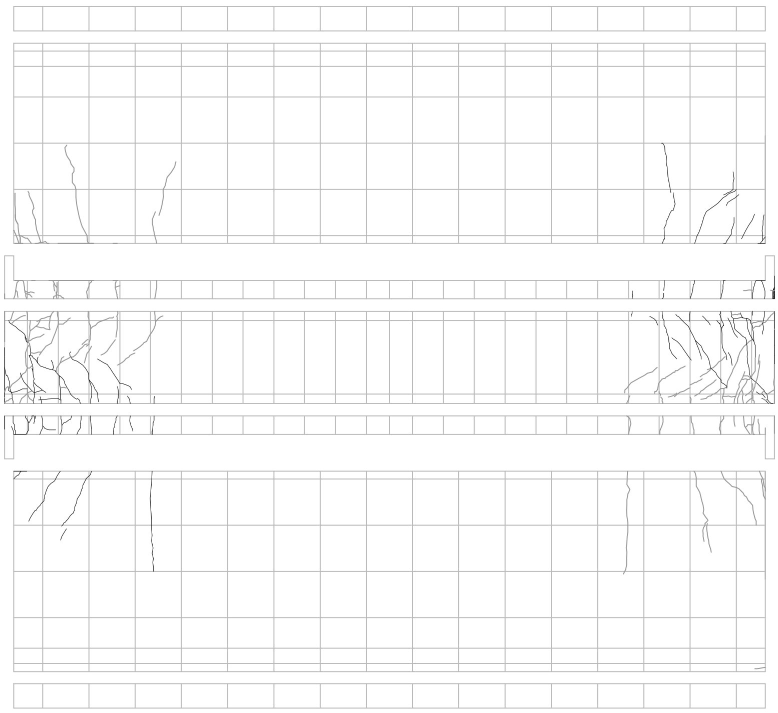

Fig (A.6) Cracks pattern of SP-S2

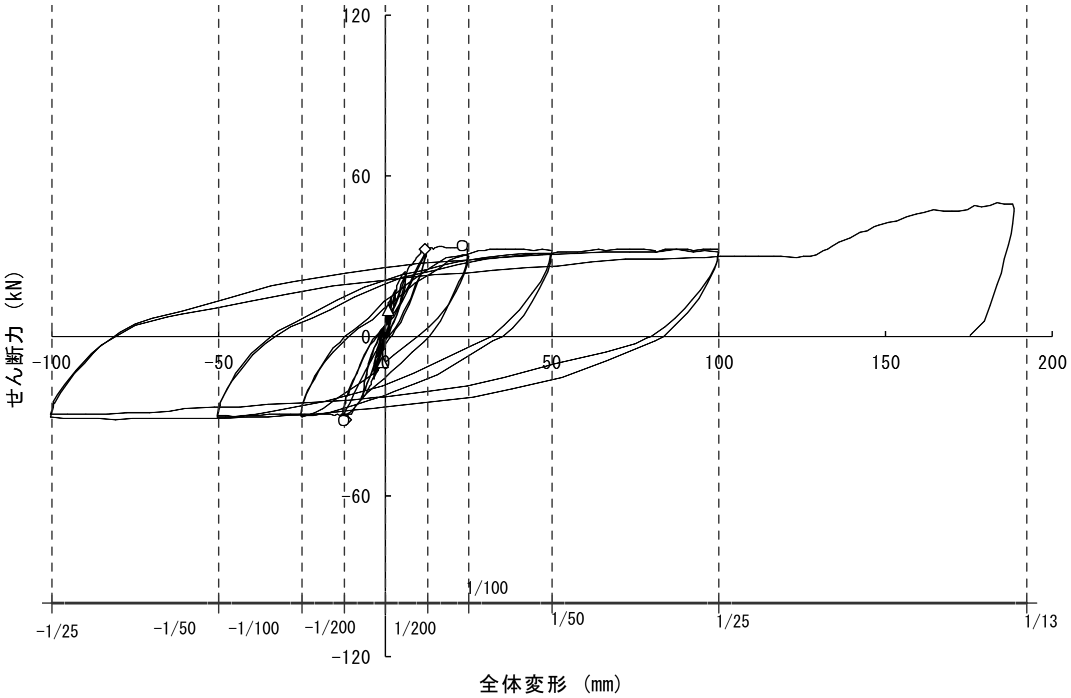

Fig (A.7) Shear force and drift angle of SP-S3

Fig (A.8) Cracks pattern of SP-S3

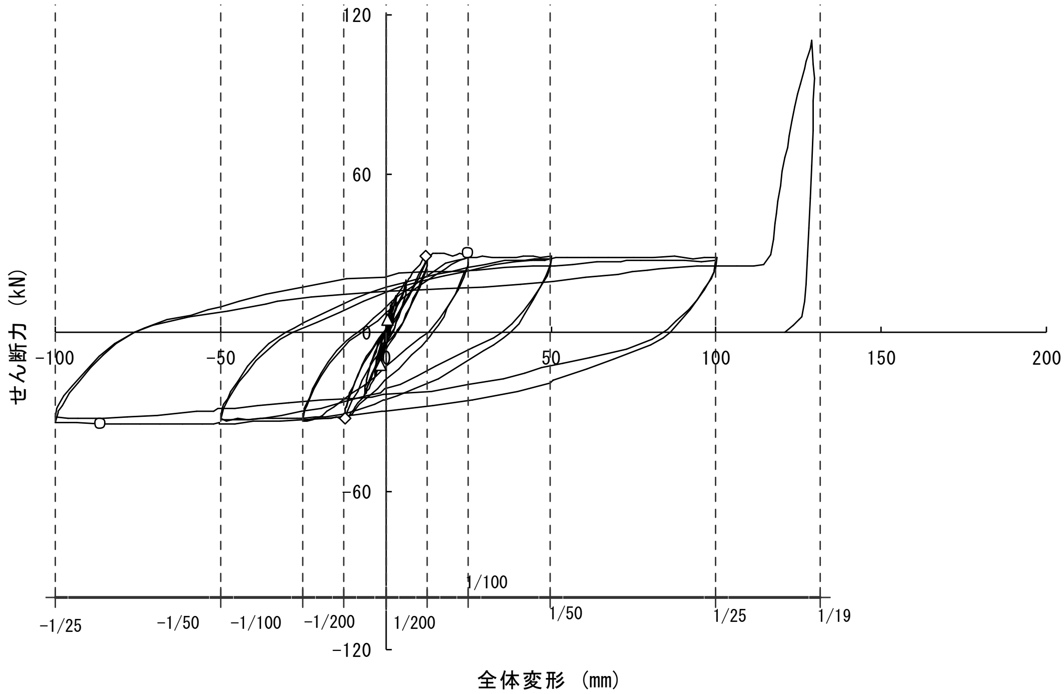

Fig (A.9) Shear force and drift angle of SP-S4

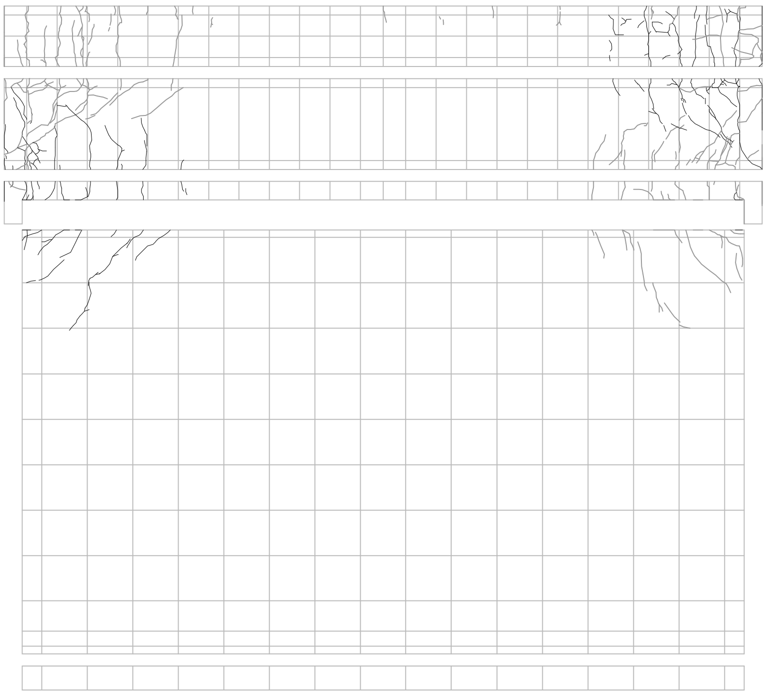

Fig (A.10) Cracks pattern of SP-S4

APPENDIX B

THE ILLUSTRATIONS OF CRACKS PATTERNS IN EACH OF STUDIED SPECIMENS

SP-S5


S.1
S.2
S.3
S.4
S.5
The positions of Reinforcement
At Positive Direction of Loading
At Negative Direction of Loading

SP-S6

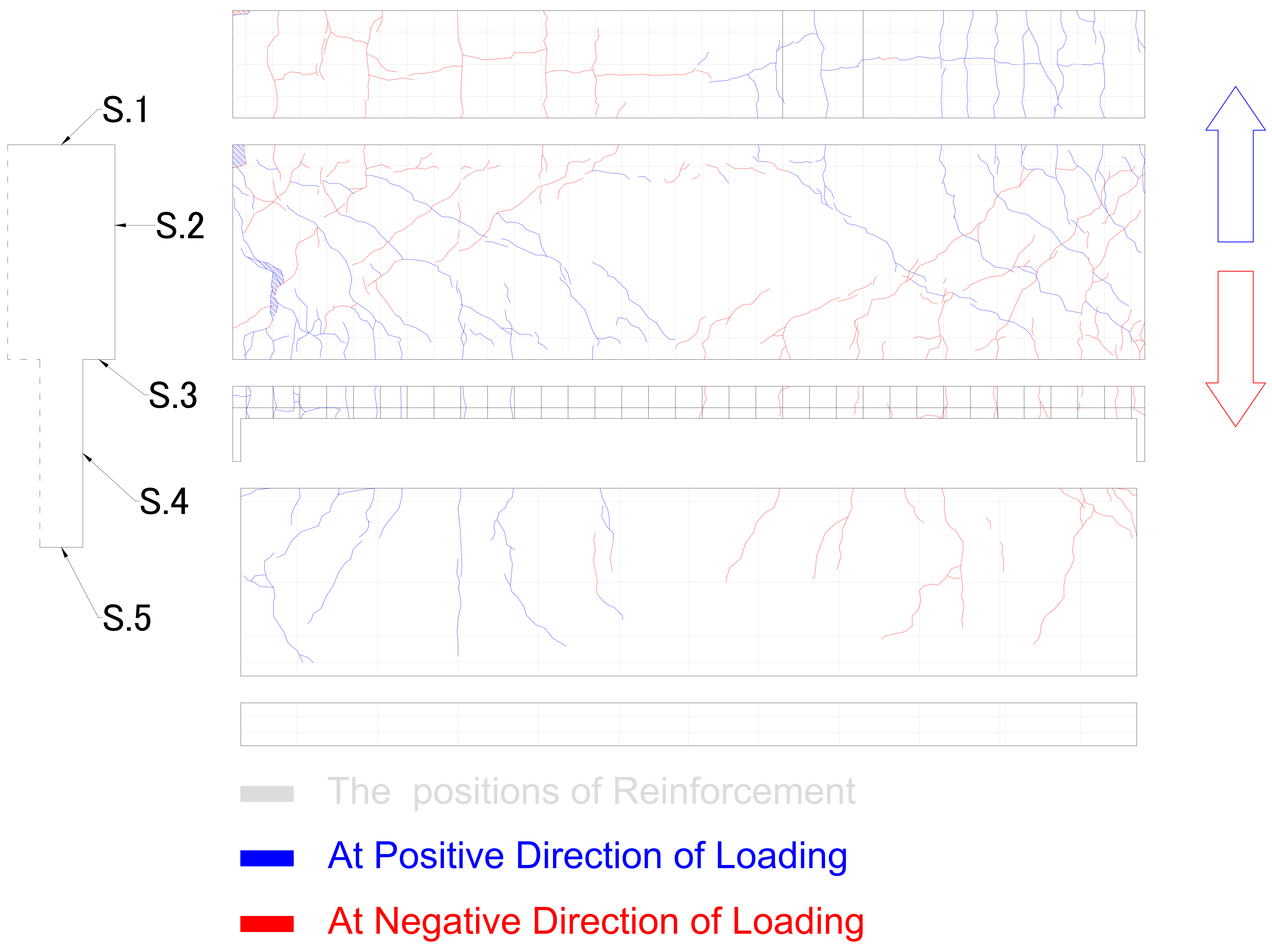
S.1
S.2
S.3
S.4
S.5
The positions of Reinforcement
At Positive Direction of Loading
At Negative Direction of Loading

SP-S6-AR

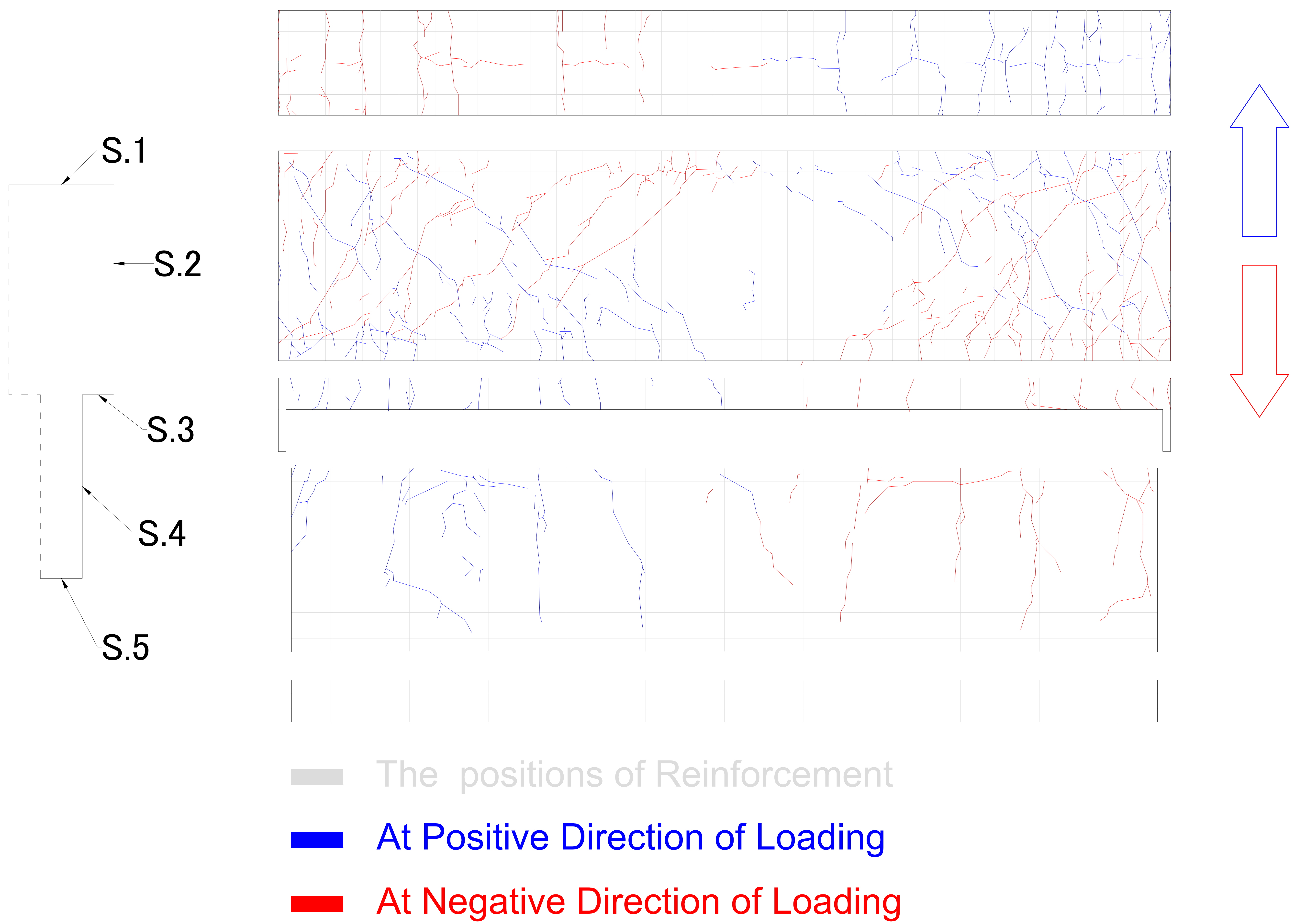
S.1
S.2
S.3
S.4
S.5
The positions of Reinforcement
At Positive Direction of Loading
At Negative Direction of Loading

SP-S6-Slab T

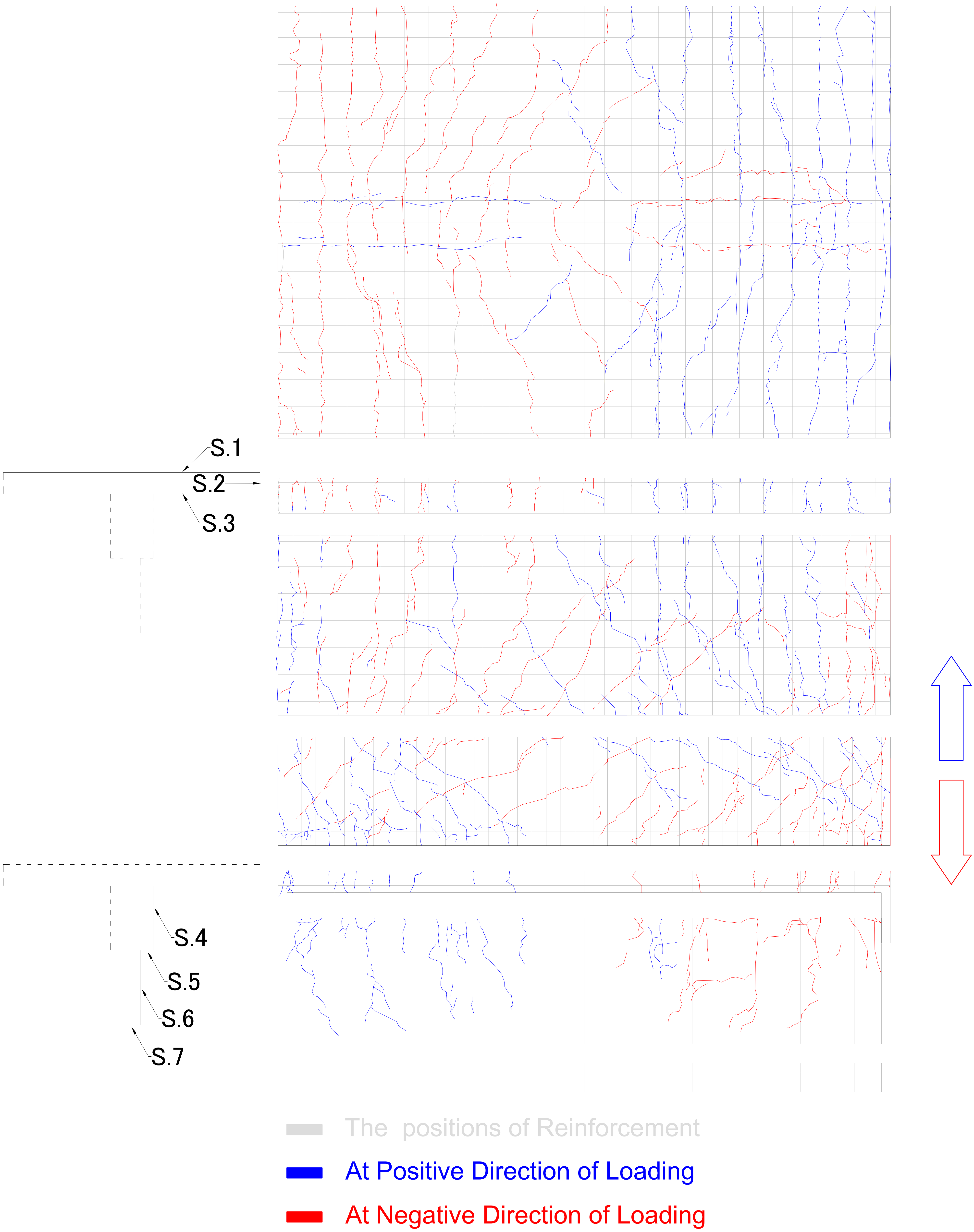

S.1
S.2
S.3
S.4
S.5
S.6
S.7
The positions of Reinforcement
At Positive Direction of Loading
At Negative Direction of Loading

SP-S6-Slab K

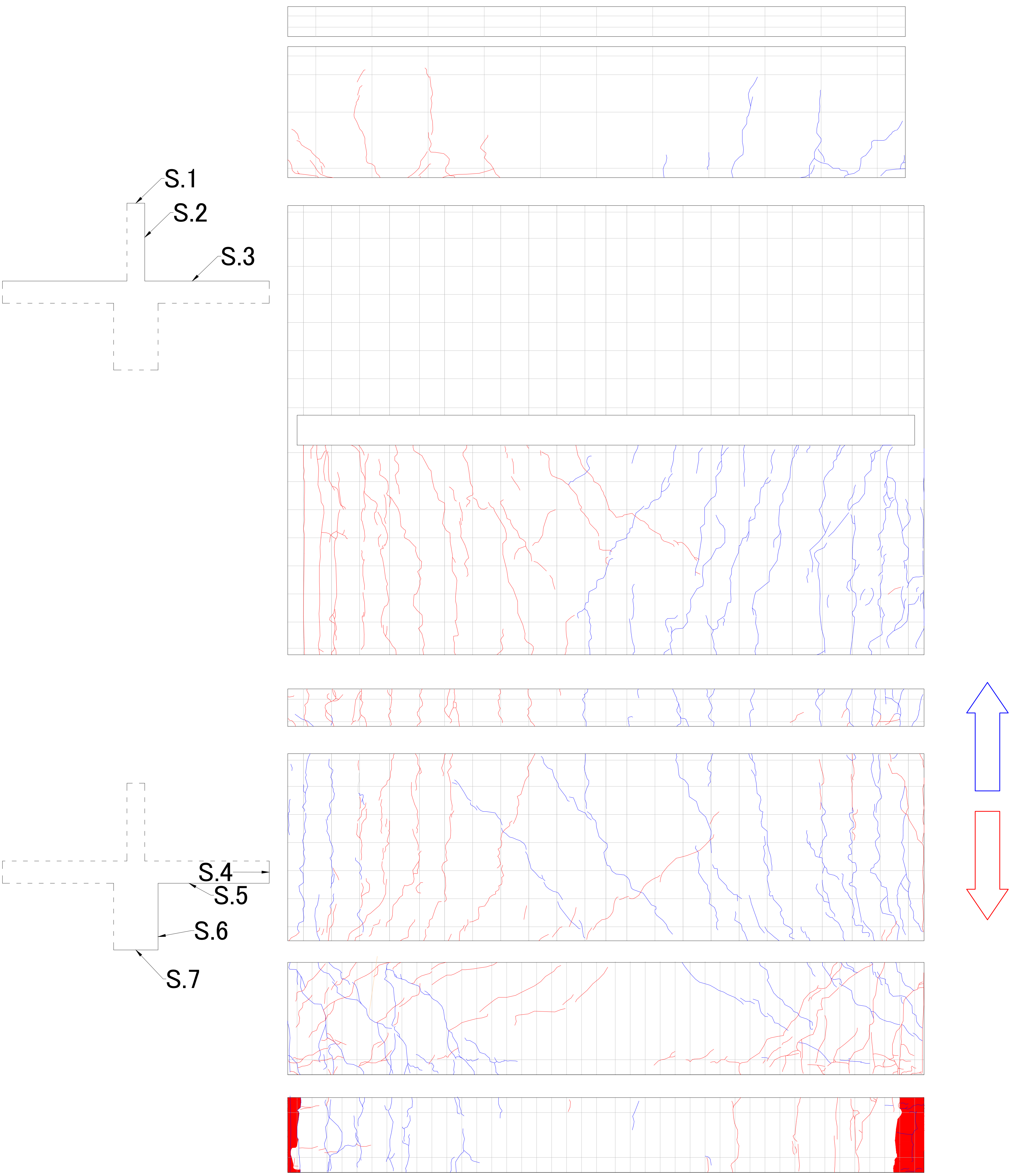

The positions of Reinforcement

At Positive Direction of Loading

At Negative Direction of Loading

SP-S5-Slab T

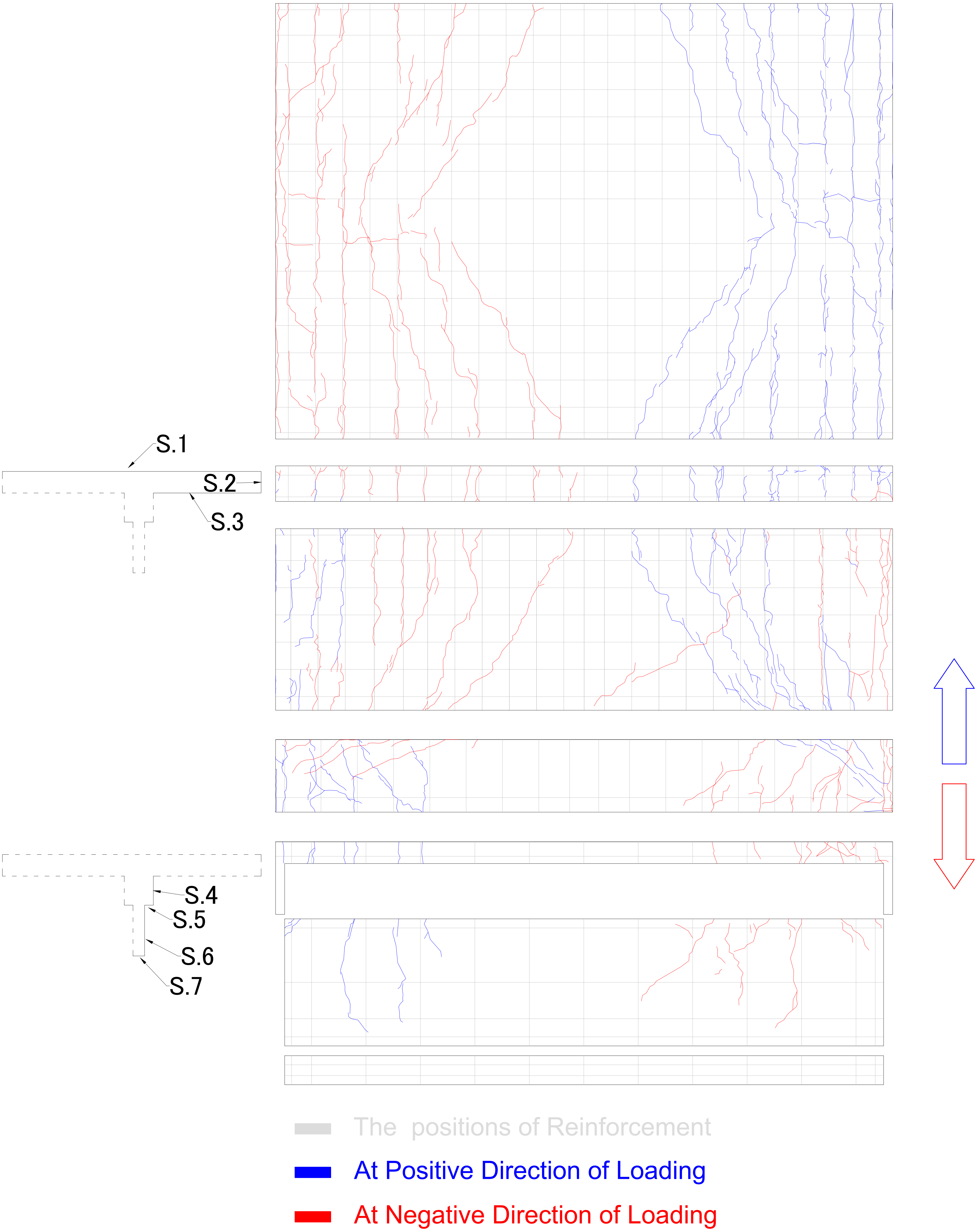

S.1
S.2
S.3
S.4
S.5
S.6
S.7
The positions of Reinforcement
At Positive Direction of Loading
At Negative Direction of Loading

APPENDIX C

CALCULATION OF STRUT-ANDTIE MODELS IN DIFFERENT CODES

[redacted] Strut strength and crack control comparison for each design specification.

Specification	Strut Compressive Capacity without Longitudinal Reinforcement	Strut Compressive Capacity w/Longitudinal Reinforcement	Minimum Crack Reinforcement Across Strut (Crack Control)
AASHTO LRFD	$f_{cu}A_{cs}$, where $f_{cu} = \dfrac{f'_c}{0.8+170\varepsilon_1} \le 0.85 f'_c$ $\varepsilon_1 = \varepsilon_s + (\varepsilon_s + .002)\cot^2\alpha_s$ (§ 5.6.3.3.3)	$f_{cu}A_{cs} + f_y A_{ss}$ (§ 5.6.3.3.4)	• Must have orthogonal grid of reinforcing bars near each face • Spacing $\le$ 12.0 in. • $\dfrac{AreaReinf_{eachdirection}}{GrossAreaConc} \ge 0.003$ (§ 5.6.3.6)
ACI 318-05	$0.85\beta_s f'_c A_{cs}$ Prismatic: β_s= 1.0 Bottle-Shaped w/reinf. satisfying crack control: β_s= 0.75 Bottle-Shaped not satisfying crack control: β_s = 0.60λ λ =1.0 for normal weight concrete λ =0.85 for sand-lightweight concrete λ =0.75 for all lightweight concrete Strut in tension members: β_s= 0.40 All other cases: β_s= 0.60 (§ A.3)	$f_{cu}A_c + f'_s A'_s$ (§ A.5)	For $f'_c \le$ 6000 psi $\sum \dfrac{A_{si}}{b_s s_i}\sin(\alpha_i) \ge 0.003$ (§ A.3.3.1)
CSA A23.3	$f_{cu}A_{cs}$, where $f_{cu} = \dfrac{f'_c}{0.8+170\varepsilon_1} \le 0.85 f'_c$ $\varepsilon_1 = \varepsilon_s + (\varepsilon_s + .002)\cot^2\alpha_s$ (§ 11.4.2.3)	$f_{cu}A_c + f'_s A'_s$ (§ 11.4.2.4)	• Must have orthogonal grid of reinforcing bars near each face • Spacing $\le$ 300mm • $\dfrac{AreaReinf_{eachdirection}}{GrossAreaConc} \ge 0.002$ (§ 11.4.5)
CSA S6-06	$f_{cu}A_{cs}$, where $f_{cu} = \dfrac{f'_c}{0.8+170\varepsilon_1} \le \alpha_1 \cdot f'_c$ $\varepsilon_1 = \varepsilon_s + (\varepsilon_s + .002)\cot^2\theta_s$ α_1 = 0.85-0.0015f'_c (§ 8.10.3.3)	$f_{cu}A_{cs} + f_y A_{ss}$ (§ 8.10.3.4)	• Must have orthogonal grid of reinforcing bars near each face • Spacing $\le$ 300mm • $\dfrac{AreaReinf_{eachdirection}}{GrossAreaConc} \ge 0.003$ • Not more than 1500 mm^2/m each face (§ 8.10.5.1)
NZS 3101	$0.85\beta_s f'_c A_{cs}$ Prismatic: β_s= 1.0 Bottle-Shaped w/rein. satisfying crack control: β_s= 0.75 Bottle-Shaped not satisfying crack control: β_s = 0.60λ λ =1.0 for normal weight concrete λ =0.85 for sand-lightweight concrete λ =0.75 for all lightweight concrete Strut in tension members: β_s= 0.40 All other cases: β_s= 0.60 (§ A5.2)	$f_{cu}A_c + f'_s A'_s$ (§ A5.5)	For $f'_c \le$ 40 MPa $\sum \dfrac{A_{si}}{b_s s_i} f_y \sin(\gamma_i) \ge 1.5MPa$ (§ A.3.3.1)
DIN1045-1	$1.0\eta_1 f_{cd} A_{cs}$ Uncracked Concrete Compressive Zones $0.75\eta_1 f_{cd} A_{cs}$ Parallel to Cracks η_1 = 1.0 for normal weight concrete η_1 = 0.4 + 0.6(ρ/2200) for lightweight concrete (§ 10.6.2)	No direct mention of subject. "design stress in strut reinforcement shall not exceed f_{yd}" (§ 10.6.2)	$\rho_w = \dfrac{A_{sw}}{s_w b_w \sin(\alpha)} \ge \rho$ $\rho = 0.16(f_{ctm}/f_{yk})$ (§ 13.2.3)*

[redacted] (Continued): Strut strength and crack control comparison for each design specification.

Specification	Strut Compressive Capacity without Longitudinal Reinforcement	Strut Compressive Capacity w/Longitudinal Reinforcement	Minimum Crack Reinforcement Across Strut (Crack Control)
1999 FIP Recommendations	$f_{cd,eff}A_c = \upsilon_1 f_{1cd}A_{cs}$ or $\upsilon_2 f_{1cd}A_c$ $\upsilon_1 = (1 - f_{ck}/250)$ rectangular, uncracked stress block $\upsilon_2 = 1.0$ uniform strain/uncracked $\upsilon_2 = 0.80$ parallel cracks w/bonded reinforcement $\upsilon_2 = 0.60$ compression across small cracks $\upsilon_2 = 0.45$ compression across large cracks (§ 5.3.2)	$A_c f_{cd,eff} + A_{sc}\sigma_{scd}$ (§ 5.3.3)	Must have orthogonal grid of “skin reinforcement” with $s_t \leq$ 100 mm $A_{st} = 0.01 s_t b_c$ for stirrups $A_{st} = 0.020 s_t b_c$ for longitudinal rein. (gen.) $A_{st} = 0.015 s_t b_c$ for longitudinal rein. (post-tensioned members) (§ 7.5.5)*
CEB-FIP Model Code 90	$f_{cd1}A_{cs}$ or $f_{cd2}A_{cs}$ Uncracked Concrete Compressive Zones $f_{cd1} = .85\left(1 - \frac{f_{ck}}{250}\right)f_{cd}$ Cracked Concrete Compressive Zones $f_{cd2} = .60\left(1 - \frac{f_{ck}}{250}\right)f_{cd}$ (§ 6.8.1.2 and 6.2.2.2)	No direct mention of subject with respect to strut-and-tie models.	Does not give much guidance. States, “A minimum amount of reinforcement…for crack control.” Gives some guidance for pure tension and flexure. (§ 7.4.5)

[redacted] Definitions for variables referenced in Table 4-1 for each design specification.

<table>
<tr><td>AASHTO LRFD</td><td>A_{cs} = area of concrete in the strut (in^2)
A_{ss} = area of steel in the strut (in^2)
f'_c = concrete compressive strength (ksi)
f_{cu} = limiting concrete compressive strength (ksi)
ε_s = the tensile strain in the concrete in direction of the tension tie (in/in)</td><td>CSA A23.3</td><td>A_{cs} = area of concrete in the strut (mm^2)
A_{ss} = area of steel in the strut (mm^2)
f'_c = concrete compressive strength (MPa)
f_{cu} = limiting concrete compressive strength (MPa)
ε_s = the tensile strain in the concrete in direction of the tension tie (mm/mm)</td></tr>
<tr><td>ACI 318-05</td><td>A'_s = area of compression steel (in^2)
A_c = area of concrete in the strut (in^2)
A_{cs} = area of concrete in the strut (in^2)
A_{si} = total area of surface reinforcement at spacing s_i (in^2)
f'_c = concrete compressive strength (ksi)
f_{cu} = effective concrete compressive strength (ksi)
α_i = the angle between the reinforcement and the axis of the strut (DEG.)</td><td>NZS 3101</td><td>A'_s = area of compression steel (mm^2)
A_c = area of concrete in the strut (mm^2)
A_{cs} = area of concrete in the strut (mm^2)
A_{si} = total area of surface reinforcement at spacing s_i (mm^2)
f'_c = concrete compressive strength (MPa)
f'_s = steel compressive strength (MPa)
f_{cu} = effective concrete compressive strength (MPa)
γ_i = the angle between the reinforcement and the axis of the strut (DEG.)</td></tr>
<tr><td rowspan="2">DIN1045-1</td><td rowspan="2">A_{sw} = sectional area of the shear reinforcement (mm^2)
b_w = width of the web (mm)
f_{cd} = design concrete compressive strength = $\alpha(f_{ck}/\gamma_c)$ (MPa)
f_{ck} = characteristic concrete compressive strength (MPa)
f_{ctm} = mean axial tensile strength of concrete (MPa)
f_{yd} = design yield strength of steel = f_{yk}/γ_s (MPa)
f_{yk} = characteristic yield strength of reinforcing steel (MPa)
s_w = spacing of the shear reinforcement elements (mm)
α = angle of the shear reinforcement to the beam axis (§ 13.2.3) (DEG.)
α = reduction factor taking into account long term affect on concrete strength = 0.85
γ_c = concrete partial safety factor = 1.5
γ_s = reinforcement partial safety factor = 1.15
ρ = density of concrete (§ 10.6.2) (kg/m^3)
ρ = minimum shear reinforcement ratio (§13.2.3)</td><td>CEB-FIP Model Code 90</td><td>f_{cd} = design values of concrete compressive strength = f_{ck}/γ_c (MPa)
f_{cd1} = uncracked compressive design strength (MPa)
f_{cd2} = cracked compressive design strength (MPa)
f_{ck} = characteristic concrete compressive strength (MPa)
γ_c = concrete partial safety factor = 1.5</td></tr>
<tr><td>1999 FIP Recommendations</td><td>A_c = area concrete compressive strut (mm^2)
A_{sc} = area of compression steel (mm^2)
A_{st} = area of crack control reinforcement (mm^2)
f_{1cd} = uniaxial compressive design strength = $\alpha(f_{ck}/\gamma_c)$ (MPa)
$f_{cd,eff}$ = effective compressive strength of strut (MPa)
f_{ck} = characteristic concrete compressive strength (MPa)
α = coefficient taking account of uniaxial strength in relation to strength control of specimen and duration of loading = 0.85
σ_{scd} = stress in compression steel (MPa))
γ_c = concrete partial safety factor = 1.5
υ_1 and υ_2 = reduction factors</td></tr>
<tr><td>CSA-S6-06</td><td>A_{cs} = area of concrete in the strut (mm^2)
A_{ss} = area of steel in the strut (mm^2)
f'_c = concrete compressive strength (MPa)
f_{cu} = limiting concrete compressive strength (MPa)
ε_s = the tensile strain in the concrete in direction of the tension tie (mm/mm)</td><td></td><td></td></tr>
</table>

[redacted] Specified tie strengths, node strengths, and α_s[1] for each design specification.

Specification	Min. α_s[1] (deg.)	Tie Nominal Capacity	Node Compressive Stress
AASHTO LRFD	-	$f_y A_{st} + A_{ps}[f_{pe} + f_y]$ (§ 5.6.4.3.1)	CCC: $0.85f'_c$ CCT: $0.75f'_c$ CTT: $0.65f'_c$ (§ 5.6.3.5)
ACI 318-05	$\alpha_s \geq 25$ (§ A.2.5)	$A_{ts} f_y + A_{tp}[f_{se} + \Delta f_p]$ (§ A.4)	$.85\beta_n f'_c$ CCC: $\beta_n = 1.0$ CCT: $\beta_n = 0.8$ CTT: $\beta_n = 0.6$ (§ A.5)
CSA A23.3	-	$f_y A_{st}$ (§ 11.4.3.1)	CCC: $0.85f'_c$ CCT: $0.75f'_c$ CTT: $0.65f'_c$ (§ 11.4.4.1)
CSA-S6-06	-	$f_y A_{st} + \mathrm{f}_{py} A_{ps}$ (§ 8.10.4.1)	CCC: $\alpha_1 \psi_c f'_c$ CCT: $0.88\alpha_1 \psi_c f'_c$ CTT: $\alpha_1 f'_c$ (§ 8.10.5.1)
NZS 3101	$\alpha_s \geq 25$ (§ A4.5)	$A_{st} f_y + A_{tp}[f_{se} + \Delta f_p]$ (§ A6.1)	$.85\beta_n f'_c$ CCC: $\beta_n = 1.0$ CCT: $\beta_n = 0.8$ CTT: $\beta_n = 0.6$ (§ A7.2)
DIN 1045-1*	$\alpha_s \geq 45$ (§ 10.6.3)	f_{yd} Max Stress of Tie $f_{p0.1k}/\gamma_s$ Max Stress in Prestressing Tie (§ 10.6.2)	$1.1\,\eta_1 f_{cd}$ CCC Nodes $0.75\,\eta_1 f_{cd}$ CCT and CTT Nodes with $\theta_s \geq 45$ $\eta_1 = 1.0$ for normal weight concrete $\eta_1 = 0.4 + 0.6(\rho/2200)$ for lightweight concrete (§ 10.6.3)
CEB-FIP Model Code 90*	$\alpha_s \approx 60$ $\alpha_s \geq 45$ (§ 6.8.1)	Max Stress of Tie f_{ytd} Max Stress in Prestressing Tie $f_{pyd,net} = 0.9f_{ptk}/\gamma_s - \sigma_{do} \leq 600$ MPA (§ 6.8.1.1 and 6.2.4)	CCC and CCT or CTT with $\theta_s \geq 55$ $0.85\left(1 - \frac{f_{ck}}{250}\right) f_{cd}$ CCT and CTT $0.60\left(1 - \frac{f_{ck}}{250}\right) f_{cd}$ (§ 6.9.2.1 and 6.2.2.2)
1999 FIP Recommendations	-	$A_s f_{yd} + A_p f_{ptd}$ (§ 5.2)	CCT and CTT $\upsilon_2 f_{1cd}$, where $\upsilon_2 = 0.85$ CCC Biaxial compression $1.20f_{1cd}$ Triaxial compression $3.88f_{1cd}$ (§ 5.6)

*Nominal stress in tie is specified rather than force.

[1] α_s = the angle between the compressive strut and adjoining tension tie (deg.)

[redacted] Definitions for variables referenced in Table 4-3 for each design specification.

AASHTO LRFD	A_{ps} = area of prestressing steel (in^2) A_{st} = total area of longitudinal steel reinforcement in the tie (in^2) f'_c = concrete compressive strength (ksi) f_y = yield strength of longitudinal steel reinforcement (ksi) f_{pe} = stress in prestressing steel due to prestress after losses (ksi)	CSA A23.3	A_{st} = total area of longitudinal steel reinforcement in the tie (mm^2) f'_c = concrete compressive strength (MPa) f_y = yield strength of longitudinal steel reinforcement (MPa)
ACI 318-05	A_{ts} = area of nonprestressed reinforcement in a tie (in^2) A_{tp} = area of prestressing steel in a tie (in^2) f'_c = concrete compressive strength (ksi) f_y = specified yield strength of reinforcement (ksi) f_{se} = effective stress in prestressing steel (after allowance for all prestress losses) (ksi) Δf_p = increase in stress in prestressing steel due to factored loads (ksi)	NZS 3101	A_{st} = area of nonprestressed reinforcement in a tie (mm^2) A_{tp} = area of prestressing steel in a tie (mm^2) f'_c = concrete compressive strength (MPa) f_y = specified yield strength of reinforcement (MPa) f_{se} = effective stress in prestressing steel (after allowance for all prestress losses) (MPa) Δf_p = increase in stress in prestressing steel due to factored loads (MPa)
DIN1045-1	f_{cd} = design value of concrete compressive strength = $\alpha(f_{ck}/\gamma_c)$ (MPa) f_{ck} = characteristic concrete compressive strength (MPa) f_{yd} = design yield strength of tie reinforcement = (f_y/γ_s) (MPa) f_y = yield stress of steel (MPa) α = reduction factor taking into account long-term effects on concrete strength = 0.85 γ_c = concrete partial safety factor = 1.5 γ_s = reinforcement partial safety factor = 1.15	CEB-FIP Model Code 90	f_{cd} = design value of concrete compressive strength = f_{ck}/γ_c (MPa) f_{ck} = characteristic concrete compressive strength (MPa) f_{ptk} = characteristic prestressing tie tensile strength (MPa) $f_{pyd,net}$ = design value for prestressing tie tensile strength (MPa) f_{ytd} = design value for tie tensile strength = f_{ytk}/γ_s (MPa) f_{ytk} = f_y = yield stress of steel (MPa) γ_c = partial safety factor for concrete = 1.5 γ_s = partial safety factor for steel = 1.15 σ_{do} = design tendon stress taken into account in the prestress loading system (MPa)
CSA-S6-06	A_{st} = total area of longitudinal steel reinforcement in the tie (mm^2) A_{ps} = cross-sectional area of tendons in tie (mm^2) f'_c = concrete compressive strength (MPa) f_{py} = yield strength of presressing steel (MPa) f_y = yield strength of longitudinal steel reinforcement (MPa) α_1 = 0.85-0.0015f'_c ψ = ratio of creep strain to elastic strain	1999 FIP Recommendations	A_s = area of nonprestressing reinforcement (mm^2) A_p = area of prestressing steel (mm^2) f_{1cd} = uniaxial design strength of concrete = $\alpha(f_{ck}/\gamma_c)$ (MPa) f_{ck} = characteristic concrete compressive strength (MPa) f_{yd} = design value for tie tensile strength = f_y/γ_s (MPa) f_y = yield stress of steel (MPa) f_{ptd} = design value for prestressing tie tensile strength = f_{pe}/γ_s (MPa) $f_{p0.1k}$ = characteristic 0.1 % Proof Stress of prestressing steel (MPa) α = coefficient taking account of uniaxial strength in relation to strength control of specimen and duration of loading = 0.85 γ_c = concrete partial safety factor = 1.5 γ_s = reinforcement partial safety factor = 1.15

[redacted] Strut provisions from additional sources.

Source	Strut Compressive Stress
AASHTO LRFD (§ 5.6.3.3.3)	$\dfrac{f'_c}{0.8+170\varepsilon_1} \le 0.85f'_c$ $\varepsilon_1 = \varepsilon_s + (\varepsilon_s + .002)\cot^2\alpha_s$
Schlaich et al. (1987)	$0.85f'_c$ "for an undisturbed and uniaxial state of compressive stress" (prismatic) $0.68f'_c$ "if tensile strains in the cross direction or transverse tensile reinforcement may cause cracking parallel to the strut with normal crack width" $0.51f'_c$ "as above for skew cracking or skew reinforcement" $0.34f'_c$ "for skew cracks with extraordinary crack width. Such cracks must be expected, if modeling of the struts departs significantly from the theory of elasticity's flow of internal forces"
Collins et al. (1991)	$\dfrac{f'_c}{0.8+170\varepsilon_1} \le 0.85f'_c$ and $\varepsilon_1 = \varepsilon_s + (\varepsilon_s + .002)\cot^2\alpha_s$ where, α_s is the smallest angle between the tie and the strut ε_s is the tensile strain in the tension-tie reinforcement (in/in)
MacGregor (1997)	$\upsilon_1\upsilon_2 f'_c$ where $\upsilon_2 = (0.55 + \dfrac{15}{\sqrt{f'_c}})$ $\upsilon_1 = 1.0$ Uncracked uniaxially stressed struts or fields $\upsilon_1 = 0.80$ Struts cracked longitudinally due to bottle shaped stress fields, containing transverse reinforcement $\upsilon_1 = 0.65$ Struts cracked longitudinally due to bottle shaped stress fields without transverse reinforcement $\upsilon_1 = 0.60$ Struts in cracked zone with transverse tensions from transverse reinforcement
Bergmeister et al. (1993)*	Fan, bottle, or prismatic struts: $\upsilon_e f'_c$ $\upsilon_e = 0.8$ for $f'_c \le 4000$ psi $\upsilon_e = 0.9\text{-}.25f'_c/1000$ for $4000 < f'_c < 10{,}000$ psi $\upsilon_e = 0.65$ for $f'_c \ge 10{,}000$ psi Compression diagonal struts: $0.6\upsilon_e f'_c$ Confined compression fields: $[\upsilon_e f'_c(A/A_b)^{0.5} + \alpha(A_{core}/A_b)f_{lat}(1\text{-}s/d)^2] \le 2.5f'_c$ $\alpha = 4.0$ for spiral confinement $\alpha = 2.0$ for square closed hoop confinement anchored with longitudinal reinforcement $\alpha = 1.0$ for square closed hoop confinement without longitudinal reinforcement anchorage

* See additional notation below

<u>Bergmeister et al.</u>

f_{lat} = lateral pressure $= 2f_yA_s/(ds)$ for $f'_c \le 7000$ psi
$= 2f_sA_s/(ds)$ for $f'_c \ge 7000$ psi

$f_s = C\mu 2s/(\pi d A_s) \le f_y$

C = Compression load

μ = Poisson's ratio

A = area of the confined concrete concentric with and geometrically similar to the bearing plate.

A_b = Area of the bearing plate

A_{core} = Area of confined strut

$A/A_b \le 4$

$1 \le A_{core}/A_b \le 3$

[redacted] Node provisions from additional sources.

Source	Node Compressive Stress
AASHTO LRFD (§ 5.6.3.5)	CCC: $0.85f'_c$ CCT: $0.75f'_c$ CTT: $0.65f'_c$
Schlaich et al. (1987)	CCC: $0.85f'_c$ CCT or CTT: $0.68f'_c$
Collins et al. (1991)	CCC: $0.85f'_c$ CCT: $0.75f'_c$ CTT: $0.60f'_c$ ($\varphi = 0.7$)
MacGregor (1997)	$\upsilon_1\upsilon_2 f'_c$ where $\upsilon_2 = (0.55 + \frac{15}{\sqrt{f'_c}})$ $\upsilon_1 = 1.0$ Joints bound by struts and bearing plates $\upsilon_1 = 0.85$ Joints anchoring one tension tie $\upsilon_1 = 0.75$ Joints anchoring more than one tension tie
Bergmeister et al. (1993)*	Unconfined nodes without bearing plates: $\upsilon_e f'_c$ $\upsilon_e = 0.8$ for $f'_c \leq 4000$ psi $\upsilon_e = 0.9\text{-}.25f'_c/1000$ for $4000 < f'_c < 10{,}000$ psi $\upsilon_e = 0.65$ for $f'_c \geq 10{,}000$ psi Confined nodes: $[\upsilon_e f'_c(A/A_b)^{0.5} + \alpha(A_{core}/A_b)f_{lat}(1\text{-}s/d)^2] \leq 2.5 f'_c$ $\alpha = 4.0.$ for spiral confinement $\alpha = 2.0$ for square closed hoop confinement anchored with longitudinal reinforcement $\alpha = 1.0$ for square closed hoop confinement without longitudinal reinforcement anchorage Unconfined nodes with bearing plates: $\upsilon_e f'_c(A/A_b)^{0.5} \leq 2.5 f'_c$ Triaxially confined node: $f_{c3} \leq 2.5 f'_c$

* See additional notation below

Bergmeister et al.

f_{lat} = lateral pressure $= 2f_yA_s/(ds)$ for $f'_c \leq 7000$ psi $= 2f_sA_s/(ds)$ for $f'_c \geq 7000$ psi

$f_s = C\mu 2s/(\pi d A_s) \leq f_y$

C = Compression Load

μ = Poisson's ratio

A = area of the confined concrete concentric with and geometrically similar to the bearing plate.

A_b = Area of the bearing plate

A_{core} = Area of confined strut

$A/A_b \leq 4$

$1 \leq A_{core}/A_b \leq 3$

REFERENCES

1) Abdul Ghaffar, Afzal Javed, Habib ur Rehman, Kafeel Ahmed, M Ilyas (2010). *Development of Shear Capacity Equations for Rectangular Reinforced Concrete Beams.* Pak. J. Engg. & Appl. Sci. Vol. 6.

2) R. Park and T. Paulay (1975). *Reinforced Concrete Structures*, Chapter 12. Published John Wiley and Sons.

3) Bertero, V., Popov, E. P. (1975). *Hysteretic Behavior of Ductile Moment-Resisting Reinforced Concrete Frame Components*. EERC 75-16, University of California, Berkeley.

4) Pau1ay, T.(1977). *Shear Strength Requirements*, Bulletin of the N.Z. Soc. for Earthquake Engineering, Vol. 10, No.2.

5) Architectural Institute of Japan (1968). *Tokachi-oki earthquake damage investigation report*, 1968.12.

6) Architectural Institute of Japan (1978). *Miyagi-oki earthquake disaster investigation report*, 1980.2.

7) WATANABE Hidekazu. (2011). *Studying the seismic performance of RC beams with secondary walls*. Thesis Doctoral Degree, Yokohama National University.

8) SUZUKI Atsushi. (2010). *Studies on the deformation capacity and flexural strength of RC beams with spandrel walls*, Journal of annual meeting of Architectural Institute of Japan 2010.

9) FUKUYAMA Hiroshi, TAJIRI Seitaro. (2009). *An experimental study on performance of RC beams with spandrel walls*, Journal of annual meeting of Architectural Institute of Japan.2009.

10)Michael,D., Brown,M.D., Sankovich,C.L., Bayrak,O., Jirsa,J.O., Breen,J.E.(2006). *Design for Shear in Reinforced Concrete Using Strut- and Tie- Models*, Report No.HWA/TX-06/0-4371-2,The University of Texas.

11) Radmila syndic-Grebovic (2014). *Experimental Analysis of Shear Strength of Beams and Application of STM.* University of Montenegro. International

Conference of Contemporary Achievements in Civil Engineering, SERBIA.
12) Barney T. Martin, Jr., Ph.D., P.E. Modjeski and Masters, Inc.(2007). Verification and Implementation of Strut-and-Tie Model in LRFD Bridge Design Specifications. University of Nevada Reno.
13) Schlaich, Jorg. (1992). Strut-and-Tie Model Design of Structural Concrete. IABSE Congress Report.
14) http://www.aij.or.jp/jpn/symposium/2009/3-3-5.pdf
15) Design Guidelines for Earthquake Resistance Reinforced Concrete Buildings Based on Inelastic displacement Concept. (1999). Architecture Institute of Japan.
16) James_K._Wight,_James_G._MacGregor (2009). Reinforced Concrete, Mechanics and Design. Sixth Edition.PEARSON.
17) Adebar, P. and Leeuwen, J. V. (1999). *Side-face reinforcement for flexural and diagonal cracking in large concrete beams*. ACI Structural Journal, 96(5), 693-704.
18) Adebar, P. (2001). *Diagonal cracking and diagonal crack control in structural concrete*. Design and Construction Practices to Mitigate Cracking, ACI, SP204, 85-116.
19) De Silva, S., Mutsuyoshi, H., Witchukreangkrai, E. and Uramatsu T. (2005). *Analysis of shear cracking behavior in partially prestressed concrete beams*. Proceedings of JCI, 27(2), 865-870.
20) De Silva, S., Mutsuyoshi, H. and Witchukreangkrai, E. (2008). *Evaluation of shear crack width in I-shaped prestressed reinforced concrete beams*. Journal of Advanced Concrete Technology, 6(3), 443-458.
21) Marta Słowik. (2014). *Shear failure mechanism in concrete beams.* Lublin University of Technology. 20th European Conference on Fracture (ECF20).
22) Angelakos, D. (1999). *The influence of concrete strength and longitudinal reinforcement ratio on the shear strength of large-size reinforced concrete*

beams with, and without transverse reinforcement. Thesis Master Degree. University of Toronto, Canada.

23)-Collins, M. P. and Mitchell, D. (1991). *Prestressed concrete structures*. Prentice-Hall Inc, Englewood Cliffs, N. J.

24) Collins, M. P., Bentz, E. C., Sherwood, E. G. and Xie, L. (2007). *An adequate theory for the shear strength of reinforced concrete structures*. University of Cambridge.

25) Sherwood, E. G., Bentz, E. C. and Collins, M. P. (2007). *Effect of aggregate size on beam-shear strength of thick slabs*. ACI Structural Journal, 104(2), 180-190. Shioya, T., Iguro, M., Nojiri, Y., Akiyama, H. and Okada, T. (1989).

26) Zararis, P. D. (2003). *Shear strength and minimum shear reinforcement of RC slender beams*. ACI Structural Journal, 100, 203-214.

27) Witchukreangkrai, W., Mutsuyoshi, H., Kuraoka, M. and Oshiro, T. (2004). *Control of diagonal cracking in partially prestressed concrete beams*. Proceedings of JCI, 26(2), 727-732.

28) Witchukreangkrai, E., Mutsuyoshi, H., Takagi, M. and De Silva, S. (2006). *Evaluation of shear crack width in partially prestressed concrete members*. Proceedings of JCI, 28(2), 823-828.

29) Hassan, H. M., Ueda, T., Tamai, S. and Okamura, H. (1985). *Fatigue test of reinforced concrete beams with various types of shear reinforcement*. Transaction of JCI, 7, 277-284.

30) Hassan, H. M. and Ueda, T. (1987). *Relative displacement along shear crack of reinforced concrete beam*. Proceedings of JCI, 9(2), 699-704.

31) Hassan, H. M. (1987). *Shear cracking behavior and shear resisting mechanism of reinforced concrete beams with web reinforcement*. Thesis Doctoral Degree. The University of Tokyo, Japan.

32) Hassan, H. M., Farghaly, S. A. and Ueda, T. (1991). *Displacements at shear crack in beams with shear reinforcement under static and fatigue loadings*. Concrete Library of JSCE, 19, 247-255.

33) Rizkalla, S. H., Hwang, L. S. and El Shahawai, M. (1983). *Transverse reinforcement effect on cracking behavior of RC members*. Canadian Journal of Civil Engineering, 10(4), 566-581.

34) Mohamed Zakaria, Tamon Ueda, Zhimin Wu and Liang Meng. *Experimental Investigation on Shear Cracking Behavior in Reinforced Concrete Beams with Shear Reinforcement.*

35) Madhu Karthik, Murugesan Rerriar.(2009). Stress-Strain Models of Unconfined and Confined concrete and Stress-BlockParameters.Texas A&M University

36) HORDIJK, D. A. Local Approach to Fatigue of Concrete. PhD thesis, Delft University of Technology, 1991.

37) D.A. Hordijk.(1992). Tensile and Tensile Fatigue of Concrete; Experiments, Models and Analysis.HERON Vol.37.NO.1.

38) Cornelissen, H. A. W., Horijk, D. A., AND Reinhardt, H. W. Experimental determination of crack softening characteristics of normal weight and lightweight concrete. Heron 31, 2 (1986). 1990.

39) Schliach, J. –Schaffer, K.: Design and Detailing of Structural Concrete Using Strut and Tie Models. *The Structural Engineer, No.6, March,1991.*

40) Broms, B. (1965). *Crack width and crack spacing in reinforced concrete members*. ACI Journal Proceedings, 62(10), 1237-1256.

41) Clark, A. P. (1956). *Cracking in reinforced concrete flexural members*. ACI Journal Proceedings, 52(8), 851-862.

42) Gergely, P. and Lutz, A. L. (1968). *Maximum crack width in reinforced concrete flexural members*. Causes, Mechanisms, and Control of Cracking in Concrete, ACI, SP20, 87-117.

43) Ma, S. M., Bertero, V. V. and Popov, E.P.(1976).*Experimental and*

Analytical Studies on the Hysteretic Behavior of Reinforced Concrete Rectangular and T-Beams, Report No. EERC 76-2, University of California.
44) Jorg Schlaich, Dieter Weischede (1982). *Detailing of Concrete Structures*, Bulletin of Information 150, Comite Euro-International du Beton, Paris.
45) S. Sugano (1970). *Experimental study on restoring force characteristics of reinforced concrete members,* Thesis Doctoral Degree, The University of Tokyo.
46) David Birrcher, Robin Tuchscherer, Matt Huizinga, Oguzhan Bayrak, Sharon Wood, James Jirsa.(2009). Strength and Serviceability Design of Reinforced Concrete Deep Beams, Report No. FHWA/TX-09/0-5253-1, The University of Texas.
47) American Concrete Institute, Building Requirements for Structural Concrete and Commentary (ACI 318M-05).